THE EFFECT OF WIND MEASUREMENT ERRORS ON LINEAR SIMULATIONS OF EQUATORIAL CIRCULATIONS

by

Robert Kuklinski

B.S., Worcester Polytechnic Institute

(1981)

SUBMITTED IN PARTIAL FULFILLMENT

OF THE REQUIREMENTS OF THE

DEGREE OF

MASTER OF SCIENCE

IN METEOROLOGY

at the

MASSACHUSETTS INSTITUTE OF TECHNOLOGY

May 1984

Signature of Author _____
Department of Earth, Atmospheric, and Planetary Sciences
May 11, 1984

Certified by _____
Mark A. Cane
Thesis Supervisor

Accepted by _____
Theodore R. Madden
Chairman, Departmental Committee on Graduate Students

TABLE OF CONTENTS

THE EFFECT OF WIND MEASUREMENT ERRORS ON LINEAR SIMULATIONS OF EQUATORIAL CIRCULATIONS

by

ROBERT KUKLINSKI

Submitted to the
Department of Earth, Atmospheric, and Planetary Sciences
on May 11, 1984 in partial fulfillment of the requirements
for the Degree of Master of Science in Meteorology

ABSTRACT

This paper examines the response of the linear shallow water equations on a zonally bounded equatorial beta-plane subject to low frequency periodic zonal wind stress. The general solutions, following Cane and Sarachik [1981], consist of sums of the eastward propagating equatorial Kelvin mode and a number of westward propagating Rossby modes.

To explore the response of a basin to small scale forcing the zonal wind stress is idealized as a delta function. The response is dominated by the sum of directly forced Rossby modes. It is demonstrated that ray theory can be used to duplicate the point source results. In both cases regions of intense response foci are found at a distance CT/4 westward of and at the equatorial image point of the forcing , where T is the period of the forcing and C is the Kelvin wave speed. Regions that experience a very weak response called shadow zones are also found.

The point source solution is used as a Green's function to obtain the response of a basin to unit forcings over an area. We find that features predicted by point forcing and ray theory appear in our "patch" forced problem. As the area we force over grows the higher Rossby modes are damped and the important response becomes confined closer to the equator.

We use the patch solution and superposition to examine the companion problem of the effect of forcing across a basin on a single observation point. The important influence on the observation point comes from four sources.

1. Strong influence from local effects.
2. Moderate influence from Rossby waves forced within 10° of the equator to the east of the observation point.
3. Intense influence from inverse focus points CT/4 east of the observation point
4. Moderate influence from Kelvin waves forced along the equator to the west of the forcing.

The patch influence functions for the first three baroclinic modes are used to examine the importance of wind measurement error in the modeling of sea surface height in the equatorial Pacific and Indian Oceans. The wind errors over the basins are represented by a difference field of two surface wind analyses. FNOC (Fleet Naval Oceangraphic Center) and NMC (National Meteorlogical Center) winds on a 2.5°x2.5° grid are used in the Pacific. ECM (European Meteorlogical Center) data and a wind analysis from Wiley and Hinton on a 2°x3° grid are used in the Indian Ocean. In the Pacific during the January 1982-June 1983 El Nino event, small sea surface errors are found in the eastern Pacific and within one degree of the equator. Serious errors are found north of the equator in the center of the basin near Fanning (9.1cm mean and 48.7cm variance deviation from zero sea surface error). North and south of the equator in the east the errors are also large; (near Rabaul 12.4cm mean + 101.4cm variance). In the Indian Ocean from December 1978 November 1979 large errors from the equator northward into the Arabian Sea are associated with the seasonal monsoon circulation.

Thesis Supervisor: Dr. Mark Cane

Title: Associate Professor of Meteorology

ACKNOWLEDGEMENTS

I would like to thank my advisor, Mark Cane for the guidance and freedom he provided me with during my stay at MIT. I would also like to thank Ed Harrison for serving as a substitute advisor when Mark was away. Members of the MIT staff and fellow graduate students Mike, Ron, Mark, Haim, Steve G., Steve Z., Wes, and Sean provided assistance and insightful disscusions. Most of all I would like to thank my wife Anne H. Kuklinski for the help, support, and love she has given me over the past two years.

INTRODUCTION

The theoretical study of forced planetary scale waves in the tropics has received considerable attention recently. These waves forced by periodic horizontal wind stress are studied using the equatorially scaled shallow water equations:

$$U_t - YV + H_x = e^{iwt} \mathcal{T}_x(X,Y) \tag{1.1}$$

$$V_t + YU + H_y = e^{iwt} \mathcal{T}_y(X,Y) \tag{1.2}$$

$$H_t + U_x + V_y = 0 \tag{1.3}$$

Here U,V, and H are the zonal velocity, meridional velocity, and height respectively. The dimensional equivalent to (1.1-1.3) can be recovered with the scaling:

$$T' = T_m T \qquad T_m = [1/\beta C]^{0.5} \tag{1.4}$$

$$X' = L_m X \qquad L_m = [C/\beta]^{0.5} \tag{1.5}$$

Here T' and X' are the dimensional time and distance; L_m and T_m the equatorial distance and time scales and C the Kelvin wave speed.

If we confine our analysis to low frequency, small zonal wavenumber waves, the system (1.1-1.3) may be rewritten as:

$$U_t - YV + H_x = e^{iwt} \mathcal{T}_x(X,Y) \tag{1.6}$$

$$YU + H_y = 0 \tag{1.7}$$

$$H_t + U_x + V_y = 0 \tag{1.8}$$

We are only examining motions with $\omega = O(\varepsilon)$ and $\partial/\partial x = O(\varepsilon)$,here $\varepsilon << 1$. We find that the meridional forcing must enter at O(1) in equation (1.7) and the zonal forcing at $O(\varepsilon)$ in equation (1.6). So if stress components are assumed to act on a scale of 1 to 5 degrees of latitude only the zonal stress need be retained.

Studies by Cane and Sarachik [1976,1977 & 1981]; Gent,O'Neill,and Cane [1983]; and others have explored low frequency solutions to this system that sum meridional modes. The solutions are constructed from the sum of the equatorial Kelvin mode and a sum of Rossby modes that have their turning points equatorward of the turning latitude at the forcing frequency. Cane and Sarachik solved (1.6-1.9) in a basin bounded by X=0 and X=Xe but unbounded meridionally. The boundaries play an important part in the solution in that they require return flow into the interior.

This paper will use these earlier results to examine the response of the equatorial ocean to a periodic zonal wind stress. The stress will be idealized as a delta function to examine small scale forcing and provide a Green's function to study more general forcings. Forcing

over an area is a more realistic situation but the response is more complex. Features from the simpler delta response will be useful in analyzing the more complicated patch forcing case.

An analysis of the character of the response is an important first step in an attempt to understand how errors in the measurement of wind stress are transformed into errors in the equatorial height field. The height field is of particular interest when using a shallow water model because in most cases the model simulates the observed properties of the height field better than the observed properties of the currents.

The paper is organized as follows: In chapter 2 the zonal wind stress is idealized as a delta function in both x and y. An analysis of the response of the U, V, and H fields along with plots of the fields in a 6000km wide basin is provided. Chapter 3 uses ray theory on Rossby waves and compares the solutions to the delta results. In chapter 4 the point source solution is used as a Green's function to solve for forcing over an area rather than at just a single point. The results of the previous chapters are used to analyze the effects of wind measurement error on sea surface height in the Pacific and Indian Oceans in chapters 5 and 6 respectively. The important results are summarized in the seventh chapter and are followed by appendices containing notation and mathematical derivations.

POINT FORCING

The problem of the response of a linear baroclinic equatorial ocean to a periodic zonal wind stress was examined by Cane and Sarachik (1981). Their solution is constructed from the periodic forced solution in the absence of boundaries plus a free wave solution added on to satisfy the boundary conditions. These solutions consist of Kelvin waves and sums of long Rossby waves. The boundary conditions are:

$$U=0 \quad \text{at} \quad X=Xe \tag{2.1}$$

$$\int U\,dy=0 \quad \text{at} \quad X=0 \tag{2.2}$$

Physically (2.1) means that Kelvin waves incident on the eastern boundary are reflected as a sum of long Rossby waves. At the western boundary U=0 would imply that long Rossby waves incident on the boundary would be reflected as the Kelvin wave and a sum of short Rossby waves. Since our solution makes use of the long wave approximation short Rossby waves are not present. Cane and Sarachik (1977) have shown that the correct long wave boundary condition for

this case is given by (2.2). The short Rossby waves form a boundary layer that when integrated meridionally can carry no net mass zonally, leaving the Kelvin wave as the only means of returning meridionally integrated zonal mass flux incident on the western boundary.

We wish to examine the effect of a small scale periodic disturbance on a model basin. To accomplish this the model is forced by a zonal wind stress idealized as a delta function of the form:

$$\tau_x(X,Y) = \delta(X-X_*)\,\delta(Y-Y_*) \tag{2.3}$$

The general form of the solution may be expressed as the sum of forced and free terms:

$$\begin{bmatrix} U \\ V \\ H \end{bmatrix} = \begin{bmatrix} U \\ V \\ H \end{bmatrix}_{FORCED} + \rho \begin{bmatrix} U \\ V \\ H \end{bmatrix}_{FREE} \tag{2.4}$$

The free and forced solutions independently satisfy equation (2.1). ρ is a constant chosen to satisfy boundary condition (2.2). Since U=0 at X=Xe, equation (1.7) implies that the height is independent of y at X=Xe; hence ρ determines the amplitude of the height field at the eastern boundary.

The solution is derived in detail in appendix 2; here we simply write the complete result:

$$\begin{bmatrix} U \\ V \\ H \end{bmatrix} = e^{\phi_* - \phi_x + \phi_T} \left[\sum_{m=1}^{N} 4m(m+1) R_{mu}(Y_*) \underset{\sim}{R}_m e^{-2(m+1)(\phi_* - \phi_x)} - M(Y_*) \underset{\sim}{M} \right] \qquad (2.5)$$

$$+ \int \left[\frac{e^{\phi - \phi_x + \phi_T}}{i\omega} \left(\underset{\sim}{M} + \sum^{N} 2 \alpha_m \underset{\sim}{R}_m e^{-2(m+1)(\phi - \phi_x)} \right) \right]$$

$$\phi = i\omega X e \qquad \phi_T = i\omega t$$

$$\phi_x = i\omega X \qquad \int = i\omega e^{\phi_* - \phi} \left[\frac{\sum^{N} 2 \alpha_m R_{mu}(Y_*) e^{-2(m+1)\phi_*} + M(Y_*)}{1 - \sum^{N} \frac{\alpha_m^2}{m(m+1)} e^{-2(m+1)\phi}} \right] \qquad \underset{\sim}{R}_m = \begin{bmatrix} R_{mu} \\ i\omega \psi_m \\ R_{mh} \end{bmatrix} \quad \underset{\sim}{M} = \begin{bmatrix} M \\ 0 \\ M \end{bmatrix}$$

$$\phi_* = i\omega X_*$$

where (2.5) is valid in the region west of the forcing ($X < X_*$). To the east of the forcing ($X > X_*$) only the free term is nonzero and we are left with (2.6).

$$\begin{bmatrix} U \\ V \\ H \end{bmatrix} = \int \left[\frac{e^{\phi - \phi_x + \phi_T}}{i\omega} \left(\underset{\sim}{M} + \sum_{m=1}^{N} 2 \alpha_m \underset{\sim}{R}_m e^{-2(m+1)(\phi - \phi_x)} \right) \right] \qquad (2.6)$$

the notatation for (2.5-2.6) is given in appendix 1 with $\underset{\sim}{R}_m$ and $\underset{\sim}{M}$ denoting the Rossby and Kelvin modes. The Rossby and Kelvin terms are defined in terms of the normalized scalar function $\psi_m(Y)$, with $H_m(Y)$ representing the mth Hermite polynomial.

$$\Psi_m(Y) = [\sqrt{\pi}\ 2^m m!\ ]^{-\frac{1}{2}} H_m(Y) e^{-\frac{Y^2}{2}} \tag{2.7}$$

The complexity of the solutions makes them difficult to analyze analytically. An asymptotic form of the eigenvalue will simplify the analysis. Morse and Feshbach (1953) showed that for large N and near the equator $\Psi_m(Y)$ may be approximated by:

$$\Psi_m = (\sqrt{2}/\pi)(2m-Y^2)^{-\frac{1}{4}} \cos[0.5Y\sqrt{2m-Y^2} - M\pi/2 + m\sin^{-1}(Y/\sqrt{2m})] \tag{2.8}$$

We may use (2.8) to see which terms in the solution are important if we consider several modes. The mth Rossby mode written in asymptotic form for U and H respectively are:

$$R_{mv} = \frac{\sqrt{2}(2m-Y^2)^{-\frac{1}{4}}}{4\pi m(m+1)} [(\frac{-(2m+1)}{2(2m-Y^2)} - 1)Y\cos[\ ] + (2m+1)[D]\sin[\ ]] \tag{2.9}$$

$$R_{mH} = \frac{2(2m-Y^2)}{4\pi m(m+1)} [(2m+1-0.5(2m-Y^2)^{-\frac{1}{4}})Y\cos[\ ] + [D]\sin[\ ]] \tag{2.10}$$

$$[D] = 0.5(2m-Y^2) - 0.5Y\ (2m-Y^2)^{-\frac{1}{2}} + m(2m-Y^2)^{-\frac{1}{2}}$$

α_m may also be expressed in asymptotic form using Stirling's formula.

$$\alpha_{2m+1} = [(2m+1)^{\frac{1}{2}}!][2^m m!]^{-1} \qquad \alpha_{2m} = 0$$

$$\alpha_{2m+1} = \frac{[\sqrt{2}\pi(2m+1)^{2m+\frac{3}{2}} e^{-(2m+1)+\frac{\Theta}{24m+12}}]^{\frac{1}{2}}}{} \tag{2.11}$$

$$\alpha_{2m+1} \approx 2\pi^{\frac{1}{4}} m^{\frac{1}{4}} e^{-1}$$

The formulae in (2.8-2.11) are valid for $Y^2 < 2m$. Since we are only interested in the response in the equatorial regions these are satisfactory. Order of magnitude statements using these asymptotic forms will highlight the structure of (2.5-2.6).

The behavior of free waves was examined in Cane and Moore 1981. The higher m terms in the sums were shown to be small (they decrease at least as fast as $m^{-\frac{3}{4}}$). This allowed the expressions to be accurately approximated as infinite sums which can written in closed form as:

$$\begin{bmatrix} U \\ V \\ H \end{bmatrix}_{free} = e^{\Phi_T}(-i\omega^{-1}\pi^{-\frac{1}{4}})\cos^{\frac{1}{2}}[-2i(\phi_x-\phi)]e^{\frac{\lambda^2}{2}\tan[2(\phi_x-\phi)]} \begin{bmatrix} -i\tan[-2i(\phi_x-\phi)] \\ i\omega Y\sec^2[-2i(\phi_x-\phi)] \\ 0 \end{bmatrix} \tag{2.12}$$

ρ has a form which allows us to use the Cane and Moore sum to rewrite it in the simplier form:

$$\rho = -\omega e^{-\Phi}\frac{\cos^{\frac{1}{2}}[-2\omega X_*]\tan[-2\omega X]\, e^{\frac{\lambda^2}{2\lambda}\tan(-2\omega X_*)}}{\pi^{\frac{1}{4}}\left[1 - \sum_{m=0} \frac{\alpha_m^2}{m(m+1)} \rho^{-2(m+1)\Phi}\right]} \tag{2.13}$$

From (2.12-2.13) we observe that the free wave times ρ is an order one term except (i) near resonance points at $\omega(X-Xe)= \pi k/4$ +-k=1,3,5... where the zonal velocity is unbounded or (ii) if the problem is forced near $\omega X_* = \pi k/4$ where ρ is large and the entire free wave term is important. All three fields oscillate rapidly away from the equator.

Along the equator we find:

$$\Psi_m = 0 \qquad R_{mU} \approx O(m^{-\frac{3}{4}}) \qquad R_{mH} \approx O(m^{-\frac{7}{4}}) \qquad M = [0.5\pi^{-\frac{1}{2}}]^{\frac{1}{2}} \tag{2.14}$$

These allow the order of forced terms to be written as:

$$U_{FORCED} = \Sigma O(m^{\frac{1}{2}}) + O(1)$$

$$V_{FORCED} = 0 \tag{2.15}$$

$$H_{FORCED} = \Sigma O(m^{-\frac{1}{2}}) + O(1)$$

The terms in the zonal velocity sums grow like m while the height terms decay like $m^{-\frac{1}{2}}$, and the meridional velocity is identically zero. The higher modes dominate the forced zonal velocity term. The U solution then should be very sensitive to the value we chose for N, the number of Rossby modes.

Away from the equator we find:

$$\Psi_m \approx O(m^{-\frac{1}{4}}) \qquad R_{mU} \approx O(m^{-\frac{5}{4}}) \qquad R_{mH} \approx O(m^{-\frac{5}{4}}) \tag{2.16}$$

The height field then will experience its largest response off the equator, while the principal response of the zonal velocity is confined near the equator. Physically this tells us that we would expect the group velocity of a packet of Rossby waves to speed up near the equator and slow down near the turning latitudes. The forced meridional velocity has terms which grow like m but are multipied by ω which is assumed to be small.

The general character of the delta forced solutions may be seen in figures [2.1-2.20]. All figures are drawn from a 51 by 41 X by Y grid. For a representative case will take C=1.0 (typical Kelvin wave speeds for the first five baroclinic modes in the Indian Ocean are 2.8, 1.7, 1.1, 0.8, and 0.6 (m/s) respectively); N=50 as a large number of Rossby modes, and we will examine a semi-annual forcing (our period T=186.2). Our model basin size is 6000km east-west and 2200km north and south of the equator or roughly the size of the Indian Ocean. In nondimensional units the basin is 28.4 by 10.4. We examine the response of the basin to delta forcings at various positions. The nondimensional relative amplitudes of the responses reveal the degree to which regions in the basin are influenced by the forcings. Dimensional values depend on scaling assumptions, such as the depth of the fluid over which the wind stress acts. It is not necessary to use the dimensional values here because the nondimensional values are adequate in our analysis.

Figures [2.1-2.3] illustrate the amplitude of the free U, V, and H fields. The general response of the three fields is contained within a sinusoidal envelope that is T/4 periodic. The outer edge of this

envelope represents the paths of the highest mode Rossby waves.

The principal response of the height field is within the envelope. The higher modes are less important and the response at the edge of the envelope is smaller than in the interior of the envelope. We see that equatorward of the turning latitudes the height field is a constant at the eastern boundary.

The zonal velocity as shown by equation (2.12) is just -itan(2ω [X-Xe]) times the height field. At (X-Xe)= - $\pi/4\omega$ and - $\pi 3/4\omega$ ($\approx$4000 and 50km) on the equator we see the singularity in the U field. At these points all Rossby modes are present and in phase. We call this region of intense response the focus. We also observe that in regions where the response of the free height field is important, the amplitude of the free zonal velocity is small.

The free meridional velocity is dominated by the higher Rossby modes. It is zero along the equator because Ψ has a zero on the equator and the Kelvin wave term is by definition zero for the meridional velocity.

Figure [2.4] is a plot of the amplitude that ρ would have if the problem were forced at various points in the basin. Since the denominator of (2.13) appoaches 1 like $m^{-\frac{3}{2}}$; the structure of this plot looks like a constant (ω^2) times a displaced free zonal velocity field. The frequency parameter ωX_* here replaces $\omega(X-Xe)$. All our solutions are a superposition of free and forced terms. If the problem is forced near $X_* = \pi/4\omega$ or $\pi 3/4\omega$ (2000 or 5950km) on the equator, ρ will be large and the free wave will dominate the solution. To

examine the structure of the forced solution alone we need to force in regions where ρ is small.

We will examine the forced solution for $(X_*,Y_*)=(5000,0)$. Here ρ is small and the free wave terms are small in comparison with the forced terms. Figures [2.5-2.7] show the amplitude of the U, V, and H fields that result from forcing at this point. The general response of these fields are sinusodial envelopes that originate at the forcing points. These envelopes are a waveguide for the Rossby waves. The sum of forced Rossby modes dominates the solutions. While the Kelvin wave is present it is small compared to the sum of Rossby modes. The zonal velocity response is large near the equator. We observe a focus on the equator approximately 4000km east of the forcing point. The height field is characterized by large responses away from the equator at the peaks of the curving U and V waveguides. V exhibits a significant response along the entire waveguide with the exception of the equator along which the forced meridional velocity is zero.

The position of the forced response pattern depends on the location of the forcing point. We observe in figures [2.5,2.8,2.9] that the entire pattern moves intact with the forcing point, with the westernmost portion of the pattern dissappearing as the forcing point is moved westward. We also observe that no important response appears east of the forcing point. This indicates that relative to the forced response, the free wave is inconsequential when considering a large number of modes or for forcings away from the resonance points.

The temporal variations in the solutions are easily analyzed. For

the real V field figures [2.10-2.12] show for the various times a qualitatively similar picture. Waves are forced at (5000,0) and travel north and south west following the waveguide. They are turned back toward the equator and are intense near the focus at approximately (1000,0). At the specified times the V waveguide is static while individual waves moving in it cause a rise and fall in the value of V at a specific point. Since our interest lies in the gross response of a basin to a forcing, we will concentrate attention on amplitude plots.

Results of forcing off the equator are shown in figures [2.13-2.15]. The zonal structure of the response is the same as for the equatorial forcing but the meridional structure is altered. The forced solutions are image symetric about the equator. So if we force at a point (X_*,Y_*) and observe a response W(X,Y) we would observe a response W(X,-Y) to forcing at a point $(X_*,-Y_*)$. The fields still follow waveguides which demonstrate the dominance of the forced Rossby sums. The focus appears at the equatorial image point roughly 4000km east of the forcing point. The waveguides become contorted sinusodial patterns around a line that runs from the forcing point to the focus.

The inviscid results are sensitive to the number of Rossby modes. Figures [2.16-2.20] depict the delta forced solutions for a modest number (N=7) of modes. Since the turning latitudes are lower for the lower modes, we observe that the responses are trapped closer to the equator. If we force poleward of the turning latitudes, the response is very weak. The contours used to plot figure [2.15] are ninety times stronger than those in figure [2.20]. In general equatorward of the

turning latitudes the response is also weaker but, the familiar pattern of curving waveguides still appears. The waveguides are not as compact as in the case of the higher modes but are qualitatively similar. The height field for example still experiences a strong response near the turning latitudes of the highest modes. In the U field we see the region 4000km east of the forcing point where a large sum of Rossby modes will create a focus.

To this point we have only considered inviscid results. The singularities in the free wave and the dominance of the higher modes in the forced solutions are a result of our neglect of friction. Although our understanding of how friction works on the model is incomplete, we know it is present and should be accounted for. Adding a Rayleigh friction will keep our free U bounded and will damp the higher modes. We may accomplish this by replacing ω with:

$$\bar{\omega} = \omega - iR \qquad (2.17)$$

As we stated the inviscid results are somewhat unrealistic in allowing higher modes to dominate and retaining a singularity at the focus. Figures [2.21,2.22] have friction in them. The spindown time R is taken as $\omega/10$ and $\omega/100$ (5 and 50 years for this case). We see that friction acts to localize the response at the forcing point. When it is moderate, R= $\omega/10$, the focus isn't reached by most of the waves. When we use a small amount of damping; $\omega/100$=R; the focus is present, but is appreciably smaller than in the inviscid case.

RAY THEORY

Ray theory provides us with an alternative way of examining the problem. The theory shows asymptotically the trajectories that a packet of waves will follow. Whitham (1961) has shown that these trajectories called 'rays' satisfy the equations:

$$\frac{DY}{Dt} = \frac{\partial \sigma}{\partial l} \tag{3.1}$$

$$\frac{DX}{Dt} = \frac{\partial \sigma}{\partial k} \tag{3.2}$$

$$\frac{Dk}{Dt} = \frac{-\partial \sigma}{\partial X} \tag{3.3}$$

$$\frac{Dl}{Dt} = \frac{-\partial \sigma}{\partial Y} \tag{3.4}$$

$$\frac{D\omega}{Dt} = \frac{-\partial \sigma}{\partial t} \tag{3.5}$$

Here k is the zonal wavenumber, l is the meridional wavenumber and the frequency. The rays are important physically because they are energy paths for a packet of waves. The theory only tells use where packets of wave will travel and doesn't distingush between free and

forced waves. We will use the theory then to describe the 'action' of the packet of Rossby waves emminating from a forcing point.

We begin with the system of equations (1.1-1.3) which can be combined into a single equation for V.

$$-V_{ttt} + V_{xxt} + V_{yyt} - Y^2 V_t + V_x = 0 \tag{3.6}$$

Equation (3.6) has a degenerate solution V = 0 which is the Kelvin wave. Ray theory won't provide us with any new information on it since it is non-dispersive and we know exactly how it behaves: it carries energy from east to west along the equator. Our asymptotic analysis has shown that the Kelvin terms are small compared to a sum of Rossby modes for large N so here we consider the behavior of the dominant Rossby terms. By only considering low frequencies and assuming the variations in X are smaller than those in Y, (3.6) can be simplified to:

$$V_{yyt} - Y^2 V_t + V_x = 0 \tag{3.7}$$

we now use WKB theory and assume V has the form

$$V = A e^{i\phi(x,y,t)} \tag{3.8}$$

where the total phase ϕ is defined by $\phi_y = l$, $\phi_x = k$, and $\phi_t = -\omega$. If the amplitude A is assumed to vary slowly compared to the phase we are left to highest order with the dispersion relation:

$$\omega = \sigma(X,Y,l,k) = -k/(l^2 + Y^2) \tag{3.9}$$

We substitute the dispersion relation (3.9) into the ray equations (3.1-3.5) to obtain the set of equations;

$$\frac{DY}{Dt} = \frac{2l\omega^2}{k} \tag{3.10}$$

$$\frac{DX}{Dt} = \frac{\omega}{k} \tag{3.11}$$

$$\frac{Dk}{Dt} = 0 \tag{3.12}$$

$$\frac{Dl}{Dt} = \frac{-2l\omega^2}{k} \tag{3.13}$$

$$\frac{D\omega}{Dt} = 0 \tag{3.14}$$

The solutions are easily found to be:

$$\omega = \omega_0 \tag{3.15}$$

$$k = k_0 \tag{3.16}$$

$$X = \omega t/k + X_0 \tag{3.17}$$

$$Y = [-k/\omega] \sin[2\omega^2 t/k + \alpha_0] \tag{3.18}$$

$$1 = [-k/\omega] \cos[2\omega^2 t/k + \alpha_0] \tag{3.19}$$

Each ray path then has a characteristic w and k by (3.15) and (3.16). (3.17) shows that a disturbance may only move westward from its initial position since only negative k is allowed by the dispersion relation.

We want to examine rays from a point disturbance. That is to say given an initial position (X_0,Y_0) k, and ω we want to plot the ray paths in (X,Y) space. At t=0, given a (X_0,Y_0) we may determine the constant α_0.

$$\alpha_0 = \sin^{-1}[Y_0(-k/\omega)\ ] \tag{3.20}$$

then X and Y may be determined by:

$$X = \omega t/k + X_0 \tag{3.21}$$

$$Y = (-k/\omega) \sin[2t\omega^2/k + \sin^{-1}(Y_0(-k/\omega)\ )] \tag{3.22}$$

t appears only as a parameter and can be eliminated. Equatorial wave theory suggests the notation:

$$-k/\omega = 2m + 1 \tag{3.23}$$

so:

$$Y = \pm [2m+1]^{\frac{1}{2}} \sin[2\omega(X-X_0) + \sin^{-1}(Y_0/(2m+1)^{-\frac{1}{2}})] \qquad (3.24)$$

(3.24) may expressed in the simple form:

$$Y = \pm [2m+1-Y_0]^{\frac{1}{2}} \sin[2\omega(X-X_0)] + Y_0\cos[2\omega(X-X_0)] \qquad (3.25)$$

The area over which a ray acts is called a 'ray tube'. Ray tubes are in effect energy channels. Hence regions in which few rays penetrate called 'shadow zones' will be regions of a weak relative response to a forcing. Regions in which rays are packed together called 'caustics' then are expected to experience a strong response and if several adjacent rays come together and cross at a focus we could expect the wave amplitude to become immense.

The foci may be found from (3.25) by finding points on the ray paths that are multivalued in M. Those are points on which:

$$\sin(2\omega(X-X_0)) = 0 \qquad (3.26)$$

$$2\omega(X-X_0) = N\pi$$

The focus then is located at:

$$(X - X_0) = \Delta X = NT/4 \tag{3.27}$$

or in dimensional units at:

$$\Delta X = CTN/4 \tag{3.28}$$

in terms of Y the focus is at:

$$Y = Y_0(-1)^N \tag{3.29}$$

Figures [3.1,3.4] are plots of ray paths that emanate from the initial points (5000,0) and (5000,1000). The plots use the same scaling as the previous figures but the number of modes used is 30. We see that the rays are packed along the outer edge of the sine packet and congregate as they near the foci. We expect then to have our largest response at the focus and in the areas that are shaded in the figures. Ray theory tells us that important responses to a point forcing occur in two regions, one adjacent to the forcing point in which energy streams north-west and south-west of the source and a second region adjacent to the equatorial image point CT/4 km west of

the source in which energy is concentrated at a focus point. Ray theory also implies that energy will be absent in the shadow zone along the line connecting the focus and the source. These ray paths do not account for the behavior of the Kelvin wave term which will be important if the forcing is near the equator.

Ray theory may also be used to find an energy density in (X,Y) space for a packet of Rossby waves. Along a given ray the magnitude of the group velocity times the energy density is a constant. So the energy density may be expressed as:

$$\langle E \rangle = \varepsilon(k_0) / \ |\vec{C}_g| \tag{3.30}$$

Where $\vec{C}_g$ is the group velocity and $\varepsilon(k_0)$ is a constant for that ray. $\vec{C}_g$ may be found from the dispersion relation (3.9).

$$\vec{C}_g = \frac{\partial \sigma}{\partial k}\hat{i} + \frac{\partial \sigma}{\partial l}\hat{j} = -(l^2+Y^2)^{-1}\hat{i} + 2kl(l^2+Y^2)^{-2}\hat{j} \tag{3.31}$$

then:

$$\langle E \rangle = \varepsilon(k_0) \ [(l^2+Y^2)^{-2} + 4k^2l^2(l^2+Y^2)^{-4}]^{-\frac{1}{2}} \tag{3.32}$$

which may be simplified with (3.18-3.19) and (3.23) to become:

$$\langle E \rangle = \varepsilon_n (2m+1)\,[1+4\omega^2(2m+1-Y^2)]^{-\frac{1}{2}} \tag{3.33}$$

Instead of using the mode number m , we could find expression for the energy density in terms of the initial position, space coordinates, frequency, and the initial energy. From (3.25) without quantization we find:

$$Y = \pm ((-k/\omega)-Y_0)^{\frac{1}{2}} \sin 2\omega\Delta X + Y_0 \cos 2\omega\Delta X \qquad (3.34)$$

and see immediately that

$$-k/\omega = [Y-Y_0\cos 2\omega\Delta X]^2 [\sin 2\omega\Delta X]^{-2} + Y_0^2 \qquad (3.35)$$

The energy density defined only along a ray path then is given as:

$$\langle E \rangle = \frac{\left(\left[\frac{Y-Y_0\cos 2\omega\Delta X}{\sin 2\omega\Delta X}\right]^2 + Y_0^2\right)\varepsilon(k_0)}{\left[1+4\omega^2\left(\left[\frac{Y-Y_0\cos 2\omega\Delta X}{\sin 2\omega\Delta X}\right]^2 + Y_0^2 - Y^2\right)\right]^{\frac{1}{2}}} \qquad (3.36)$$

If we had an explicit expression for $\varepsilon(k_0)$ we could use (3.36) to draw a continuous energy density plot. We have a discrete approximation from modal theory for $\varepsilon(k_0)$. Figures [3.3,3.6] are drawn using the discrete modes. The figures show the energy density that would result from equally spaced rays. At the turning latitudes we see a lot of energy. This is caused by the fact that the waves take a long time to turn. Near the foci the actual amount of energy per ray is small because the waves move through these regions quickly. The total amount of energy here is expected to be large though because the ray tubes come together and the area over which the energy acts becomes

vanishingly small. In short the two factors that govern energy density are the area over which the ray tube acts and the intensity of the energy along the tube. Both factors are significant for our problem.

Cane and Sarachik (1981) showed that ray theory is inadequate if the Kelvin wave or reflected Rossby waves are important. The actual total energy $[(U^2 + V^2 + H^2)/2]$ from modal theory should resemble the ray theory results in our case since both the Kelvin and free terms are small compared to the sum of forced Rossby modes. Figures [3.2, 3.5] are the total energy plots. The agreement between the results is clear. We see in both plots that the largest concentration of energy is near the foci and turning latitudes. We also observe shadow regions in the same location in both sets of figures. These plots illustrate how effective ray theory can be in determining the essence of the solutions with a simple, analytic method.

PATCH FORCING

We have analyzed the response of a model basin to a point source distrubance. With the exception of cataclysmic events such as earthquakes or nuclear explosions, the forcing of long period waves in the real ocean occurs over a region rather than at a single point. The point forced solutions (2.5-2.6) may be used as a Green's function and integrated over a forcing region to obtain the response of the basin to a regional forcing. We will examined the response of the basin to a square patch of a unit zonal periodic wind stress.

That is :

$$U,V,H\ [X,Y] = \iint_{FORCING} \tau_x(X_*,Y_*)\, G_{U,V,H}\ (X,Y,X_*,Y_*)\, dX\ dY \qquad (4.1)$$

We take :

$$\tau_x = \begin{cases} 1 & |X-X| < \Delta X\ ;\ |Y-Y| < \Delta Y \\ 0 & \text{elsewhere} \end{cases} \qquad (4.2)$$

The complete derivation is given Appendix 3. The results for the region $X < (X' - \Delta X)$ are:

$$\begin{bmatrix} U \\ V \\ H \end{bmatrix} = \begin{bmatrix} 2\omega^{-1} e^{\phi'-\phi_X+\phi_T} \left[\sum_{m=1} I_R \underset{\sim}{R}_m \sin((2m+1)\phi_\Delta) e^{-2(m+1)(\phi'-\phi_X)} \right] - \\ \left[2\omega^{-1} e^{\phi'-\phi_X+\phi_T} \left[\pi^{\frac{1}{4}} (\mathrm{erf}(Yn)-\mathrm{erf}(Ys)) \underset{\sim}{M} \sin\phi_\Delta \right] + \right. \\ \left. \rho \left[-i\omega^{-1} e^{\phi-\phi_X+\phi_T} \left(\underset{\sim}{M} + \Sigma\, 2\alpha_m \underset{\sim}{R}_m e^{-2(m+1)(\phi-\phi_X)} \right) \right] \right. \end{bmatrix} \quad (4.3)$$

$$\phi' = i\omega X' \qquad Yn = Y' + \Delta Y \qquad X' = X$$

$$\phi_\Delta = \omega \Delta X \qquad Ys = Y' - \Delta Y \qquad Y' = Y$$

$$I_R = -(\Psi(Yn) - \Psi(Ys) + (2m+1)^{-1} \int_{-Y_S}^{Y_N} \Psi Y$$

$$\rho = 2ie^{\phi'-\phi} \frac{[\pi^{\frac{1}{4}} [\mathrm{erf}(Yn)-\mathrm{erf}(Ys)] \sin\phi_\Delta + \Sigma \frac{2\alpha_m}{4m(m+1)} I_R \sin(\phi_\Delta(2m+1)) e^{-2(m+1)\phi'}}{1 - \sum_{m=1} \frac{\alpha_m^2}{m(m+1)} e^{-2(m+1)\phi}}$$

for the region $X > (X' + \Delta X)$

$$\begin{bmatrix} U \\ V \\ H \end{bmatrix} = \rho \left[-i\omega^{-1} e^{\phi-\phi_X+\phi_T} \left(\underset{\sim}{M} + \sum_{m=1} 2\alpha_m \underset{\sim}{R}_m e^{-2(m+1)(\phi-\phi_X)} \right) \right] \quad (4.4)$$

and for the region $(X' - \Delta X) < X < (X' + \Delta X)$

$$\begin{bmatrix} U \\ V \\ H \end{bmatrix} = \begin{bmatrix} iw^{-1}\Sigma\, I_R \underset{\sim}{Re}^{-(\phi'-\phi_x+\lambda\phi_D)+\phi_T} + J \end{bmatrix} + J_2 + \quad (4.5)$$
$$\rho^{*} \left[-i\omega^{-1}e^{\phi-\phi_x+\phi_T}\left(\underset{\sim}{M} + \sum_{m=1} 2\alpha_m \underset{\sim}{R}_m e^{-\lambda(m+1)(\phi-\phi_x)}\right)\right]$$

$$J = \begin{bmatrix} i\omega^{-1}e^{\phi_T}\,\Sigma\, -I_R R_{mU} \\ e^{\phi_T}\,\Sigma\, I \int R_{mH}\,dY \\ i\omega^{-1}e\;\;\Sigma\, -I_R R_{mH} \end{bmatrix}$$

$$J_2 = \begin{bmatrix} -\pi^{\frac{1}{2}}[\mathrm{erf}(Yn)-\mathrm{erf}(Ys)]M[1-e^{\phi'-\phi_x+\lambda\phi_D}]i\omega^{-1}e^{\phi_T} \\ -\pi^{\frac{1}{2}}\mathrm{erf}(Y)\,[\mathrm{erf}(Yn)-\mathrm{erf}(Ys)]e^{\phi_T} \\ -\pi^{\frac{1}{2}}[\mathrm{erf}(Yn)-\mathrm{erf}(Ys)]M[1-e^{\phi'-\phi_x+\lambda\phi_D}]i\omega^{-1}e^{\phi_T} \end{bmatrix}$$

The solution is defined in three distinct regions; for $X < X-\Delta X$ the entire forced portion is felt; for $X-\Delta X < X < X+\Delta X$ only a portion of the forced term is experienced ; and west of the forcing region only the free term remains.

An asymptotic analysis will prove useful in illuminating the structure of the 'box' solution. The only new terms that appear in the solutions are the integral of the R_{mU} and the R_{mH} terms. For large N using equation (2.8) we find that:

$$(\Psi(Yn)-\Psi(Ys)+(2m+1)^{-1}\int_{Ys}^{Yn} Y\Psi_m) \approx O(m^{-\frac{1}{4}}) \quad (4.6)$$

The order of the forced terms that are forced and observed on the equator may be estimated using (4.6).

$$\begin{aligned} U &= \Sigma\, O(1/\omega m) + O(1/\omega) \\ V &= 0 \\ H &= \Sigma\, O(1/\omega m^2) + O(1/\omega) \end{aligned} \tag{4.7}$$

We note that the higher modes are damped like (m^{-1}) in the zonal velocity field and like (m^{-2}) in the height field. The response then is not as sensitive to the higher modes as the delta case is. By forcing over a patch rather than at a single point phase interference has destroyed the high frequency response within the forcing region. We are still left with an important forced reponse though because of the (ω^{-1}) factor which by assumption must be large.

To obtain the box solutions we performed an X_* integral, which introduced a $[\omega(2m+1)]^{-1}$ factor to the Rossby terms. Our quantization condition (3.23) expresses (2m+1) as a function of the meridional wavenumber l ; and the distance from the equator Y. At the turning latitudes we know that l=0. Our box solution then has divided the delta forced Rossby terms by Y^2. This is equivalent to saying the importance of the higher modes is reduced. It should be noted that the strongest response occurs very near the equator in the patch case.

The sum of forced Rossby modes no longer completely dominates the solution. The Kelvin wave term is the same order as the Rossby term if, as in (4.7), we assume that we force over a large box(O(4°x4°)) and ϕ_Δ is an order one term. We would expect to see the Kelvin response on the equator in both the U and H fields. If the forcing area is small(O(25x25km)) the Kelvin wave term is order one and not $O(\omega^{-1})$. A small box in this case then should strongly resemble the delta case and be dominated by the Rossby terms. The box forcing solutions normalized by $\Delta X \Delta Y$ approach the delta forced solutions (2.3-2.4) in the limit as ΔX and ΔY approach zero.

The free wave in the box case is the same as in the delta case. It is multiplied by $\bar{\rho}$ instead of ρ . ρ is simply the Kelvin wave and its Rossby reflection at the eastern boundary times a periodic function of the zonal forcing position and the zonal basin length. When we integrate ρ over X_* and Y_* to find $\bar{\rho}$ we again see that the higher Rossby modes are attenuated. We expect then that $\bar{\rho}$ will be large only near the equator and that the focusing effect is tempered by the attenuation of the higher modes.

The relative importence of the free wave in the box case should be much greater than in the delta case because the forced box solution is much smaller. $\bar{\rho}$ will determine how much the free wave contributes to the total response.

Figures [4.1-4.12] illustrate the inviscid the box solutions. The amplitude of all fields are displayed. The box solution's sensitivity to ΔX and ΔY is examined along with the number of Rossby modes and the position of the forcing. The solutions are normalized by $\Delta X \Delta Y$.

Figures [4.1-4.3] are the $\hat{\rho}$ terms for three different box sizes. The first is a very small box 20km by 20km (0.09 by 0.09 in non-dimensional units). It is small enough to resemble ρ . We observe a weak focus and note the only real difference is that $\hat{\rho}$ is large on the eguator in regions where ρ is small. As an intermediate case figure [4.2] shows a 2° by 2° box. Here the focus is weak as are the higher Rossby modes that allowed ρ to be large away from the equator. The last figure is for a 4° by 4° box (1.05 by 1.05 in nondimensional units. No evidence of a focus is observed. $\hat{\rho}$ is large only within 5° of the equator. Outside of the focus regions $\hat{\rho}$ is larger than near ρ the equator. As the box size grows , parts of the box extend into regions where only high Rossby modes are present. The high modes are less energetic, so only the parts of the box in which the lower modes are present contribute significantly to $\hat{\rho}$. We see then that $\hat{\rho}$ will be large only near the equator no matter how large of an area we force over because forcing away from the equator can only produce weak influences.

The U, V, and H fields for a 4° by 4° box centered at (5000,0) are shown in figures [4.4-4.6]. The effect of the attenuation of the higher modes is seen. The zonal velocity response is large west of the forcing across the equator. The maxima of the zonal response are still near the forcing point and at the focus. The 2° by 2° box in figure [4.7] has a more pronounced focus and extends farther from the equator. The response of the height field is also large near the forcing. The main response of the height field is still off the equator. The response of the meridional velocity is similar to the delta case but it is weaker by a factor of 10.

The response with N=7 modes is shown in figures [4.8-4.10]. The general response is similar to the N=50 case. Unlike the delta case our solution is less sensitive to the number of modes because the higher modes are attenuated.

Results of forcings in the western half of the basin are shown in figures [4.11-4.12]. We see that a free zonal velocity response appears to the east of the forcing. This indicates that the Kelvin wave contributes to the total response near the equator. The contribution of the Kelvin wave is difficult to see for forcings in the eastern part of the basin because it appears as part of a superposition of free and forced responses in which the forced response is very complicated near the equator.

We may add friction to the box solution with equation (2.17). A given amount of friction will not alter results as impressively as it did in the delta case because the highest modes are already damped. It will still prove useful to examine what effect some arbitary spindown time will have on the model solutions.

Figures [4.13-4.14] show the responses with friction, corresponding to a spindown time of 25 years. The zonal velocity response is only slightly affected indicating, that the higher modes don't contribute much to the solution.

AN ANALYSIS OF THE EFFECT OF WIND MEASUREMENT ERRORS ON EXPECTED CIRCULATIONS IN THE EQUATORIAL PACIFIC

To this point we have examined the effects of an isolated regions of periodic zonal wind stress on a model basin. We will use the results of the previous chapters to determine the response at a single point to long period waves forced throughout a basin. This analysis will allow us to gauge the importance of errors in the measurement of surface winds in the modeling of sea surface height in the equatorial Pacific.

The forcing over the real ocean is basin wide. The response of the ocean at a single station then is governed by a field of wind stresses. The model we developed is linear. Linearity allows us to represent the height or current at a single location as that which would result from a sum of individual forcings. The delta case assumes an impulse forcing is representitive of the forcing that occurs within a region. The patch forcing assumes that the stress is uniform over a region. We will divide a basin into a discrete number of regions and use either the delta or patch assumption to examine the total effect of basin wide forcing at a station.

The patch and delta solutions may be used to calculate a response

function for an observation point (X,Y). The response function tells us how much influence waves forced in the basin will have on the observation point. We find the response function by first dividing the basin into a grid of forcing points. For the delta case each forcing point represents the forcing over the area between adjacent points. In the patch forcing case each forcing point is the center of a rectangular region of uniform stress that extends halfway to the adjacent grid points. We fix X and Y and solve equations (4.3-4.5) and (2.5-2.6) at each grid point to find the response function $W(\omega,X,Y,M,\Delta X,\Delta Y,X',Y')$ or $W(\omega,X,Y,M,X_*,Y_*)$. The response function is defined for a single forcing frequency and a single baroclinic mode M.

To solve the equations we could have taken our transform in space instead of time, but for the problem under consideration a frequency analysis of wind errors is a more straightforward and insightful approach. The time dependence of the problem is naturally periodic in the sense that the winds that contain the measurement errors are seasonally cyclic. We would not expect the wind errors to be as periodic spatially; hence our analysis is done in the frequency domain.

In determining the response function we assumed a unit forcing over a region. It is necessary then to weight the response function by the observed forcing at each frequency to determine the sea surface height. By superposition the total sea surface error at a station will be a product of the response function and the error in the zonal stress summed over all forcing frequencies, baroclinic modes, and

forcing points. The total error, $\bar{\eta}$,at a station is written as:

$$\bar{\eta}(X,Y,t) = \sum_{\substack{\text{FORCING} \\ \text{GRID}}} \sum_{m=1}^{M} \sum_{\omega=1}^{\infty} \eta_m W(\omega,X,Y,X_*,Y_*,M)\,\tau\,(\omega,X_*,Y_*)\,e^{i\omega\bar{\tau}} \qquad (5.1)$$

η_m is the sea level scale that translates a height into sea level.

We will model the Pacific Ocean as a rectangular basin with straight north- south aligned coastlines at 120E and 70W. The basin is unbounded at the north and south from 30N to 30S. Surface wind data for the Pacific is available over a 2.5° by 2.5° grid. We will adopt this size to be that of our forcing grid. In the patch case this yields 68 by 24 2.5° boxes of uniform stress.

The scaling we use is based on observations of Eriksen et al 1983 using CTD casts to determine reasonable stratification profiles in the Pacific at 179W near the Equator. We scale distance by L and time by T . The wind stress is assummed to act as a body force over the depth of the mixed layer. Below the mixed layer no stress is felt. With these assumptions the sea level scale η_m is defined, following Cane (1983) by:

$$\eta_m = [\tau/(\rho_w\, gD)]\; A_m^2(0)\; L_m \qquad (5.2)$$

$A_m(0)$ is the surface amplitude of the horizontal structure function which is constant in the mixed layer, D is the depth of the ocean and ρ_w is the density of the water.

The stress at the surface is parameterized with

$$\tau_x = \rho_a C_D U_x |\underset{\sim}{U}| \tag{5.3}$$

C_D is the drag coeffeicent taken to be 1.8X10-3, ρ_a is the air density, U_x is the zonal component of the surface wind, and $|\underset{\sim}{U}|$ is the magnitude of the surface wind. With these assumptions and a zonal wind stress of one dyne we have the scaling parameters that appear in Table 5-1 for the first four baroclinic modes. Table 5-1 shows that away from any focus points the first and second baroclinic modes will dominate the sea surface height over most of the basin.

TABLE 5-1

MODE	C (m/s)	L (km)	T (days)	$A_m(0)$	η_m
1	2.91	361	1.43	4.22	1.436
2	1.78	282	1.83	4.02	1.026
3	1.13	225	2.30	2.05	0.212
4	0.83	190	2.66	1.61	0.110

We will examine the sea surface errors at 10 islands located near the equator in the Pacific. The names and location of these stations

are listed in Table 5-2 and illustrated in figure [5.1]. These islands have tidal gauges which recorded the sea surface height during the El Nino event of January 1982 - June 1983.

TABLE 5-2

STATION	LATITUDE	LONGITUDE
GALAPAGOS	1S	90W
CHRISTMAS	2N	157W
FANNING	4N	159W
JARVIS	.5S	161W
CANTON	3S	172W
KWAJALEIN	8.5N	168E
NAURU	1S	167E
TRUK	7N	151E
RABAUL	4S	152E
MALAKAL	7N	134E

For each island we must develop a set of response functions (one for each forcing frequency). We will drive the model with a time series of 18 monthly mean stress errors at each forcing point. The response functions are valid for a single frequency so the time series of stress errors must be transformed into the frequency domain to find the magnitude of the forcing at that frequency. The time series is

resolved in a dc(ω=0), 9 positive, and 9 negative forcing frequencies with the Fourier transform. Since we are transforming real data, the negative frequency stresses are simply the complex conjugates of the positive frequencies.

$$\tau_x(X_*,Y_*,t) \longrightarrow \hat{\tau}_x \quad (X_*,Y_*,\omega)$$

$$\omega=2\pi/T \qquad T=\infty,+-18/n \qquad n=1,..9$$

$$\hat{\tau}_x(-\omega) = \hat{\tau}_x^*(\omega) \tag{5.4}$$

T = Forcing Periods = ∞,18,9,6,18/4,18/5,3,18/7,18/8,2 Months

The response function also possesses this property, that is $W(\omega) = W^*(-\omega)$ Since the product of complex conjugates is the complex conjugate of the product, we need only consider the positive and dc forcing frequencies. We account for the negative frequencies when we sum over all frequencies by introducing a factor of 2 in the positive frequencies. By symmetry the imaginary response sums to zero and we are left with a real time series of sea surface errors.

Figures [5.2-5.16] show the amplitude of the response functions at Fanning for the first baroclinic mode for both the delta and patch forcing cases. We use this station to illustrate the properties of typical response functions. We assume a spindown time of 5 years in all the response functions. The number of Rossby modes is 20. The number of modes is not a critical parameter except very close to the observation points for long forcing periods. The Rayleigh friction assumption we used does not damp the solutions at the observation point. 20 modes appear to be a value for N that keeps the importance

of the response function near the obervation point reasonable. In any event the number of modes does not significantly effect our analysis.

The delta and patch response functions are similar with the exception of the dc forcing. The dc response is a local phenomenom in the patch case. It is felt over a much larger region in the delta case. In the patch case we see that the only important forcing occurs about a line that runs north and south of the observation point. Unless the wind errors are dramatically incoherent meridionally, significant north south phase cancellation keeps the importance of the response about this line small. The delta case contains this feature along with a significant response to the east of Fanning. At the other frequencies the delta influence is felt further north and south of the observation point because as we discussed in the previous chapter the patch case attenuates the higher modes that are important off the equator.

We observe at all forcing frequencies Fanning is significantly affected by forcing immediately adjacent to the island and from Rossby waves forced within 10 of the equator to the east of the island. For forcing periods shorter than 18/4 months we see a maximum in the response function at the equatorial image point to and CT/4 east of Fanning. This maximum, called the inverse focus, corresponds to the place where Rossby waves that focus at Fanning originated. For forcing periods shorter than 18/8 months we see a second inverse focus at the same latitude CT/2 eastward of Fanning. This maximum corresponds to the region in which Rossby waves that have their second focus at Fanning originated. The second inverse focus is weaker than the first because of the inclusion of friction.

To the west of Fanning near the equator, Kelvin waves and Rossby waves that are reflected off the western boundary at several frequencies influence the height field at the island. The response functions for the other baroclinic modes reveal features similar to those of those of the first baroclinic mode. To sum up the response function shows that the regions in the basin that strongly influence the station are:

1. a strong local response at the observation point
2. a moderate broad response to the east of the island within 10° of the equator
3. a moderate response west of the island along the equator
4. intense responses from inverse focus points east of the island

The importance of each of these contributions at each station depends on the location of the station and the forcing frequency. Figures [5.17-5.22] show response functions for some other stations. For stations in the east away from the equator only local effects are felt. For stations in the east near the equator, such as at the Galapagos, the Kelvin wave influence is large. Stations off the equator in the central and western Pacific are influenced primarily by Rossby waves. Kwajalein, Truk, and Rabaul response functions show the strong influence of the Rossby waves. In the center of the basin near the equator at Jarvis we see that all four of the effects contribute to the response.

The sea surface errors may now be determined if we have a representation for the stress errors over the basin. We will take a difference field of two frequently utilized surface wind analyses to represent the wind error over the basin. These are translated into stress errors with the parameterization (5.3). This parameterization of the stress as the zonal velocity squared will likely lead to large stress errors in regions of strong zonal wind. The wind fields we used were the FNOC (Fleet Naval Oceanqraphic Center) analysis on a 2.5° x2.5° grid (120E-70W and 30N-30S) and the NMC (National Meteorlogical Center) surface wind over the same region on a 5°x5° grid. These analyses are monthly mean winds for 18 months from January 1982 - June 1983. The NMC data was linearly interpolated down to a 2.5°x2.5° grid to conform to the FNOC analysis.

The monthly NMC surface zonal stress fields (in dynes) are shown in figures [5.23-5.31]. The negative sign indicates stress imparted on the ocean by an easterly wind. During the first six months of 1982 the Pacific was forced by a typical wind stress pattern. Strong easterlies between 5N-25N across the basin exert a strong negative zonal stress during the period. Near 15N 170W we see stress over 2 dynes in March. Near the equator the stresses are generally weak. South of the equator the easternly stress pattern is broken from the western boundary to approximately 170E. At the western boundary moderate westerly stress oscillates from approximately 10S to 10N during a typical yearly cycle. From July 1982 to April 1983 anomalous westerly winds are seen to extend far into the basin. These anomalous westerlies drove Kelvin waves across the basin that caused dramatic 30-40cm rises in sea

surface height in the eastern Pacific during the El Nino event. The extent of the westerly stress was enormous. In September 1982 westerly mean monthly wind stress ranged from the western boundary to 120W. By April 1983 the forcing over the basin reverted back to a more normal condition.

The difference field of the NMC and FNOC zonal stresses is a representation of the wind measurement error over the basin. The difference field is not a true error field. Small differences could occur in data poor regions where both fields are erroneous. The entire measurement error could be contained in one data set, but at present it is impossible to say which data set is better. The response then of the basin is uncertain to the order of this difference field. These differences are likely to be large in regions of high wind gradients, large wind variability where the wind is inherently difficult to measure, or where there is little data. The degree to which these are well correlated spatailly or temporally will determine the magnitude of the sea surface errors.

The amplitude of the Fourier transform of the stress error fields are shown in figures[5.32-5.36]. The largest errors appear from 10N to 20N across the basin in the dc frequency (the dc component is just the mean of the error time series). Some of the errors are over 1/2 dyne in this region. The errors for the higher frequencies are generally smaller than the errors for the lower forcing frequencies. At all frequencies we observe that the largest errors occur in the strong easterly wind belts at 15N and 15S across the basin. The largest errors on the equator are near 130W for the six month period forcing.

These transform plots are multipied point by point with the response function and summed over all frequencies, baroclinic modes, and forcing point to find the total error.

Figures [5.37-5.46] show time series of predicted sea surface errors at each of the islands. In the sea surface error plots, the dotted line with the longer space is the error in the first baroclinic mode in the delta case. The dotted line with the shorter space is the error in the first three baroclinic modes in the delta case. The thin black line represents the patch error due to the first baroclinic mode. The thick black line is the error due to the sum of the first three baroclinic modes in the patch case. The first baroclinic mode in the patch case contains much of the information that is in the sum of the first three modes.

We have seen that amplitude of the response functions for the delta and patch forcing are similar. At individual stations however small differences in the response functions cause significant variations in the total sea surface error. Wind stress data at grid points are actually area averages so the patch case is more appropriate. Energetics on smaller scales than is resolved by the patch would obviously influence the comparison of delta and patch results at a point station. At Nauru the error plots bear faint resemblence to each other. The delta response functions are inadequate for determining actual sea surface error and we will rely only on the patch case.

The means and variances of the sea surface errors from zero at each island are listed in Table 5-3. The error in the first three modes is greater than in the first mode alone at each station. Rather than the

errors of the baroclinic modes summing out of phase to produce smaller errors, we see the opposite is true.

TABLE 5-3

STATION	MEAN ERROR		SAMPLE VARIANCE	
	1st mode	1st 3 modes	1st mode	1st 3 modes
GALAPAGOS	2.26	3.27	1.87	4.43
CHRISTMAS	3.99	6.14	5.00	10.76
FANNING	6.45	9.08	24.89	48.72
JARVIS	3.02	4.00	3.75	6.01
CANTON	4.44	7.13	10.34	27.63
KWAJALEIN	6.32	8.58	20.71	38.16
NAURU	2.92	4.99	6.63	16.71
TRUK	7.37	9.08	18.08	30.10
RABAUL	8.30	12.35	40.97	101.39
MALAKAL	9.47	11.48	31.98	62.31

The smallest sea surface errors occur over the eastern Pacific. Here the sea surface height is effected primarily by Kelvin waves. At the Galapagos the influence function for a 9 month period forcing shows that errors in the zonal stress near the equator from 130E to 70W will be important. The stress errors over the equator were generally small. The sea surface error at the Galapagos reaches a maximum of 8

cm in May of 1983. The maximum El Nino signiture in this region was over 35cm. Wind measurement errors are not important in the modeling of sea surface height in the eastern Pacific during this time.

In the central Pacific the errors are important away from the equator. At Fanning a mean error of 9.08 cm is found. Even more troublesome are the 48.72 cm variance and the variablity of this error. Nearer the equator at Christmas the errors are smaller but still significant. Within half a degree of the equator in the same longitude belt the cyclic six months error pattern seen at Christmas and Fanning is present at Jarvis but not nearly as large. Cane and Busalacchi 1984 in a hindcast of the 1982-1983 El Nino event found important discrepancies between observed and modeled sea level at Fanning and Chirstmas. The results suggest that it is likely that the problems they had modeling sea surface at Christmas and Fanning were caused by an inaccurate wind analysis to the east of the stations. It is obvious from the fact that the errors in this longitude belt decrease as we near the equator that the important source of error at Fanning and Christmas comes from Rossby waves forced to the east of the islands. One wind analysis we used resolved the winds poorly to the east of the islands and this error manifested itself as large sea surface errors off the equator near Fanning and Christmas. If the wind errors came from west of the islands they be would carried by Kelvin waves and the maximum sea surface error would appear on the equator.

Over the Western Pacific the errors are generally worse to the south of the equator and as we move away from the equator to the north. At Rabaul south of equator large mean errors of 12.35 cm are seen. The observed sea surface signal here ranged from 20 to 15 cm during the event. If we drove a model with either of these wind fields and compared the results to the observations wind measurement errors are large enough that it would be impossible to in any sense verify the model here.

In general the sea surface errors are not significant in the eastern Pacific or near the equator. North and south of the equator in the central and western Pacific the errors are important. These are regions that are primarily influenced by Rossby waves forced to the east of the stations. The winds in the regions influencing these stations are generally strong easterlies. Large sea surface errors may result in regions influenced by areas of strong zonal winds containing relatively modest errors.

AN ANALYSIS OF THE EFFECT OF WIND MEASUREMENT ERRORS ON EXPECTED CIRCULATIONS IN THE INDIAN OCEAN

We will examine the sea surface errors in the Indian Ocean. Unlike the Pacific, the Indian Ocean is generally devoid of islands that serve as an observation network of sea surface heights. We have chosen 10 points near the equator scattered across the Indian basin to serve as our observation network. These stations are identified with a letter and their position is shown in figure [6.1].

The Indian Ocean is modeled from 20N to 20S and from 96E to 45E. Our forcing grid is a 2° latitude by 3° longitude grid. We have chosen our forcing grid to conform to available wind analyses. We use the same model and assumptions we used in the Pacific with the exception of a typical stratification value. This correspondingly changes several of the scaling parameters that appear in Table 6-1. The higher baroclinic modes are insignificant. The contribution of the second baroclinic mode appears to be the most important.

TABLE 6-1

MODE	C (m/s)	L (km)	T (days)	$A_m(0)$	η_m
1	2.80	356	1.47	3.9	1.104
2	1.73	280	1.87	5.5	1.726
3	1.11	224	2.34	2.5	0.286
4	0.80	187	2.75	2.1	0.168

The wind stress errors will again be represented by a difference field of two frequently used wind fields parameterized by equation (5.3). The wind fields we used used were a European Meteorlogical Center (ECM) analysis and a wind analysis from Wiley and Hinton. These analyses provided winds over the basin for the period December 1978 to November 1979 for a 2° x 3° latitude x longitude grid. Because we are dealing with a 12 month time series we will only examine a dc,12,6,4,3,12/5,and 2 month period forcing. The wind stress over land areas (India, Africa, and Madagascar) was taken to be zero.

The ECM zonal wind stresses over the basin are shown in figures [6.2-6.13]. The dotted line shows stress imparted on the surface by easterly wind and the solid lines by westerly wind. South of the

equator the winds are easterly throughtout the year. North of the equator the wind stress pattern shows the strong seasonal monsoon circulation. In June we see zonal stress of almost 3 dynes at 10N near the entrance of the Arabian Sea. In the eastern Indian Ocean north of the equator strong cyclonic activity is present in May.

The Fourier transform of the stress errors are shown in figures[6.14-6.17]. The errors are over 0.5 dynes in the Arabian Sea at all forcing frequencies. The ECM stress is calculated from 5 day averages while the Wiley and Hinton data comes from monthly means that supress short time cyclonic activity. We see errors in the mouth of the Bay of Bengal because of this. South of the equator in the strong easterly wind belt the errors are also large. Near the equator the errors are generally small.

Table 6-2 lists the location and the mean and variance of the errors in the Indian Ocean. By locating the stations on the equator the Kelvin wave terms should be large because the Kelvin wave decays exponentially away from the equator. The first baroclinic mode in the Indian Ocean is not as important as it was in the Pacific as seen in the Table.

TABLE 6-2

STATION	LATITUDE	LONGITUDE	MEAN ERROR		SAMPLE VARIANCE	
			1st mode	1st 3 modes	1st mode	1st 3 modes
A	0	91E	2.05	3.63	2.13	6.88
T	7N	91E	3.50	6.78	4.53	13.60
H	5S	91E	3.29	9.00	5.10	21.63
X	0	72E	1.39	2.98	1.51	13.51
F	5S	72E	4.14	11.01	5.83	19.78
G	6N	70E	4.38	11.39	8.78	42.19
B	0	54E	3.38	6.79	6.66	54.47
W	6N	52E	9.78	13.26	26.65	142.52
Q	10S	49E	2.03	3.98	1.71	11.10
Z	0	49E	3.06	6.29	5.09	44.86

Figures [6.18-6.39] are response functions and sea surface error plots for stations in the Indian Ocean. The response function of the second baroclinic mode at station A shows the strong influence of the Kelvin waves. The response functions in the Indian Ocean posses the same properties that those in the Pacific did.

The errors over the Indian Ocean are huge from the equator north into the Arabian Sea. The fluctuations in sea surface height are large

in the Arabian Sea. In some places as much as a meter. At stations Z, B, and W, Rossby waves forced north and east of the stations in the regions of large errors are very important. The sea surface errors reflect the monsoon cycle from April to July at each of the stations. Our use of only zonal stress in this region also poses a problem since the seasonal monsoon circulation is not strickly zonal. Important errors are also seen north of the equator in the central Indian Ocean. Here the easternmost region of the large errors are felt locally at the north central Indian station. At the equator in the central Indian Ocean at station X the cyclonic errors are felt. Rossby waves carry large errors from the east that distrubs a virtually nonexistent sea surface error plot in June and July. The smallest errors appear in the east where the winds are lighter.

The errors are generally weaker near the equator and worse off the equator especially in the Arabian Sea. The Indian errors are larger than those seen in the Pacific. The errors are larger because the forcing over the basin is so much larger. In modeling the sea surface fluctuations in the Indian Ocean we have seen that wind errors can be serious. The wind analyses we used could be responsible for 13 cm mean errors in the Arabian Sea.

DISCUSSION

We have explored the response of the linear shallow water equations in a meridionally unbounded basin to an oscillatory zonal wind stress. Solutions are found making use of the long wave assumption for a single low frequency ω and include both a free basin wave and a directly forced term. The free and forced terms consist of the equatorial Kelvin wave and a sum of Rossby modes. The highest number of modes is a parameter we choose.

The zonal wind stress is first idealized as a delta function in X and Y, to measure the response to very small scale forcings and to obtain a Green's function for more general types of forcing. Some ray theory results demonstrate that the essense of the delta solutions may be captured using simple asymptotic methods. The insight gained in examining these solutions is useful in understanding the case of a spatially uniform stress over a rectangular region.

The point source solution is dominated by the sum of forced Rossby modes independent of forcing location. The free wave term is small enough that no important response east of the forcing is found. The important response is contained within a sinusoidal envelope whose

inner and outer edges represent the lowest and highest mode Rossby waves respectively.

The envelope originates at the forcing point and waves travel westward in two branches toward the turning latitudes. At the turning latitudes the Rossby waves are forced to turn back toward the equator to conserve vorticity. All the modes in both branches come together at the equatorial image point of the forcing point. The envelope there is a single point called the focus. The focus is a region of intense response. Past the focus the envelope again diverges in two branches. Between the lowest modes in the two branches no Rossby waves penetrate. This region experiences a weak response and is called the shadow zone.

The response of the U,V,and H fields within the envelope differ. The meridional velocity is dominated by the higher modes. The important response is found along the outer edges of the waveguide throughout the basin. The meridional velocity response is the weakest of the three fields. The zonal velocity is also dominated by the higher modes. The response near the turning latitudes is small. The height field is less dependent on the higher modes so the response is larger near the inner part of the envelope then in either of the current fields. The response of the height field is smallest near the equator and largest near the turning latitudes.

Ray theory allows us to find the location of the focus relative to the location of the forcing. If the forcing is at a point (X,Y) then the first focus appears at (X-CT/4,-Y): here (X=0) is the western boundary, C is the

Kelvin wave speed, and T is the period of the forcing. The shadow zone is shown to be centered about the line connecting the focus and forcing points. Ray theory was also useful in explaining the spatial energy density. We find that energy is concentrated at the focus (because many modes influence a small area) and near the turning latitudes (because the waves move so slowly here).

While point forcing and ray theory provide simple solutions, they also posses some unattractive properties. The high mode response is very sensitive to the presence of a frictional mechanism. We added a Rayleigh friction term saw that it acted to localize the response near the source. The inviscid solution is sensitve to the number of Rossby modes and the viscid solution to the value of the Rayleigh damping term.

The delta solution is used as a Green's function and integratred over an arbitary rectangle to derive the patch solution. The integration introduces a factor of $(2m+1)^{-1}$ in the Rossby terms which damps the higher modes. This is equivalent, throught the quantization condition, to dividing the Rossby terms by Y^2 . The major response in the box solution is closer to the equator than it is in the delta case. Phase interference within the box has destroyed the higher mode response, and away from the forcing region the response is built principally from the lower modes. The box solution sensitivity to the number of modes included in the sums is less.

The box size is a critical parameter that characterizes the type of response we expect to find.

Case 1: small scale forcing ; 25km > ΔX, 25km > ΔY:

For forcings over areas this size or smaller the response is virtually identical to the predictions of ray theory or delta forcing.

Case 2: large scale forcing : 4° < ΔX, 4° < ΔY:

The foci no longer exist. The Kelvin and free wave terms are important. The important response independent of the forcing location is trapped near the equator. Beyond 10° north and south of the equator the response is insignificant. The reason is that parts of a patch that lie away from the equator respond only in terms of higher modes which are small. The only important response then occurs if parts of the box extends into the low latitudes. The response then is only felt in these low latitudes.

Case 3: imtermediate forcing : 4° > ΔX > 25km, 4° > ΔY > 25km:

The foci are observed but not as large as in the small scale forcing case. We also see traces of shadow zones. The response away from the equator decreases as the box grows.

The size of the box used will be determined by the resolution of the available data. The resolution required by case 1 is difficult to find and since we are exploring a simple linear model it is doubtful the response of the real ocean is as simple as the point source solution.

Case 3 with uniform forcing over a huge area is also somewhat unrealistic. Since wind stress data at 2.5° intervals is often available we conclude that the intermediate case is the most useful as well as the most practical to compare will observations.

Linear dynamics allow us to examine the effect of basin wide forcing on a single point. The basin is assumed to be divided into a grid of boxes with uniform stress. A superposition of patch solutions yields the influence of basin wide forcing on a single point. The total response at a single point is a sum over all forcing frequencies, baroclinic modes, and stress points. We find that independent of station location four distinct regions in the basin strongly influence the height field at the observation point. Near the observation point any wind forcing will have a strong influence. A broad region to the east of the observation point within 10 of the equator has a moderate influence on the station. This is the region in which Rossby waves originated that pass through the observation point. CT/4 east of the observation point at the equatorial image point to the forcing the intense influence caused by the inverse focus is seen. This is the region where Rossby waves that focus at the observation point originated. Moderate influence is exerted on stations near the equator in the eastern part of the basin by Kelvin waves forced along the equator to the west. The Kelvin waves were more important than when we examined isolated forcings because each isolated patch near the equator excites Kelvin waves in the same location. In effect at the observation point we are seeing the evidence of a sum of Kelvin waves along the equator.

We used the patch model to examine the problem of the effects of wind measurement error on predicted sea surface height. We took the Raleigh damping to have a spindown time of 5 years and used 20 Rossby modes in the sums. These parameters do not have an important effect on the results. As an estimate of the wind error we took a difference field of two common wind analyses.

In the Pacific we used FNOC (Fleet Naval Oceanagraphic Center) and NMC (National Meteorological Center) monthly mean winds on a 2.5°x2.5° grid during the Jan82-Jun83 El Nino event. During the entire period insignificant errors are found in the eastern Pacific and within one degree equator. Moderate sea surface errors are present north of the equator in the western Pacific. In the central Pacific near Fanning and in the western Pacific near Rabaul large errors are present. The largest sea surface errors are caused by poor wind analyses east of the stations. The areas that are only influenced by Kelvin wave dynamics have smaller errors because the wind analyses over the equator are generally good.

In the Indian Ocean we used ECM (European meteorological center) and WH (Wiley and Hinton) winds on a 3^{o} x2^{o} grid from Dec78-Nov79. Large errors are found from the equator northward into the Arabian Sea and along the equator in the central Indian Ocean. The monsoon circulation causes the large errors in the Arabian Sea. Tropical cyclones in the eastern Indian ocean are not resolved well in the ECM data. This causes errors in the sea surface height on the equator in the center of the basin. The errors in the winds south of the equator are large near 5S but decrease further south of the equator.

The important point to retain from the error analyses is that the differences that are present in frequently used wind analyses are significant enough to cause large spatially correlated differences in equatorial sea surface heights. These errors are large enough in places to make the verification of numerical models impossible.

REFERENCES

Blandford, R. 1966. Mixed gravity-Rossby waves in the ocean. Deep Sea Res., 26a, 1033-1050.

Bretherton, F. P. The general linearized theory of wave propagation. In: W. H. Reid (editor) Mathematical Problems in the Geophysical Sciences. Am. Math. Soc., Providence, R.I., 13: 61-102.

Cane, M.A., 1983. Modeling sea level during El Nino. J. Phys. Oc. (to appear in)

Cane, M.A. and A.J. Busalacchi. Hindcast of the 1982-1983 Pacific sea level. J. Phys. Oc. (submitted)

Cane, M.A. and D.W. Moore. 1981 A note on low frequency equatorial basin modes. J. Phys. Ocean., 11, 1578-1584.

Cane, M.A. and E.S. Sarachik. 1976. Forced baroclinic ocean motions. I. The linear equatorial unbounded case. J. Mar. Res., 34, 629-665.

--------- 1977. Forced baroclinic ocean motions. II. The linear equatorial bounded case. J. Mar. Res., 35, 395-432.

--------- 1981. The response of a linear baroclinic equatorial ocean to periodic forcing. J. Mar. Res., 39, 651-693.

Gent, P.R., K. O'Neill and M.A. Cane. 1983. A model of the semiannual oscillation in the equatorial ocean. J. Phys. Oc. (in press)

LeBlond, P.H. and L.A. Mysak. 1978. Waves in the Ocean. Elsevier Scientific New York, 602 pp.

Messiah A. 1961. Quantum Mechanics. North-Holland, 504 pp.

Morse P.M. and H. Feshbach. 1953. Methods of Theoretical Physics 1st Edn: McGraw-Hill, New York, 1978 pp.

Patton, R. J. A numerical model of equatorial waves with application to the seasonal upwelling in the Gulf of Guinea. MS Thesis, MIT.

Pedlosky, J. 1979. Geophysical Fluid Dynamics. Springer-Verlag, New York, 624 pp.

Scholf, P., D.T.L. Anderson and R. Smith. 1981. Beta-dipersion of low frequency Rossby waves. Dyn. Atmos. and Oceans, 5, 187-214.

Whitham, G.B., 1960. Anote on group velocity. J. Fluid Mech., 9, 347-352.

APPENDIX 1

Normalized Hermite functions Ψ_m are given by:

$$\Psi_m(\gamma) = [\pi^{\frac{1}{2}} 2^m m!]^{-\frac{1}{2}} H_m(\gamma) e^{-\frac{\gamma^2}{2}} \tag{A1.1}$$

where H_m are Hermite polynomials of order $|m|$.

The α_m term is defined as:

$$\int_{-\infty}^{\infty} \gamma \Psi_{2m+1} \, d\gamma \equiv 2\pi^{\frac{1}{4}} \alpha_{2m+1}$$

$$\alpha_{2m+1} = [2^m m!]^{-1} [(2m+1)!]^{\frac{1}{2}} \tag{A1.2}$$

$$\alpha_{2m} = 0$$

for $m = 0,1,2,\ldots$

Note that only odd α_m's are defined since the even eigenfunctions Ψ are symmetric.

The Rossby and Kelvin modes are functions of the Ψ's and are denoted by $R_{m()}$ and M_k. Here () denotes the U or H Rossby terms. They are given by:

$$M_K = \frac{1}{\sqrt{2}} \Psi_0 \tag{A1.3}$$

$$R_{mU} = \frac{-1}{4m(m+1)} [(2m+1)\Psi_m' + \gamma \Psi_m] \tag{A1.4}$$

$$R_{mH} = \frac{1}{4m(m+1)} [(2m+1)\Psi_m \gamma + \Psi_m'] \tag{A1.5}$$

APPENDIX 2

The solution to the shallow water model (1.6-1.8) satisfying boundary conditions (2.1-2.2) is given in (Cane and Sarachik 81) as:

$$\begin{bmatrix} U \\ H \end{bmatrix} = \frac{1}{i\omega} e^{i\omega t} \left[\begin{array}{l} a_K(x) M + \sum_{m=1} a_m(x) \underset{\sim}{R}_m + \\ \rho \left[M e^{-i\phi\xi} + \sum_{m=1}^{N} 2\alpha_m \underset{\sim}{R}_m e^{i\phi\xi(2m+1)} \right] \end{array} \right] \quad \text{(A2.1)}$$

Here:

$$\rho = \frac{\sum_{m=0}^{N} \left[\frac{a_m \alpha_m}{2m(m+1)} \right] - [a_K]\,|_{\xi=-1}}{e^{i\phi} \left[1 - e^{-2i\phi} \sum_{m=0} \frac{\alpha_m^2}{m(m+1)} e^{-2im\phi} \right]} \qquad \phi = \omega X_E \qquad \xi = \frac{x - X_E}{X_E}$$

$$a_K(x) = -\int_{\xi}^{0} D_K(\xi') e^{i\phi(\xi'-\xi)} i\phi \, d\xi' \quad \text{(A2.2)}$$

$$a_m(x) = \int_{\xi}^{0} r_m(\xi') e^{-i(2m+1)\phi(\xi'-\xi)} (2m+1) i\phi \, d\xi' \quad \text{(A2.3)}$$

$$D_K(\xi') = \frac{1}{\sqrt{2}} \int_{-\infty}^{\infty} F(x';y) \psi_0 \, dy \quad \text{(A2.4)}$$

$$r_m(\xi') = \int_{-\infty}^{\infty} \left[F(x';y)_y - \frac{1}{2m+1} \gamma F(x';y) \right] \psi_m \, dy \quad \text{(A2.5)}$$

We take the forcing to have the form:

$$F(x,y) = \delta(y-y_*)\delta(x-x_*) \tag{A2.6}$$

We now may evaluate (A2.1) explicitly beginning with (A2.4) and (A2.5).

$$D_K(\zeta') = \frac{1}{\sqrt{2}} \int_{-\infty}^{\infty} \delta(y-y_*)\,\delta(x'-x_*)\,\psi_0\,dy$$

$$D_K(\zeta') = \delta(x'-x_*)\,\frac{1}{\sqrt{2}} \int_{-\infty}^{\infty} \psi_0\,\delta(y-y_*)\,dy$$

$$D_K(\zeta') = \delta(x'-x_*)\,\frac{1}{\sqrt{2}}\,\psi_0(y_*)$$

So:
$$D_K(\zeta') = \delta(x'-x_*)\,M_K(y_*) \tag{A2.7}$$

Similarly: $r_m = \int_{-\infty}^{\infty} \left[\left[\delta(x'-x_*)\delta(y-y_*)\right]_y - \frac{1}{2m+1}\,y\,\delta(x'-x_*)\delta(y-y_*)\right]\psi_m\,dy$

$$r_m = \delta(x'-x_*)\int_{-\infty}^{\infty}\left[\delta(y-y_*)_y - \frac{1}{2m+1}\,y\,\delta(y-y_*)\right]\psi_m\,dy$$

$$r_m = \delta(x'-x_*)\left[-\psi_m'(y_*) - \frac{1}{2m+1}\,y_*\,\psi_m(y_*)\right]$$

$$r_m = \delta(x'-x_*)\,\frac{-4m(m+1)}{4m(m+1)(2m+1}\left[(2m+1)\psi_m'(y_*) - y_*\psi_m(y_*)\right]$$

$$r_m = \delta(x'-x_*)\,\frac{4m(m+1)}{2m+1}\,R_{mv}(y_*) \tag{A2.8}$$

(A2.7) and (A2.8) may now be used in (A2.2) and (A2.3) to find $A_k(x)$ and $A_m(x)$

$$a_K(x) = -\int_{\xi}^{0} \delta(x'-x_*)\, M_K(\gamma_*)\, e^{-i\phi(\xi'-\xi)}\, i\phi\, d\xi'$$

or equivalently:

$$a_K(x) = -\int_{x}^{x_\epsilon} M_K(\gamma_*)\, \delta(x'-x_*)\, e^{-iw(x'-x)}\, iw\, dx'$$

$$a_K(x) = -M_K(\gamma_*)\, iw \int_{x}^{\infty} \delta(x'-x_*)\, e^{iw(x'-x)}\, dx'$$

$$\boxed{\begin{array}{ll} a_K(x) = -M_K(\gamma_*)\, iw\, e^{-iw(x_*-x)} & \text{FOR } x<x_* \\ 0 & x_*<0 \end{array}} \qquad \text{(A2.9)}$$

Similarly:

$$a_m(x) = \int_{\xi}^{0} \delta(x'-x_*)\, \frac{4m(m+1)}{2m+1}\, R_{mv}(\gamma_*)\, e^{-i(2m+1)\phi(\xi'-\xi)}\, (2m+1)\, i\phi\, d\xi'$$

$$a_m(x) = iw\, 4m(m+1)\, R_{mv}(\gamma_*) \int_{x}^{\infty} e^{-i(2m+1)w(x'-x)}\, dx'$$

(A2.10)

$$\boxed{\begin{array}{ll} a_m(x) = -iw\, 4m(m+1)\, R_{mv}(\gamma_*)\, e^{-i(2m+1)w(x_*-x)} & x<x_* \\ 0 & x_*<x \end{array}}$$

Expressions (A2.9) and (A2.10) are substituted into (A2.1) to obtain the solution:

$$a_K(x)\Big|_{\substack{\xi=-1 \\ x=0}} = -M_K(\gamma_*)\, iw\, e^{iw(x_*)}$$

$$a_m(x)\Big|_{\substack{\xi=-1 \\ x=0}} = iw\, 4m(m+1)\, R_{mv}(\gamma_*)\, e^{-i(2m+1)wx_*}$$

ρ then becomes:

$$\rho = i\omega e^{-i\phi}\left[\frac{\sum_{m=0}^{N} 2\alpha_m R_{mv}(\gamma_*) e^{-i(2m+1)\omega x_*} + M_K(\gamma_*) e^{i\omega x_*}}{1 - \sum_{m=0}^{N} \frac{\alpha_m^2}{m(m+1)} e^{-2(m+1)i\phi}}\right]$$

$$\rho = i\omega e^{-i\phi + i\omega x_*}\left[\frac{\sum_{m=0}^{N} 2\alpha_m R_{mv}(\gamma_*) e^{-2i(m+1)\omega x_*} + M_K(\gamma_*)}{1 - \sum_{m=0}^{N} \frac{\alpha_m^2}{m(m+1)} e^{-2(m+1)i\phi}}\right] \quad \text{(A2.11)}$$

Then for $x < x_*$

$$\begin{bmatrix} v \\ H \end{bmatrix} = e^{i\omega t}\left[-M_K(\gamma_*) M_K e^{i\omega(x_*-x)} + \sum_{m=0} 4m(m+1) R_{mv}(\gamma_*) \underset{\sim}{R}_m e^{-i(2m+1)\omega(x_*-x)}\right.$$

$$\left. + e^{-i\phi + i\omega x_*}\left[\frac{\sum 2\alpha_m R_{mv}(\gamma_*) e^{-2i(m+1)\omega x_*} + M_K(\gamma_*)}{1 - \sum_{m=0} \frac{\alpha_m^2}{m(m+1)} e^{-2(m+1)i\phi}}\right] e^{i\phi - i\omega x}\left[M + \sum_{m=0} 2\alpha_m \underset{\sim}{R}_m e^{i(2m+2)(\phi-\omega x)}\right]\right]$$

This is simplified with the definitions:

$i\omega t = \phi_T$

$i\phi = \phi$

$i\omega x_* = \phi_*$

$i\omega x = \phi_x$

and redefine ρ as $\bar{\rho}$

$$\bar{\rho} = \left[\frac{M_K(\gamma_*) + \sum_{m=1} 2\alpha_m R_{mv}(\gamma_*) e^{-2(m+1)\phi_*}}{1 - \sum_{m=0} \frac{\alpha_m^2}{m(m+1)} e^{-2(m+1)\phi}}\right]$$

The final form using the above symbols is obtained by taking in front the common factor $e^{\phi_t - \phi_x + \phi_*}$; this leaves:

For $x<x_*$

$$\begin{bmatrix} U \\ H \end{bmatrix} = e^{\phi_t - \phi_x + \phi_*} \begin{bmatrix} \sum 4m(m+1) R_{mU}(\gamma_*) \underset{\sim}{R}_m e^{-2(m+1)(\phi_* - \phi_x)} - M_K(\gamma_*) M_K \\ + \bar{\rho} \left[M_K + \sum_{m=1}^{N} 2\alpha_m \underset{\sim}{R}_m e^{-2(m+1)(\phi - \phi_x)} \right] \end{bmatrix} \quad \text{(A2.12)}$$

For the region $x_* < x$ $A_m = A_k = 0$ so we are left with only the 'free' solution.

For $x > x_*$

$$\begin{bmatrix} U \\ H \end{bmatrix} = e^{\phi_t - \phi_x + \phi_*} \bar{\rho} \left[M_K + \sum_{m=1} 2\alpha_m \underset{\sim}{R}_m e^{-2(m+1)(\phi - \phi_x)} \right] \quad \text{(A2.13)}$$

To calculate our V we use equation (3):

$$H_T + U_x + V_y = 0$$

$$V = -\int [H_T + U_x] \, dy$$

$$V = -\int \left[\begin{array}{l} i\omega e^{\phi_t - \phi_x + \phi_*} \left[\begin{array}{l} \sum 4m(m+1) R_{mH}(\gamma_*) e^{-2(m+1)(\phi_* - \phi_x)} - M_K(\gamma_*) M_K \\ + \bar{\rho} \left[M_K + \sum_{m=1} 2\alpha_m R_{mH} e^{-2(m+1)(\phi - \phi_x)} \right] \end{array} \right] \\ \\ + i\omega e^{\phi_t - \phi_x + \phi_*} \left[\begin{array}{l} \sum 4m(m+1) R_{mU}(\gamma_*) e^{-2(m+1)(\phi_* - \phi_x)} + M_K(\gamma_*) M_K \\ + \bar{\rho} \left[-M_K + \sum_{m=1} 2(2m+1) \alpha_m R_{mU} e^{-2(m+1)(\phi - \phi_x)} \right] \end{array} \right] \end{array} \right] dy \quad \text{(A2.14)}$$

(A2.14) may be simplified easily:

$$V = -\int \left[i\omega e^{\phi_T - \phi_X + \phi_*} \sum R_{mV}(\gamma_*)\left[R_{mH} + (2m+1)R_{mV}\right] e^{-2(m+1)(\phi_* - \phi_X)} \frac{}{4m(m+1)} \right.$$
$$\left. + \bar{\rho} \sum_{m=1} 2\alpha_m \left[R_{mH} + (2m+1)R_{mV}\right] e^{-2(m+1)(\phi - \phi_X)} \right] dy$$

So

$$V = -i\omega e^{\phi_* - \phi_X + \phi_T} \left[\sum_{m=1}^{N} R_{mV}(\gamma_*) 4m(m+1) e^{-2(m+1)(\phi_* - \phi_X)} \int \left[R_{mH} + (2m+1)R_{mV}\right] dy \right.$$
$$\left. + \bar{\rho} \sum_{m=1}^{M} 2\alpha_m e^{-2(m+1)(\phi - \phi_X)} \int \left[R_{mH} + (2m+1)R_{mV}\right] dy \right] \quad \text{(A2.15)}$$

Using the properties of Hermite polynomials we may solve the integrals exactly.

$$\int \left[R_{mH} + (2m+1)R_{mV}\right] dy = \int \frac{1}{4m(m+1)} \left[-(2m+1)^2 \psi_m' - (2m+1)\gamma\psi_m + (2m+1)\gamma\psi_m + \psi_m'\right] dy$$

$$= \int \frac{1}{4m(m+1)} \left[-(2m+1)^2 + 1\right] \psi_m' \, dy \quad \text{(A2.16)}$$

$$= -\int \psi_m' dy = -\psi_m = \int \left[R_{mH} + (2m+1)R_{mV}\right]$$

SO THEN FOR $X < X_*$

$$V = i\omega e^{\phi_* - \phi_X + \phi_T} \left[\sum_{m=1} 4m(m+1) R_{mV}(\gamma_*)\psi_m e^{-2(m+1)(\phi_* - \phi_X)} \right.$$
$$\left. + \bar{\rho} \sum_{m=1} 2\alpha_m \psi_m e^{-2(m+1)(\phi - \phi_X)} \right] \quad \text{(A2.17)}$$

And for $x > x_*$ $A_m = A_k = 0$. So

$$V = i\omega e^{(\phi_* - \phi_x + \phi_T)} \left[\bar{\rho} \sum_{m=1}^{N} 2\alpha_m \psi_m e^{-2(m+1)(\phi - \phi_x)} \right] \qquad \text{(A2.18)}$$

APPENDIX 3

We want to force in a box centered at a point (x',y'). Take

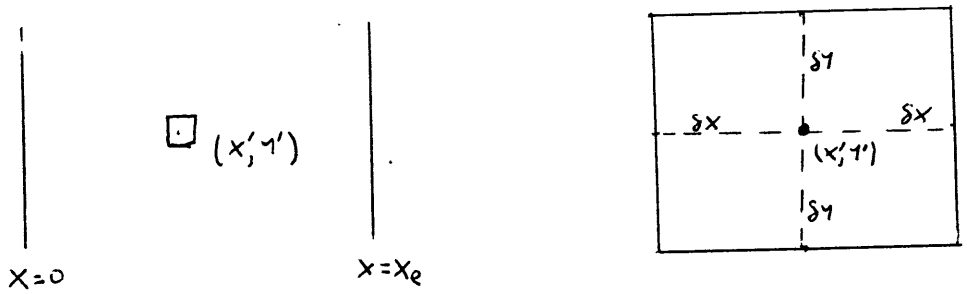

First we will examine the response away from the forcing; that is in the regions $x'+\delta x < x$ and $x'-\delta x > x$.

Then

$$\left[U(x,y), H(x,y), V(x,y)\right] = \int_{x'-\delta x}^{x'+\delta x}\int_{y'-\delta y}^{y'+\delta y}\left[U(x,x_*,y,y_*), V(x,x_*,y,y_*), H(x,x_*,y,y_*)\right]dy_*\,dx_* \qquad \text{(A3.1)}$$

First solve for the U and H fields for $x'-\delta x < x$.

$$\left[U,H\right] = \int_{y'-\delta y}^{y'+\delta y}\int_{x'-\delta x}^{x'+\delta x} e^{\phi_x}\left[\begin{array}{l}\sum 4m(m+1)R_{mv}(y_*)\underset{\sim}{R}_m e^{-(2m+1)(\phi_*-\phi_x)} - M_K(y_*)M_K e^{(\phi_*-\phi_x)} \\ +\left[\dfrac{M_K(y_*)e^{\phi_*}+\sum 2\alpha_m R_{mv}(y_*)e^{-(2m+1)\phi_*}}{e^{\phi}\left[1-\sum\frac{\alpha_m^2}{m(m+1)}e^{-2(m+1)\phi}\right]}\right]\times \\ \left[M_K e^{(\phi-\phi_x)}+\sum 2\alpha_m \underset{\sim}{R}_m e^{-(2m+1)(\phi-\phi_x)}\right]\end{array}\right] dx_*\,dy_* \qquad \text{(A3.2)}$$

Integrating over x_x first

$$\int_{x'-\delta x}^{x'+\delta x} F(T,x,\gamma,\gamma_*)\, e^{(\phi_*-\phi_x)}\, d\gamma_* = F(T,x,\gamma,\gamma_*)\, e^{-\phi_x} \int_{x-\delta x}^{x+\delta x} e^{i\omega x_*}\, dx_*$$

$$= \frac{F(T,x,\gamma,\gamma_*)\, e^{-\phi_x}}{i\omega}\, e^{i\omega x_*} \Big|_{x'-\delta x}^{x'+\delta x}$$

$$= \frac{F(T,x,\gamma,\gamma_*)\, e^{-\phi_x}}{\omega}\, e^{i\omega x'} \left[\frac{e^{i\omega\delta x} - e^{-i\omega\delta x}}{i}\right]$$

$$= \frac{F(T,x,\gamma,\gamma_*)\, e^{-\phi_x + i\omega x'}}{\omega}\, 2\sin\omega\delta x$$

Let: $\omega\delta x = \phi_\delta$ and since x' is just the center of our 'box' we will call: $i\omega x' = \phi'$.

So

$$\int_{x'-\delta x}^{x'+\delta x} F(T,x,\gamma,\gamma_*)\, e^{(\phi_*-\phi_x)} = \frac{2}{\omega} \sin\phi_\delta\, F(T,x,\gamma,\gamma_*)\, e^{\phi'-\phi_x} \qquad \text{(A3.3)}$$

Similarly

$$\int_{x'-\delta x}^{x'+\delta x} F(T,x,\gamma,\gamma_*)\, e^{-(2m+1)(\phi_*-\phi_x)} = \frac{2}{\omega(2m+1)} \sin\left[(2m+1)\phi_\delta\right] F(T,x,\gamma,\gamma_*)\, e^{-(2m+1)(\phi'-\phi_x)} \qquad \text{(A3.4)}$$

The results of (A3.3) and (A3.4) are substituted into (A3.2).

$$\left[U,H\right] = \int_{\gamma'-\delta\gamma}^{\gamma'+\delta\gamma} \frac{2}{\omega} e^{(\phi_\gamma+\phi'-\phi_x)} \left[\sum \frac{\alpha_m(m+1)}{2m+1} R_{mw}(\gamma_w) \sin\left[(2m+1)\phi_\delta\right] e^{2(m+1)(\phi'-\phi_x)} \underset{\sim}{R}_m - \sin\phi_\delta\, M_K(\gamma_w) M_K \right.$$

$$\left. + \left[\frac{M_K(\gamma_w)\sin\phi_\delta + \sum \frac{2\alpha_m}{2m+1} R_{mw}(\gamma_w) e^{-2(m+1)\phi'} \sin(\phi_\delta(2m+1))}{1 - \sum \frac{\alpha_m^2}{m(m+1)} e^{-2(m+1)\phi}}\right] \times \left[M_K + \sum 2\alpha_m \underset{\sim}{R}_m\, e^{-2(m+1)(\phi-\phi_x)}\right]\right] \qquad \text{(A3.5)}$$

Now integrate over y_*

$$\int_{y'-\delta y}^{y'+\delta y} M_k(y_*)\,dy_* = \int_{y'-\delta y}^{y'+\delta y} \frac{1}{\sqrt{2}\,\pi^{\frac{1}{4}}} H_0 e^{-\frac{y_*^2}{2}}\,dy_*$$

$$= \pi^{\frac{1}{4}} \frac{1}{\sqrt{2\pi}} \int_{y'-\delta y}^{y'+\delta y} e^{-\frac{y_*^2}{2}}\,dy_*$$

LET $\quad y'+\delta y = y_N \qquad y'-\delta y = y_S \qquad H_0 = 1$

The integral is just an error function so

$$\int_{y'-\delta y}^{y'+\delta y} M_k(y_*)\,dy_* = \pi^{\frac{1}{4}} \left[ERF(y_N) - ERF(y_S)\right] \tag{A3.6}$$

$$\int_{y'-\delta y}^{y'+\delta y} R_m(y_*)\,dy_* = \int_{y_S}^{y_N} \frac{-1}{y_m(m+1)} \left[(2m+1)\psi_m' + y_*\psi_m\right] dy_*$$

$$= \frac{-1}{y_m(m+1)} \left[(2m+1)\psi_m(y_*) + y_*\psi_m(y_*)\right] \Big|_{y_S}^{y_N}$$

$$= \frac{-(2m+1)}{y_m(m+1)} \left[\psi_m(y_N) - \psi_m(y_S) + \frac{1}{2m+1}\int_{y_S}^{y_N} y_*\psi_m(y_*)\,dy_*\right] \tag{A3.7}$$

Our final solutions are found by substituting (A3.7) and (A3.6) into (A3.5) and noting that $A_m = a_k = 0$ for $(x' + \delta x) > X$ to obtain:

For $x < (x' - \delta x)$

$$\left[U, H\right] = \frac{2}{\omega} e^{\phi' - \phi_x + \phi_T} \left[\begin{array}{l} -\sum_{m=1} \left(\psi(y_N) - \psi(y_S) + \frac{1}{2m+1}\int_{y_S}^{y_N} y_*\psi_m(y_*)\,dy_*\right) \underset{\sim}{R}_m e^{-2(m+1)(\phi' - \phi_x)} \sin\left((2m+1)\phi_\delta\right) \\ -\pi^{\frac{1}{4}} \left[ERF(y_N) - ERF(y_S)\right] M_K \sin\phi_\delta \\ +\beta \left[M_K + \sum 2\alpha_m \underset{\sim}{R}_m e^{-2(m+1)(\phi - \phi_x)}\right] \end{array} \right] \tag{A3.8}$$

For $x > (x' + \delta x)$:

$$[U, H] = \frac{2}{\omega} e^{\phi' - \phi_x + \phi_T} \hat{P} \left[M_K + \sum 2\alpha_m \underset{\sim}{R}_m e^{-2(m+1)(\phi - \phi_x)} \right] \quad \text{(A3.9)}$$

Here

$$\hat{P} = \left[\frac{\pi^{\frac{1}{2}} [ERF(\gamma_N) - ERF(\gamma_S)] \sin\phi_y - \sum \frac{2\alpha_m}{\gamma_m(m+1)} \left(\psi(\gamma_N) - \psi(\gamma_S) + \frac{1}{2m+1} \int_{\gamma_S}^{\gamma_N} \gamma_N \psi(\gamma_N) \right) e^{-2(m+1)\phi} \sin(\phi_y(2m+1))}{1 - \sum \frac{\alpha_m^2}{m(m+1)} e^{-2(m+1)\phi}} \right] \quad \text{(A3.10)}$$

The solution for V may be found using

$$V = -\int [H_T + U_x] \, dy$$

This calculation was done with different constants in (A2.14)-(A2.16) and the results are analogous. The V solutions then are found by replacing

$$\begin{bmatrix} \underset{\sim}{M}_K & \text{WITH} & 0 \\ \underset{\sim}{R}_m & \text{WITH} & i\omega \Psi_m \end{bmatrix}$$

to obtain for $x < (x' - \delta x)$

$$V = 2i e^{(\phi' - \phi_x - \phi_T)} \left[-\sum \left(\psi(\gamma_N) - \psi(\gamma_S) + \frac{1}{2m+1} \int_{\gamma_S}^{\gamma_N} \gamma_N \Psi_m \right) \Psi_m e^{-2(m+1)(\phi' - \phi_x)} \sin((2m+1)\phi_y) \right] \quad \text{(A3.11)}$$

$$+ \hat{P} \sum_{m=1} 2\alpha_m \Psi_m e^{-2(m+1)(\phi - \phi_x)} \Bigg]$$

And for $x > (x' + \delta x)$

$$V = 2i\, e^{(\phi' - \phi_x + \phi_T)} \overset{\square}{p} \sum_{m=1} 2\alpha_m \psi_m \rho^{-2(m+1)(\phi - \phi_x)} \tag{A3.12}$$

The solutions have been of the form:

$x < x_*$ field = forced + $\overset{\square}{p}$ free

$x > x_*$ field = $\overset{\square}{p}$ free

So if we want a solution within the box we will have

$$\text{Field} = \int_x^{x'+\delta x} \text{Forced}\, dx_* + \int_{x-\delta x}^{x+\delta x} \overset{\square}{p}\, \text{Free}\, dx_*$$

For $x' - \delta x < x < x' + \delta x$.

Using the results from the previous calculation for (U,H) we see

$$\begin{aligned}[U,H] = \int_x^{x+\delta x} e^{\phi_x - \phi_x - \phi_T} \Bigg[& -\sum_{m=1} (\psi_{\mu m} + \psi(\mu_5)) + \frac{1}{2m+1} \int_{\mu_5}^{\mu_m} \psi_x \psi_* \Big) \underset{\sim}{R}_m (2m+1) \rho^{2(m+1)(\phi_x - \phi_x)} \Bigg] dx_* \\ & - \pi^{-\frac{1}{2}} \left[\text{ERF}(\mu_m) - \text{ERF}(\mu_5) \right] M_K \end{aligned} \tag{A3.13}$$

$$+ \overset{\square}{p} \frac{2}{\omega} e^{(\phi' - \phi_x + \phi_T)} \left[M_K + \sum 2\alpha_m \underset{\sim}{R}_m \rho^{-2(m+1)(\phi - \phi_x)} \right]$$

All we have to evaluate directly are the $\int_x^{x'+\delta x}$ integrals.

$$\int_x^{x'+\delta x} e^{\phi_{x_*}-\phi_x}\, dx_* = \frac{1}{i\omega} e^{i\omega x_* - i\omega x}\Big|_x^{x'+\delta x}$$

$$= \frac{1}{i\omega}\left[e^{i\omega x' - i\delta x\omega + i\omega x} - 1\right]$$

$$= \frac{1}{i\omega}\left(e^{\phi' - \phi_x + i\phi_\delta} - 1\right) \qquad \text{(A3.14)}$$

Similarly

$$\int_x^{x'+\delta x} e^{-(2m+1)(\phi_{x_*}-\phi_x)} = \frac{-1}{i\omega(2m+1)}\left(e^{(2m+1)(\phi'+i\phi_\delta-\phi_x)} - 1\right) \qquad \text{(A3.15)}$$

So substituting (A3.14) and (A3.15) into (A3.13) we have:

$$[U,H] = e^{\phi_T}\left[\begin{array}{l} -\frac{i}{\omega}\left[\left(\Sigma(+(\gamma_N)-\Psi(\gamma_S)+\frac{1}{2m+1}\int_{\gamma_S}^{\gamma_N}\gamma_{x_*}\psi(\gamma_{x_*})\right)\underset{\sim}{R}_m\left(e^{-(2m+1)(\phi'+i\phi_\delta-\phi_x)}-1\right)\right] \\ -\frac{i}{\omega}\left[\pi^{-1}\left(ERF(\gamma_N)-FRF(\gamma_S)\right)\underset{\sim}{M}_K\left(1-e^{\phi'+i\phi_\delta-\phi_x}\right)\right] + \\ \frac{2}{\omega}e^{\phi-\phi_x}\int\left[M_K+\Sigma 2\alpha_m\tilde{R}_m e^{-2(m+1)(\phi-\phi_x)}\right] \end{array}\right] \qquad \text{(A3.16)}$$

The solution for V is complicated by the 1 that appears in the brackets but much of it has been calculated before in (A2.14-A2.16)

$$-\Psi_\gamma = i\omega H + U_x$$

For the Rossby terms in the forced part:

$$-(V_{RF})_\gamma = i\omega K_1 R_{mH}\left[e^{-(2m+1)(\phi' + i\phi_\delta - \phi_x)} - 1\right]$$

$$+ i\omega K_1 (2m+1) R_{mv}\left[e^{-(2m+1)(\phi' + i\phi_\delta - \phi_x)}\right]$$

$$= i\omega K_1 e^{-(2m+1)(\phi' + i\phi_\delta - \phi_x)}\left[R_{mH} + (2m+1) R_{mv}\right] - i\omega K_1 R_{mH}$$

$$= i\omega K_1\left[e^{-(2m+1)(\phi' + i\phi_\delta - \phi_x)}\left[-\psi_m'\right] - R_{mH}\right]$$

$$V_{RF} = i\omega K_1\left[e^{-(2m+1)(\phi' + i\phi_\delta - \phi_x)}\psi_m + \int R_{mH}\, d\gamma\right] \qquad \text{(A3.17)}$$

We also have a non-zero contribution from the forced Kelvin term.

$$-(V_{FK})_\gamma = i\omega K_2 M\left[1 - e^{(\phi' + i\phi_\delta - \phi_x)}\right]$$
$$+ i\omega K_2 M\, e^{(\phi' + i\phi_\delta - \phi_x)}$$

$$-(V_{KF})_\gamma = i\omega K_2 M$$

which was shown in (A3.6) to be just an error function. So

$$V_{KF} = -i\omega K_2 \pi^{\frac{1}{2}} ERF(\gamma) \qquad \text{(A3.18)}$$

So combining our results

For $x-\delta x < x < x+\delta x$:

$$V = e^{\phi_T}\Big[\Big[\sum\big(\psi(y_N)-\psi(y_S)+\tfrac{1}{2m+1}\int_{y_S}^{y_N} y_*\psi(y_*)\,dy_*\big)\Big]\times$$
$$\Big[e^{-(2m+1)(\phi'+\alpha\phi_\delta-\phi_x)}\psi_m+\int R_{m+1}\,dy\Big]$$
$$-\pi^{\frac{1}{2}}\,E R_1(y)\,\big[ERF(y_N)-ERF(y_S)\big]$$
$$+2\alpha e^{(\phi'-\phi_x)}\int_0^{\infty}\sum_{m=1}^{\infty}2\alpha_m\psi_m e^{-2(m+1)(\phi-\phi_x)}\Big] \qquad \text{(A3.19)}$$

TABLE OF FIGURES

FIGURE	FIELD	# MODES	X	Y	^	R	TIME	CONTOUR INTERVAL
2-1	FREE U	50						5.0
2-2	FREE V	50						5.0
2-3	FREE H	50						5.0
2-4		50						0.02
2-5	U	50	5000	0				9.0
2-6	V	50	5000	0				9.0
2-7	H	50	5000	0				9.0
2-8	U	50	3500	0				9.0
2-9	U	50	1000	0				9.0
2-10	REAL V	50	5000	0			0	9.0
2-11	REAL V	50	5000	0			$\pi/4$	9.0
2-12	REAL V	50	5000	0			$\pi/2$	9.0
2-13	U	50	5000	500				9.0
2-14	U	50	5000	-500				9.0
2-15	U	50	5000	1000				9.0
2-16	U	7	5000	0				2.0
2-17	V	7	5000	0				1.0
2-18	H	7	5000	0				2.0
2-19	U	7	5000	500				2.0
2-20	U	7	5000	1000				0.1
2-21	U	50	5000	0		5		4.5
2-22	U	50	5000	0		50		9.0
3-1	RAY PATHS	30	5000	0				
3-2	TOTAL ENERGY	30	5000	0				60.0
3-3	<E>	30	5000	0				60.0
3-4	RAY PATHS	30	5000	1000				
3-5	TOTAL ENERGY	30	5000	1000				60.0
3-6	<E>	30	5000	1000				60.0
4-1		50			10			0.04
4-2		50			111.2			0.04
4-3		50			222.4			0.04
4-4	U	50	5000	0	222.4			1.5
4-5	V	50	5000	0	222 4			1.5
4-6	H	50	5000	0	222.4			1.5
4-7	U	50	5000	0	111.2			1.5
4-8	U	7	5000	0	222 4			1.0
4-9	V	7	5000	0	222.4			0.5
4-10	H	7	5000	0	222.4			1.0
4-11	U	50	1000	0	222.4			1.5
4-12	U	50	1000	500	222 4			1.5
4-13	U	50	5000	0	222.4	25		1.5
4-14	U	50	5000	1000	222.4	25		1.0

FIGURE	PLOT	BAROCLINIC MODE	TIME	PERIOD	CONTOUR INTERVAL
5-1	PACIFIC BASIN				
5-2	FANNING RESPONSE FUNCTION	1			0.2
5-3	FANNING RESPONSE FUNCTION	1		18	0.2
5-4	FANNING RESPONSE FUNCTION	1		9	0.2
5-5	FANNING RESPONSE FUNCTION	1		6	0.2
5-6	FANNING RESPONSE FUNCTION	1		18/4	0.2
5-7	FANNING RESPONSE FUNCTION	1		18/5	0.2
5-8	FANNING RESPONSE FUNCTION	1		3	0.2
5-9	FANNING RESPONSE FUNCTION	1		18/7	0.2
5-10	FANNING RESPONSE FUNCTION	1		18/8	0.2
5-11	FANNING RESPONSE FUNCTION	1		2	0.2
5-12	FANNING RESPONSE FUNCTION - DELTA CASE	1			0.2
5-13	FANNING RESPONSE FUNCTION - DELTA CASE	1		18(months)	0.2
5-14	FANNING RESPONSE FUNCTION - DELTA CASE	1		6	0.2
5-15	FANNING RESPONSE FUNCTION - DELTA CASE	1		3	0.2
5-16	FANNING RESPONSE FUNCTION - DELTA CASE	1		2	0.2
5-17	GALAPAGOS RESPONSE FUNCTION	1		9	0.2
5-18	GALAPAGOS RESPONSE FUNCTION	1		6	0.2
5-19	JARVIS RESPONSE FUNCTION	1		6	0.1
5-20	KWAJALEIN RESPONSE FUNCTION	1		9	0.1
5-21	TRUK RESPONSE FUNCTION	1		9	0.1
5-22	RABAUL RESPONSE FUNCTION	1		18	0.25
5-23	NMC ZONAL STRESS		JAN 82		0.25(dynes)
5-24	NMC ZONAL STRESS		MAR 82		0.25
5-25	NMC ZONAL STRESS		MAY 82		0.25
5-26	NMC ZONAL STRESS		JUL 82		0.25
5-27	NMC ZONAL STRESS		SEP 82		0.25
5-28	NMC ZONAL STRESS		NOV 82		0.25
5-29	NMC ZONAL STRESS		JAN 83		0.25
5-30	NMC ZONAL STRESS		MAR 83		0.25
5-31	NMC ZONAL STRESS		MAY 83		0.25
5-32	STRESS ERROR TRANSFORM				0.25
5-33	STRESS ERROR TRANSFORM			18	0.25
5-34	STRESS ERROR TRANSFORM			6	0.1
5-35	STRESS ERROR TRANSFORM			3	0.1
5-36	STRESS ERROR TRANSFORM			2	0.1
5-37	GALAPAGOS SEA SURFACE ERROR				
5-38	CHRISTMAS SEA SURFACE ERROR				
5-39	FANNING SEA SURFACE ERROR				
5-40	JARVIS SEA SURFACE ERROR				
5-41	CANTON SEA SURFACE ERROR				
5-42	KWAJALEIN SEA SURFACE ERROR				
5-43	NAURU SEA SURFACE ERROR				
5-44	TRUK SEA SURFACE ERROR				
5-45	RABAUL SEA SURFACE ERROR				
5-46	MALAKAL SEA SURFACE ERROR				

FIGURE	PLOT	BAROCLINIC MODE	TIME	PERIOD	CONTOUR INTERVAL
6-1	INDIAN BASIN				
6-2	ECM ZONAL STRESS		DEC 78		0.25(dynes)
6-3	ECM ZONAL STRESS		JAN 79		0.25
6-4	ECM ZONAL STRESS		FEB 79		0.25
6-5	ECM ZONAL STRESS		MAR 79		0.25
6-6	ECM ZONAL STRESS		APR 79		0.25
6-7	ECM ZONAL STRESS		MAY 79		0.25
6-8	ECM ZONAL STRESS		JUN 79		0.25
6-9	ECM ZONAL STRESS		JUL 79		0.25
6-10	ECM ZONAL STRESS		AUG 79		0.25
6-11	ECM ZONAL STRESS		SEP 79		0.25
6-12	ECM ZONAL STRESS		OCT 79		0.25
6-13	ECM ZONAL STRESS		NOV 79		0.25
6-14	STRESS ERROR TRANSFORM				0.1
6-15	STRESS ERROR TRANSFORM			12	0.1
6-16	STRESS ERROR TRANSFORM			6	0.1
6-17	STRESS ERROR TRANSFORM			2	0.1
6-18	A RESPONSE FUNCTION	2			0.1
6-19	A RESPONSE FUNCTION	2		12	0.1
6-20	A RESPONSE FUNCTION	2		6	0.1
6-21	A RESPONSE FUNCTION	2		2	0.1
6-22	H RESPONSE FUNCTION	2		4	0.4
6-23	X RESPONSE FUNCTION	2		3	0.1
6-24	F RESPONSE FUNCTION	1		12	0.2
6-25	F RESPONSE FUNCTION	2		12	0.2
6-26	B RESPONSE FUNCTION	2		6	0.1
6-27	B RESPONSE FUNCTION	3		6	0.1
6-28	W RESPONSE FUNCTION	2		6	0.4
6-29	Q RESPONSE FUNCTION	2		3	0.4
6-30	A SEA SURFACE ERROR				
6-31	T SEA SURFACE ERROR				
6-32	H SEA SURFACE ERROR				
6-33	X SEA SURFACE ERROR				
6-34	F SEA SURFACE HEIGHT				
6-35	Q SEA SURFACE ERROR				
6-36	B SEA SURFACE ERROR				
6-37	W SEA SURFACE ERROR				
6-38	Q SEA SURFACE ERROR				
6-39	Z SEA SURFACE ERROR				

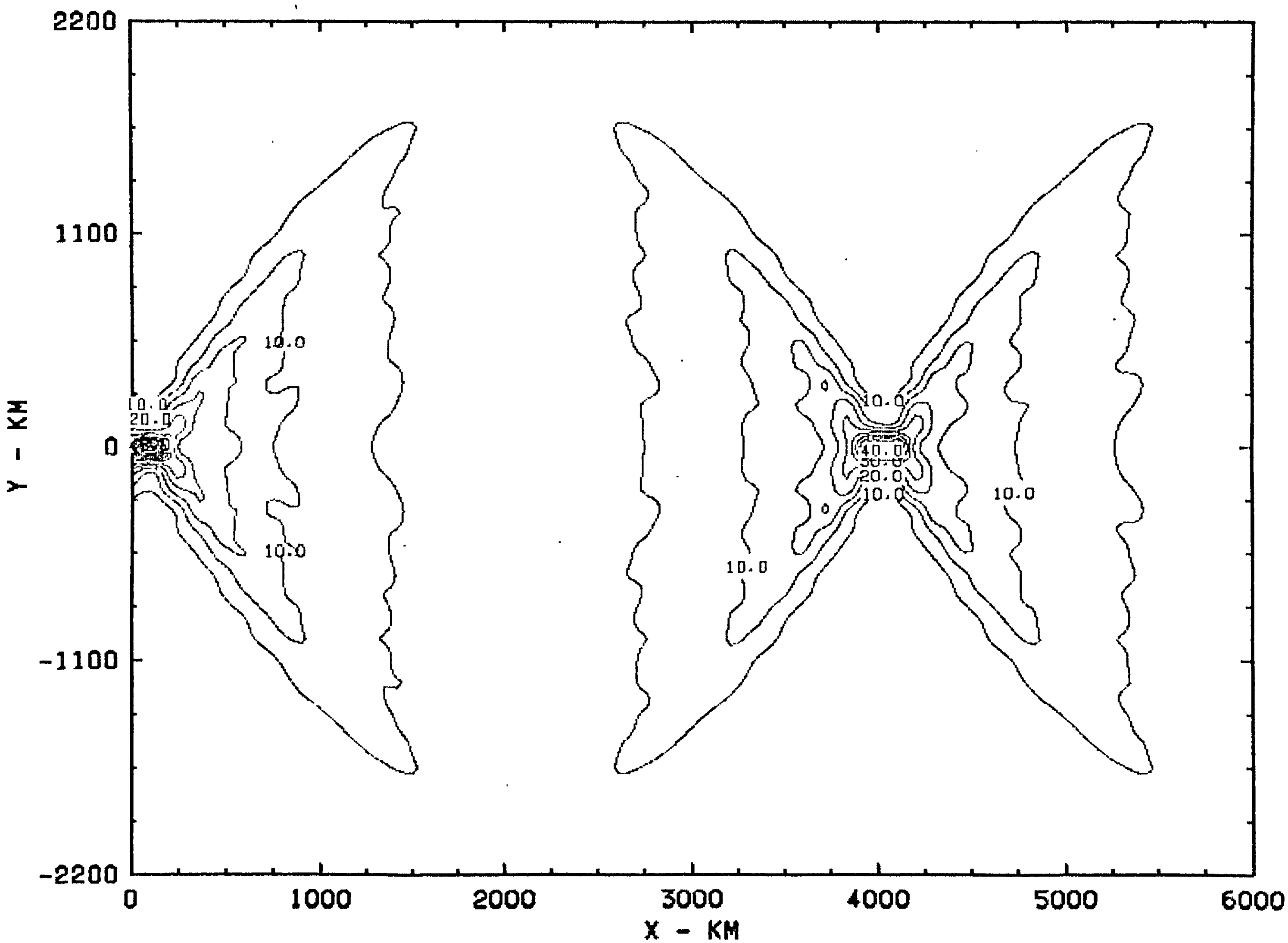

FIGURE 2.1

Free Wave - Zonal Velocity

FIGURE 2.2

Free Wave - Zonal Velocity

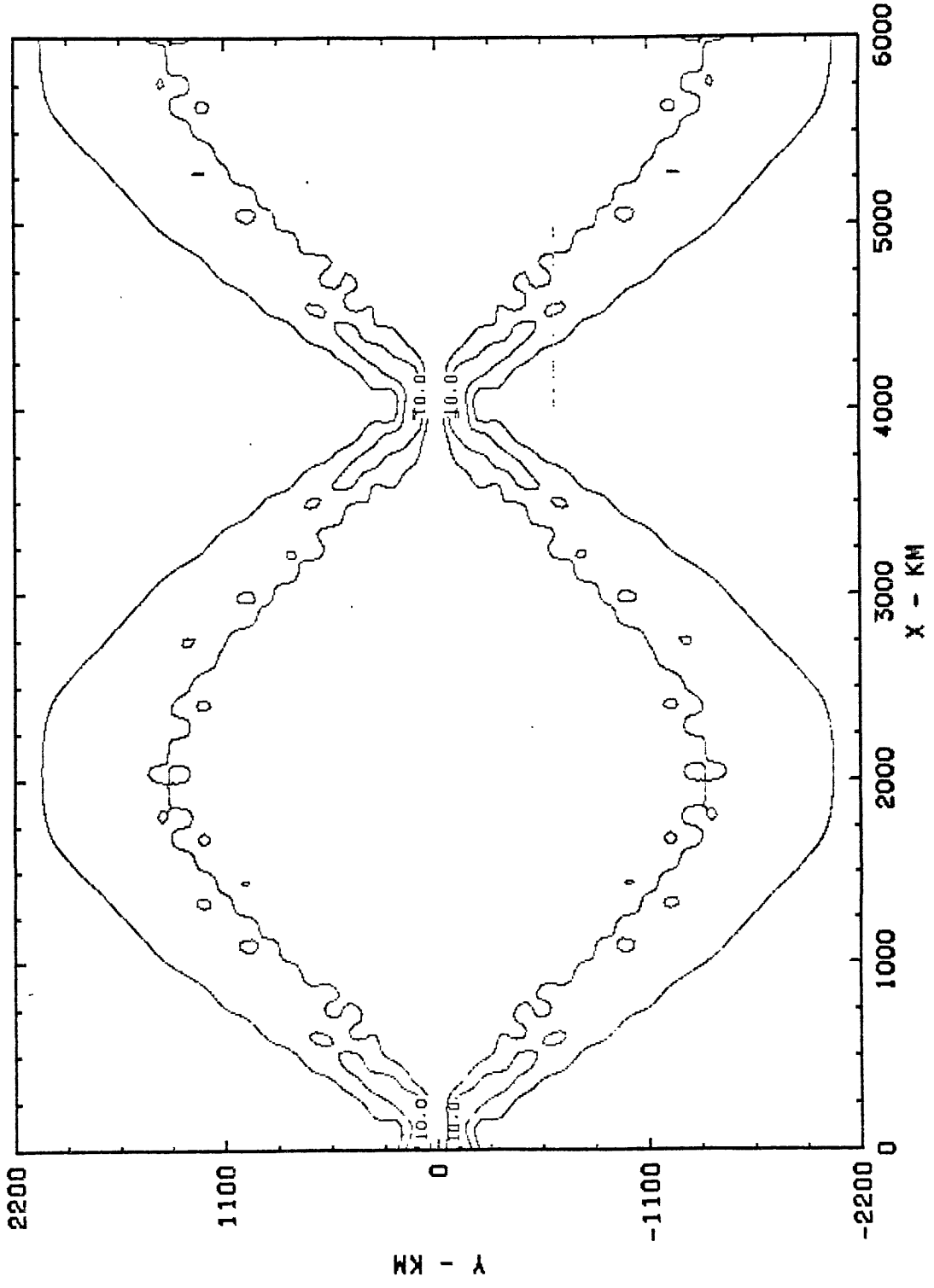

FIGURE 2.3

Free Wave - Height Field

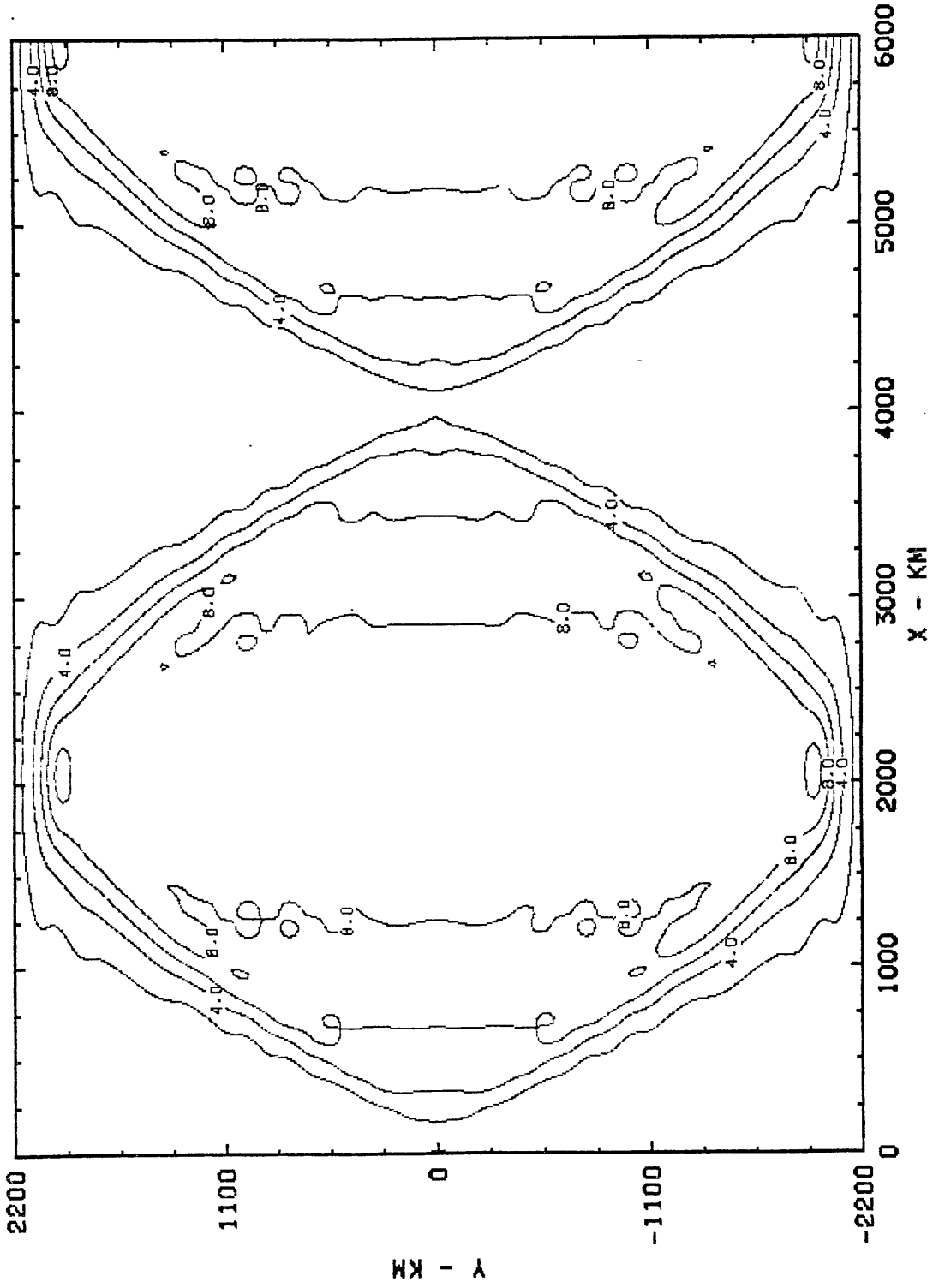

FIGURE 2.4

Rho Amplitude

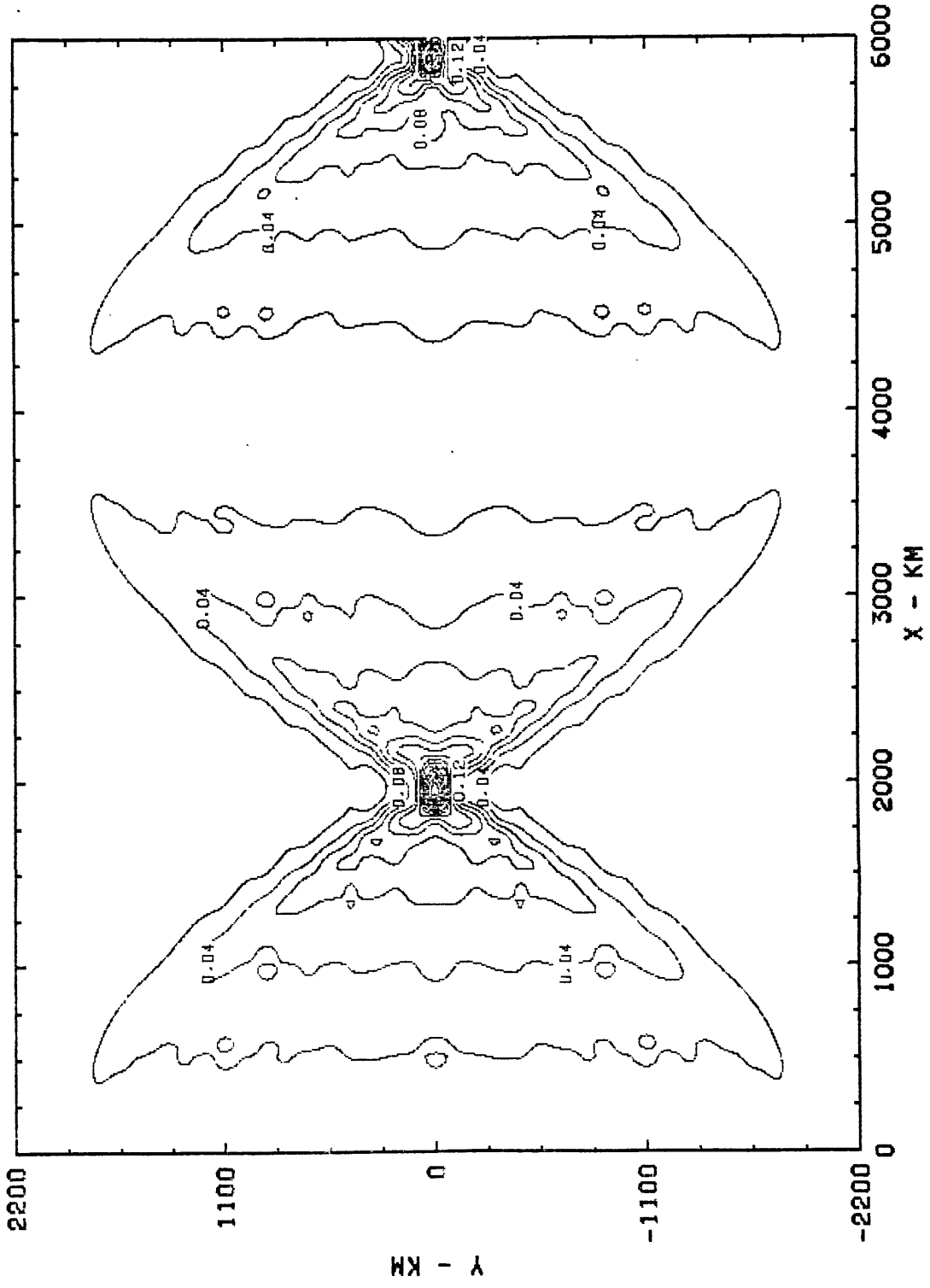

FIGURE 2.5

Zonal Velocity Amplitude
$(X_*, Y_*) = (5000, 0)$

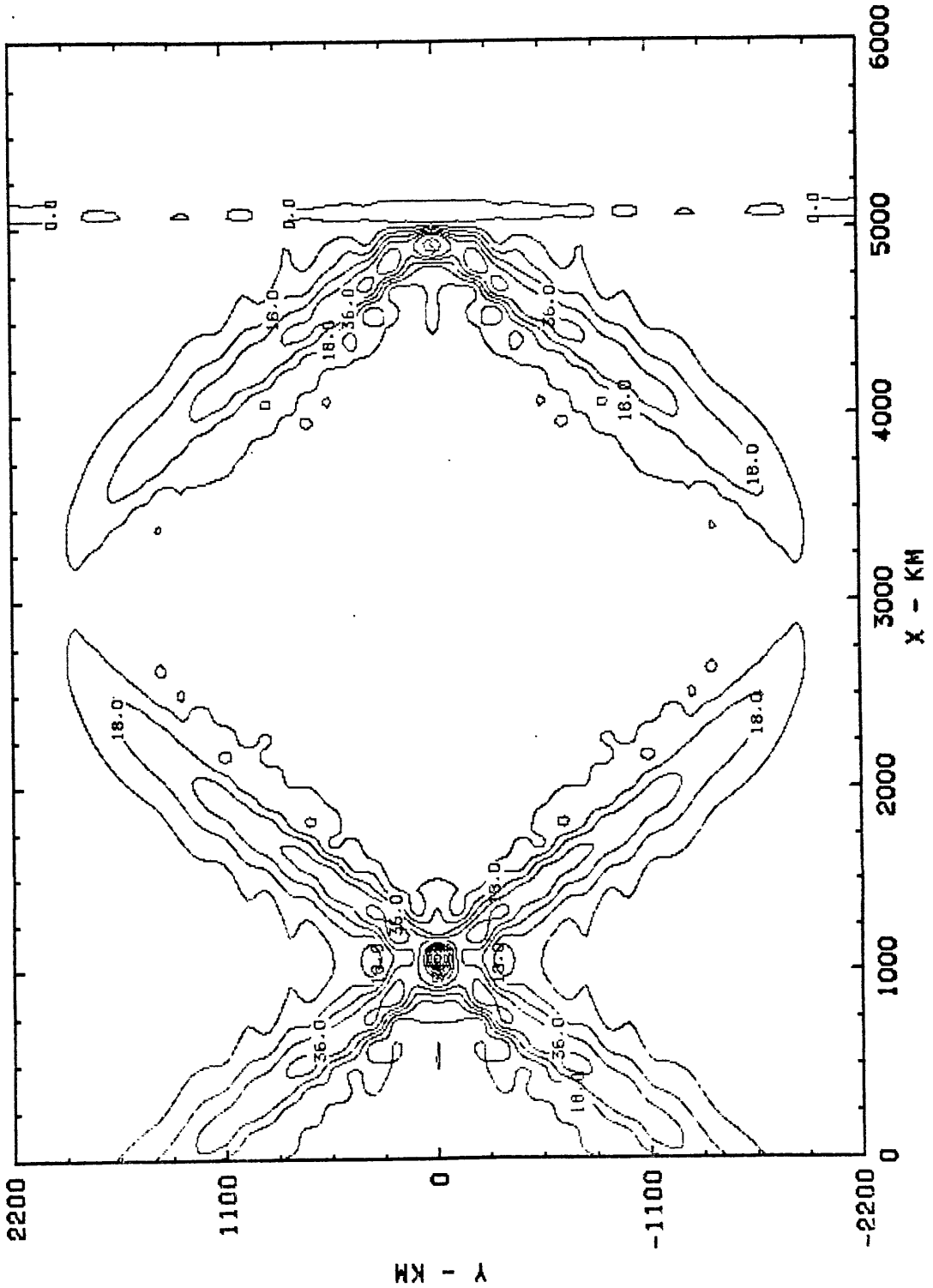

FIGURE 2.6

Meridional Velocity Amplitude
$(X_*, Y_*) = (5000, 0)$

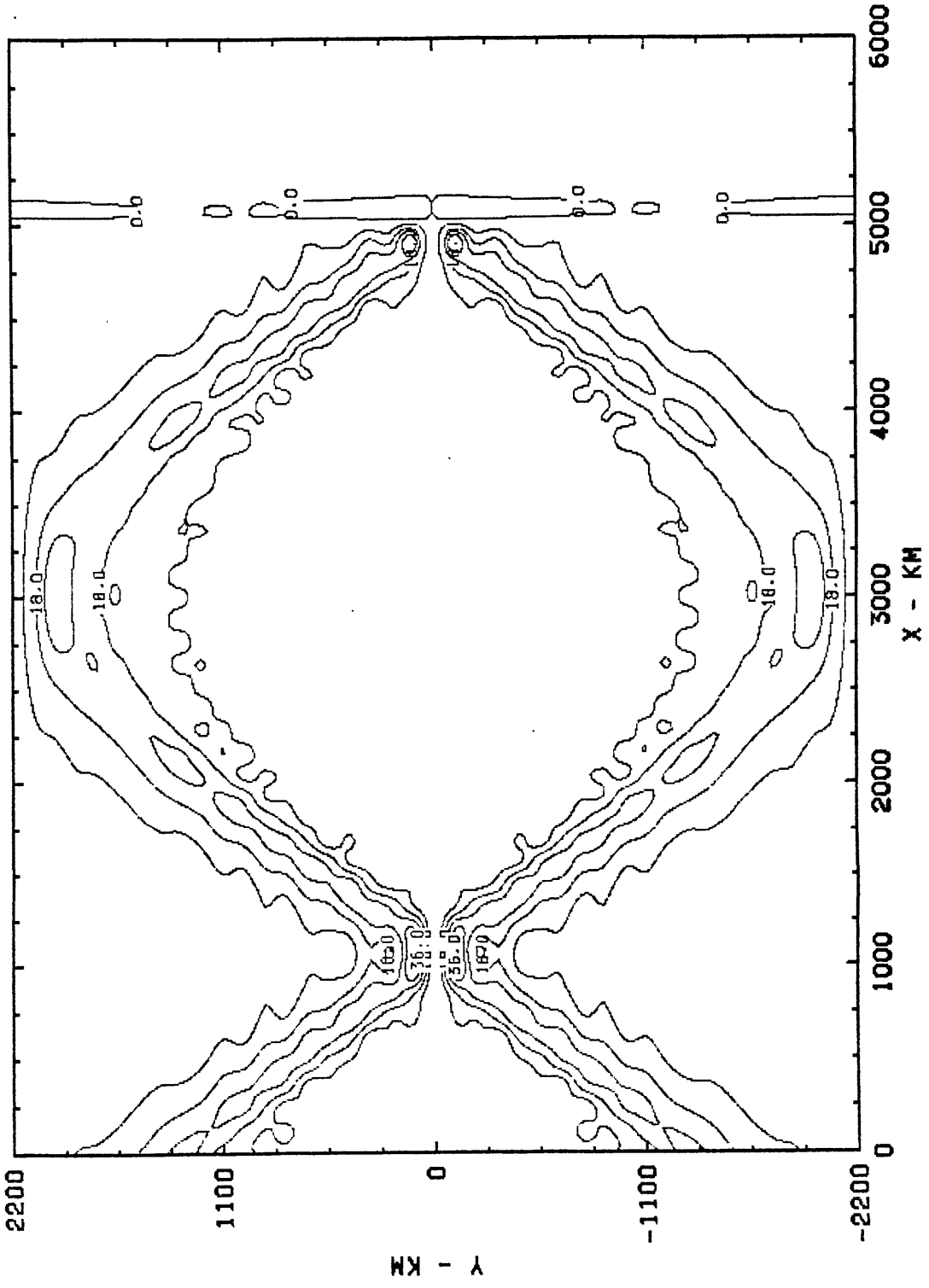

FIGURE 2.7

Height Field Amplitude
$(X_*, Y_*) = (5000, 0)$

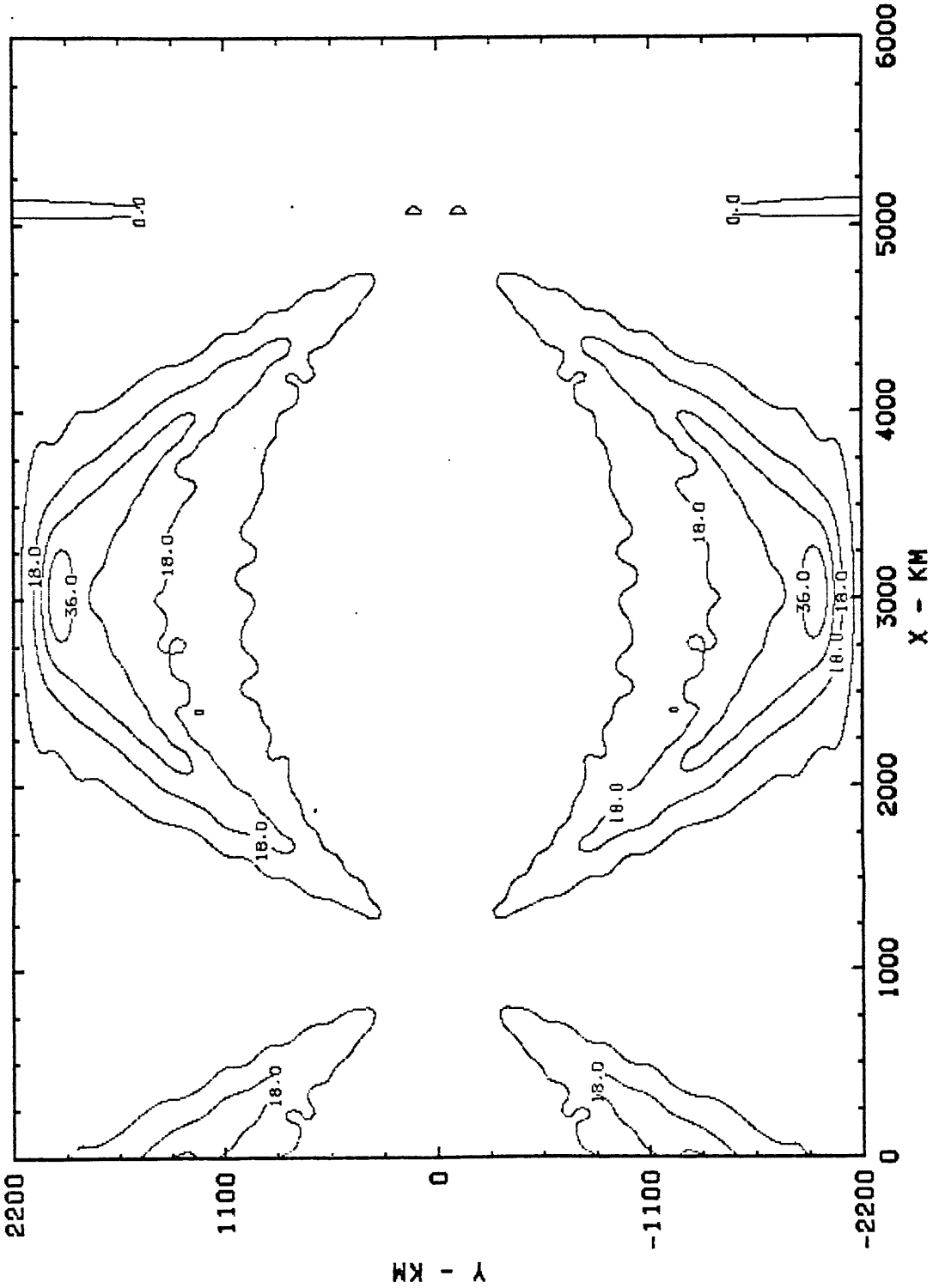

FIGURE 2.8

Zonal Velocity Amplitude
$(X_*, Y_*) = (3500, 0)$

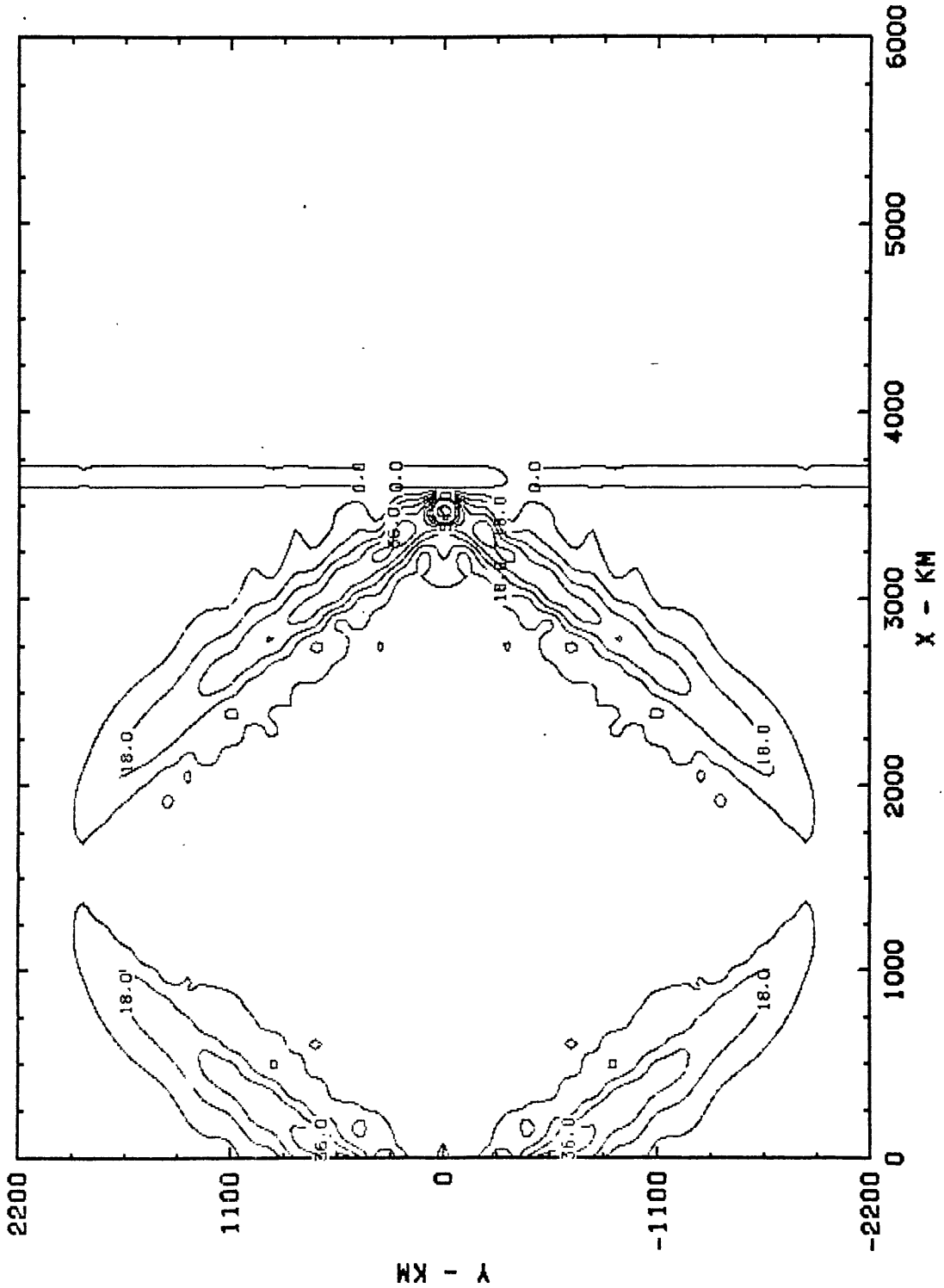

FIGURE 2.9

Zonal Velocity Amplitude
$(X_*, Y_*) = (1000, 0)$

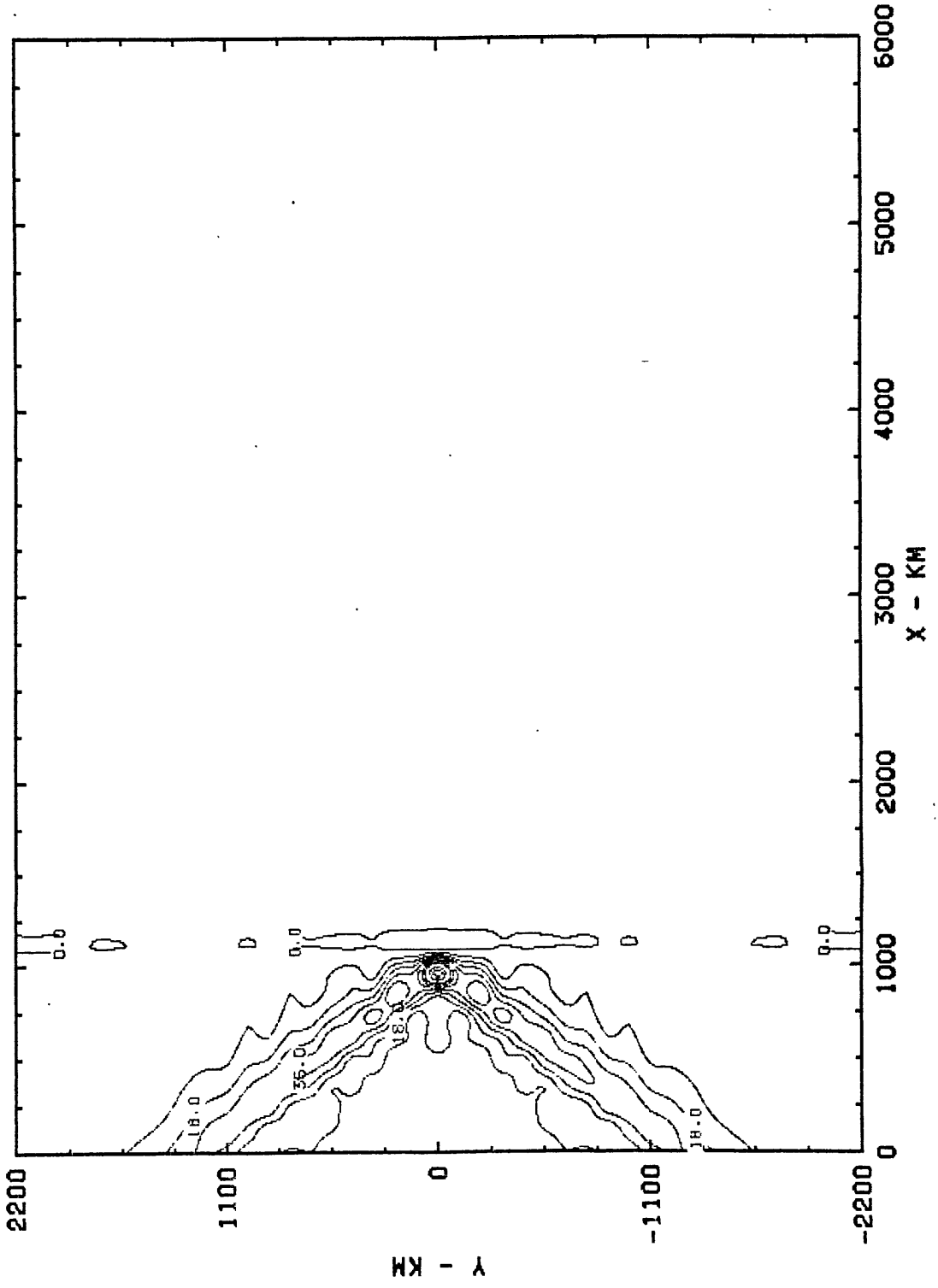

FIGURE 2.10

Meridional Velocity Real Part
$(X_*, Y_*) = (5000, 0)$ Time=0

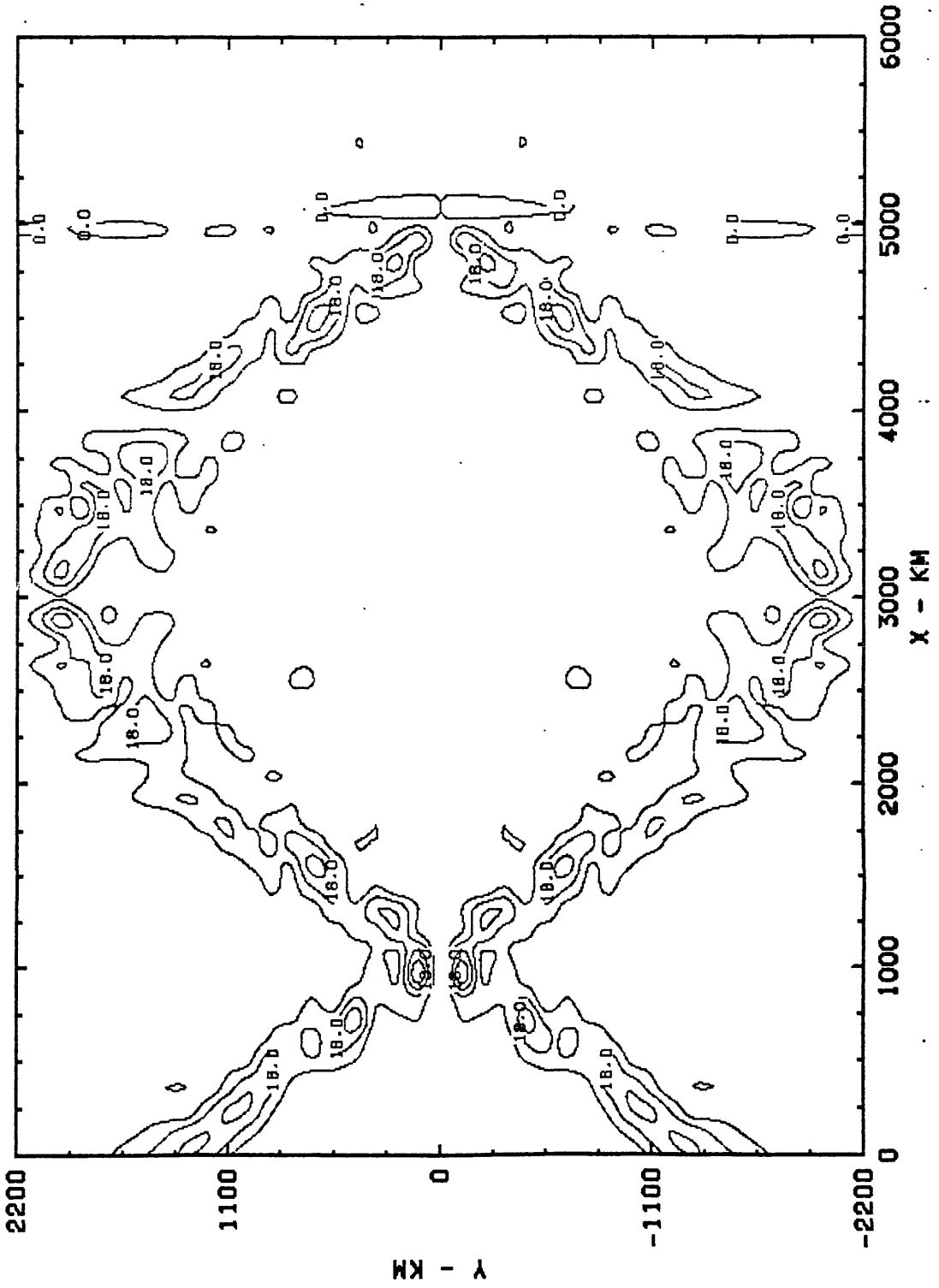

FIGURE 2.11

Meridional Velocity Real Part
$(X_*, Y_*) = (5000, 0)$ Time=$\frac{\pi}{4}$

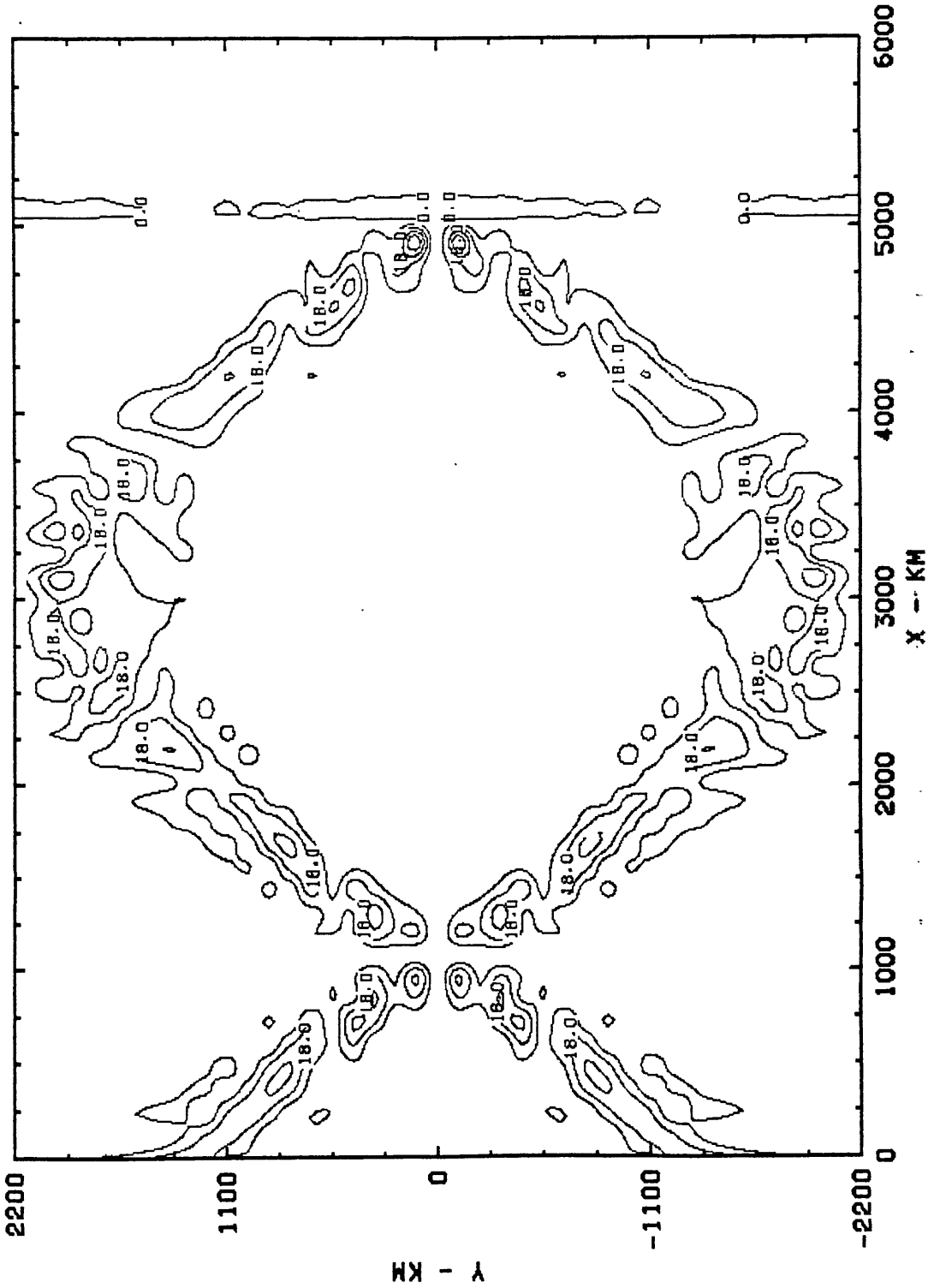

FIGURE 2.12

Meridional Velocity Real Part
$(X_*, Y_*) = (5000, 0)$ Time=$\pi/2$

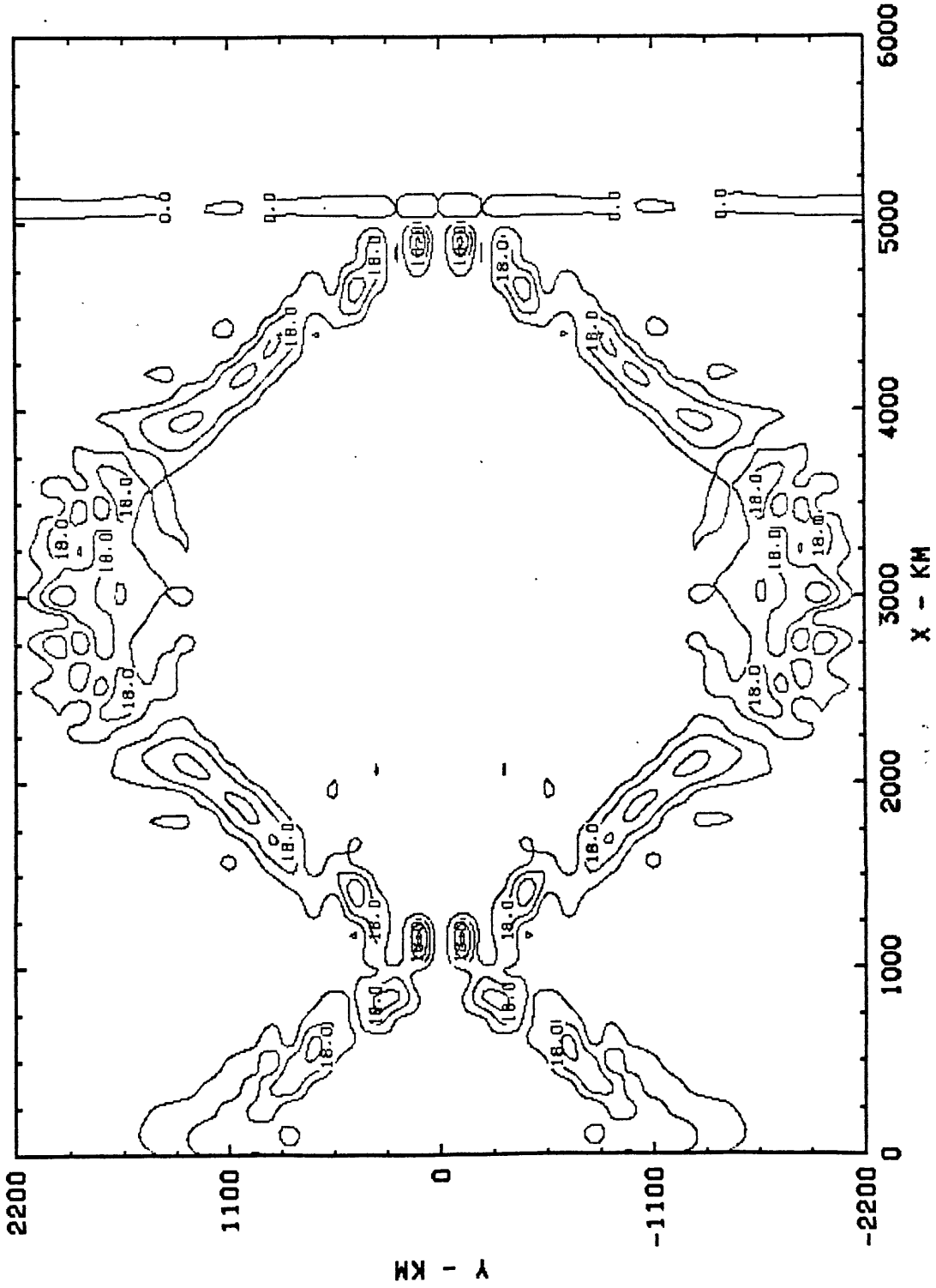

FIGURE 2.13

Zonal Velocity Amplitude
$(X_*, Y_*) = (5000, 500)$

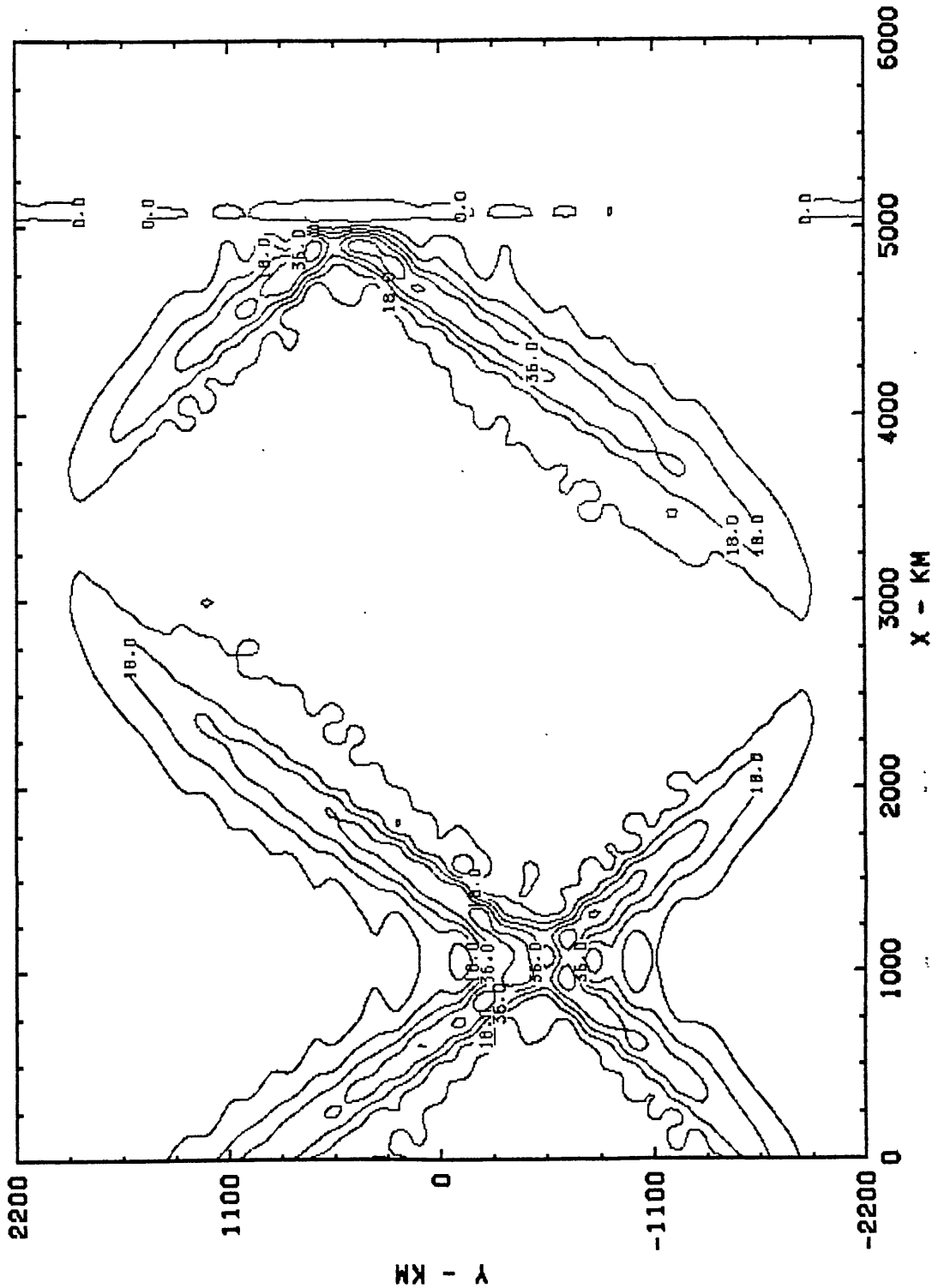

FIGURE 2.14

Zonal Velocity Amplitude
$(X_*, Y_*) = (5000, -500)$

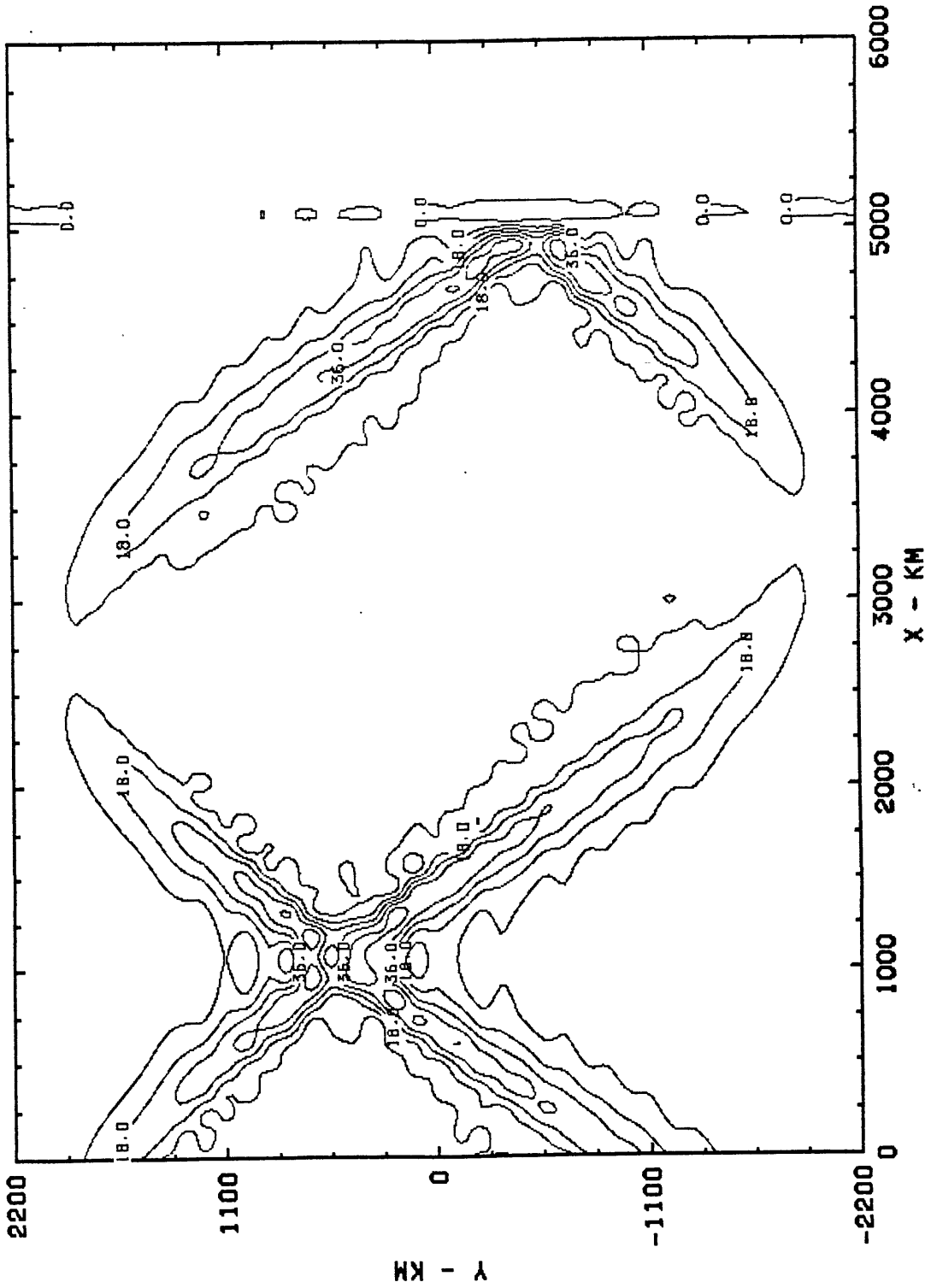

FIGURE 2.15

Zonal Velocity Amplitude
$(X_*, Y_*) = (5000, 1000)$

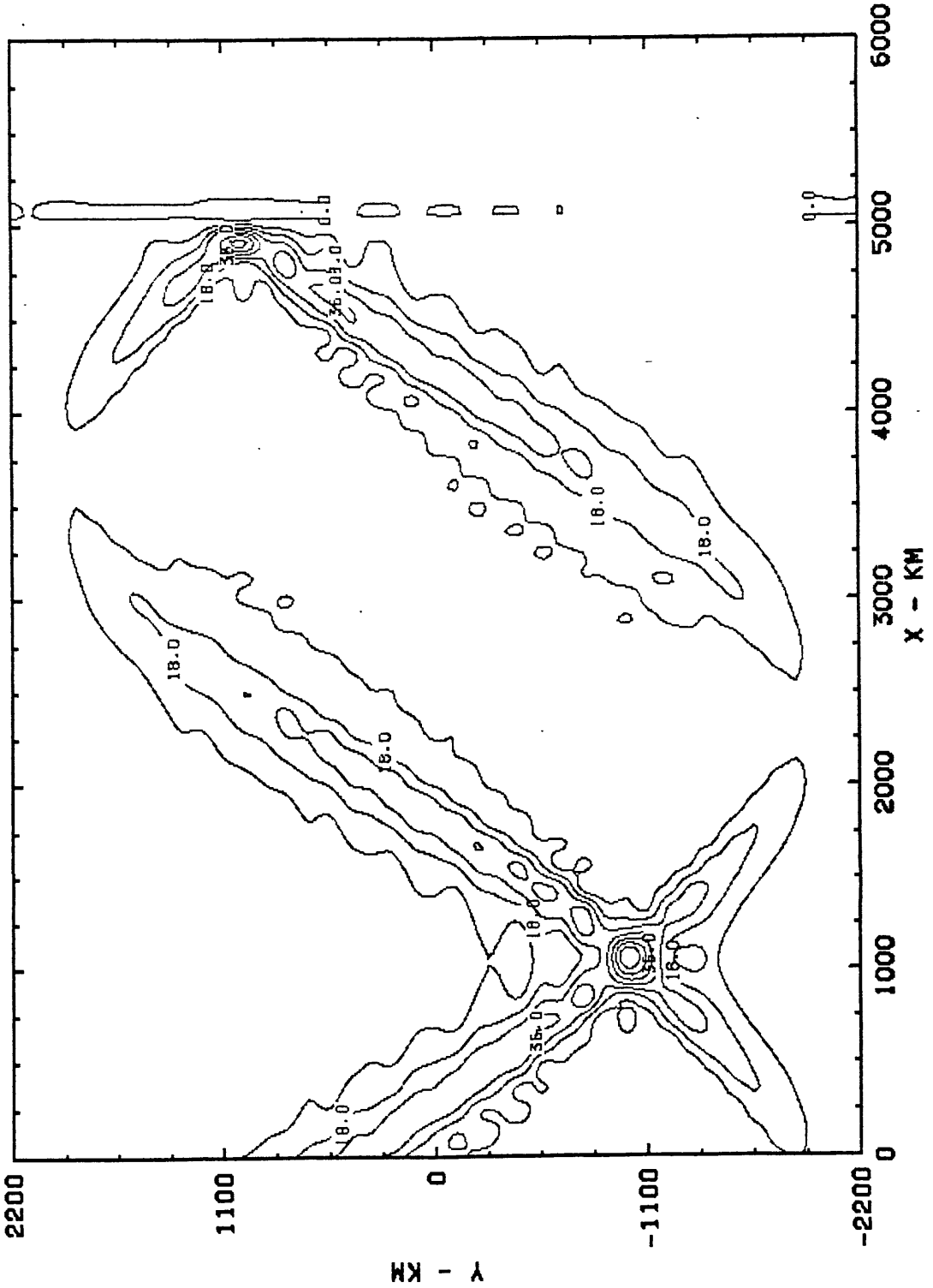

FIGURE 2.16

Zonal Velocity Amplitude
$(X_*, Y_*) = (5000, 0)$ Modes=7

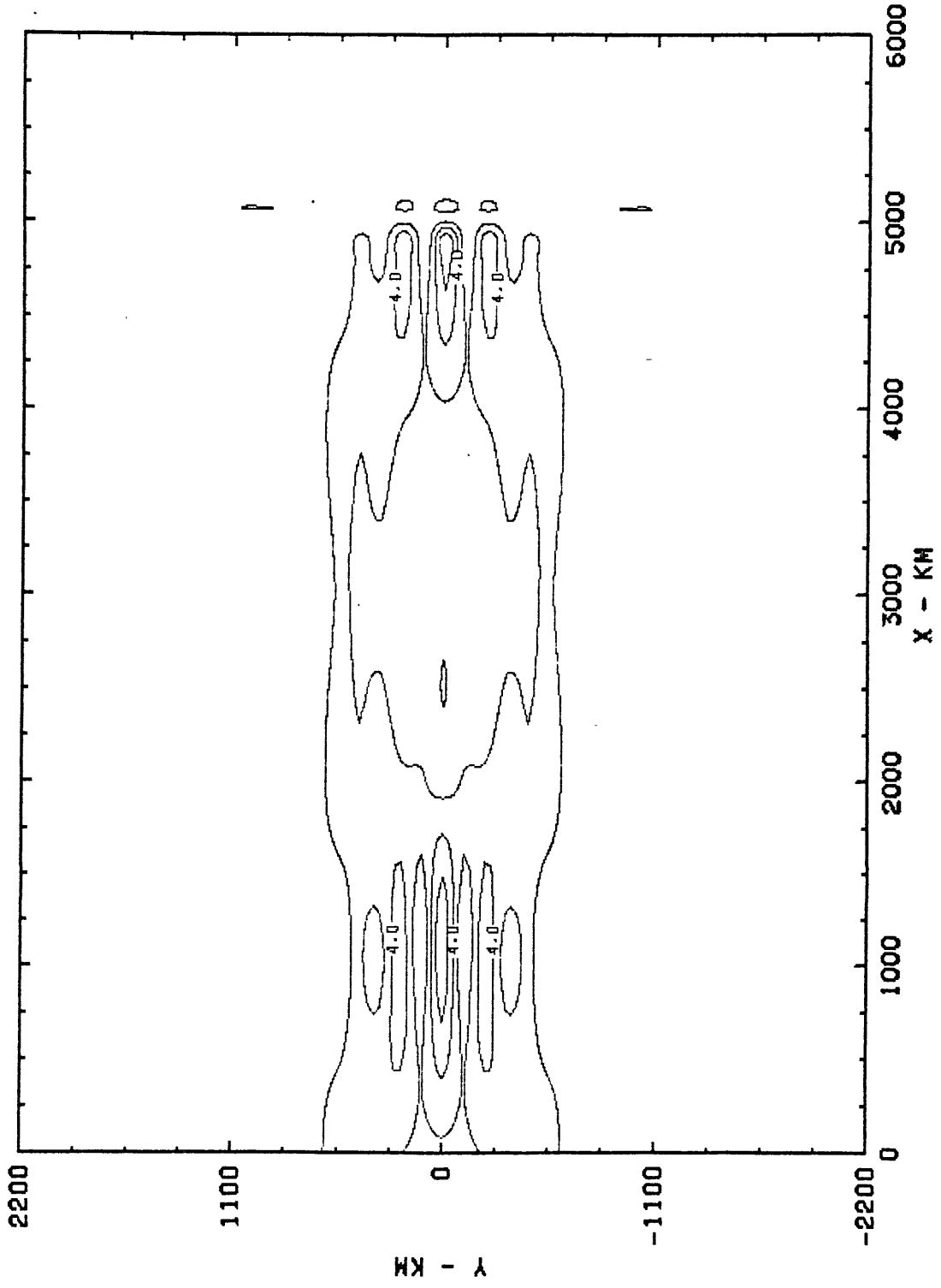

FIGURE 2.17

Meridional Velocity Amplitude
(X_*, Y_*) = (5000,0) Modes=7

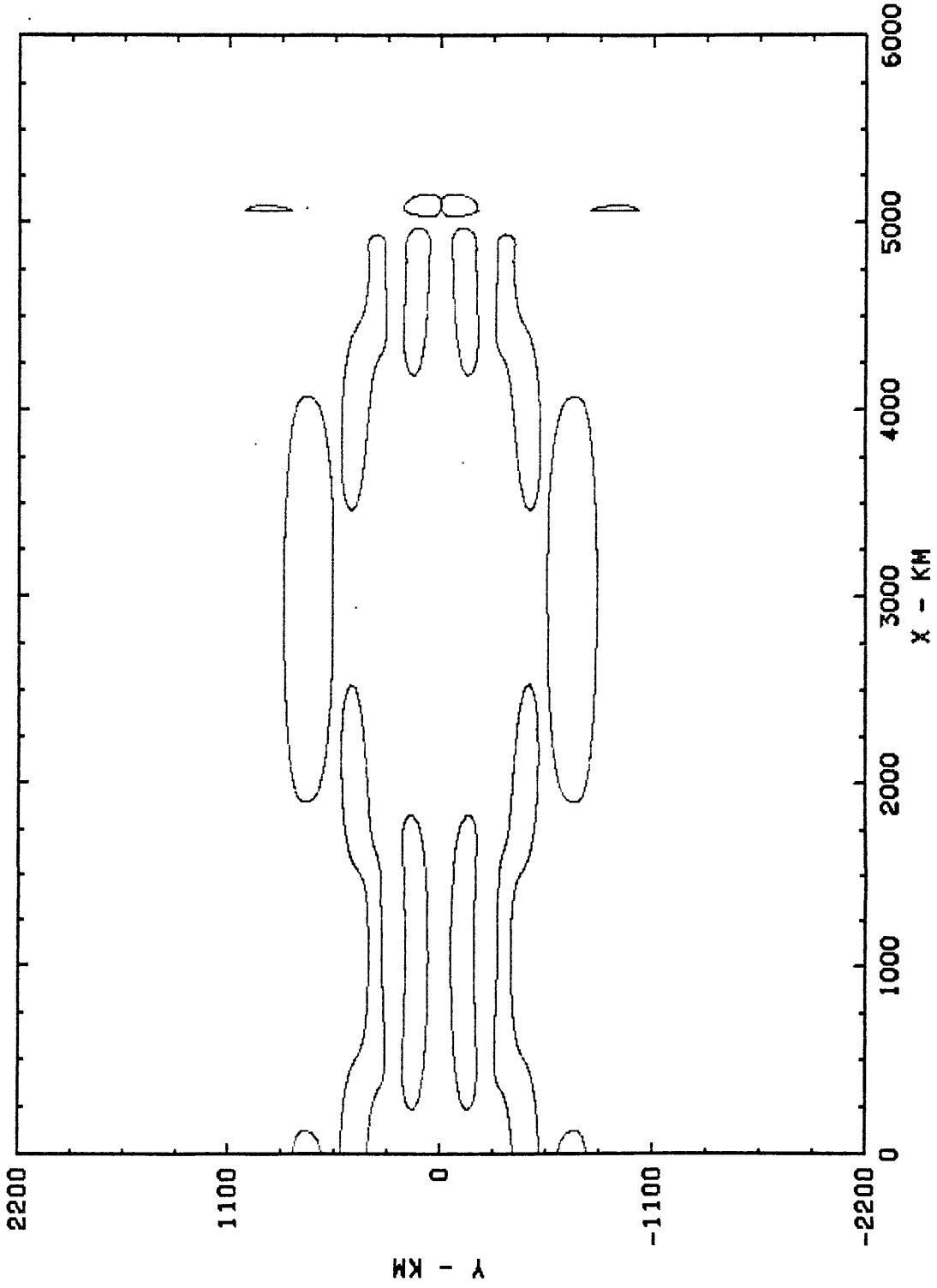

FIGURE 2.18

Height Field Amplitude
(X_*, Y_*) = (5000,0) Modes=7

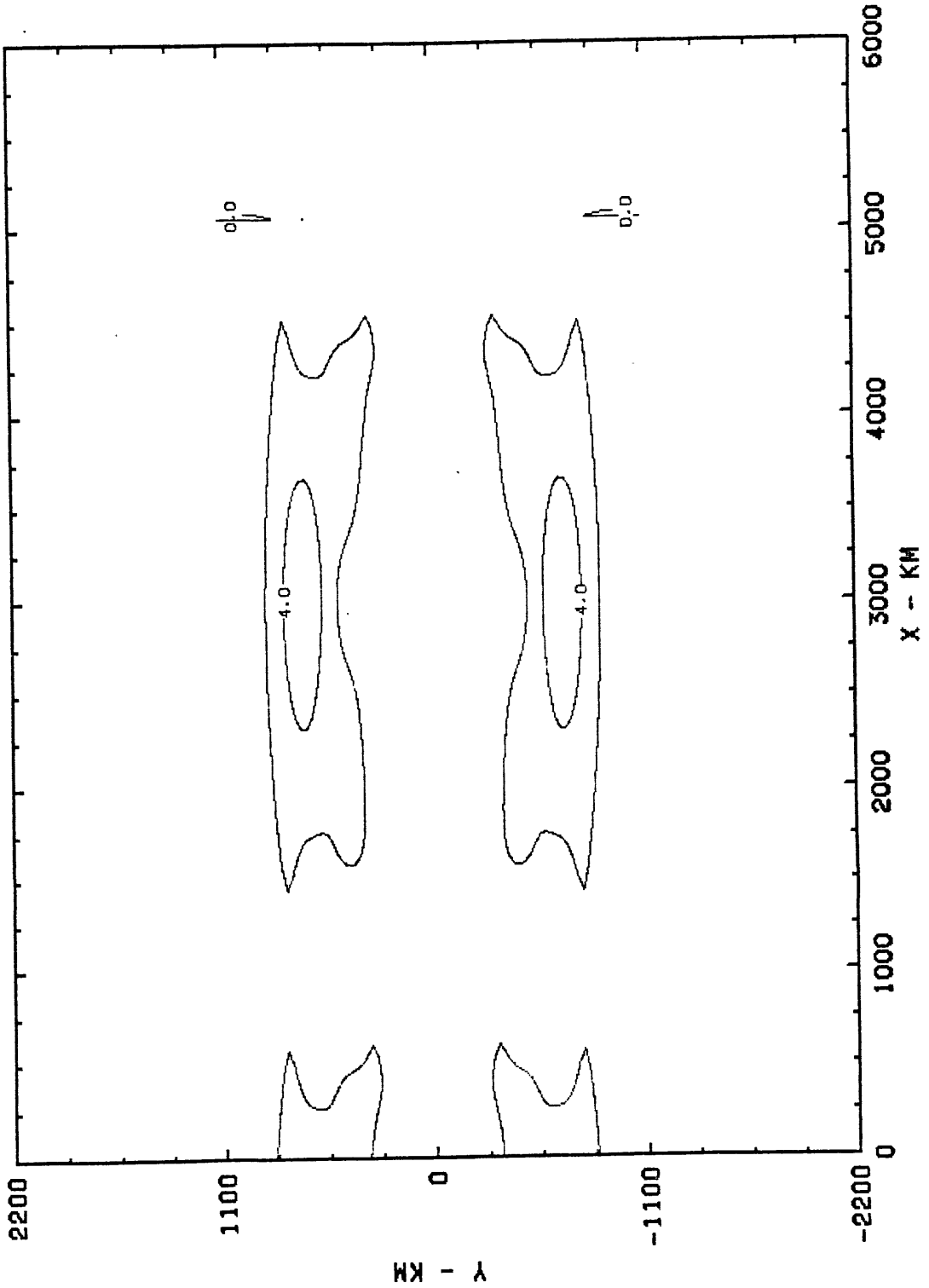

FIGURE 2.19

Zonal Velocity Amplitude
(X_*, Y_*) = (5000,500) Modes=7

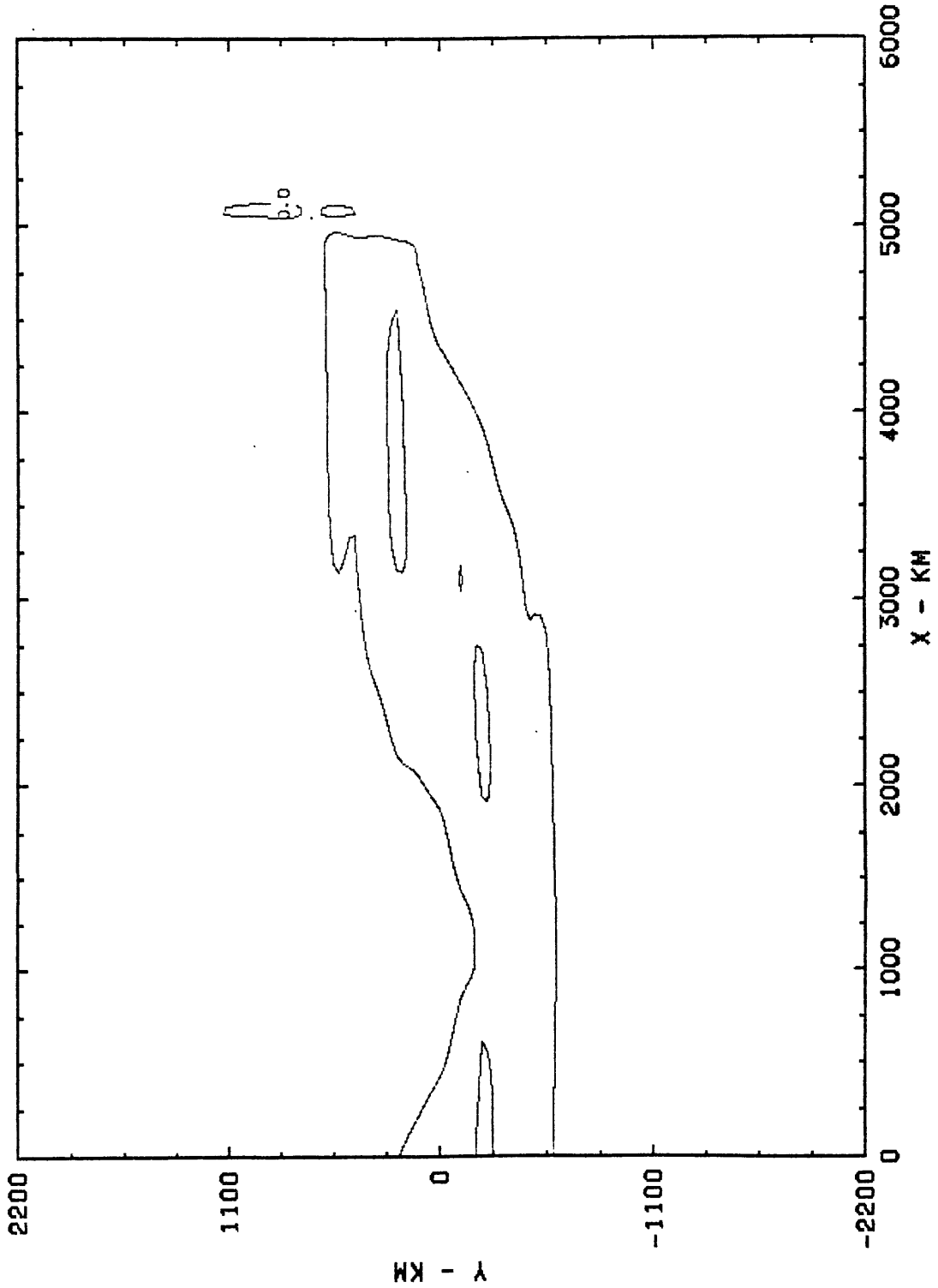

FIGURE 2.20

Zonal Velocity Amplitude
(X_*, Y_*) = (5000,1000) Modes=7

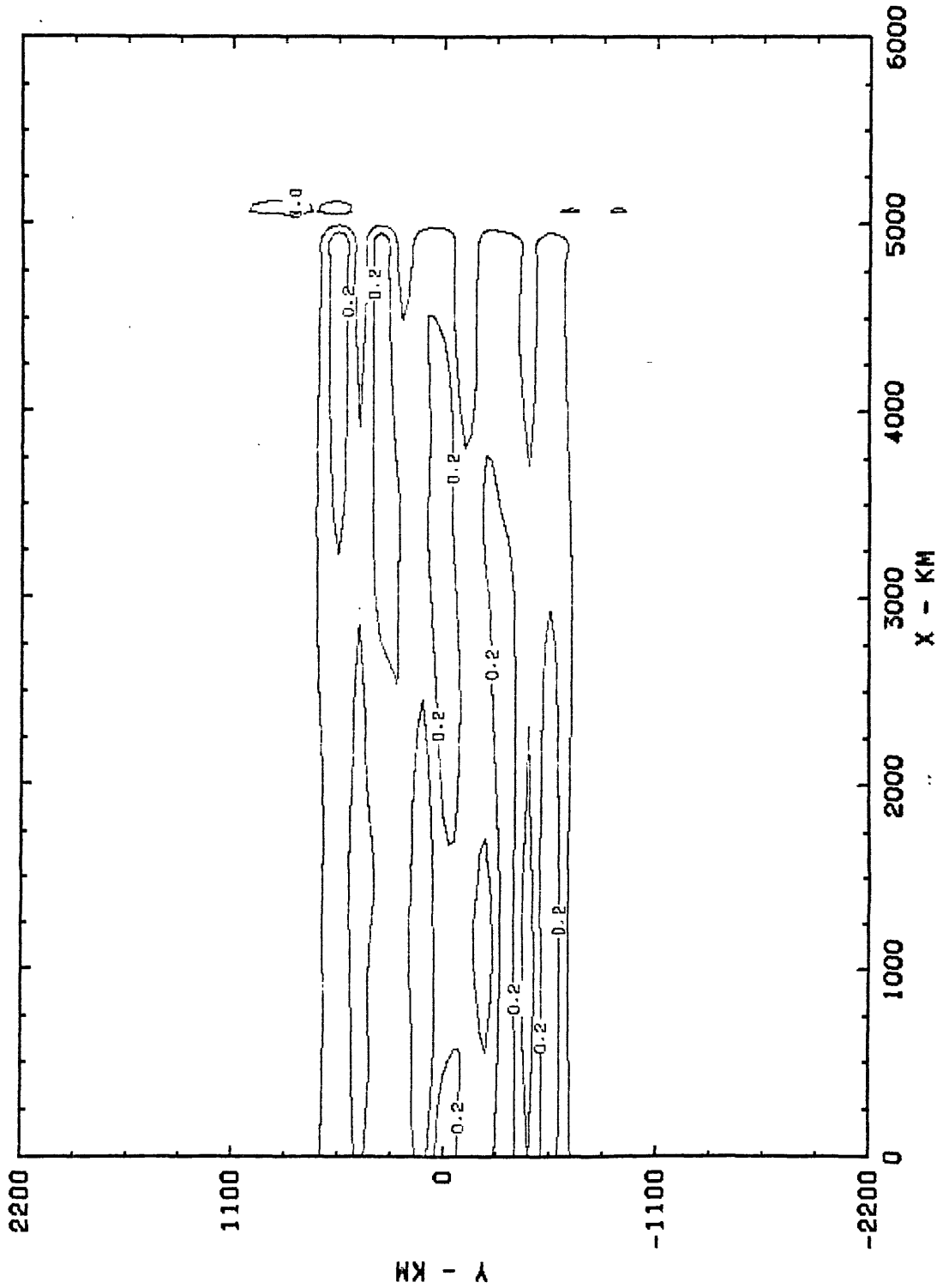

FIGURE 2.21

Zonal Velocity Amplitude
(X_*, Y_*) = (5000,0) R=5 Years

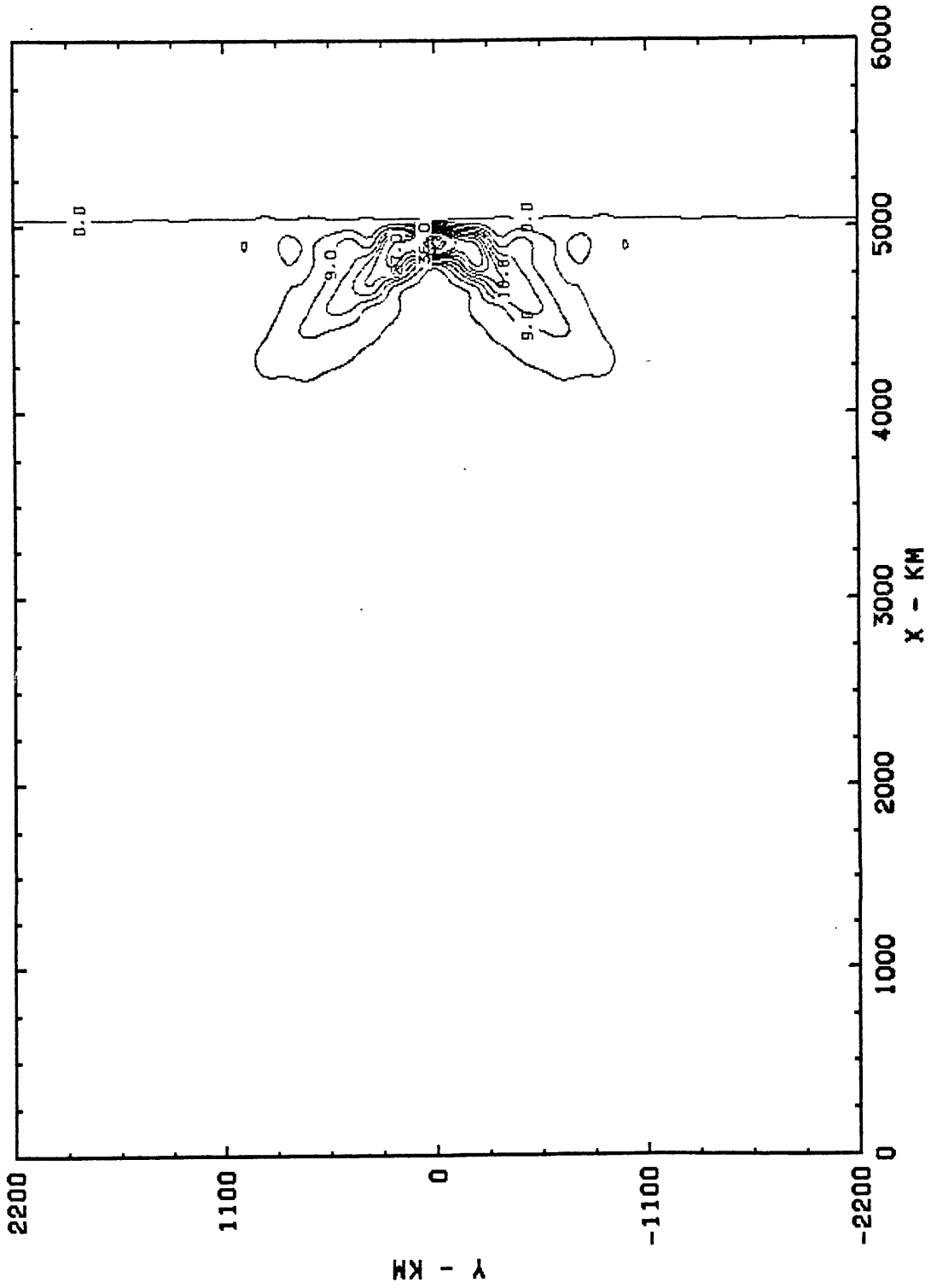

FIGURE 2.22

Zonal Velocity Amplitude
(X_*, Y_*) = (5000,0) R=50 Years

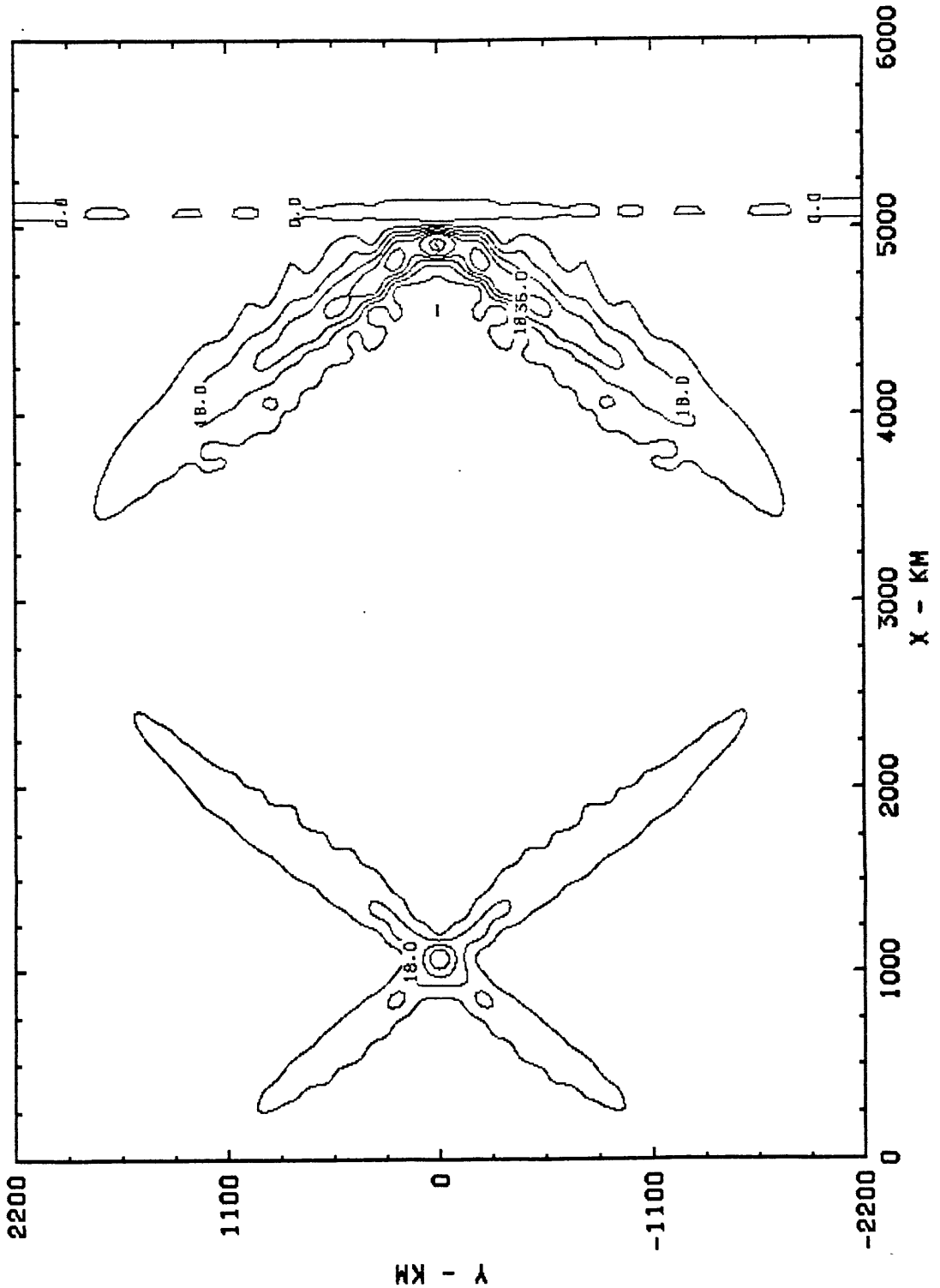

FIGURE 3.1

Ray Paths
$(X_*, Y_*) = (5000, 0)$

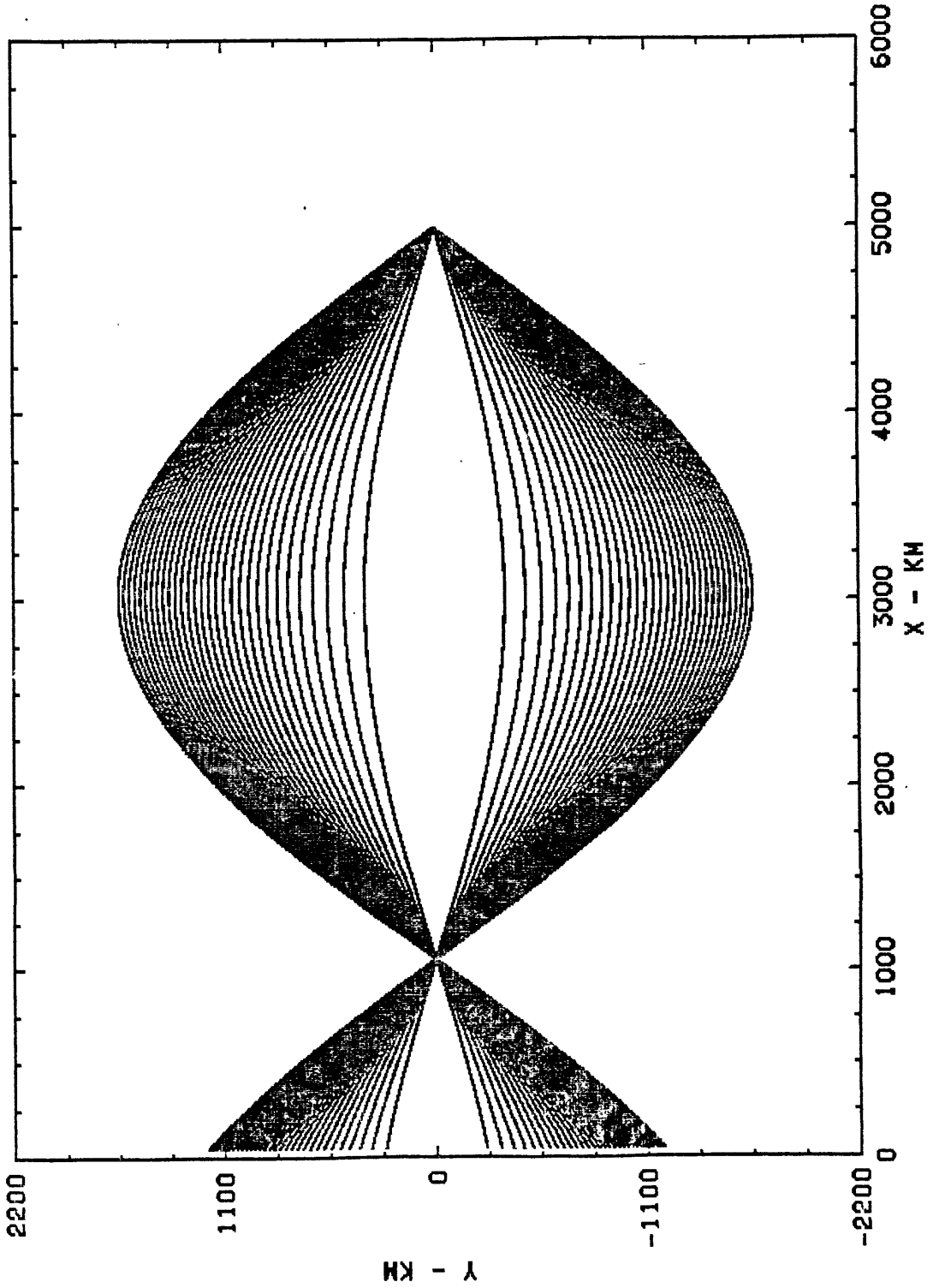

FIGURE 3.2

Total Energy
$(X_*, Y_*) = (5000, 0)$

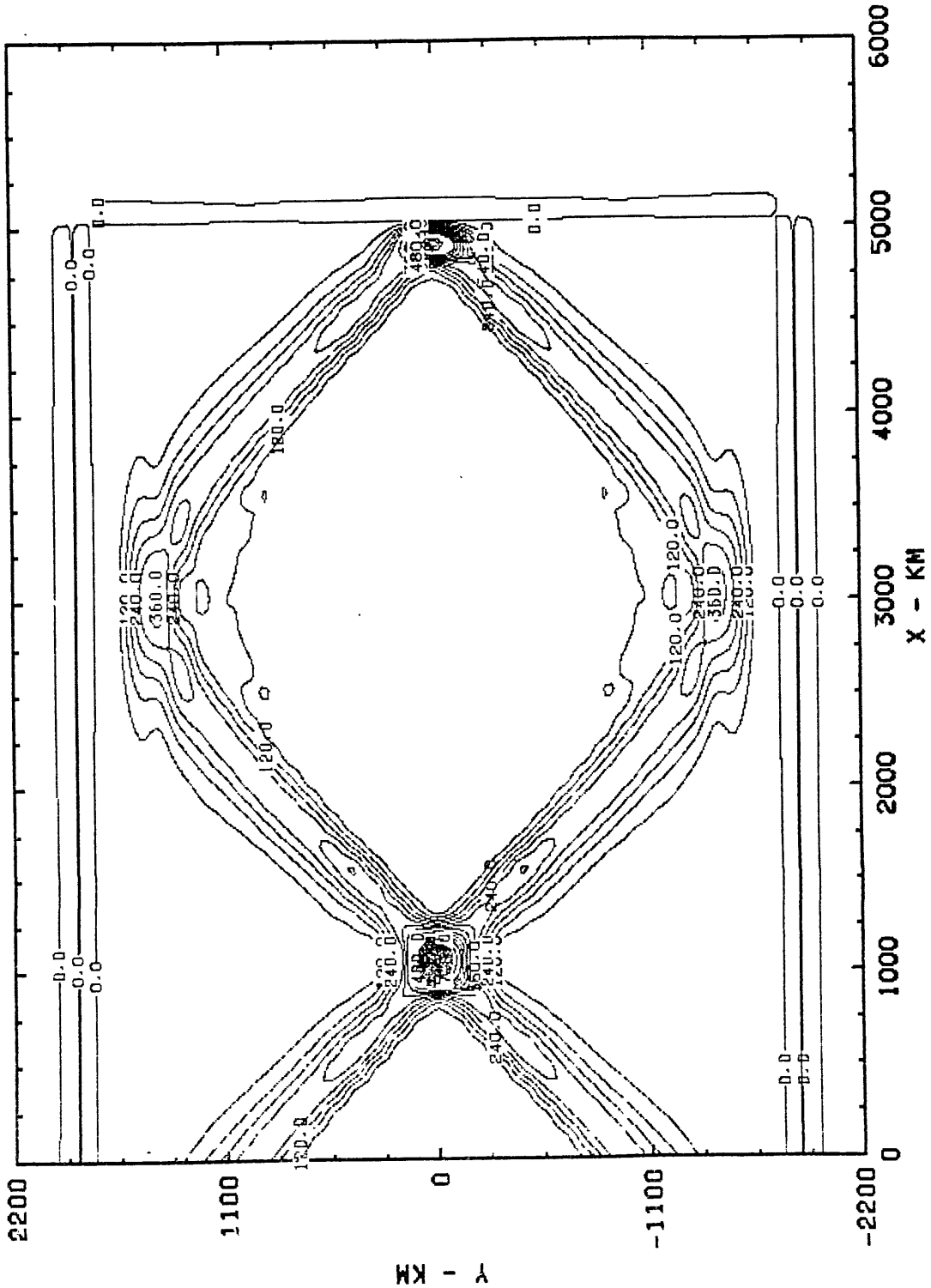

FIGURE 3.3

Ray Energy Density
$(X_*, Y_*) = (5000, 0)$

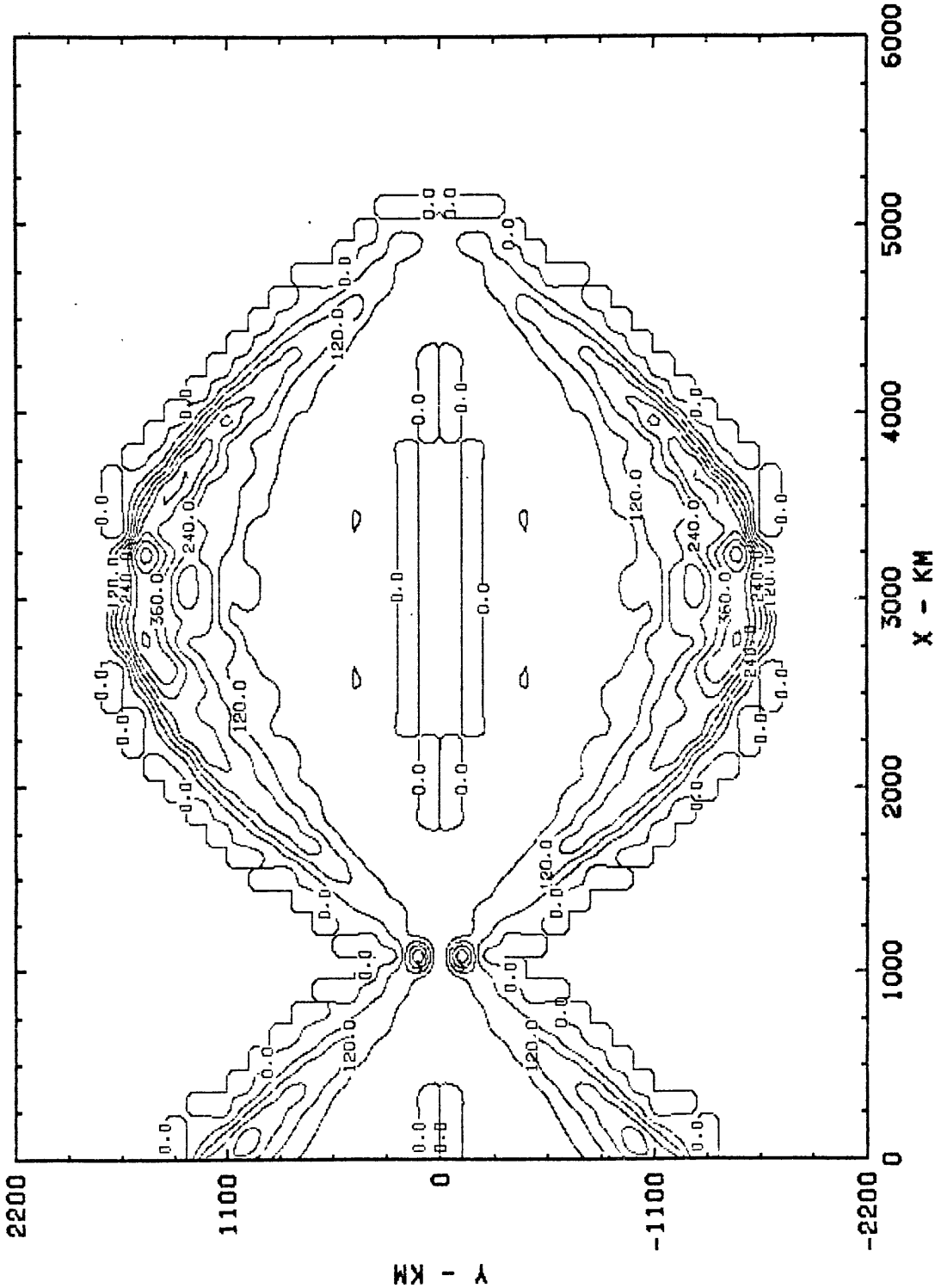

FIGURE 3.4

Ray Paths
$(X_*, Y_*) = (5000, 1000)$

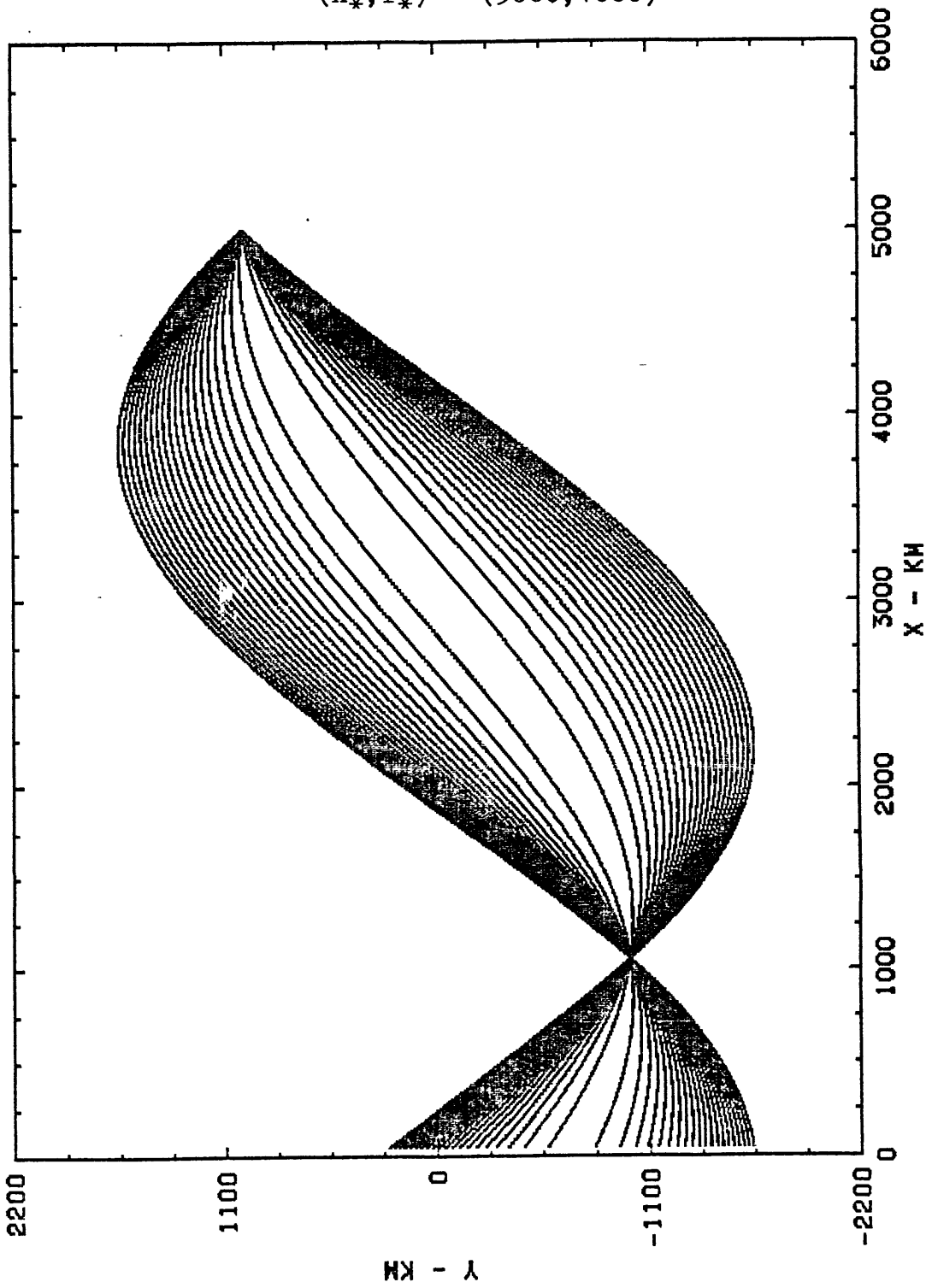

FIGURE 3.5

Total Energy
$(X_*, Y_*) = (5000, 1000)$

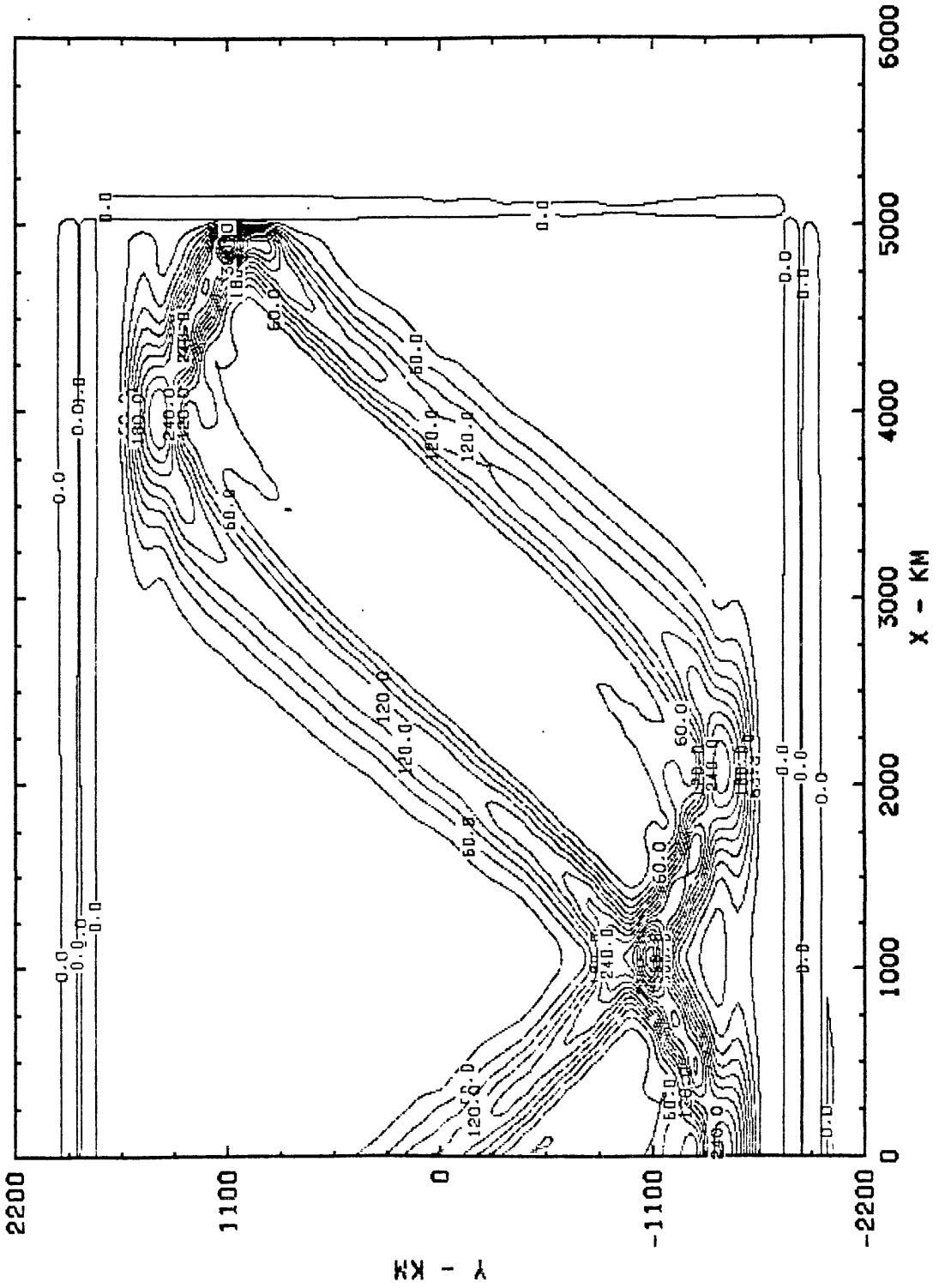

FIGURE 3.6

Ray Energy Density
$(X_*, Y_*) = (5000, 1000)$

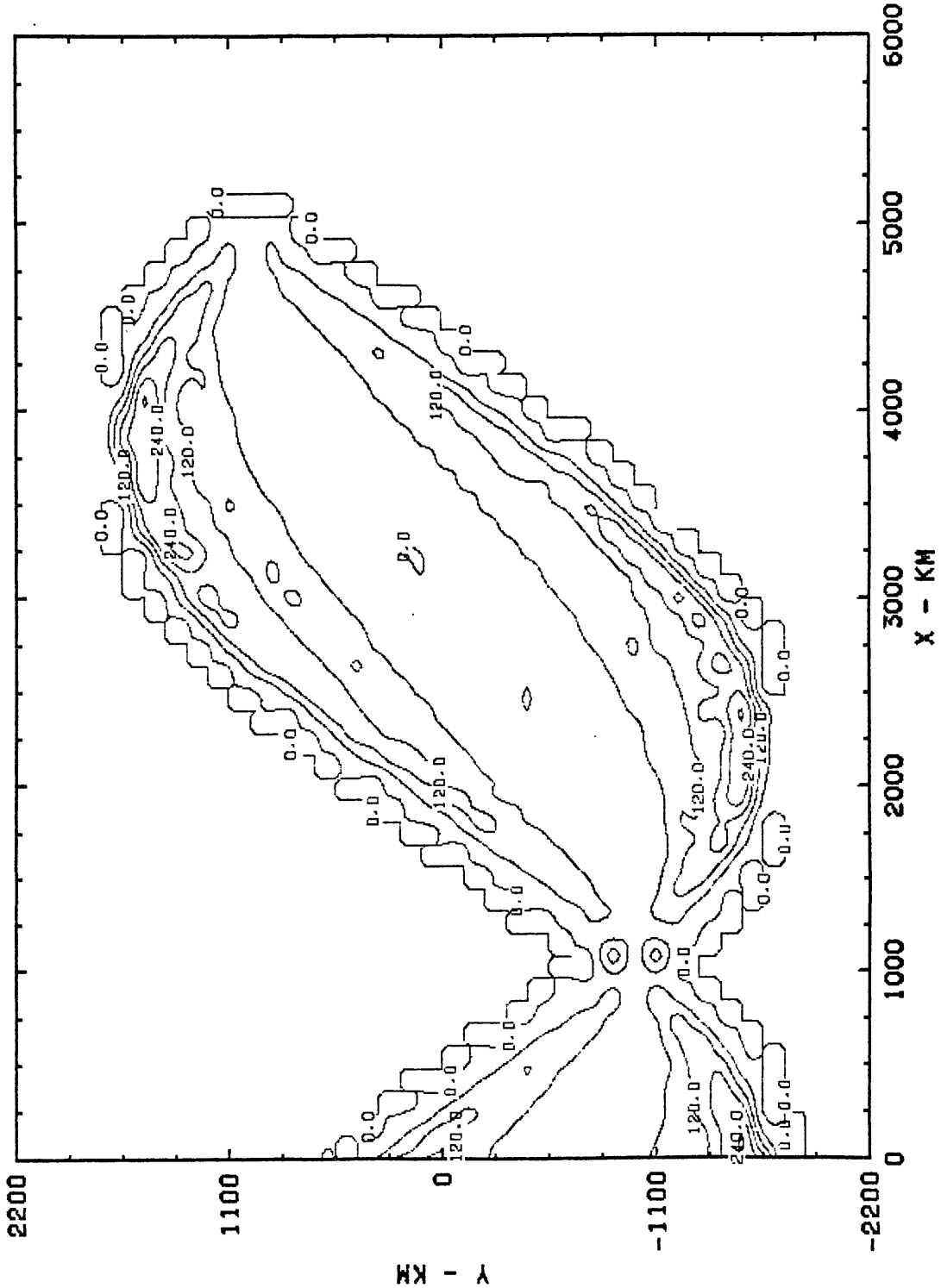

FIGURE 4.1

Patch Rho Amplitude
Box = (20km x 20km)

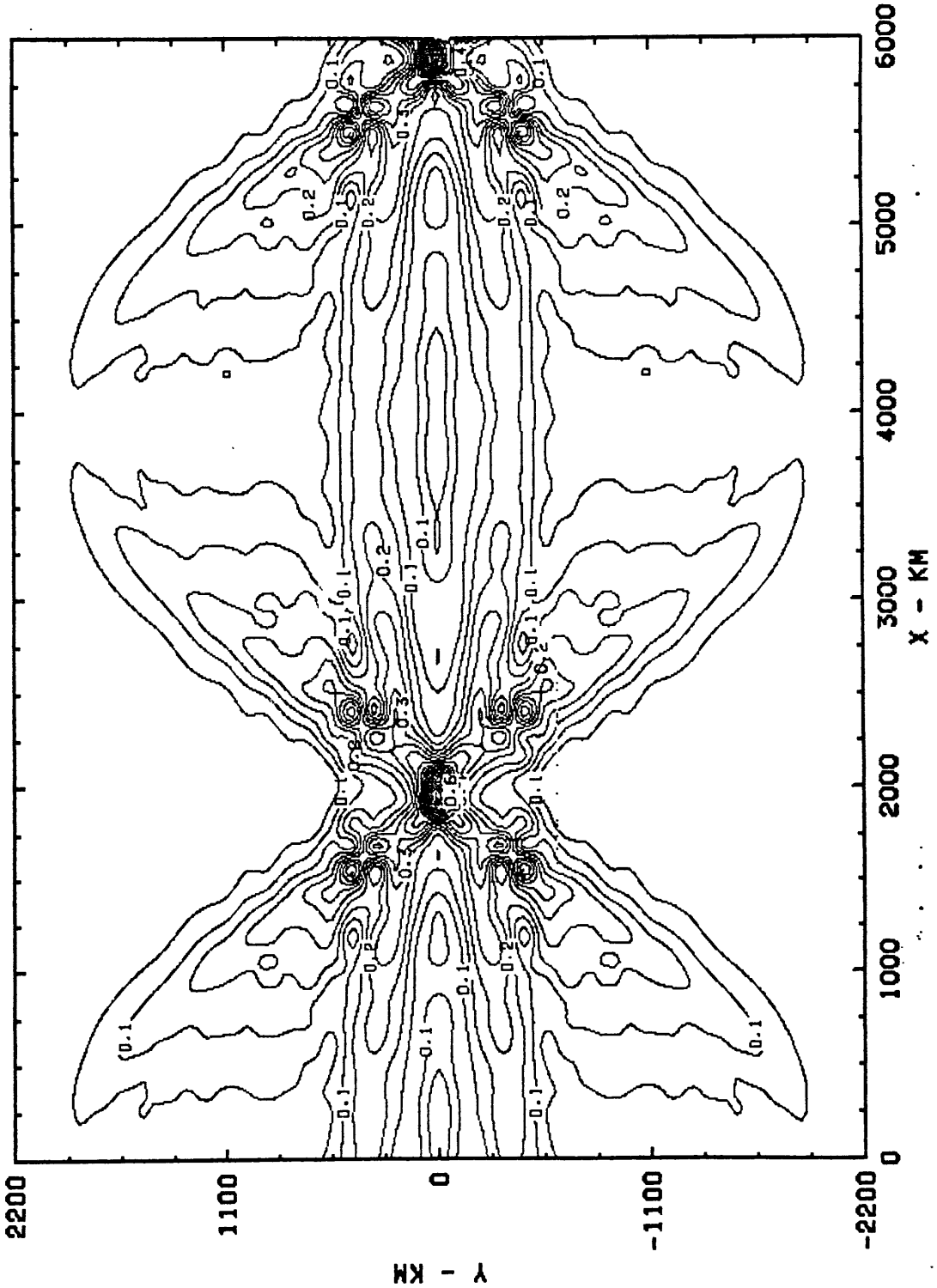

FIGURE 4.2

Patch Rho Amplitude
Box = (2° x 2°)

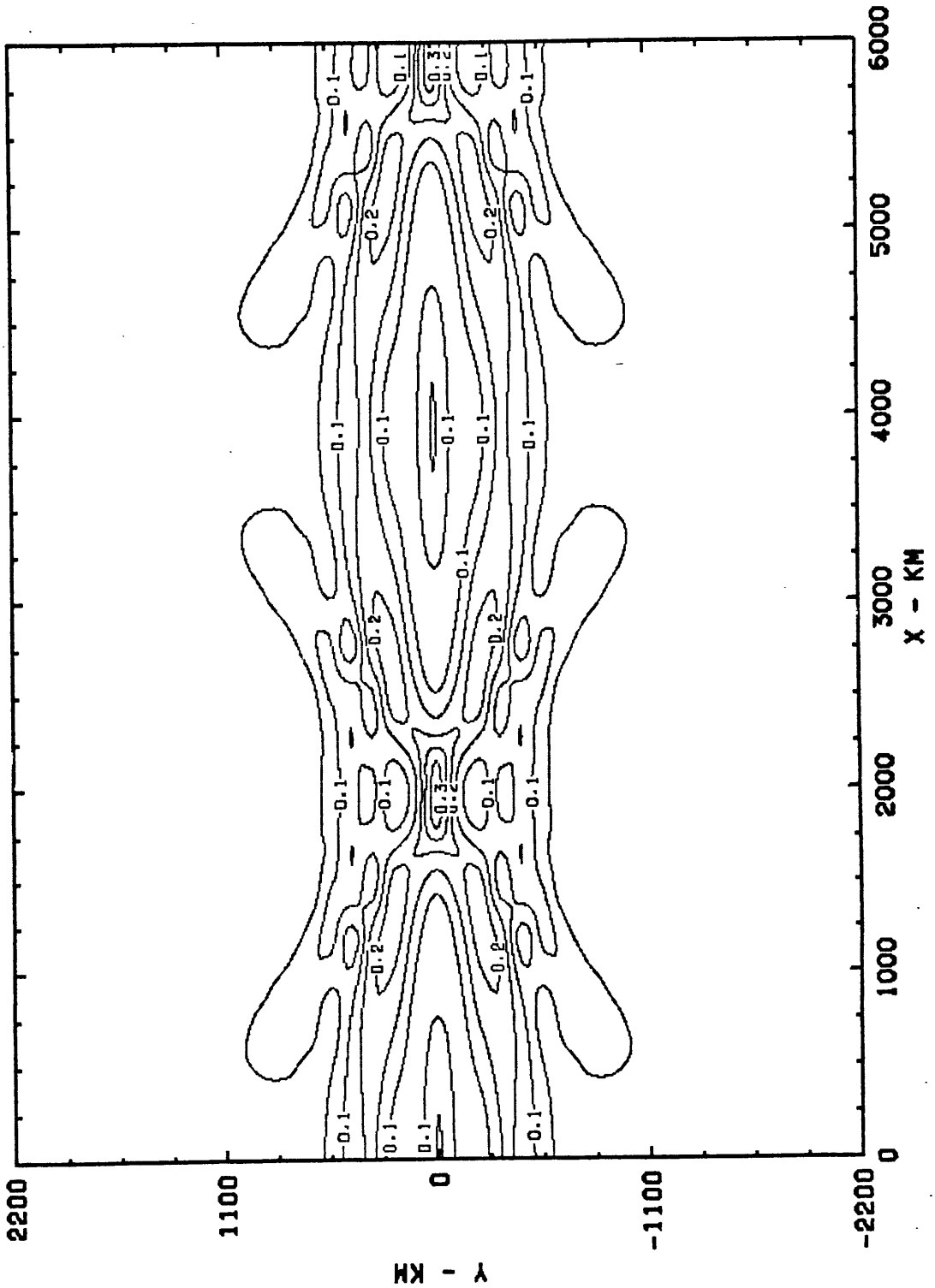

FIGURE 4.3

Patch Rho Amplitude
Box = (4° x 4°)

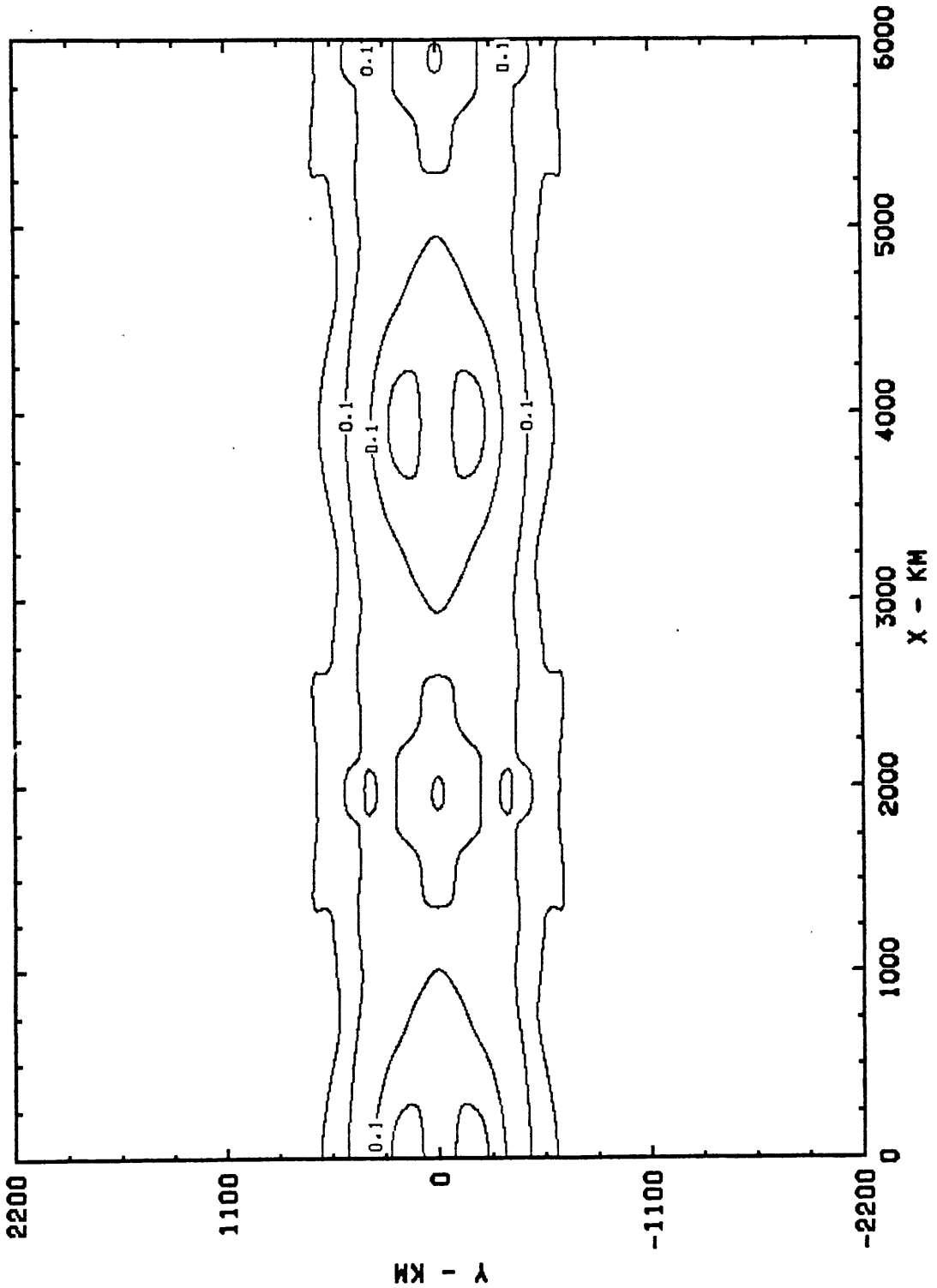

FIGURE 4.4

Patch Zonal Velocity
(X',Y')=(5000,0) Box=(4° x4°)

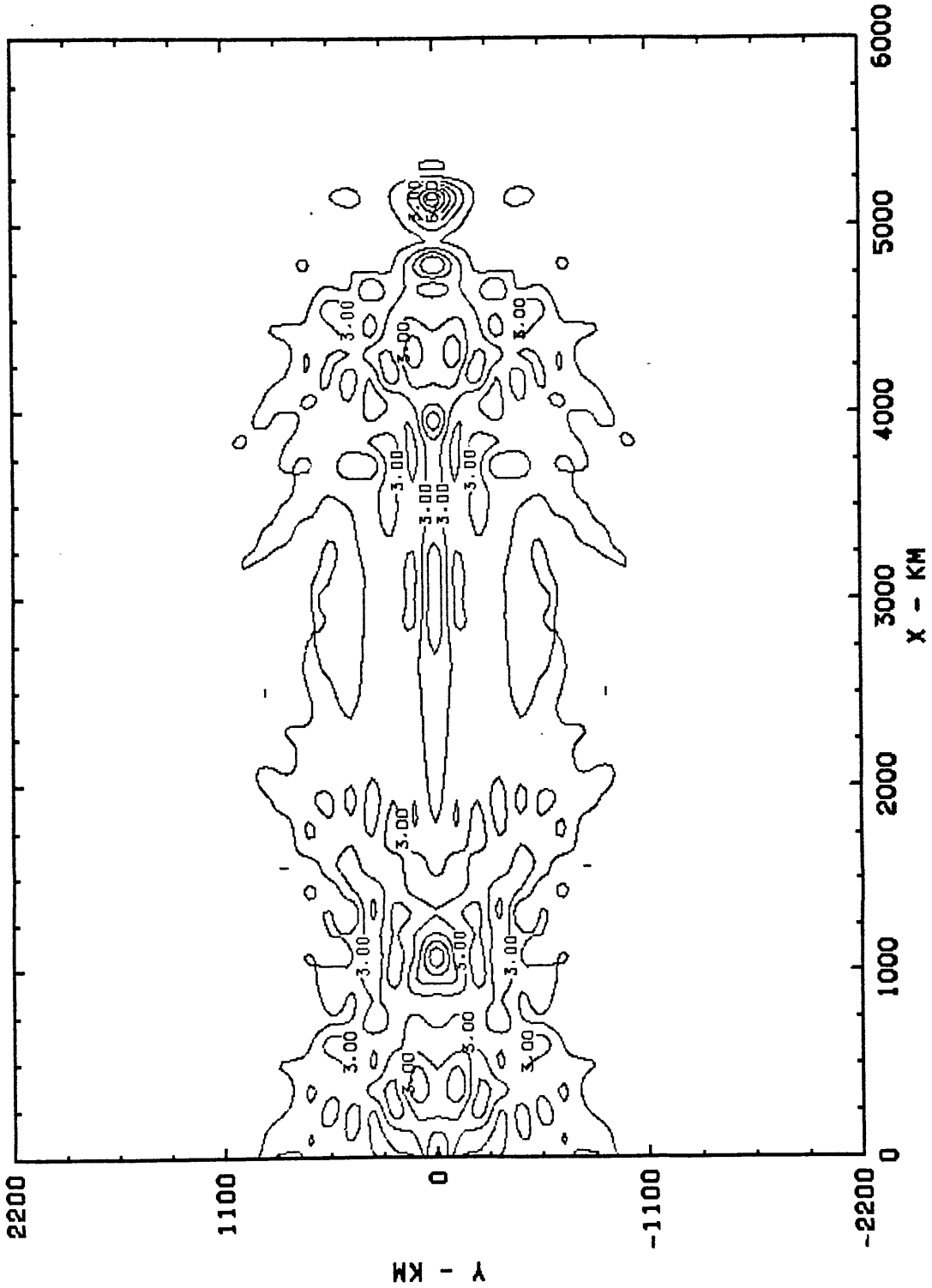

FIGURE 4.5

Patch Meridional Velocity
(X',Y')=(5000,0) Box=(4° x4°)

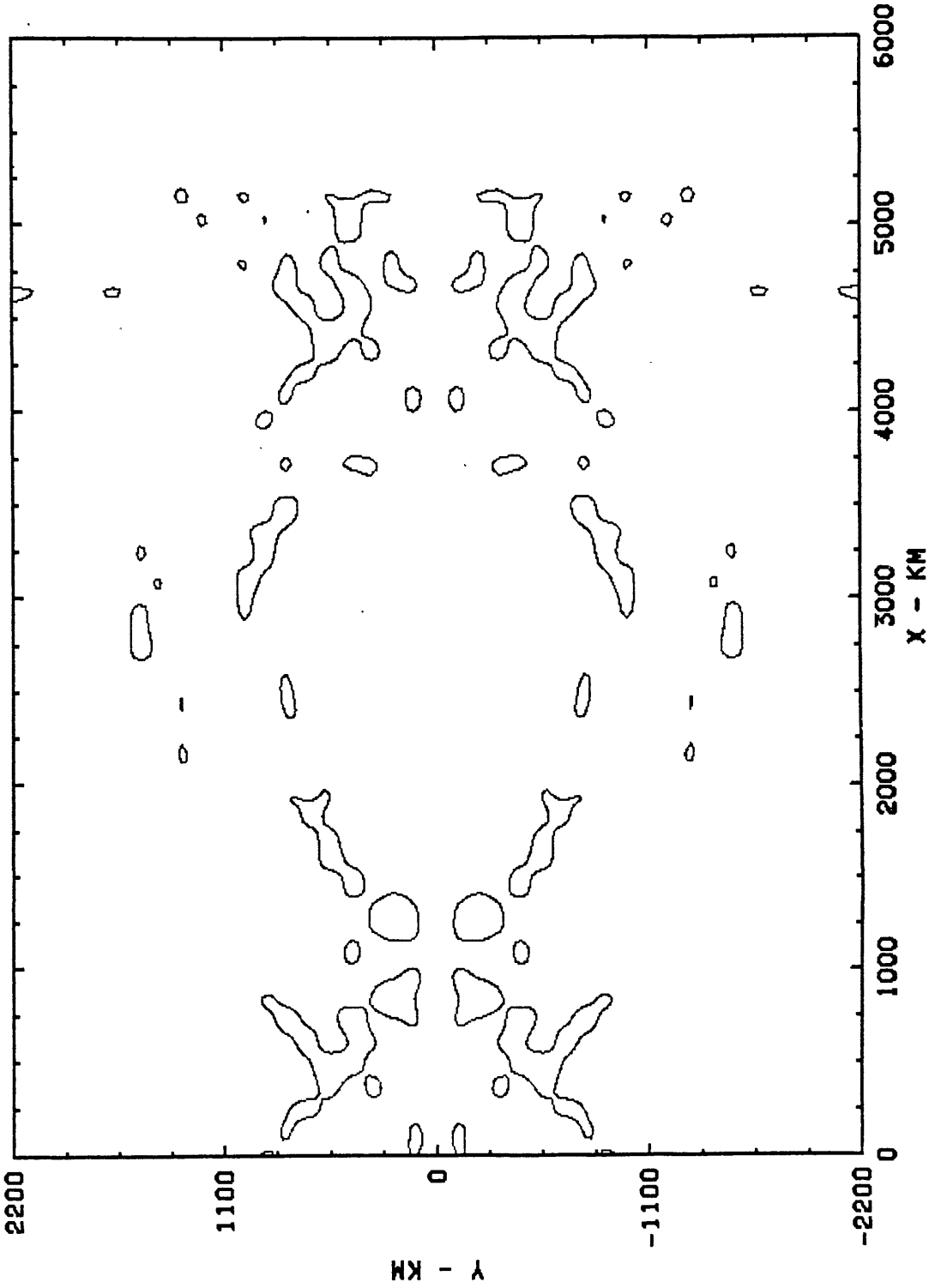

FIGURE 4.6

Patch Height Field
(X',Y')=(5000,0) Box=(4^{o}x4^{o})

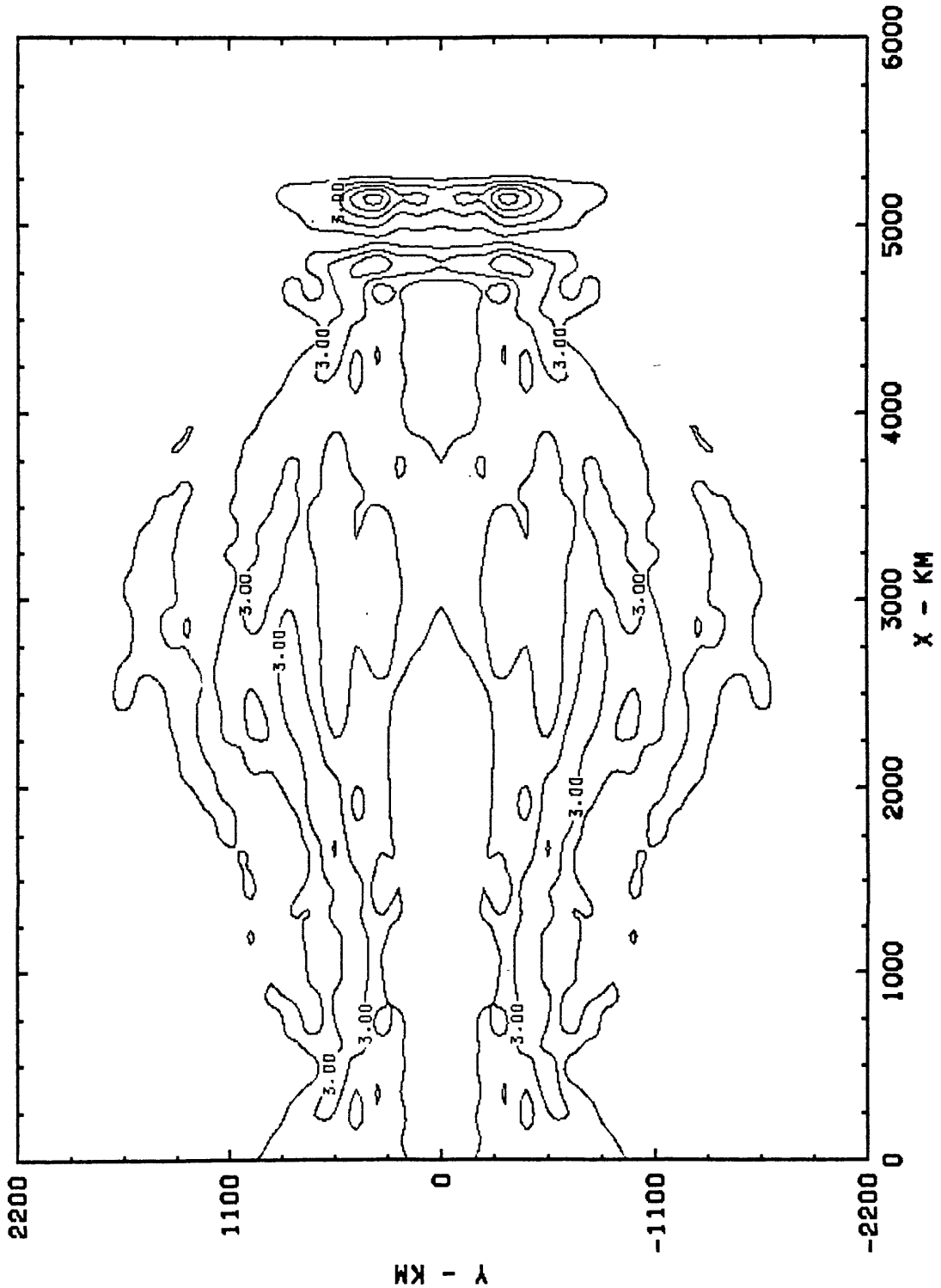

FIGURE 4.7

Patch Zonal Velocity
(X',Y')=(5000,0) Box=(2^c x2^o)

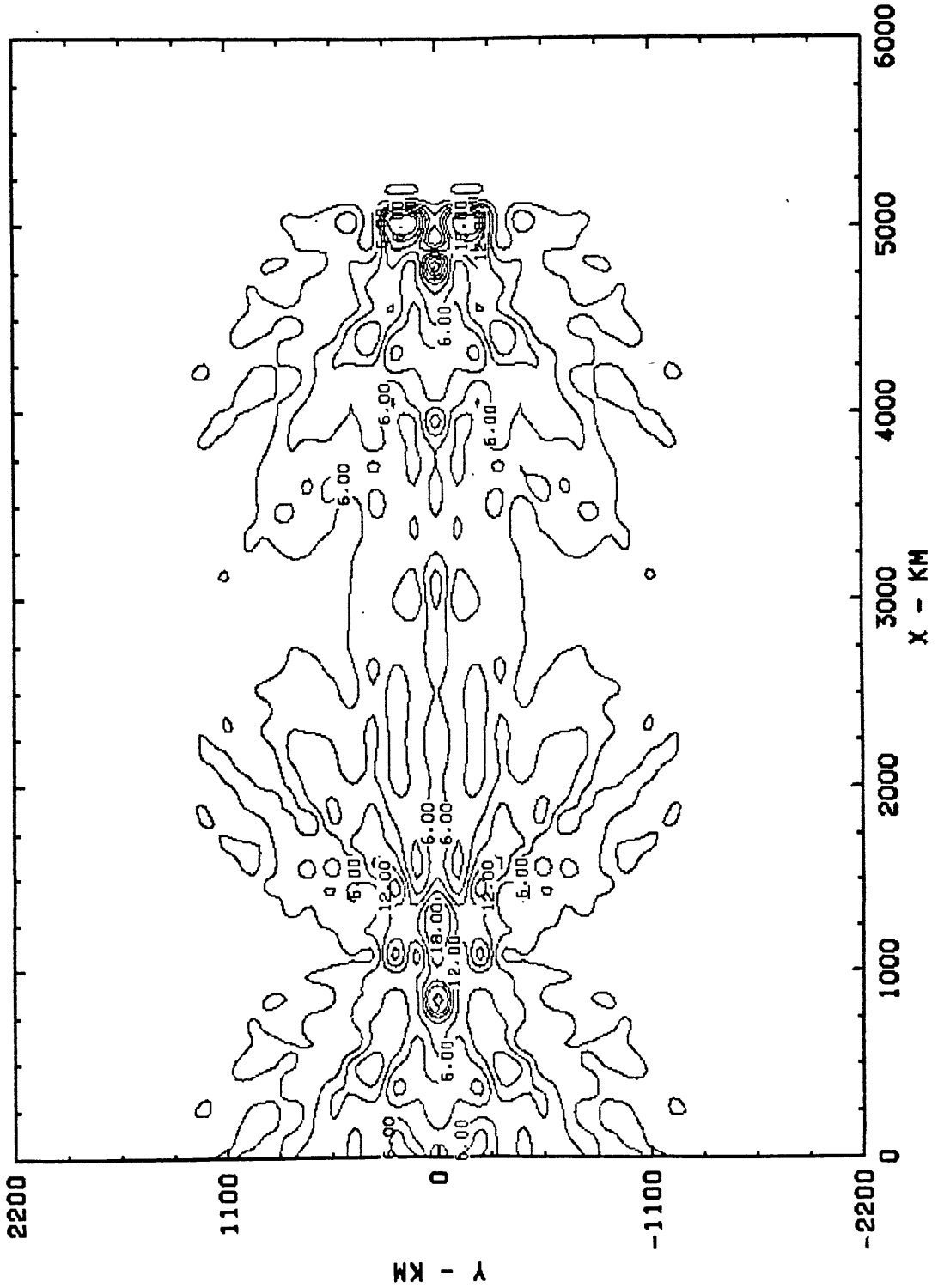

FIGURE 4.8

Patch Zonal Velocity
(X',Y')=(5000,0) Box=(4° x4°) Modes=7

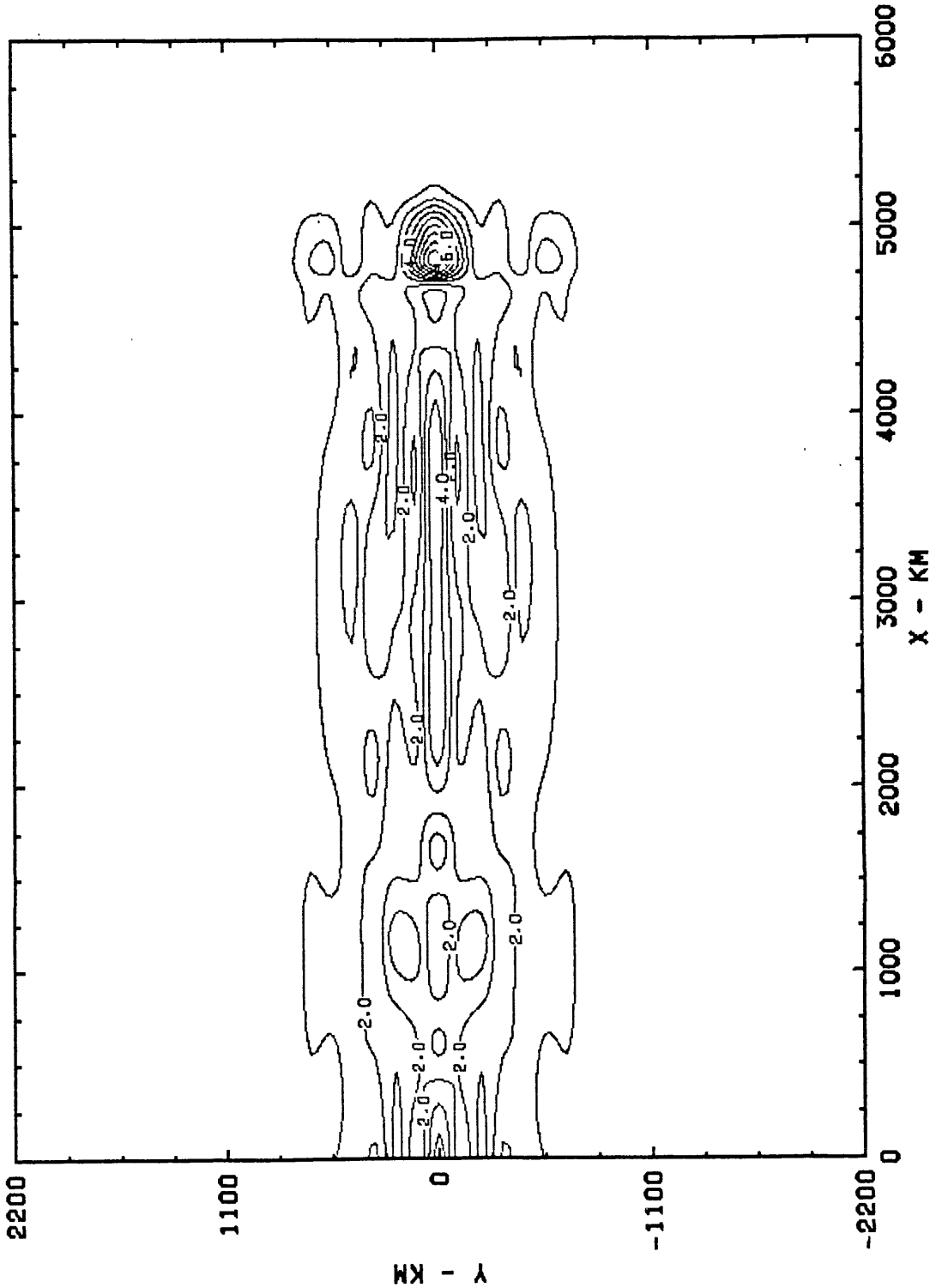

FIGURE 4.9

Patch Meridional Velocity
(X',Y')=(5000,0) Box=(4°x4°) Modes=7

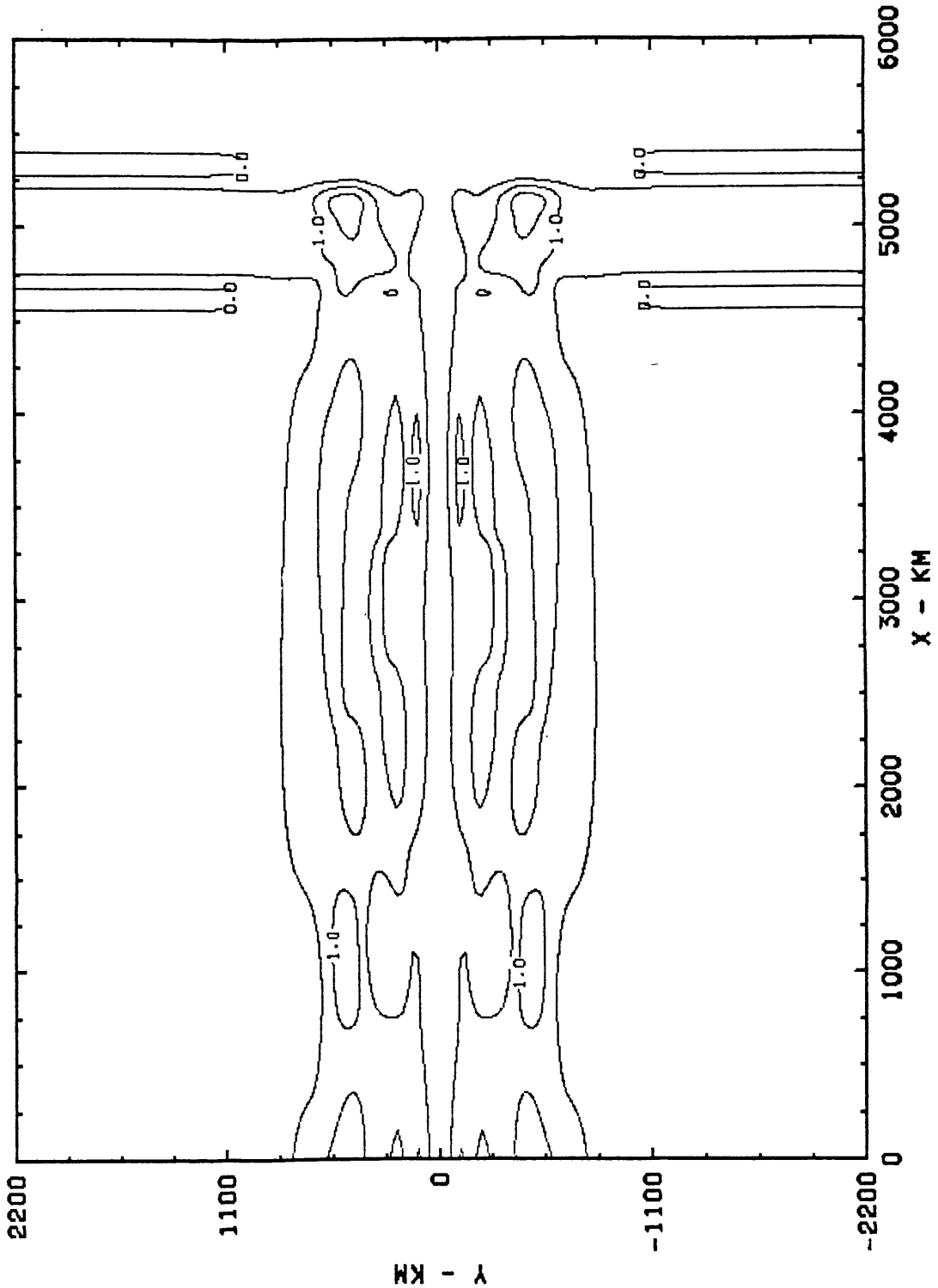

FIGURE 4.10

Patch Height Field
(X',Y')=(5000,0) Box=(4°x4°) Modes=7

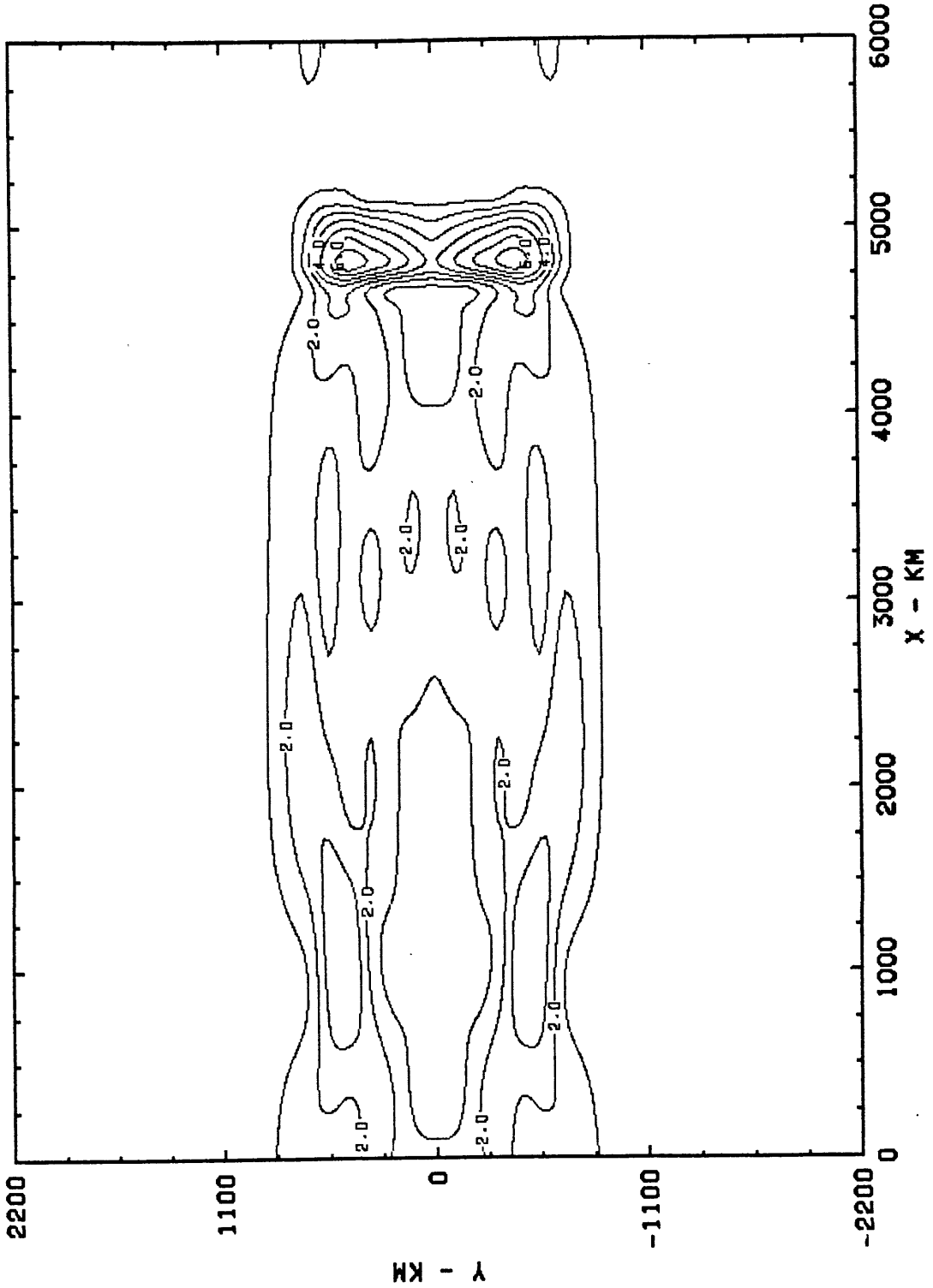

FIGURE 4.11

Patch Zonal Velocity
(X',Y')=(1000,0) Box=(4° x4°)

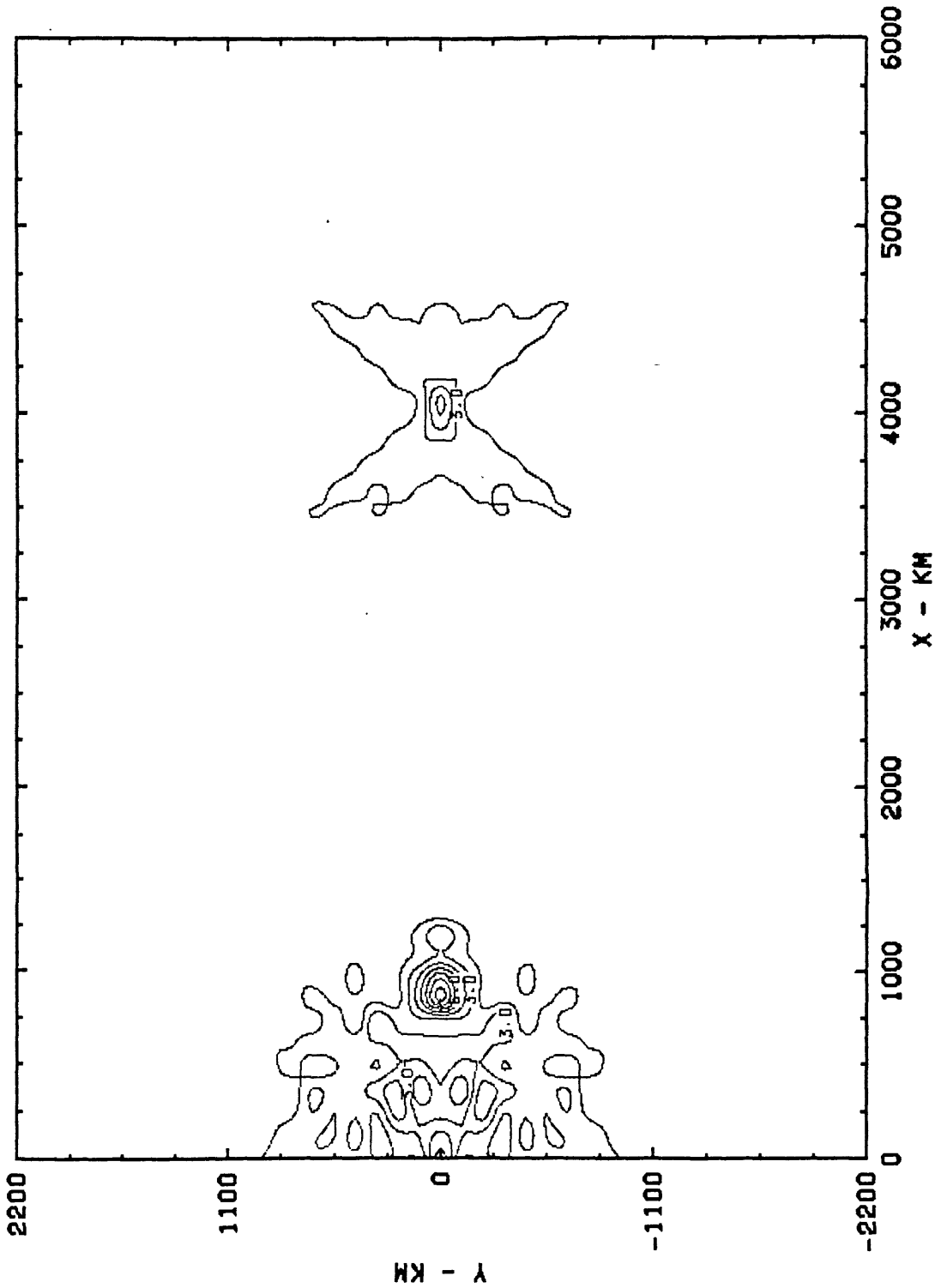

FIGURE 4.12

Patch Zonal Velocity
(X',Y')=(1000,500) Box=(4^c x 4^o)

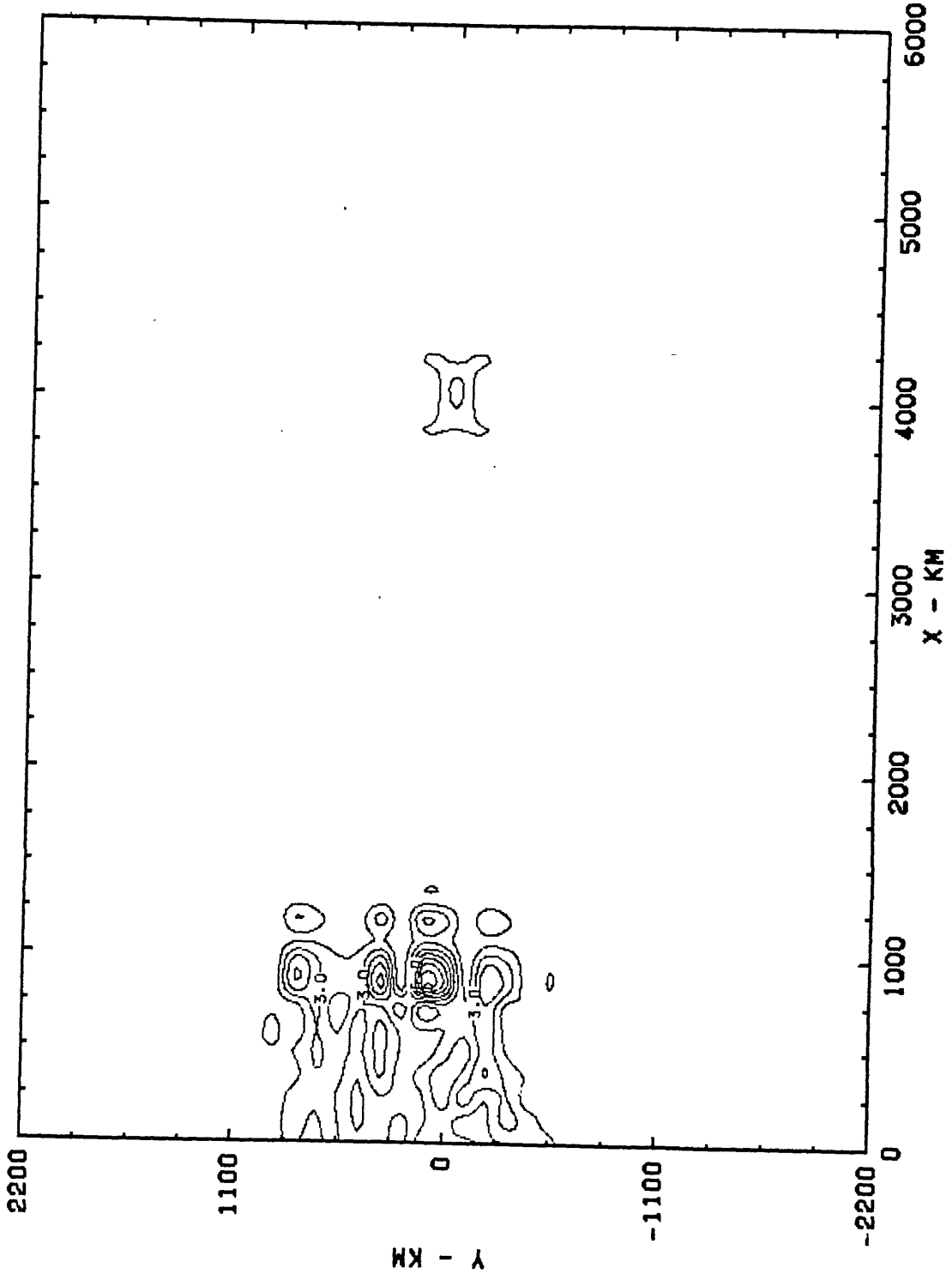

FIGURE 4.13

Patch Zonal Velocity
(X',Y')=(5000,0) Box=(4 x4) R=25 years

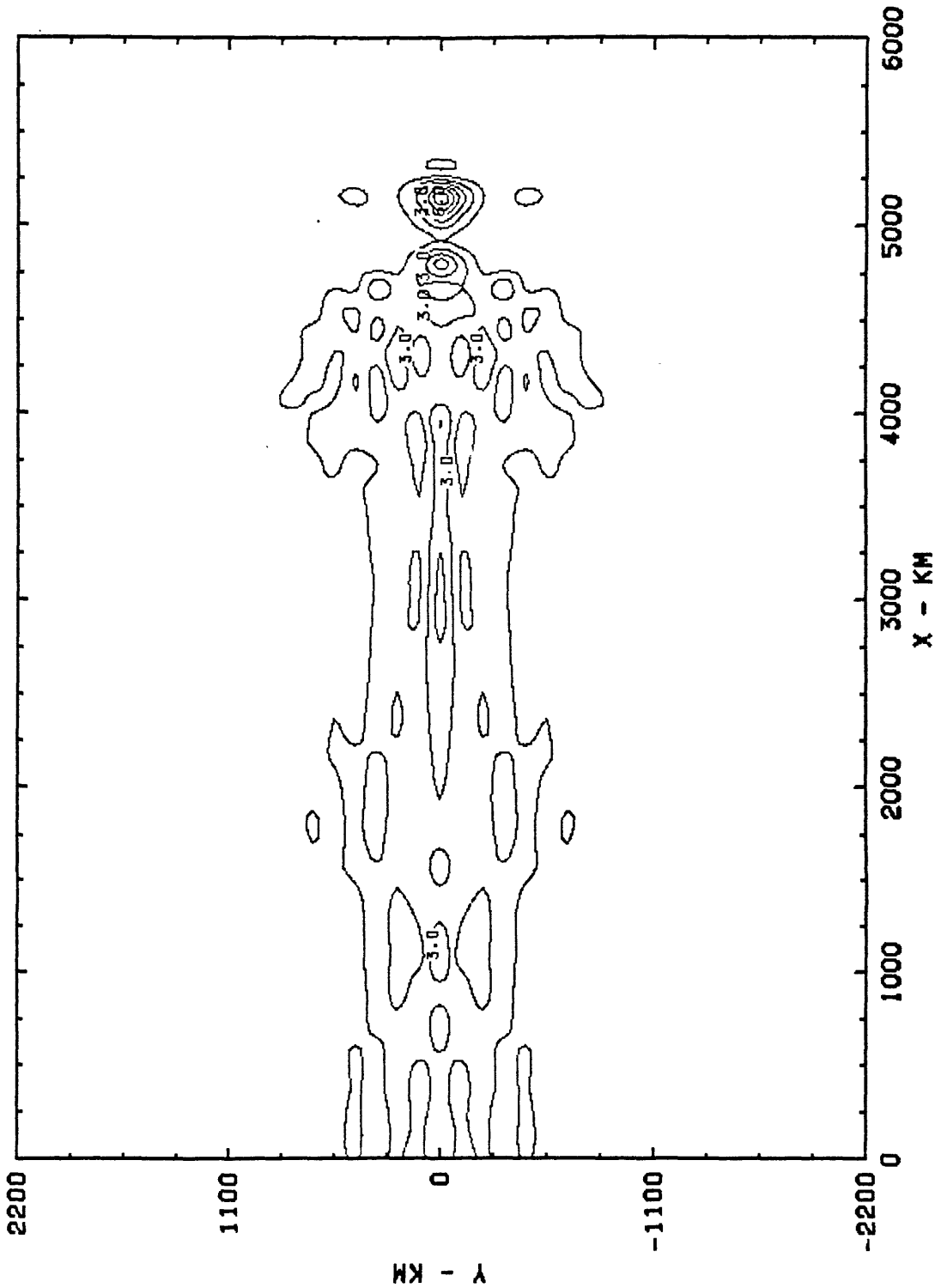

FIGURE 4.14

Patch Zonal Velocity
(X',Y')=(5000,1000) Box=(4^{o} x4^{o}) R=25 years

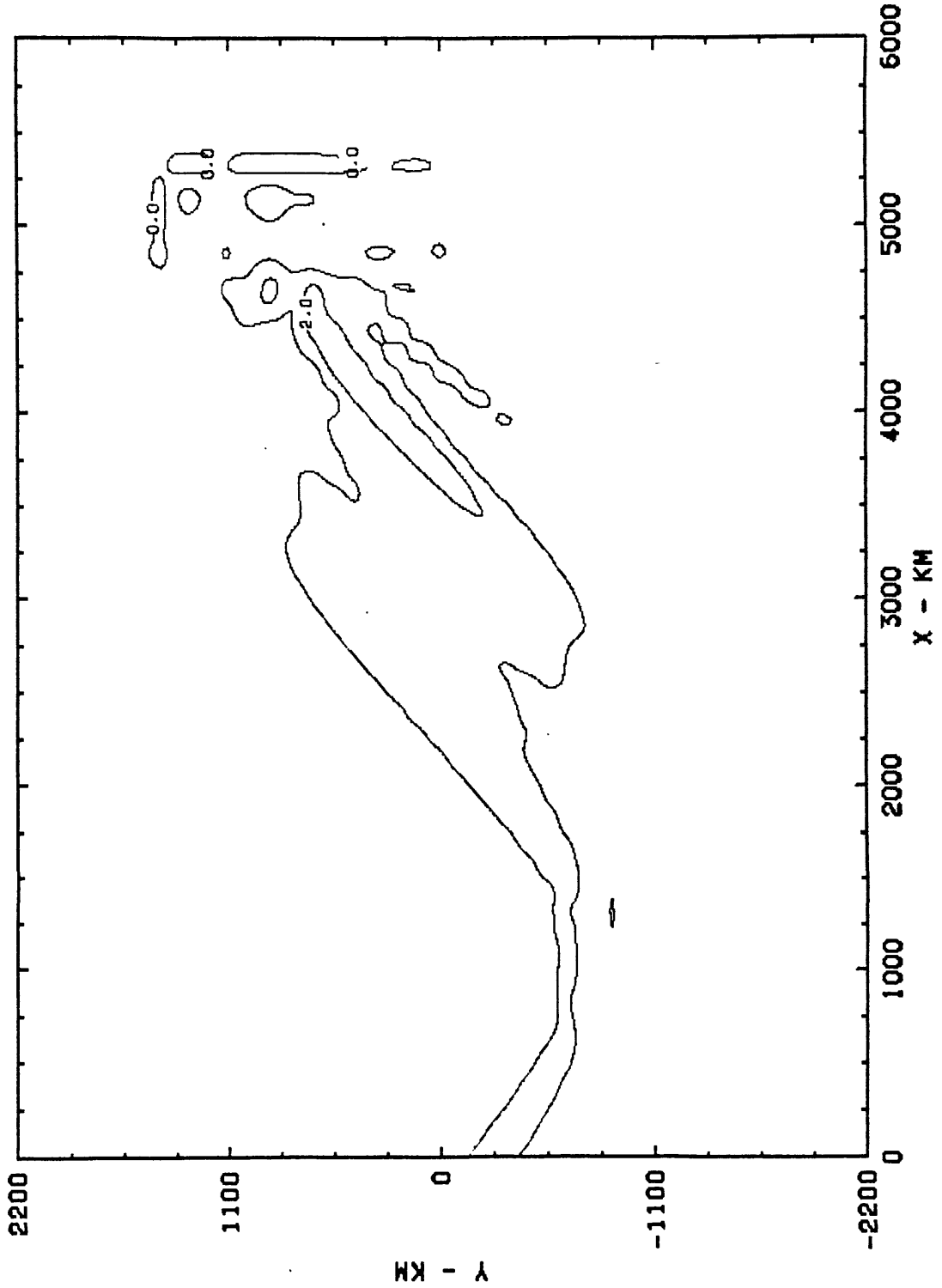

FIGURE 5.1

Pacific Islands Stations

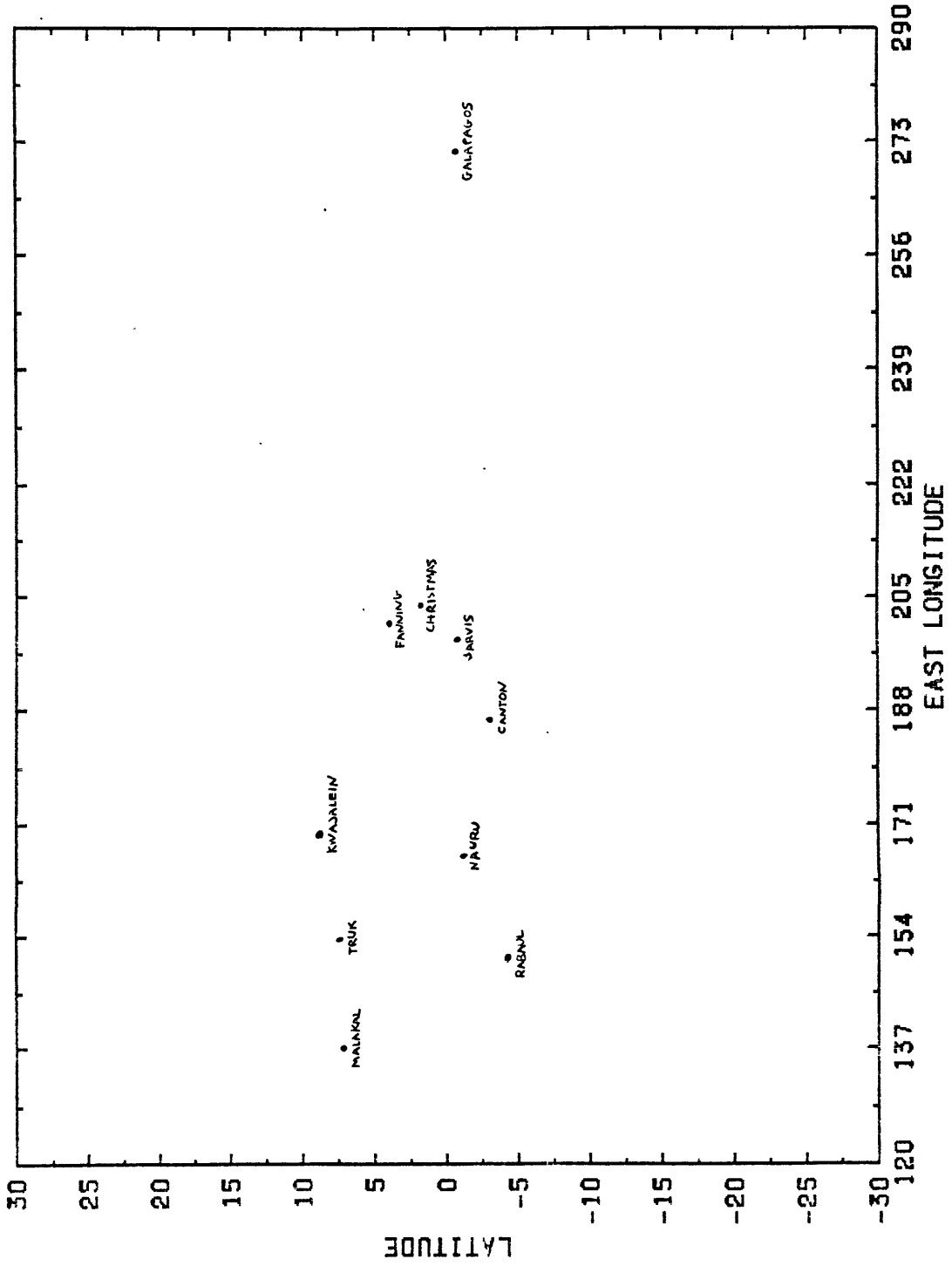

FIGURE 5.2

Fanning (4N,159W) Response Function
Forcing Period = DC

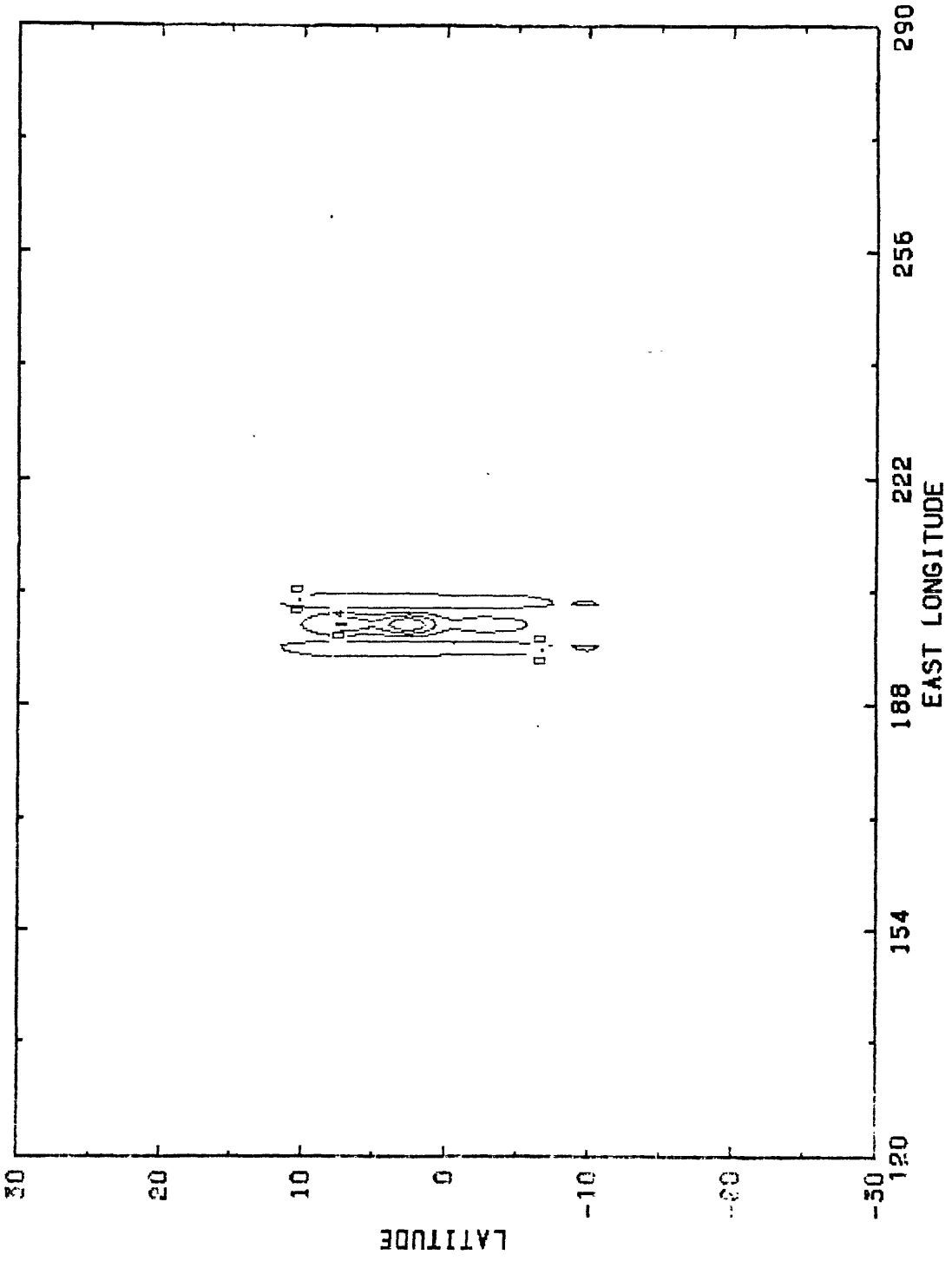

FIGURE 5.3

Fanning (4N,159W) Response Function
Forcing Period = 18 Months

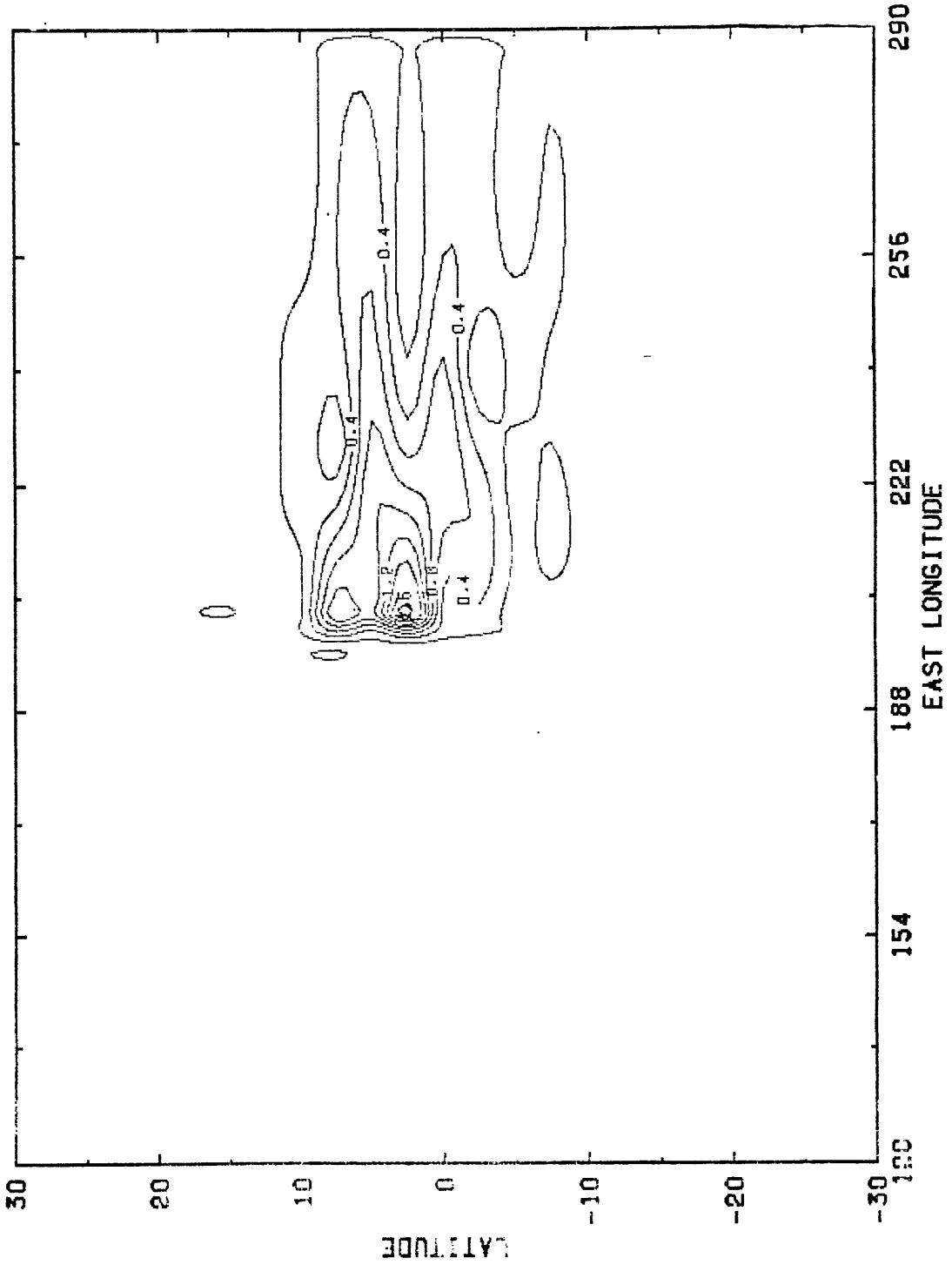

FIGURE 5.4

Fanning (4N,159W) Response Function
Forcing Period = 9 Months

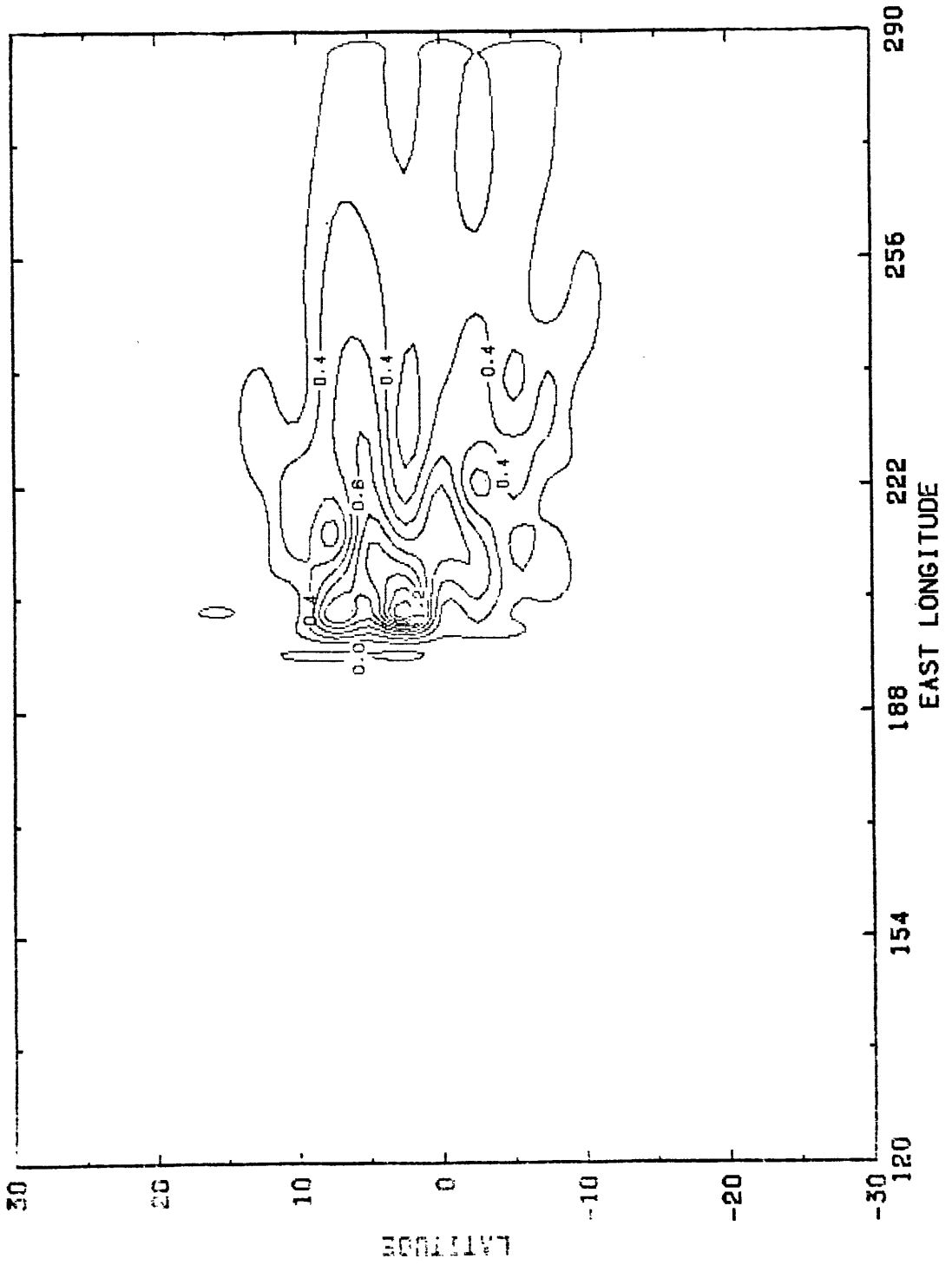

FIGURE 5.5

Fanning (4N,159W) Response Function
Forcing Period = 6 Months

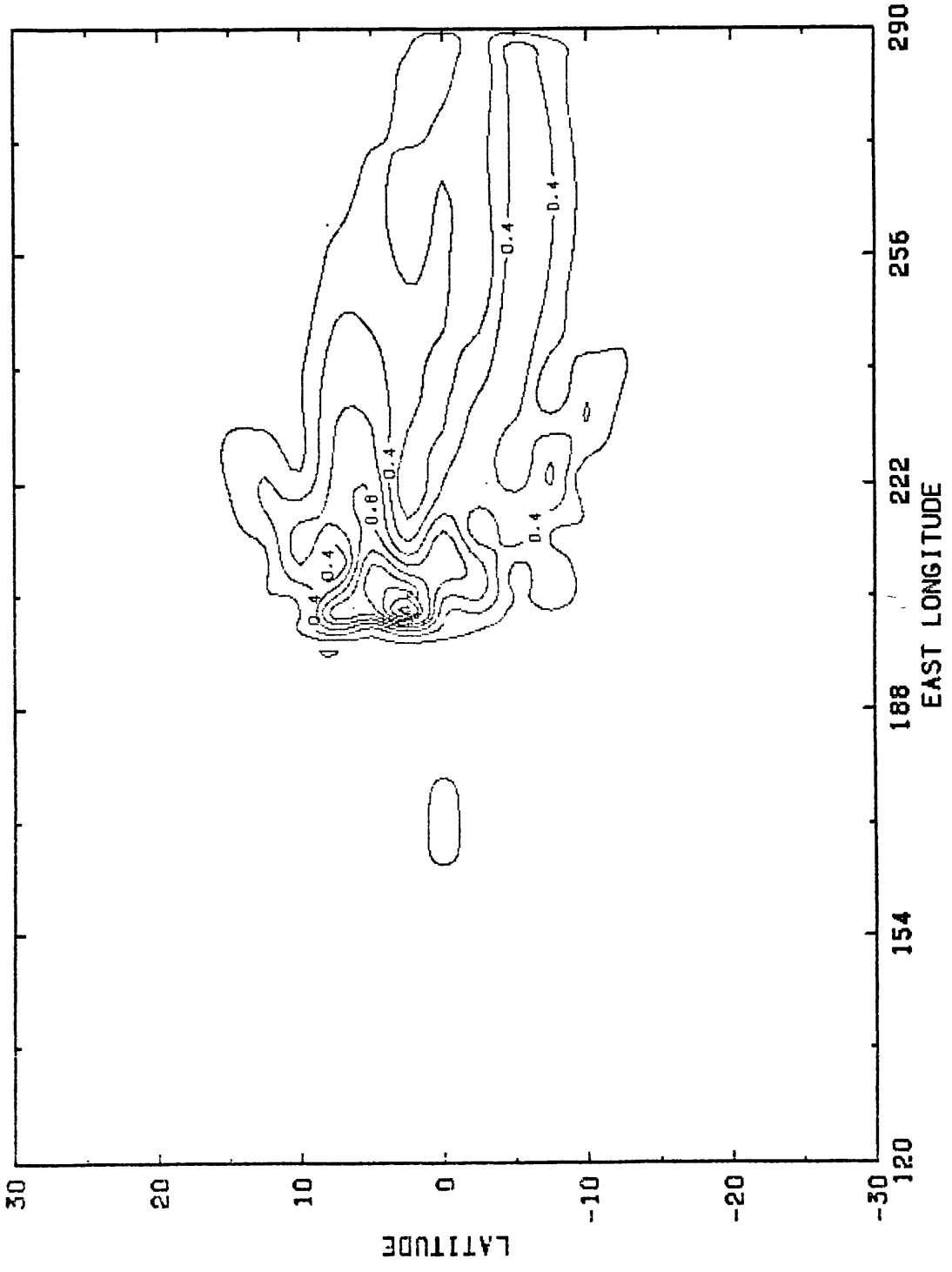

FIGURE 5.6

Fanning (4N,159W) Response Function
Forcing Period = 18/4 Months

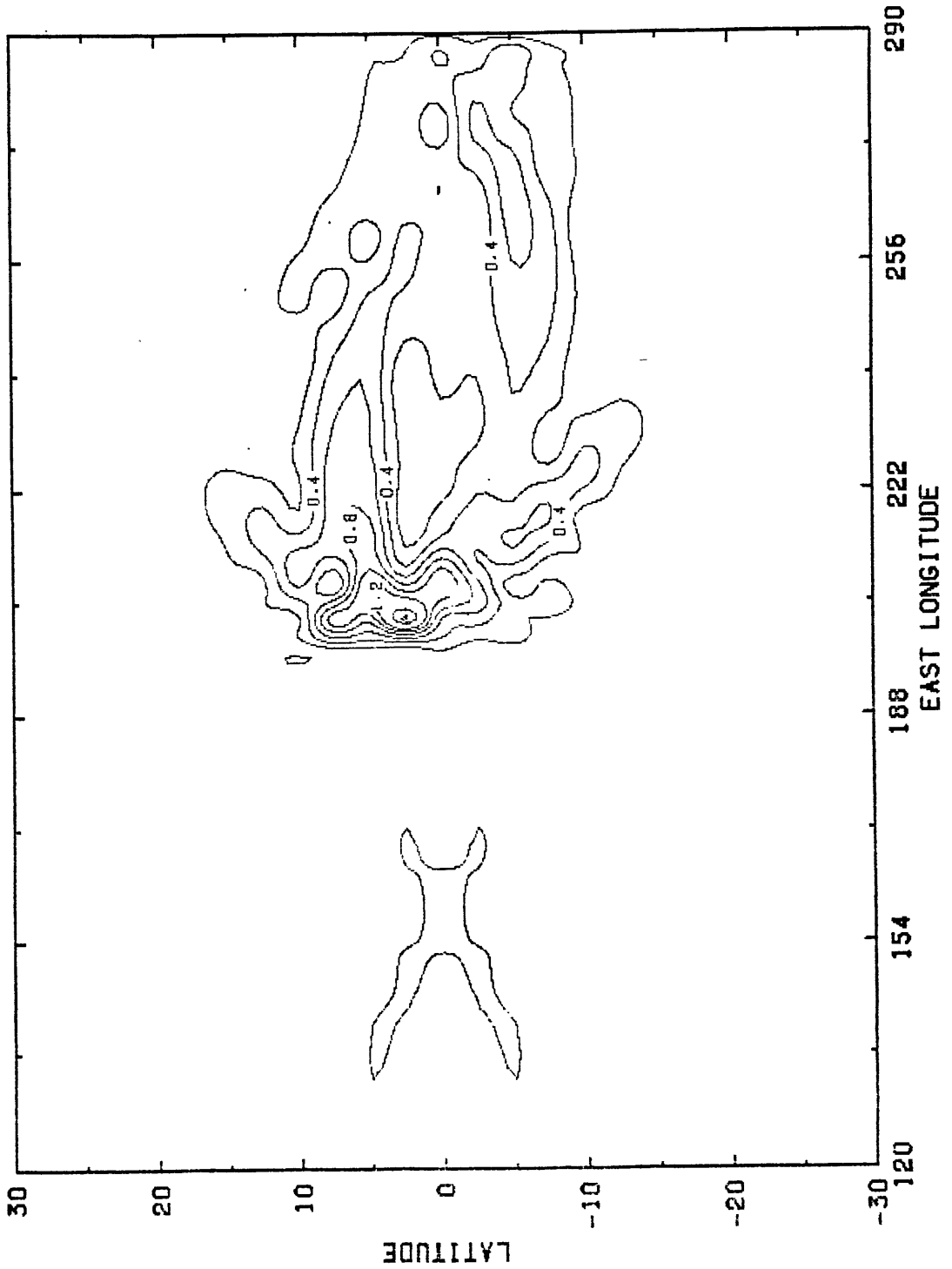

FIGURE 5.7

Fanning (4N,159W) Response Function
Forcing Period = 18/5 Months

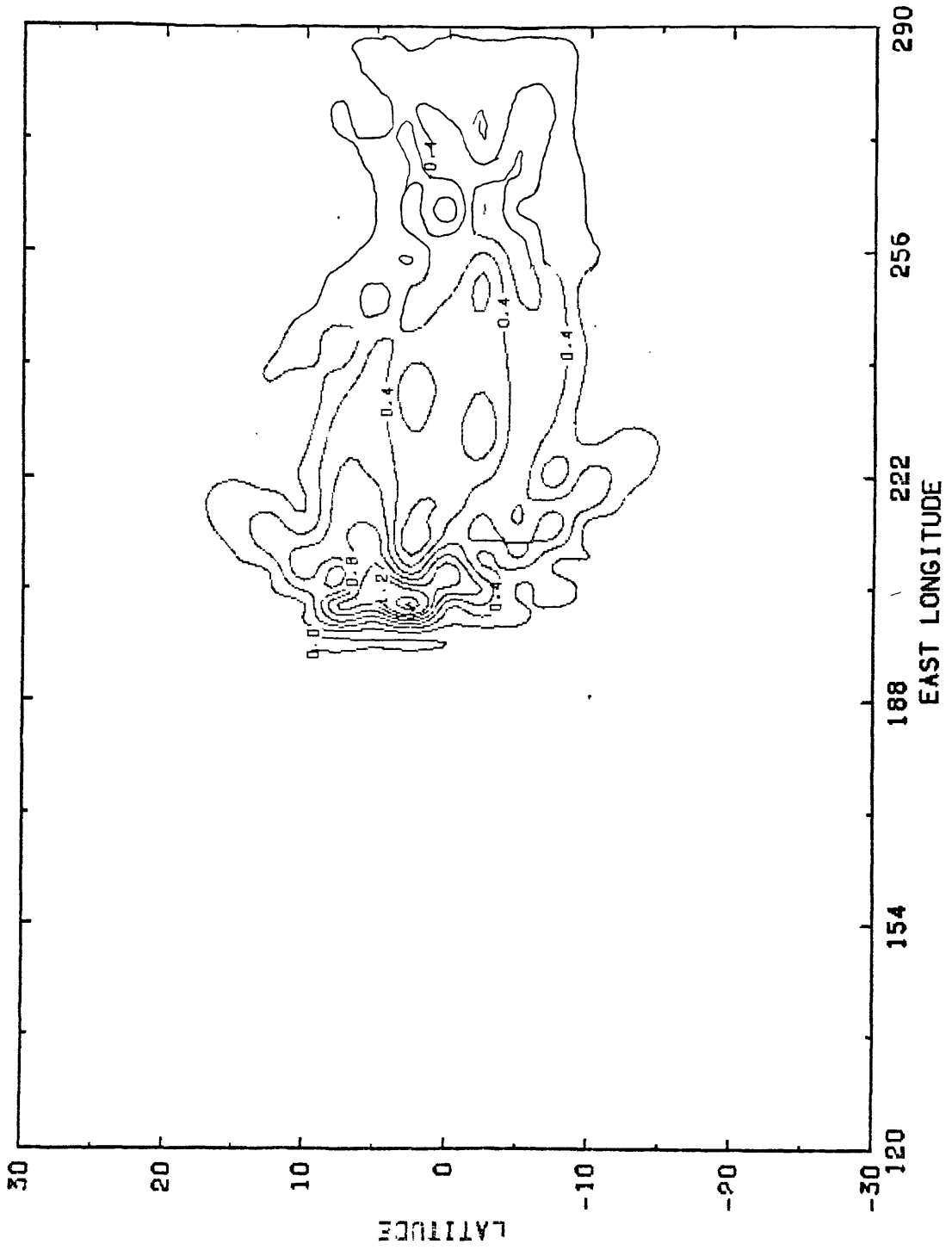

FIGURE 5.8

Fanning (4N,159W) Response Function
Forcing Period = 3 Months

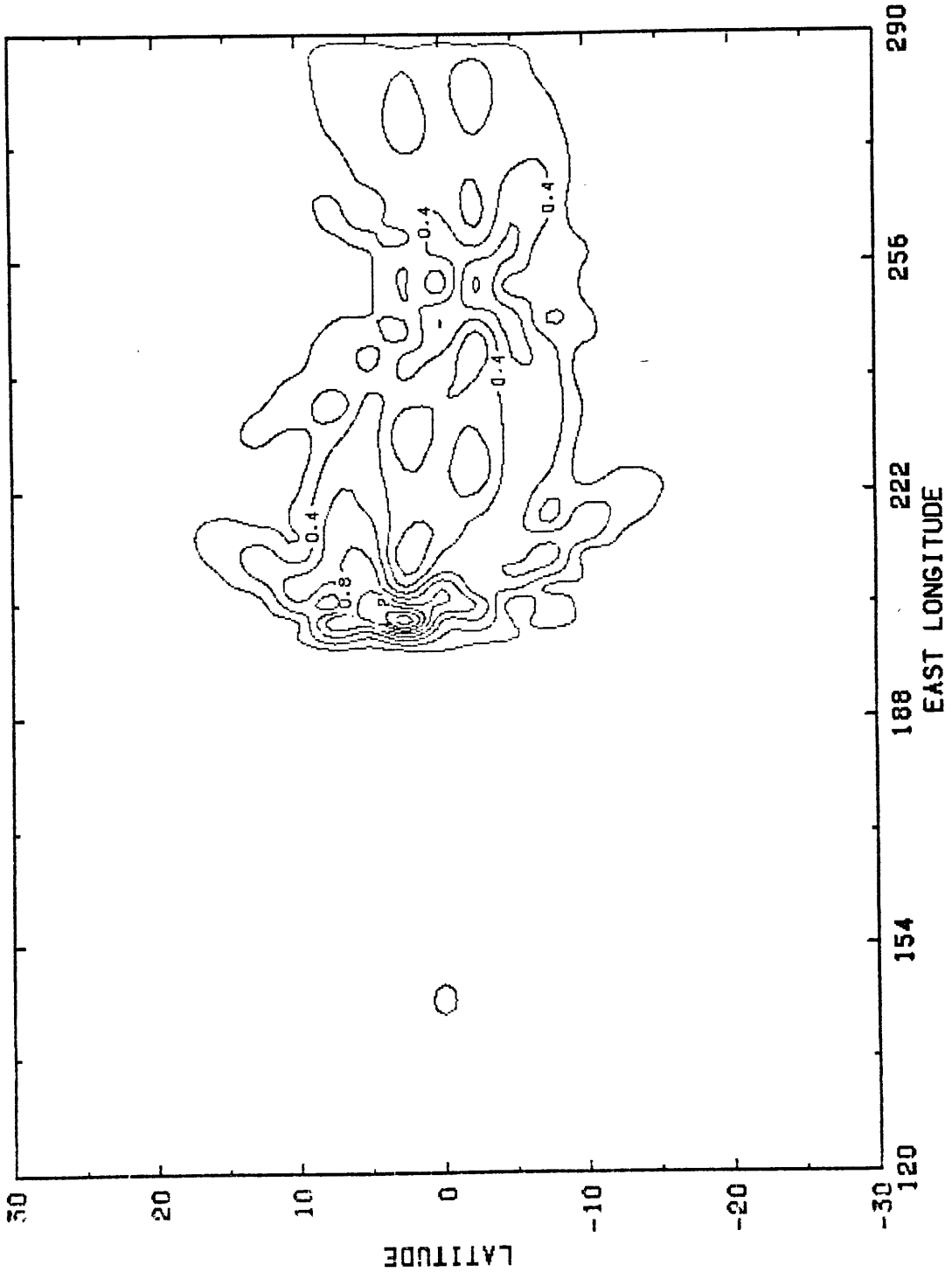

FIGURE 5.9

Fanning (4N,159W) Response Function
Forcing Period = 18/7 Months

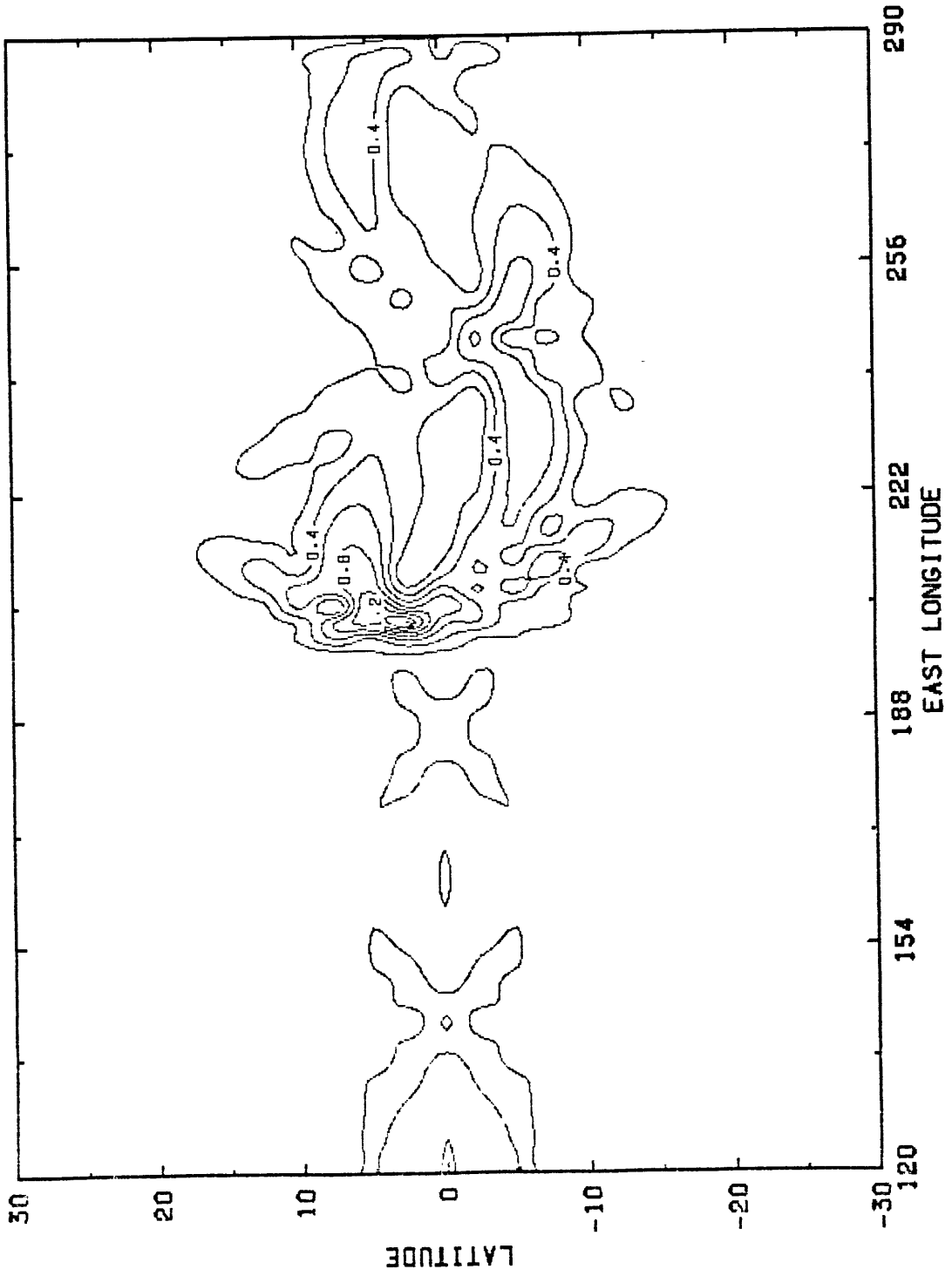

FIGURE 5.10

Fanning (4N,159W) Response Function
Forcing Period = 18/8 Months

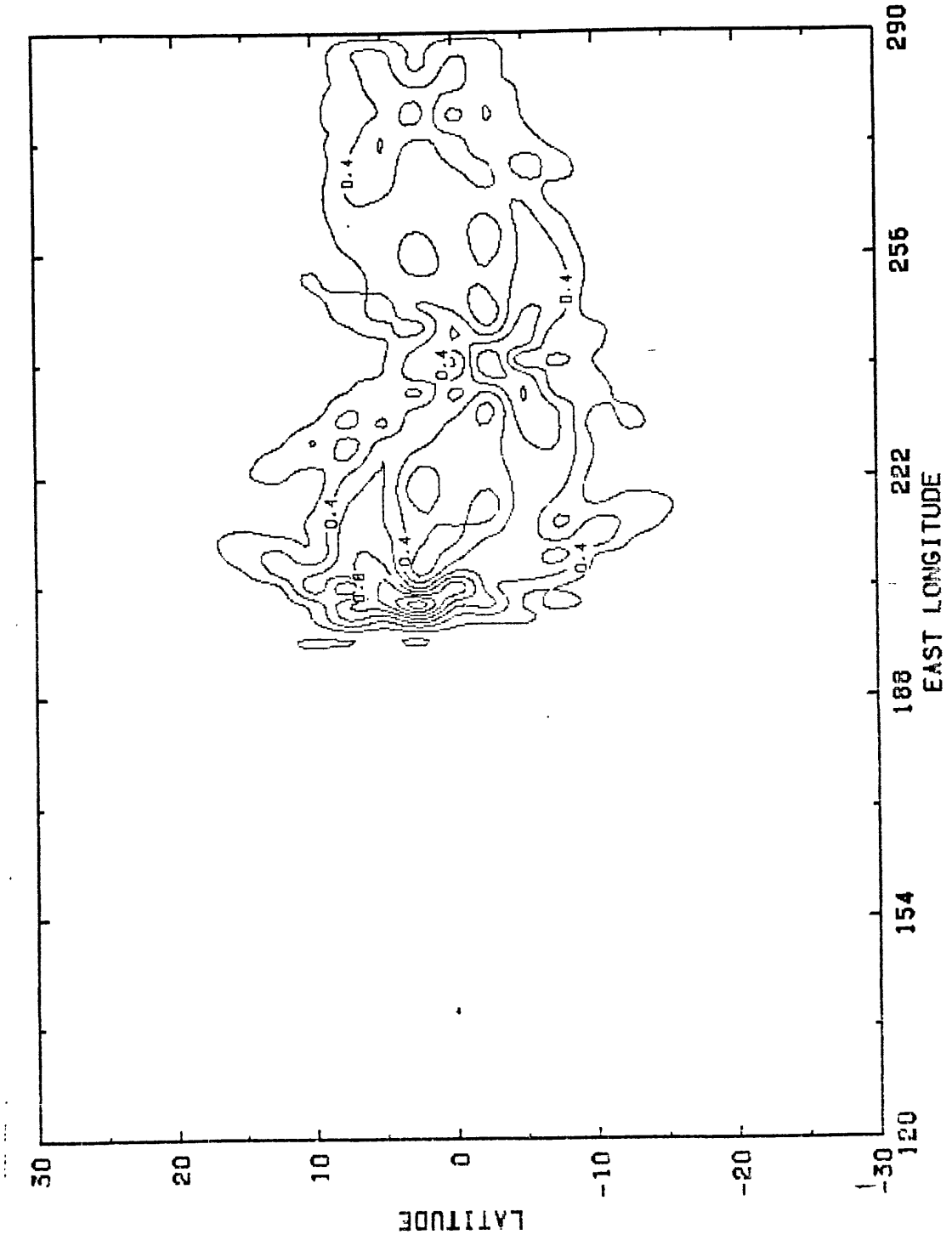

FIGURE 5.11

Fanning (4N,159W) Response Function
Forcing Period = 2 Months

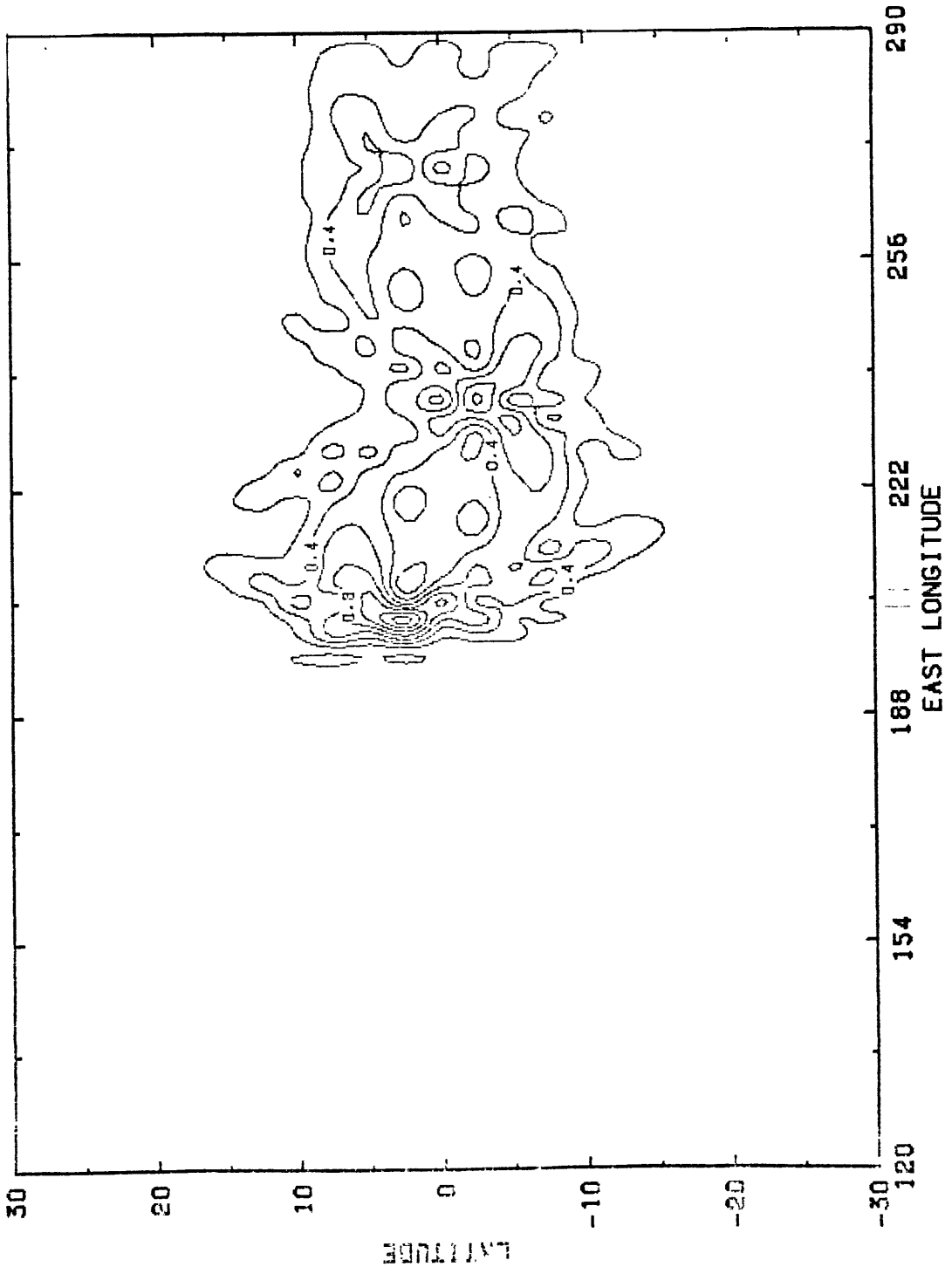

FIGURE 5.12

Fanning (4N,159W) Response Function
Delta Case - Forcing Period = DC

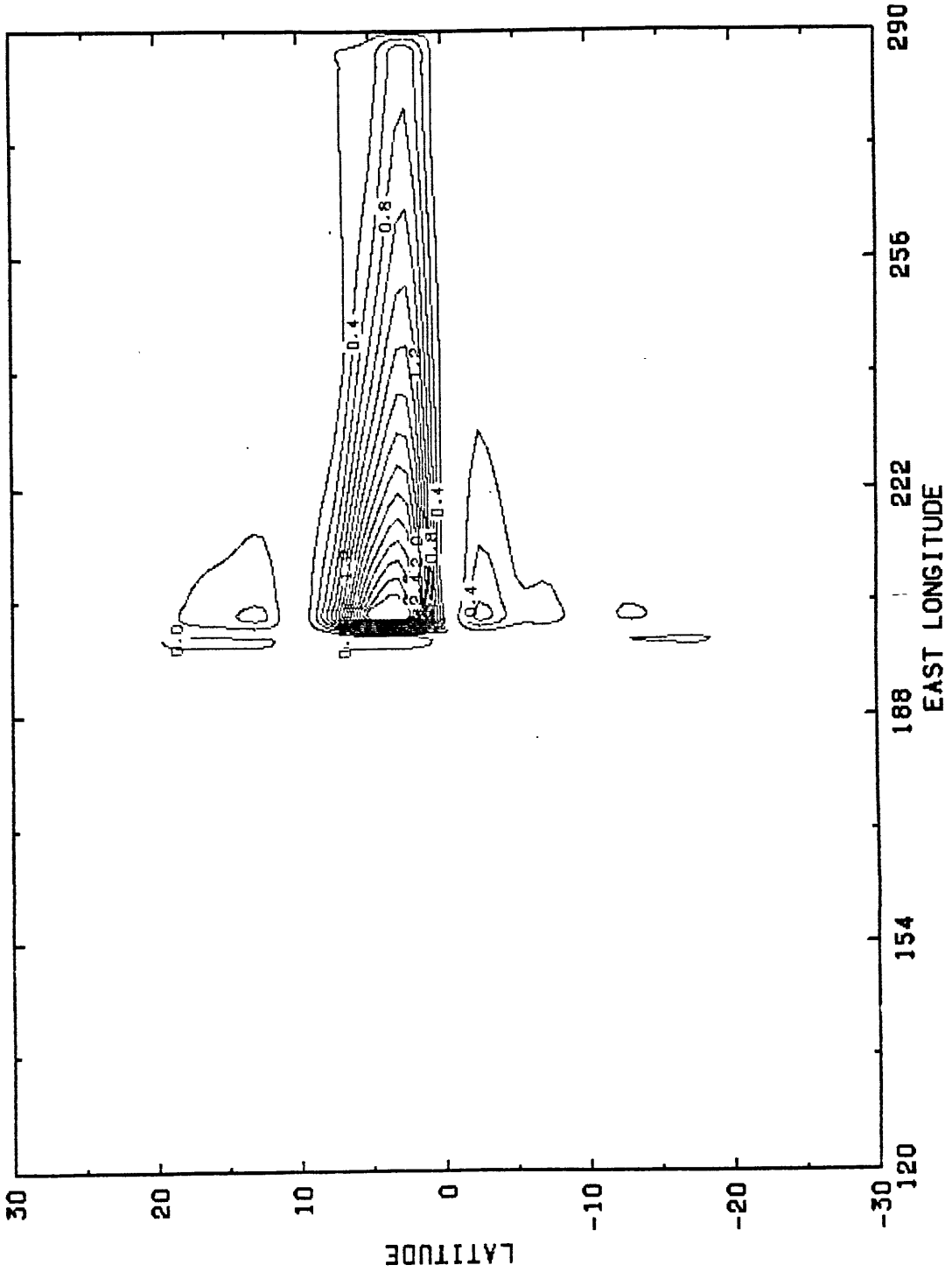

FIGURE 5.13

Fanning (4N,159W) Response Function
Delta Case - Forcing Period = 18 Months

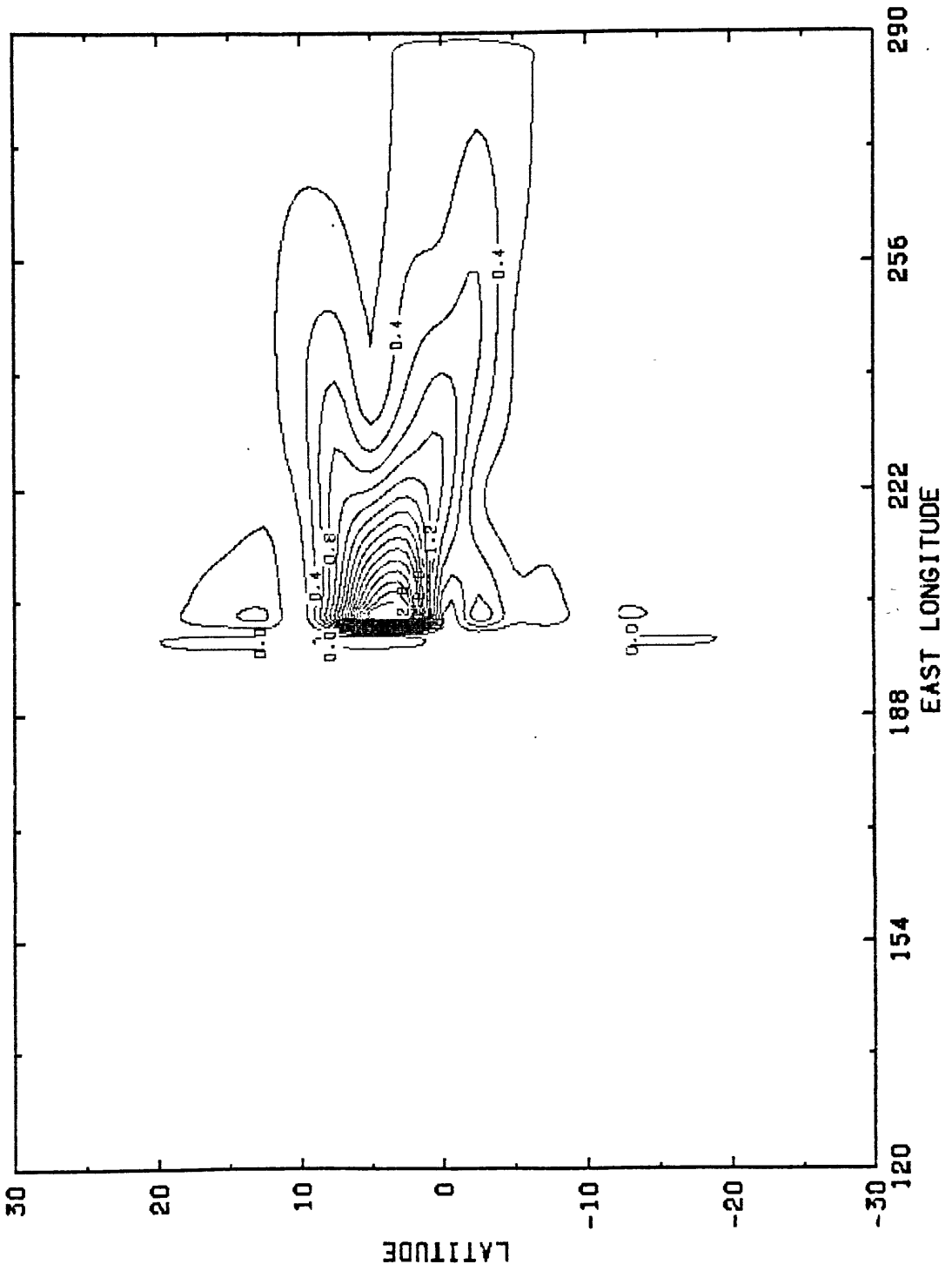

FIGURE 5.14

Fanning (4N,159W) Response Function
Delta Case - Forcing Period = 6 Months

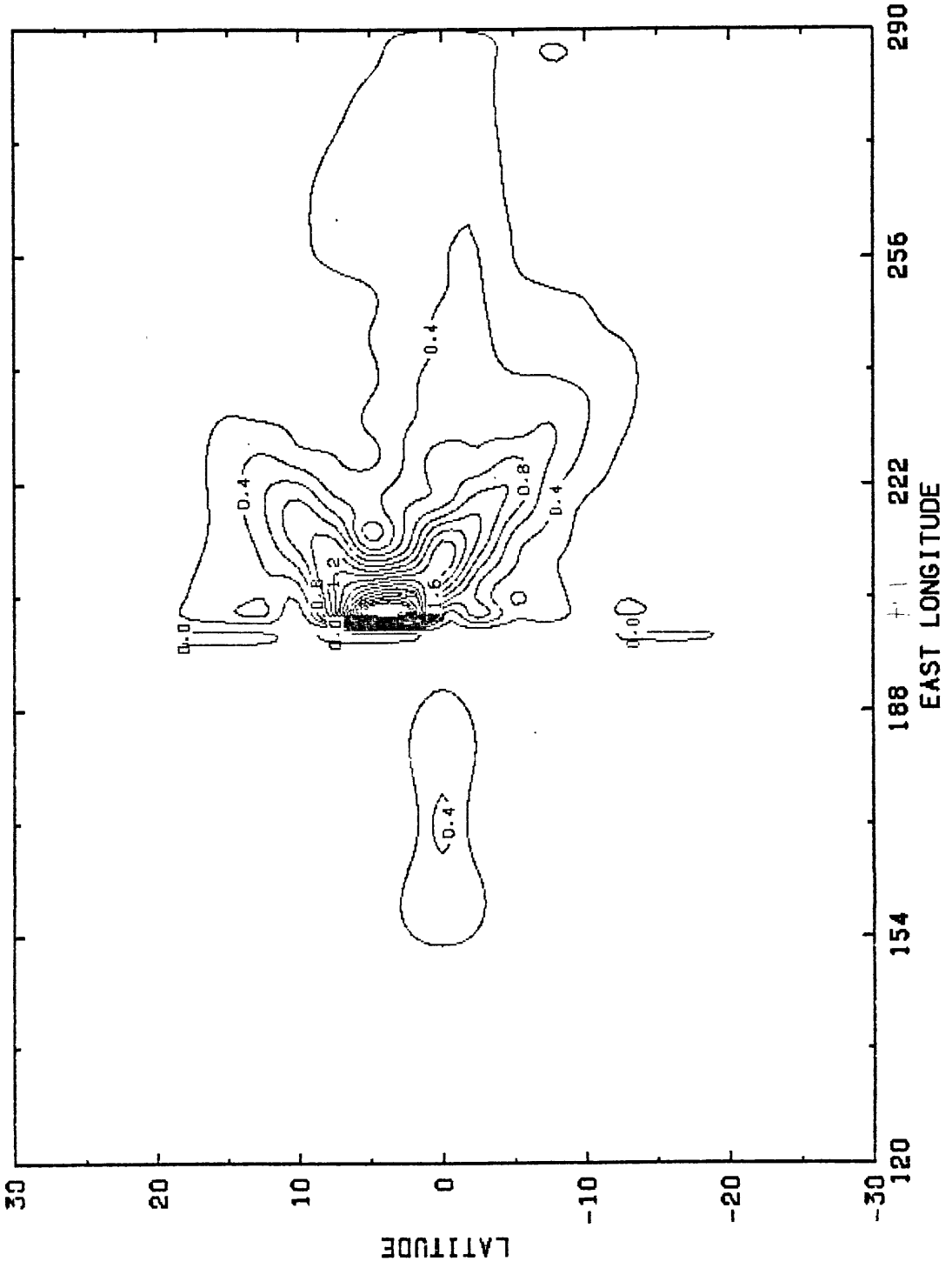

FIGURE 5.15

Fanning (4N,159W) Response Function
Delta Case - Forcing Period = 3 Months

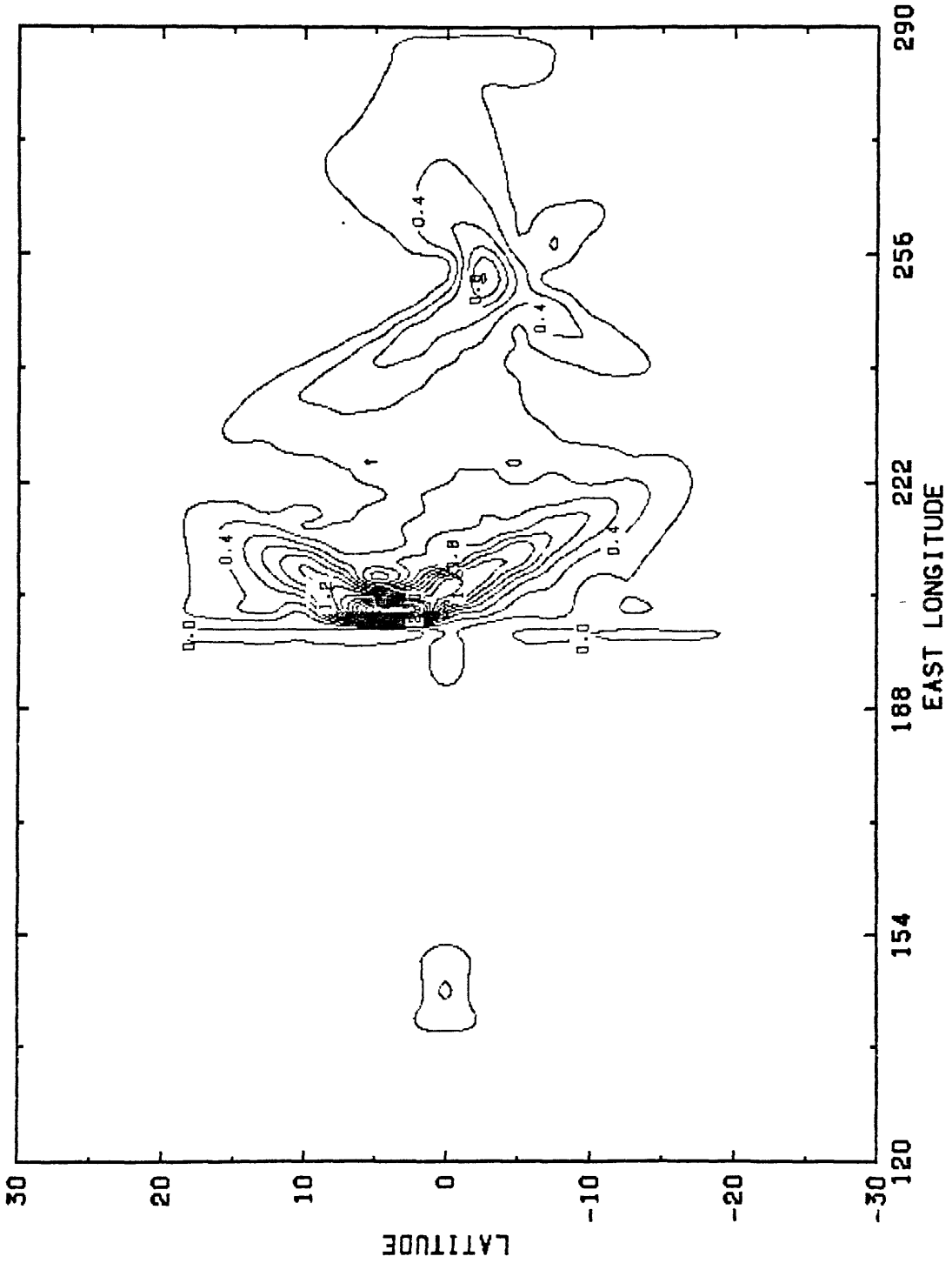

FIGURE 5.16

Fanning (4N,159W) Response Function
Delta Case - Forcing Period = 2 Months

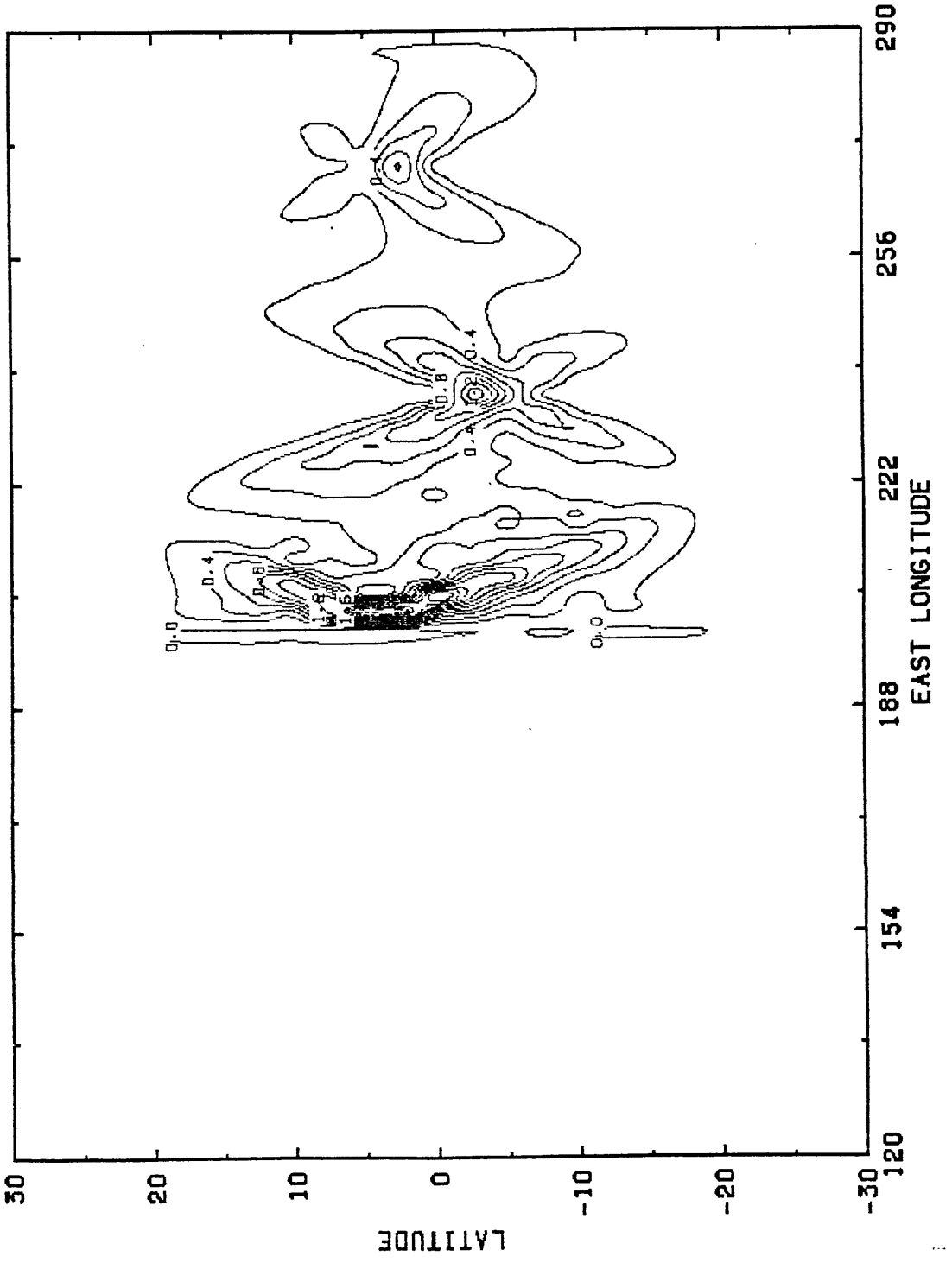

FIGURE 5.17

Galapagos (1S, 90W) Response Function
Forcing Period = 9 Months

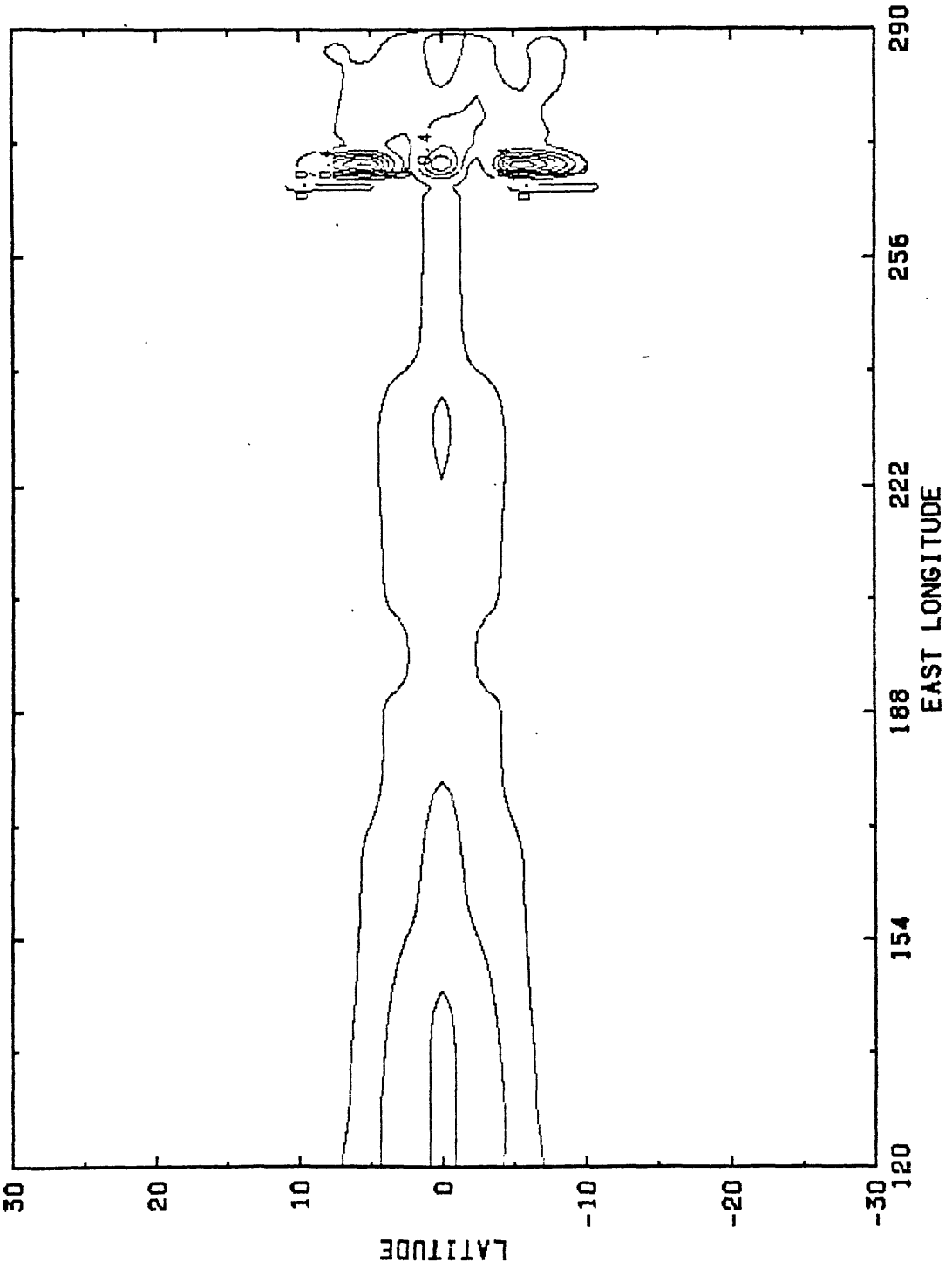

FIGURE 5.18

Galapagos (1S,90W) Response Function
Forcing Period = 6 Months

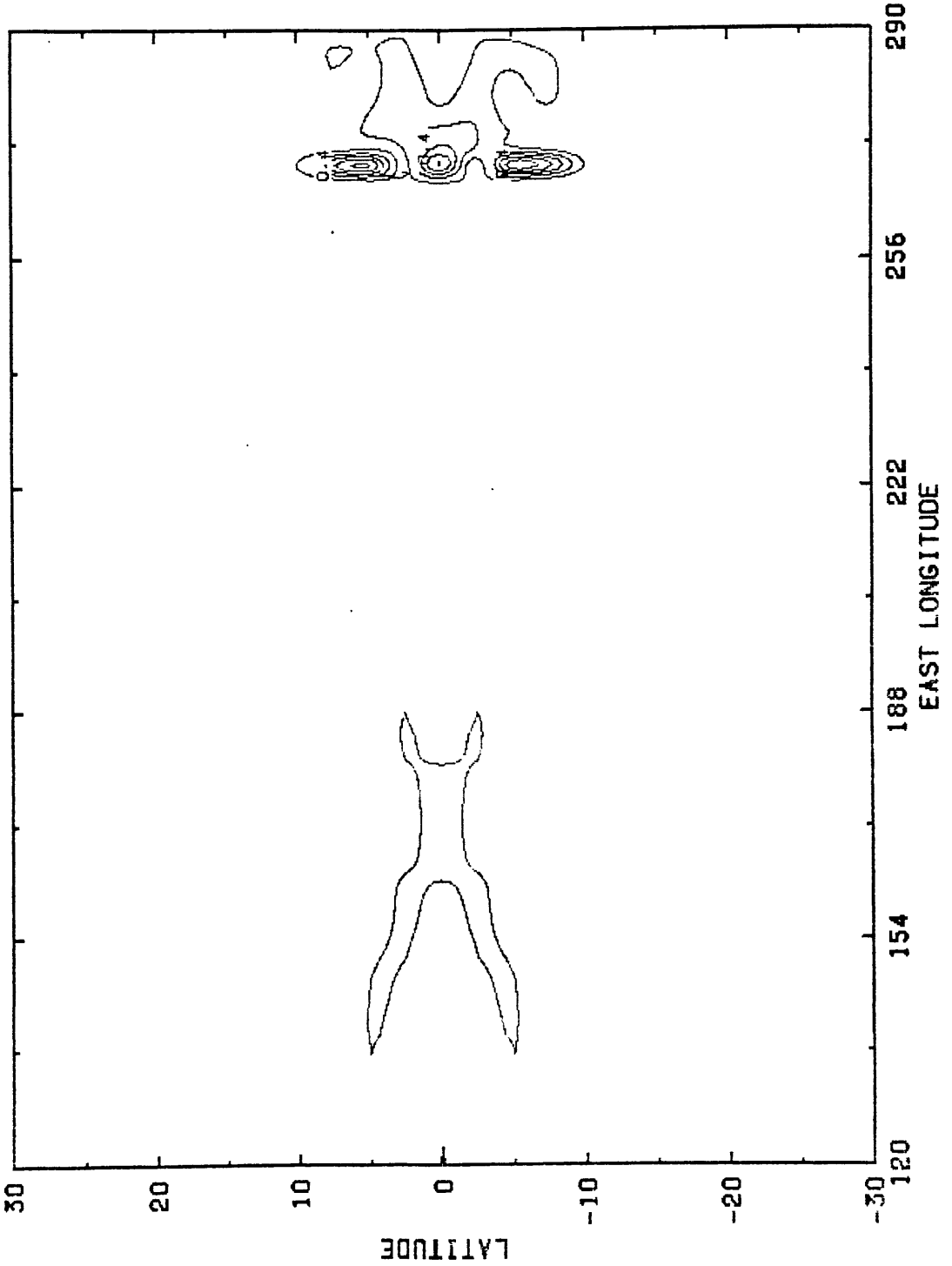

FIGURE 5.19

Jarvis (0.5S,161W) Response Function
Forcing Period = 6 Months

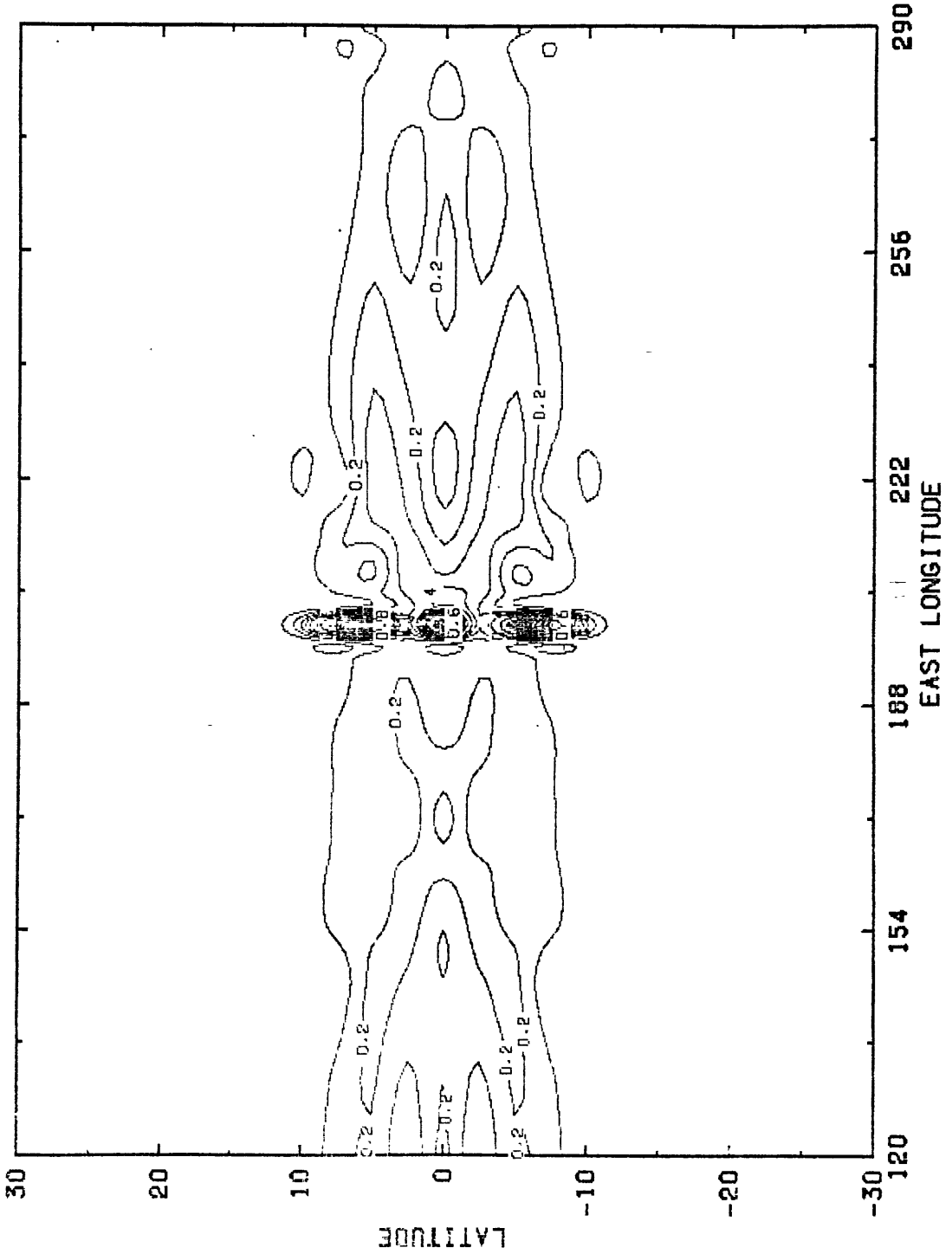

FIGURE 5.20

Kwajalein (8.5N,168E) Response Function
Forcing Period = 9 Months

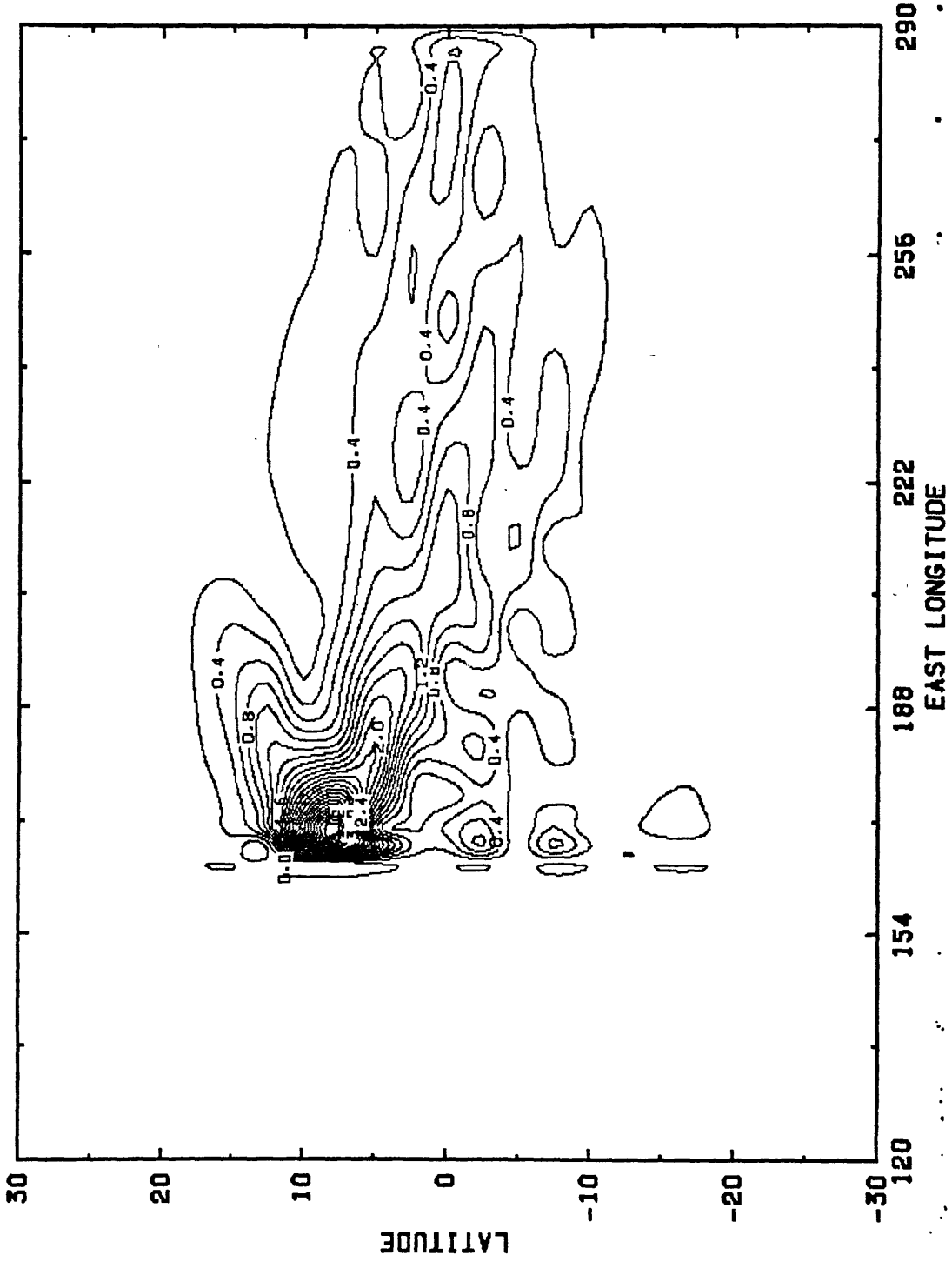

FIGURE 5.21

Truk (7N,151E) Response Function
Forcing Period = 9 Months

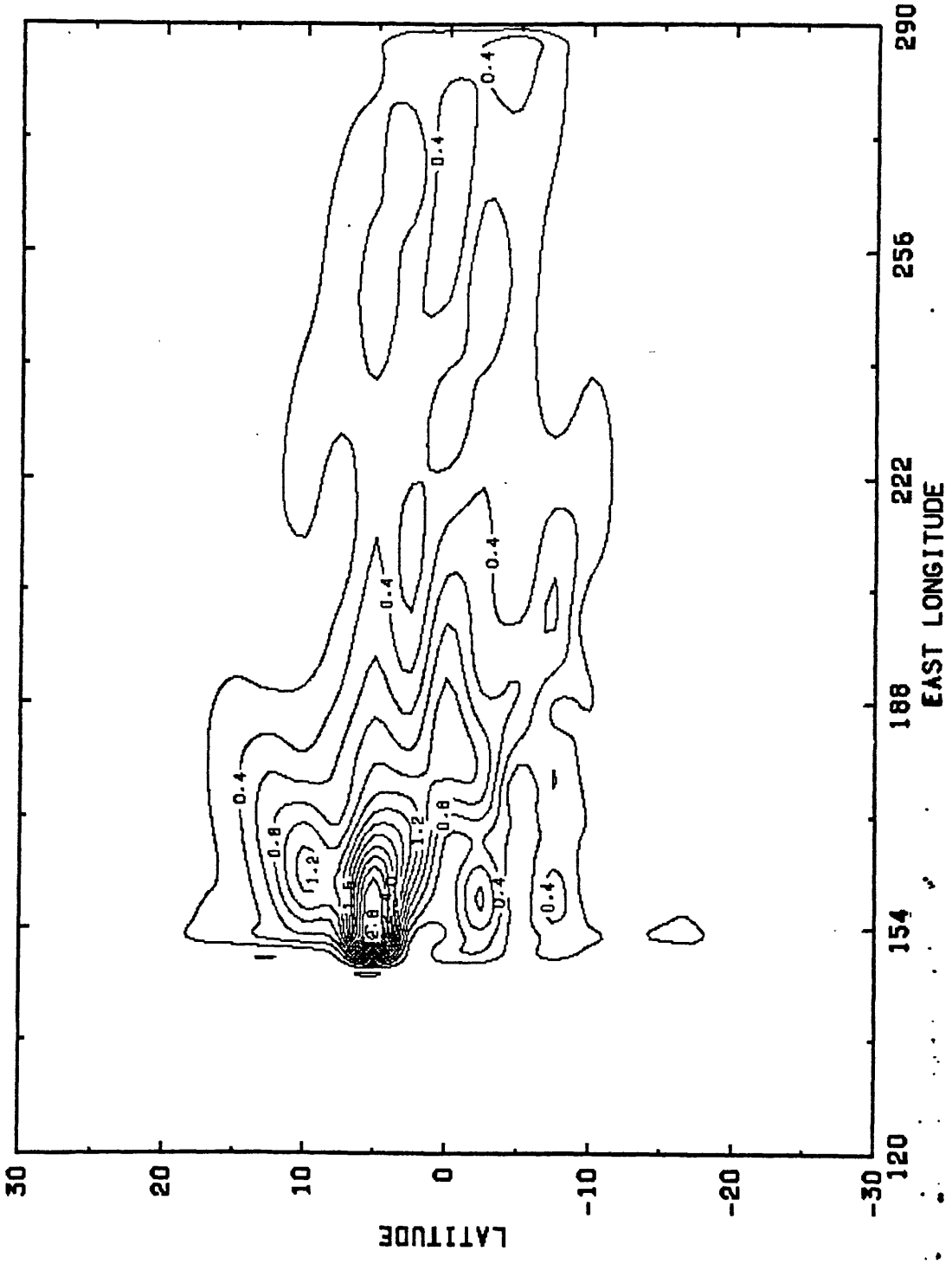

FIGURE 5.22

Rabaul (4S,152E) Response Function
Forcing Period = 18 Months

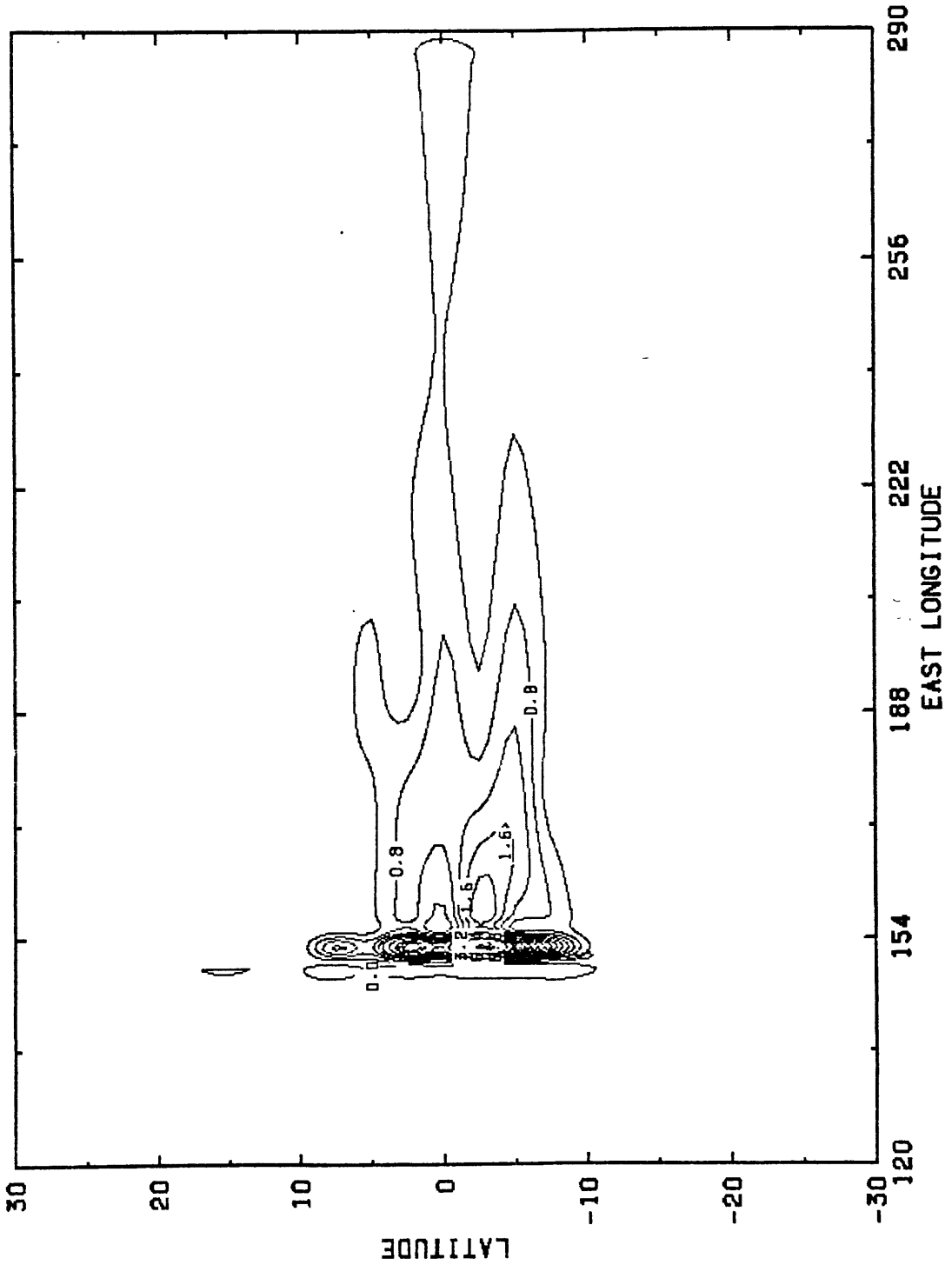

FIGURE 5.23

NMC Zonal Stress (dynes)
January 1982

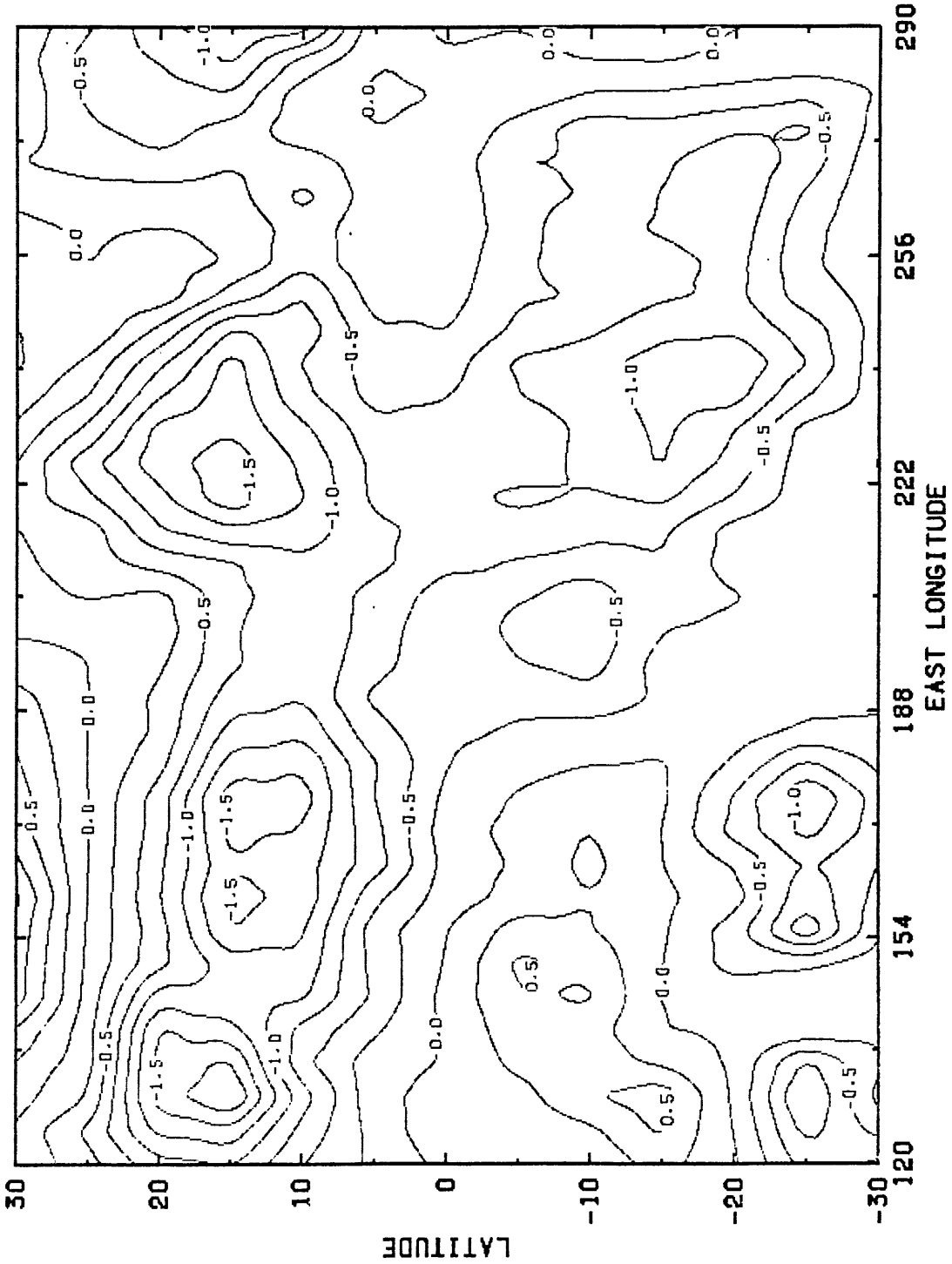

FIGURE 5.24

NMC Zonal Stress (dynes)
March 1982

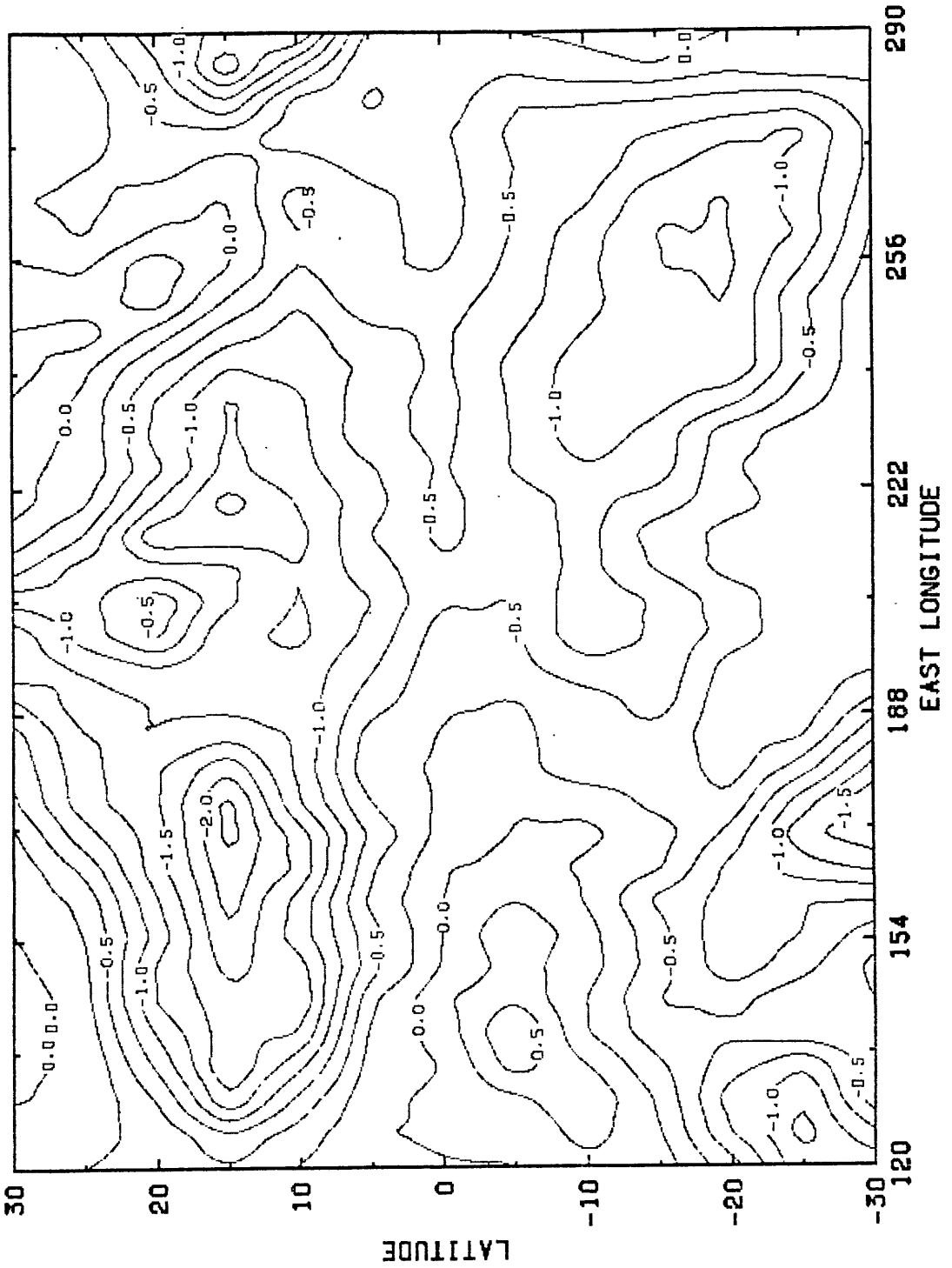

FIGURE 5.25

NMC Zonal Stress (dynes)
May 1982

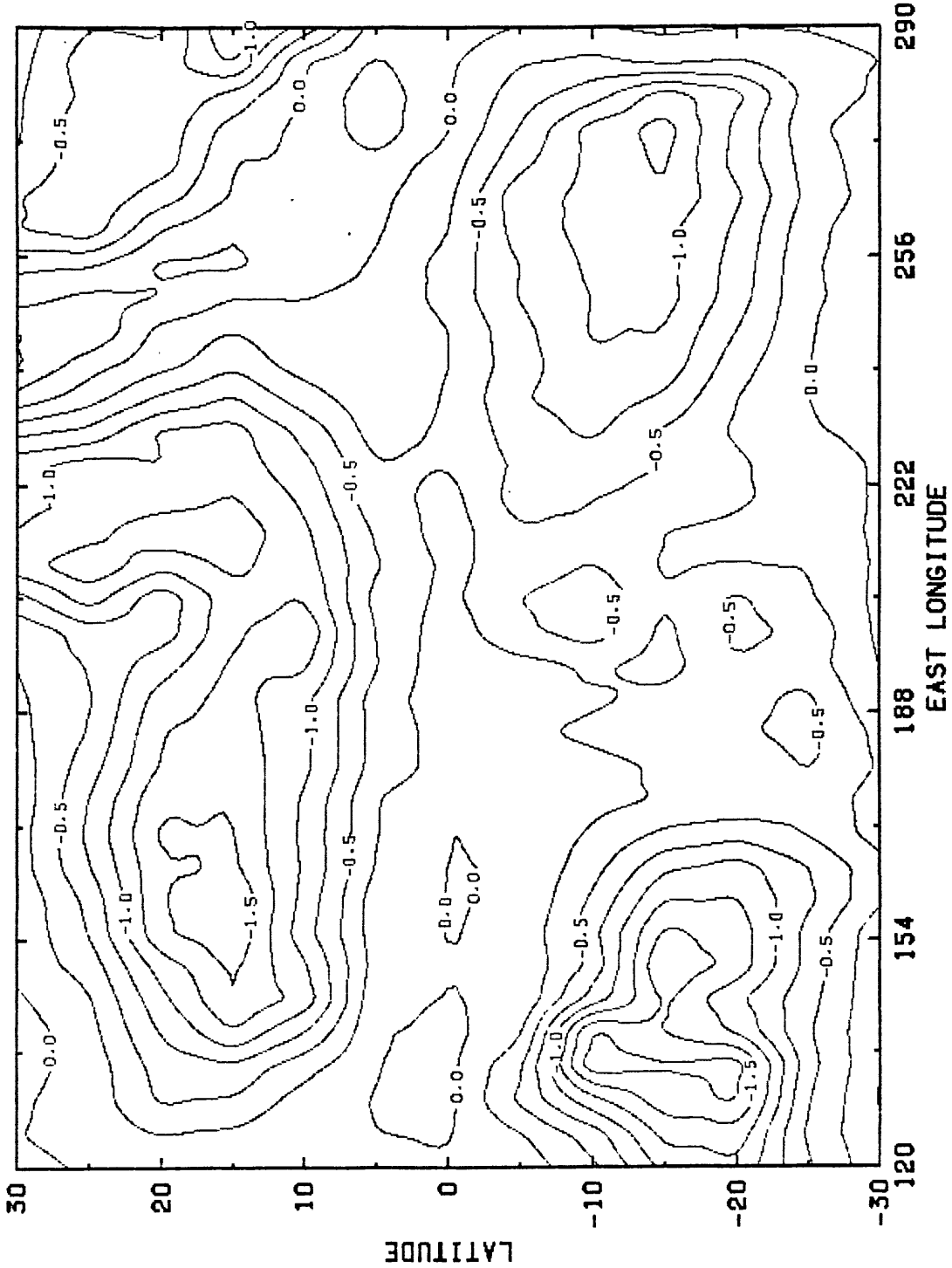

PIGURE 5.26

NMC Zonal Stress (dynes)
July 1982

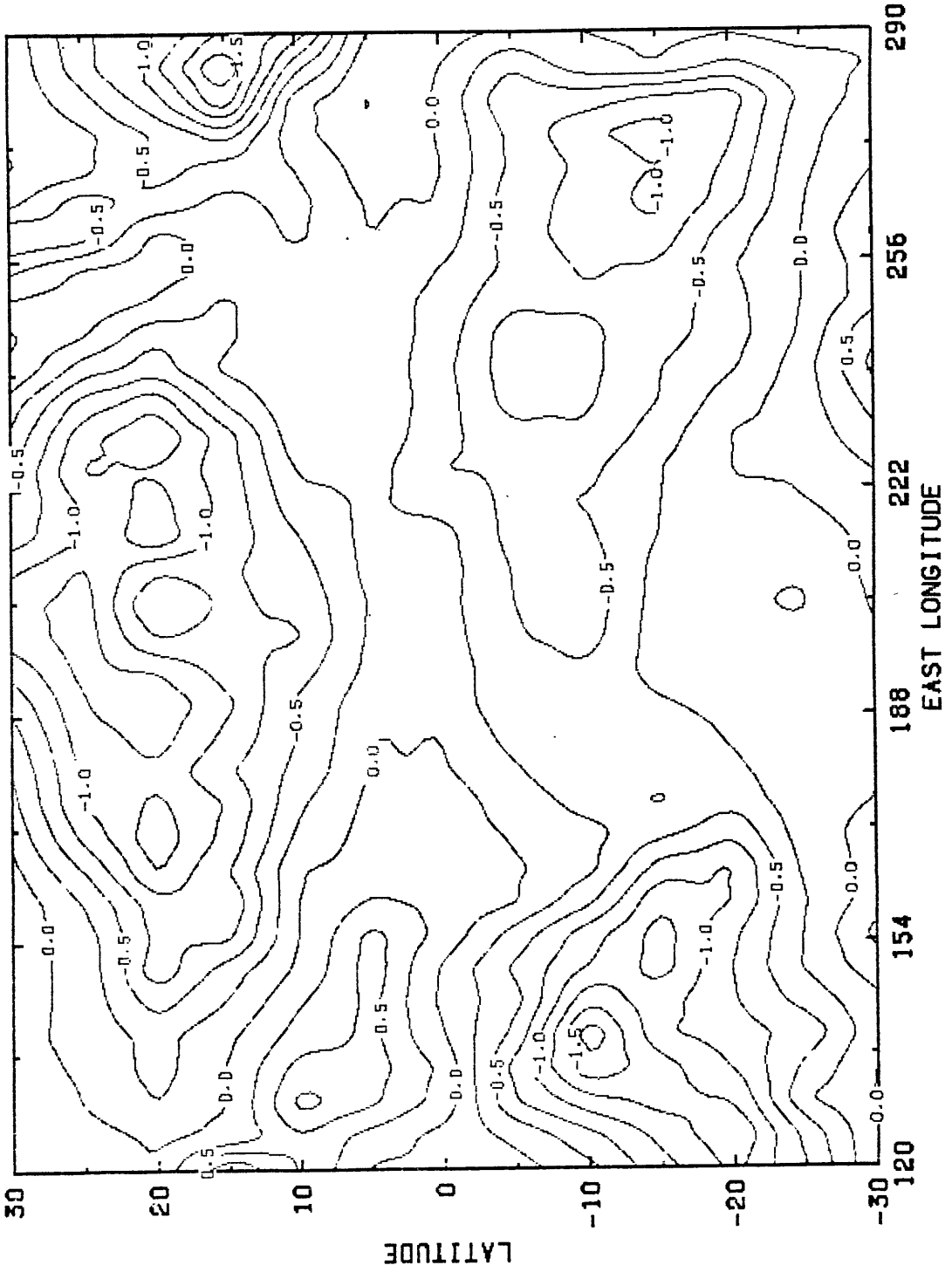

FIGURE 5.27

NMC Zonal Stress (dynes)
September 1982

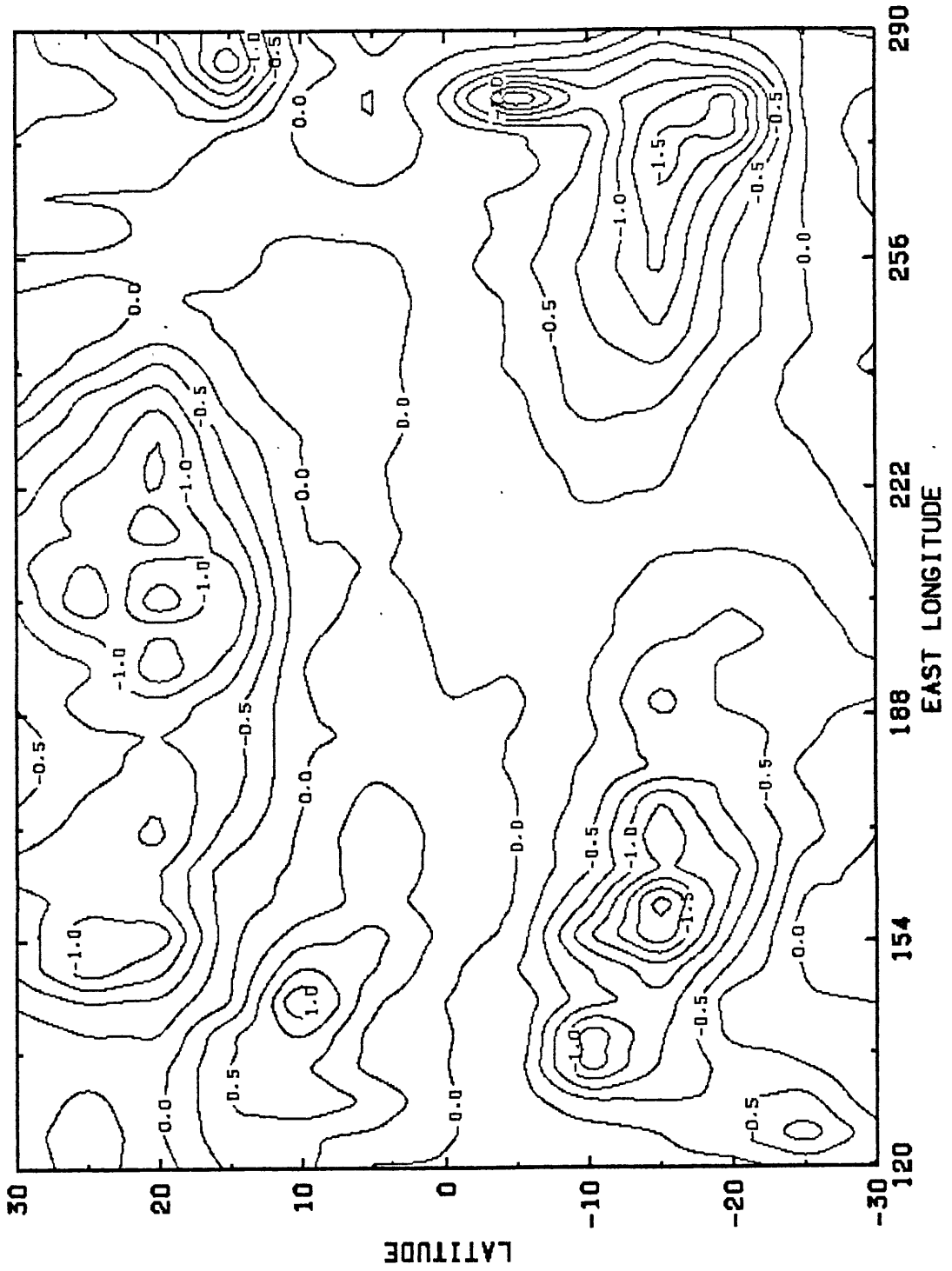

FIGURE 5.28

NMC Zonal Stress (dynes)
November 1982

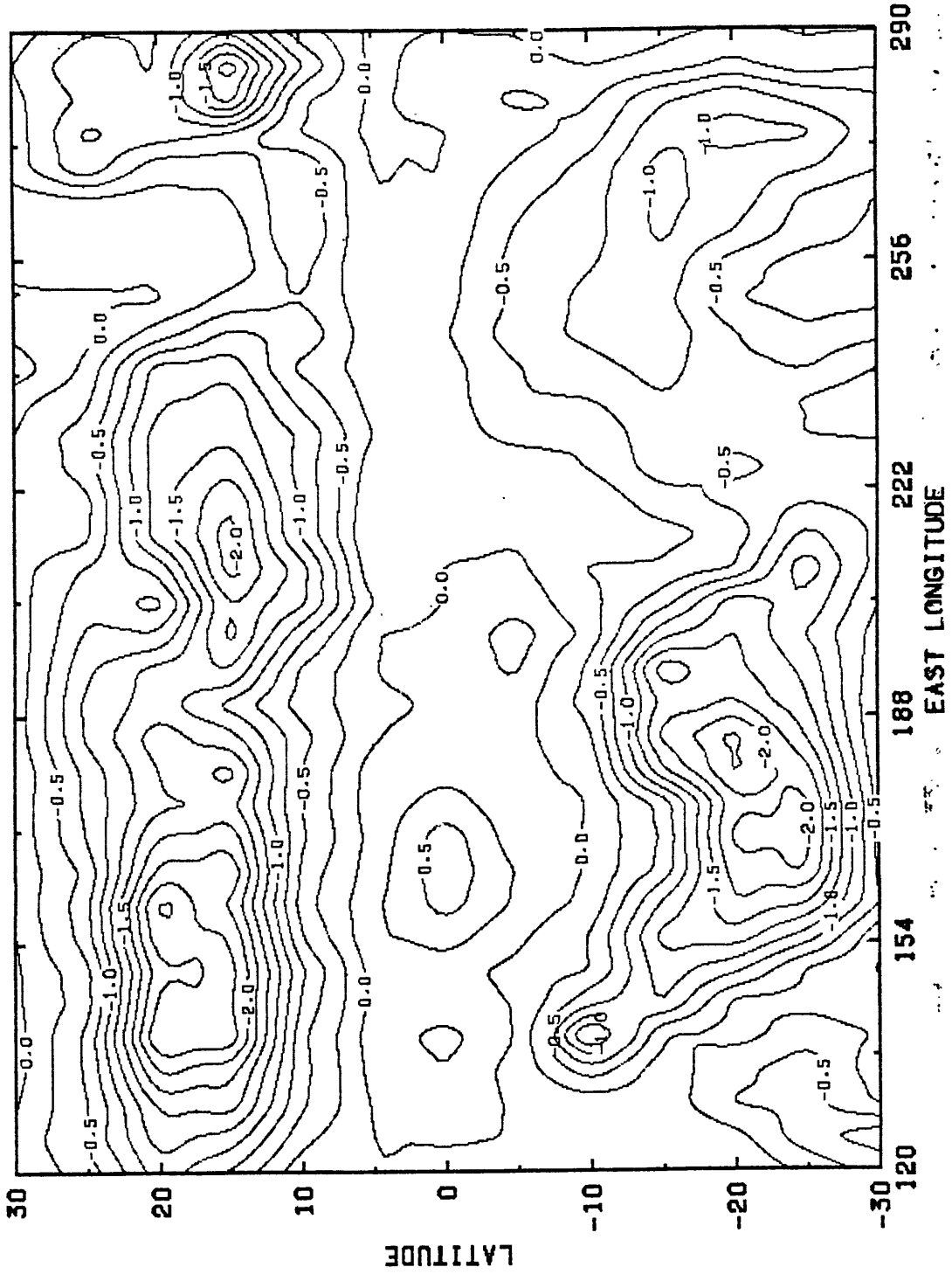

FIGURE 5.29

NMC Zonal Stress (dynes)
January 1983

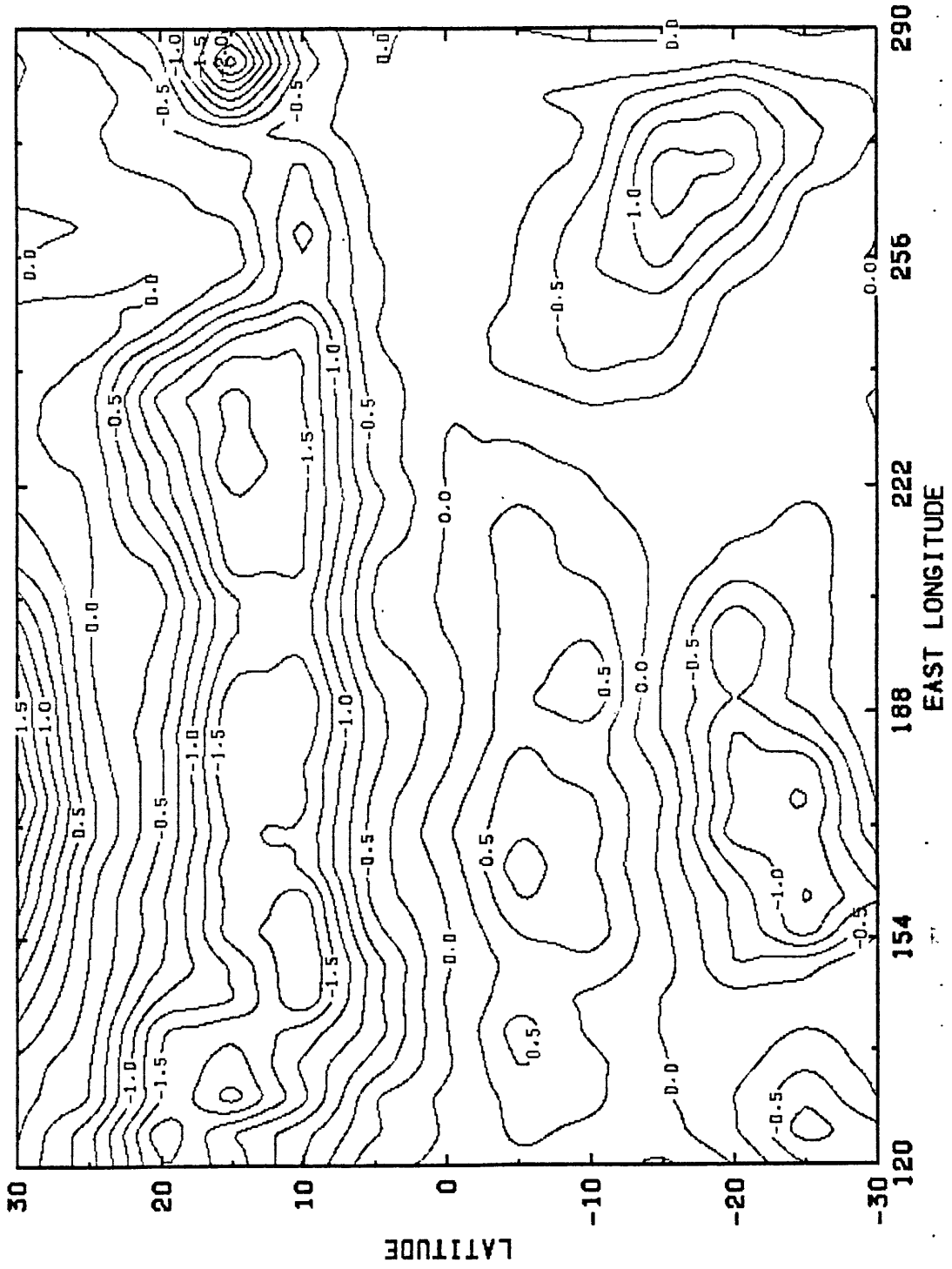

FIGURE 5.30

NMC Zonal Stress (dynes)
March 1983

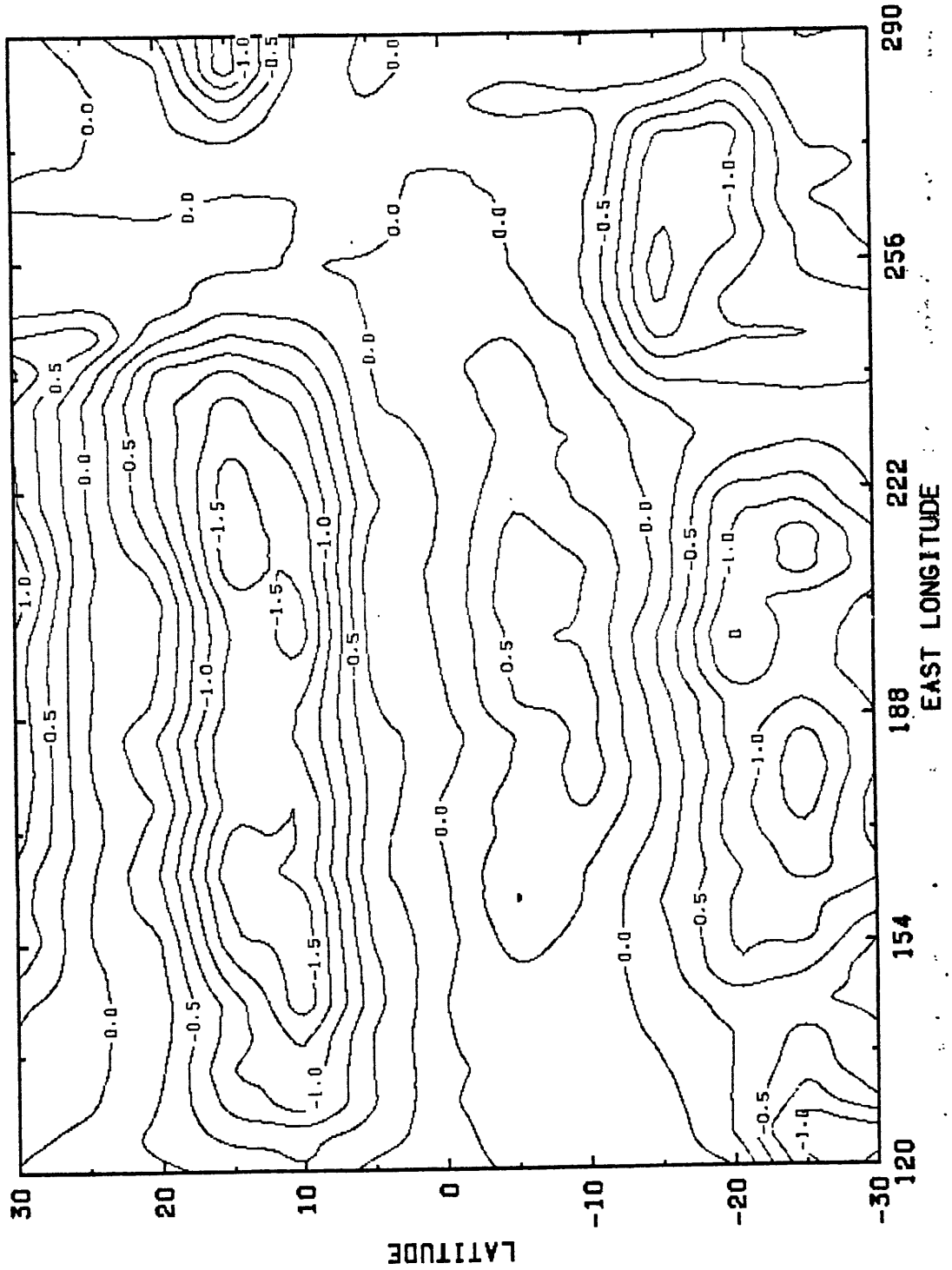

FIGURE 5.31

NMC Zonal Stress (dynes)
May 1983

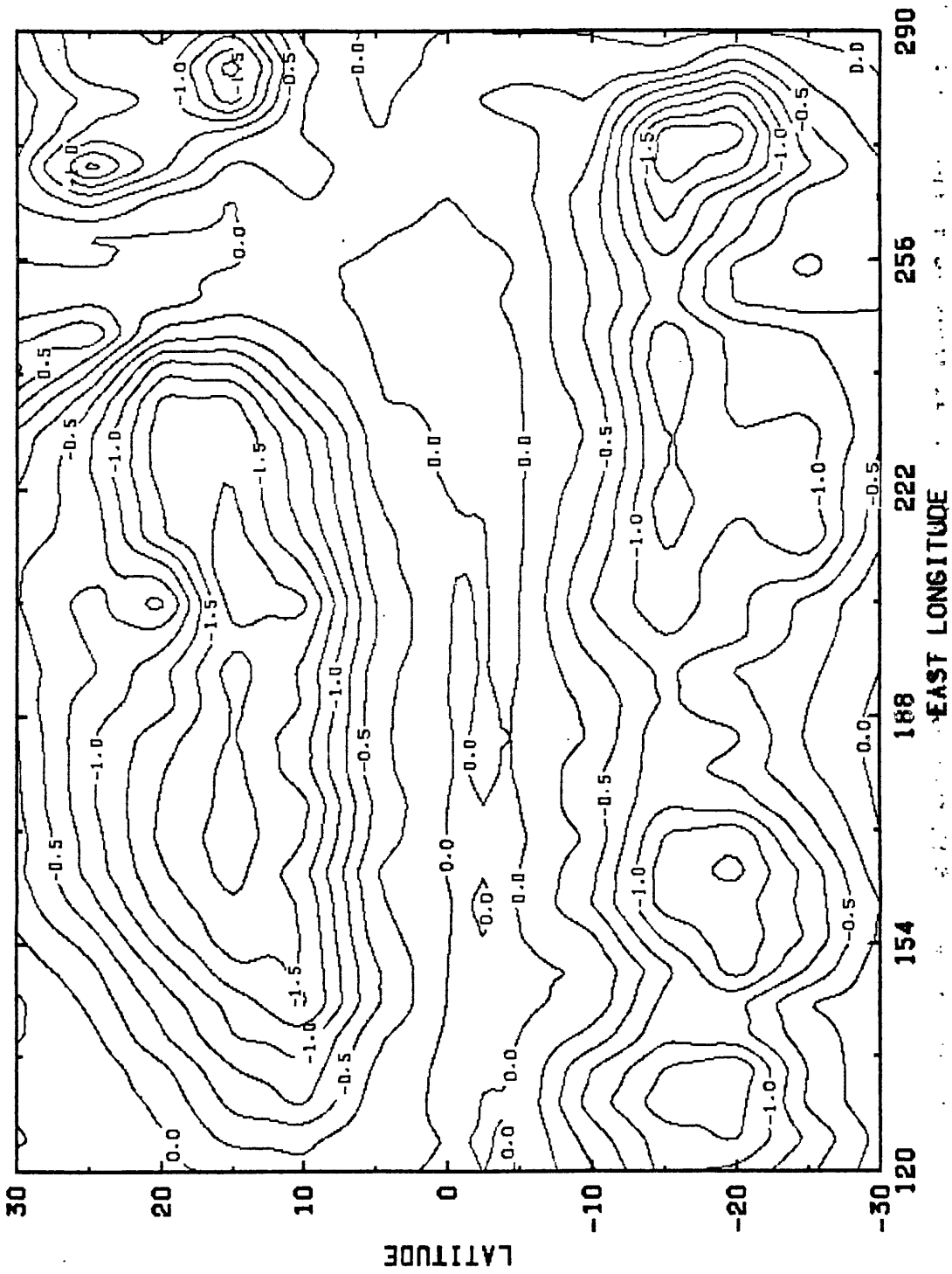

FIGURE 5.32

Stress Error Transform
Forcing Period = DC

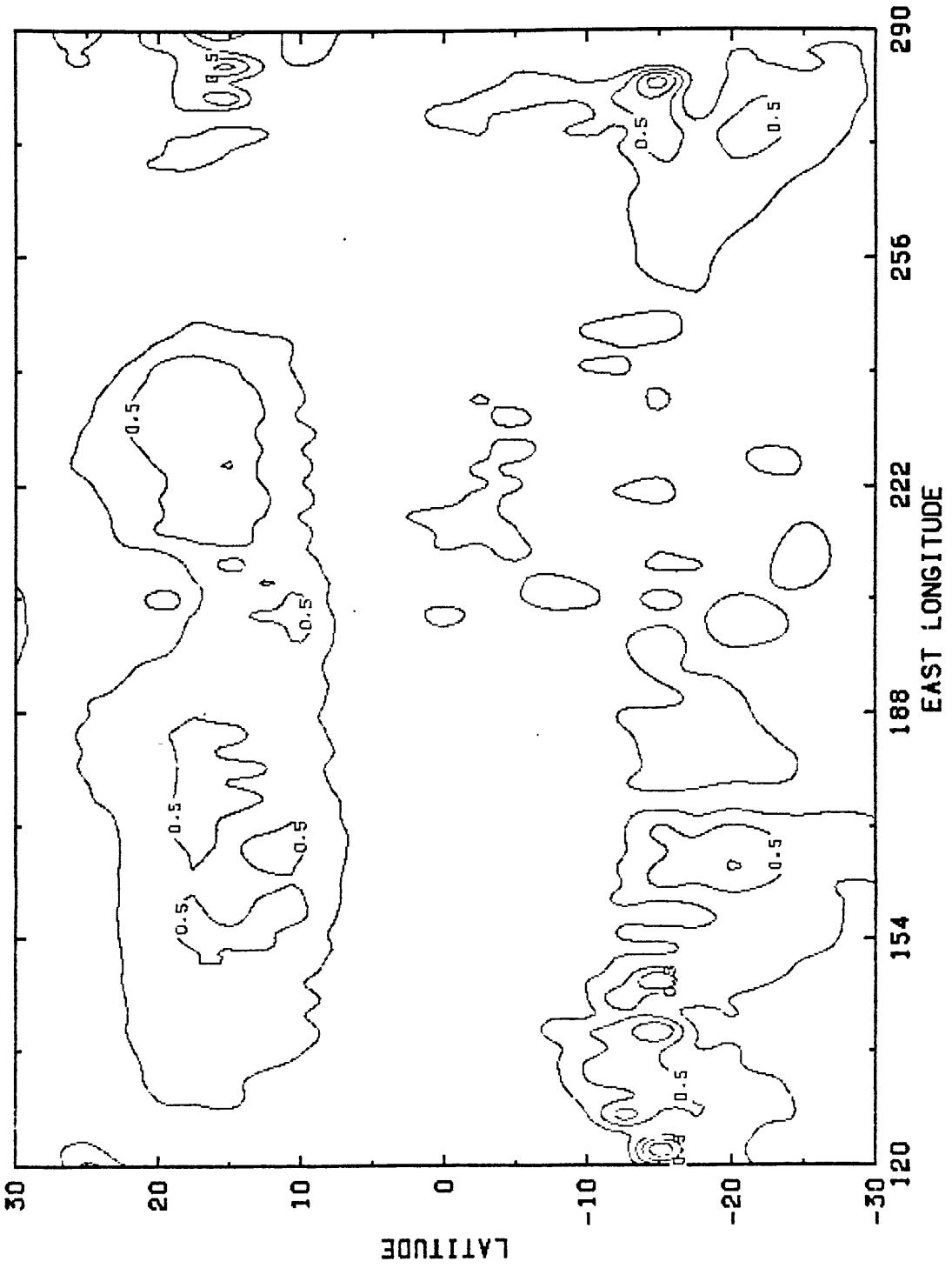

FIGURE 5.33

Stress Error Transform
Forcing Period = 18 Months

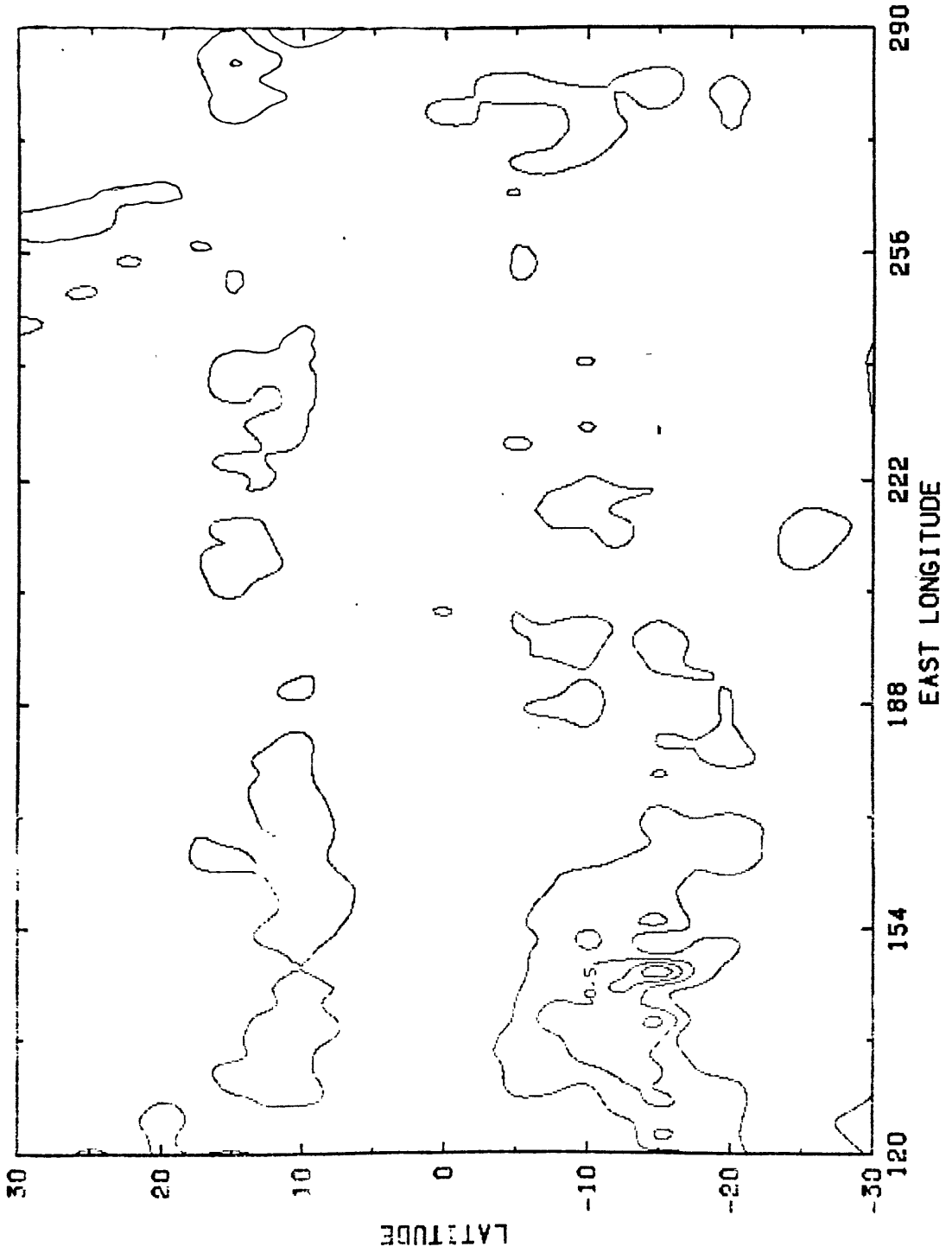

FIGURE 5.34

Stress Error Transform
Forcing Period = 6 Months

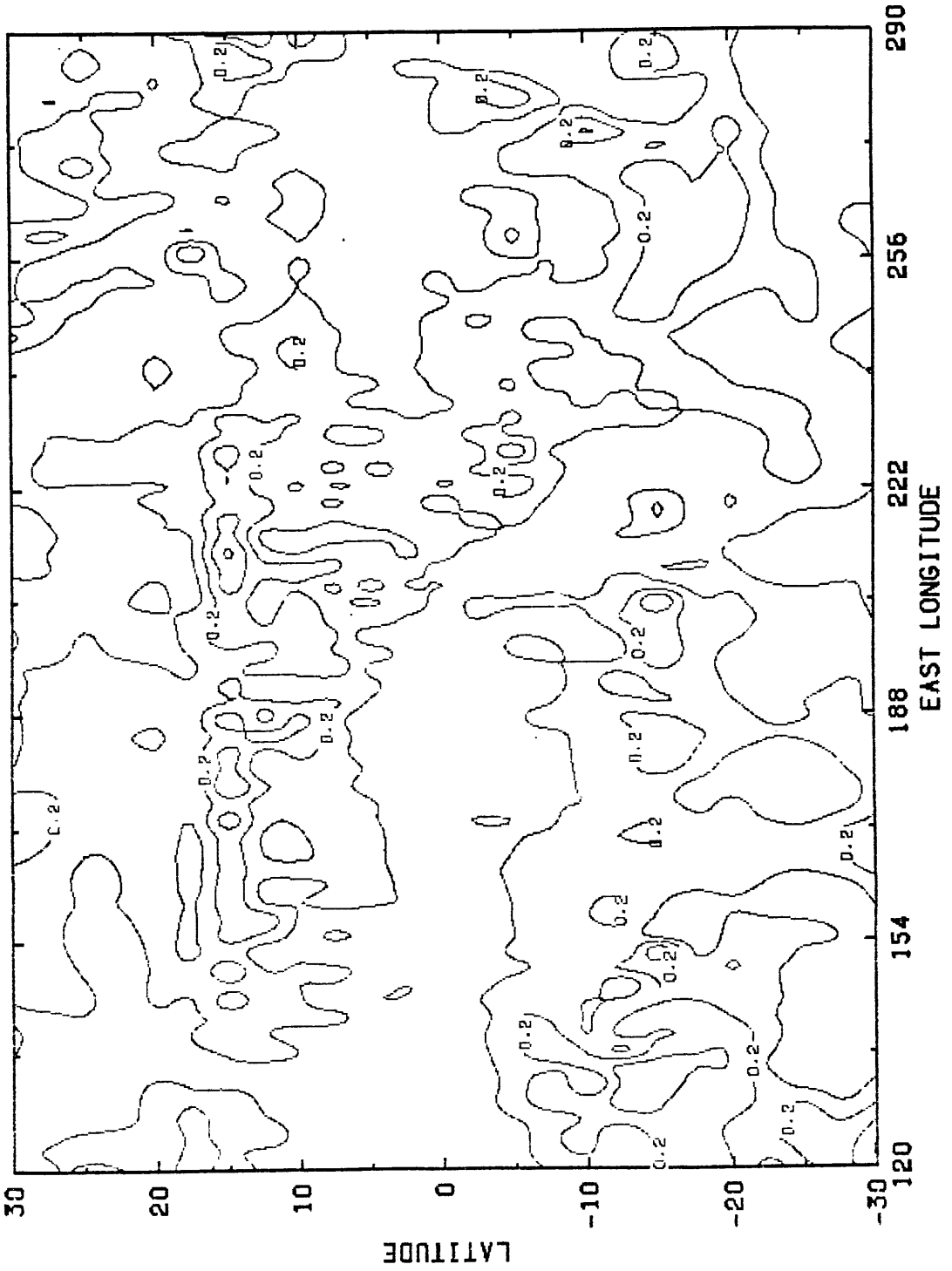

FIGURE 5.35

Stress Error Transform
Forcing Period = 3 Months

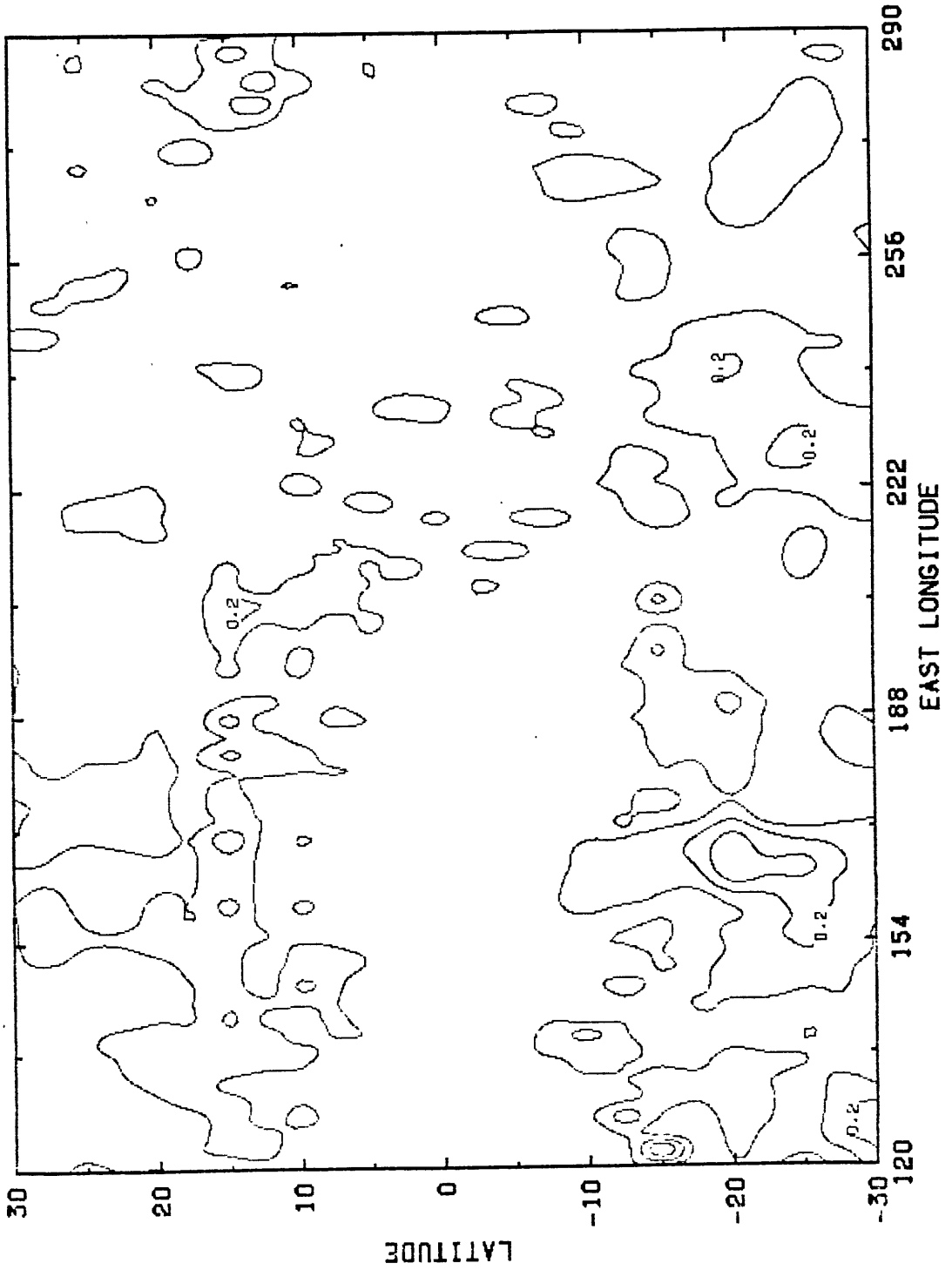

FIGURE 5.36

Stress Error Transform
Forcing Period = 2 Months

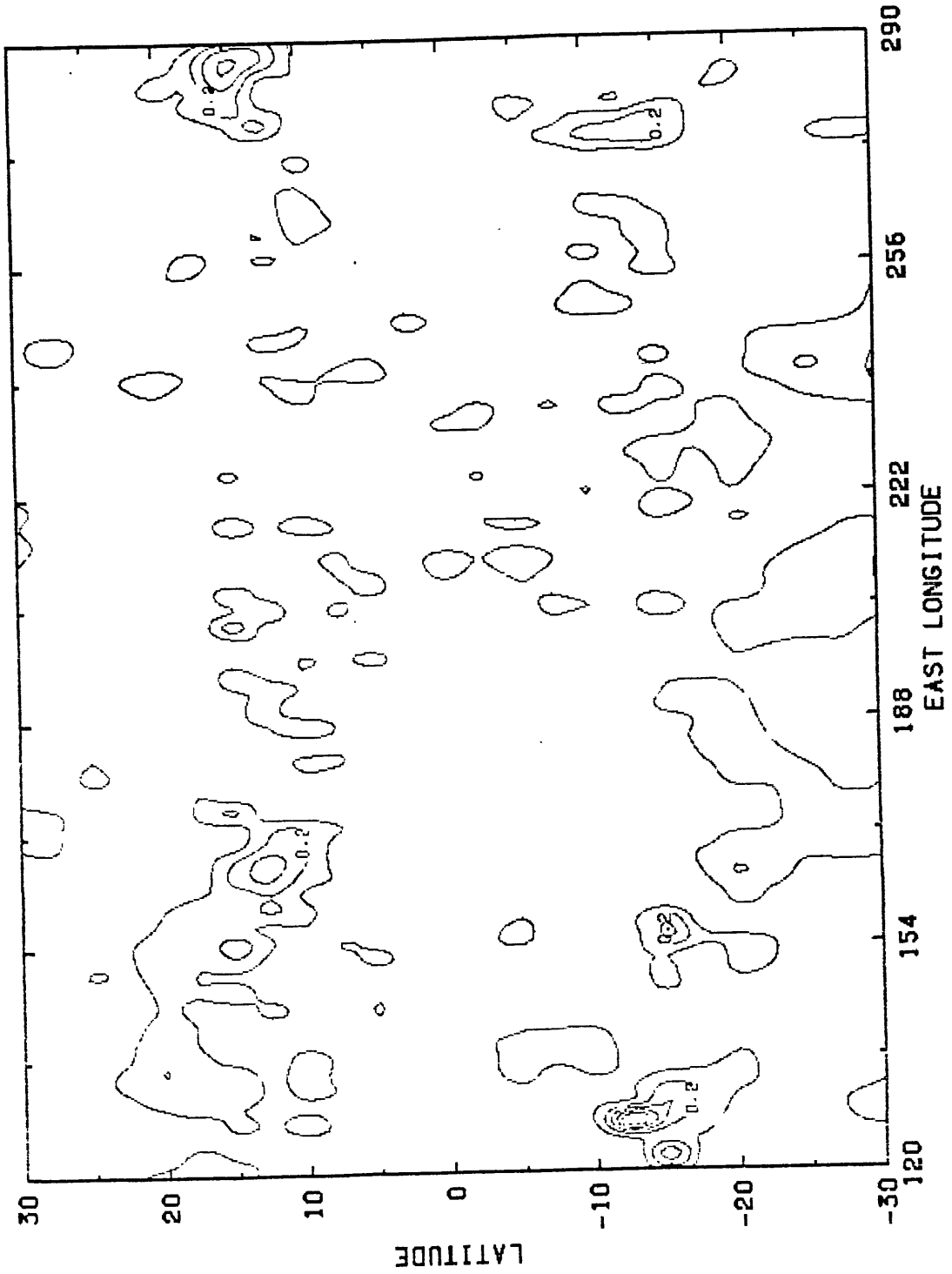

FIGURE 5.37

Galapagnos (1s,90w)
Sea Surface Error

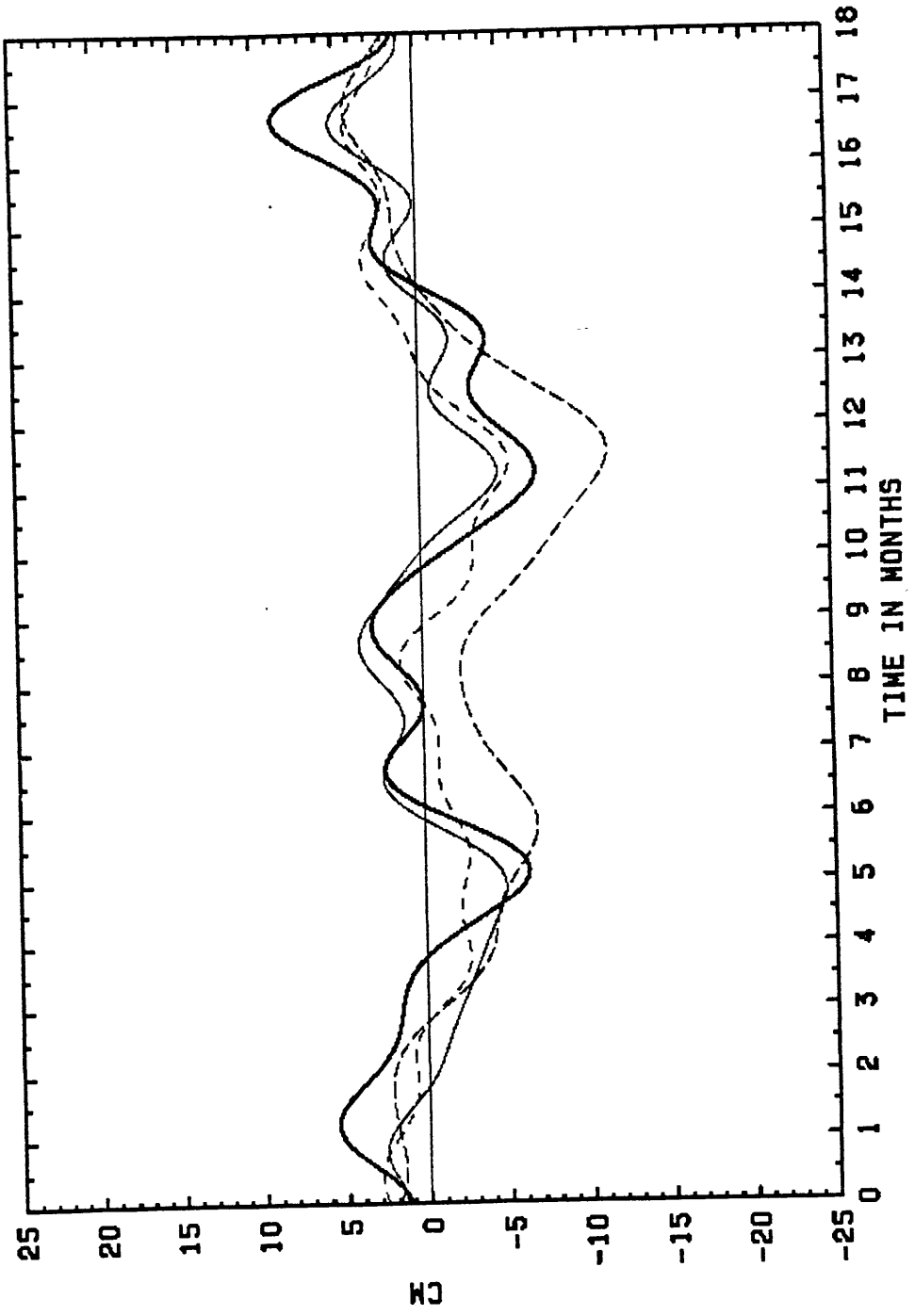

FIGURE 5.38

Christmas (2N,157W)
Sea Surface Error

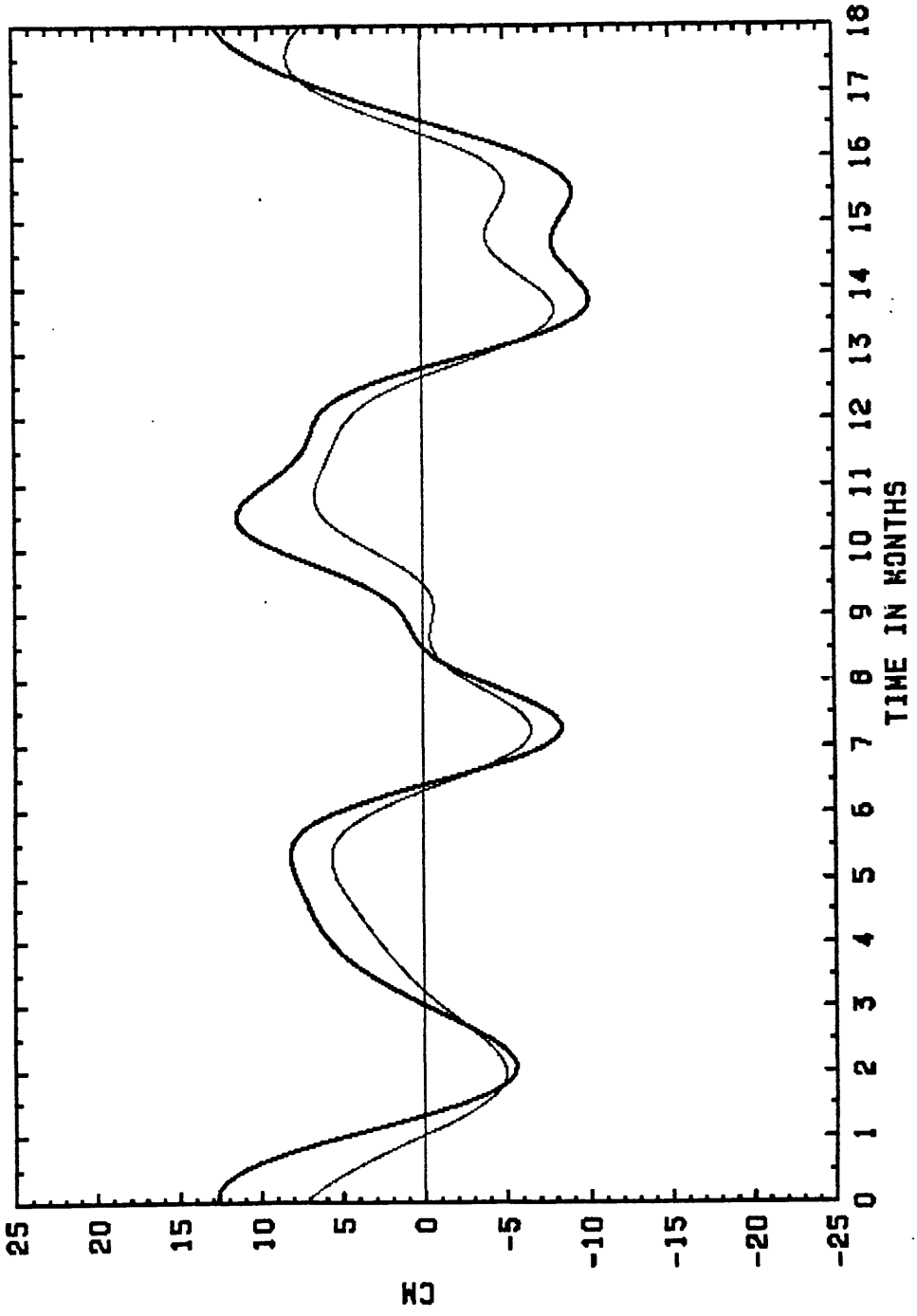

FIGURE 5.39

Fanning (4N,159W)
Sea Surface Error

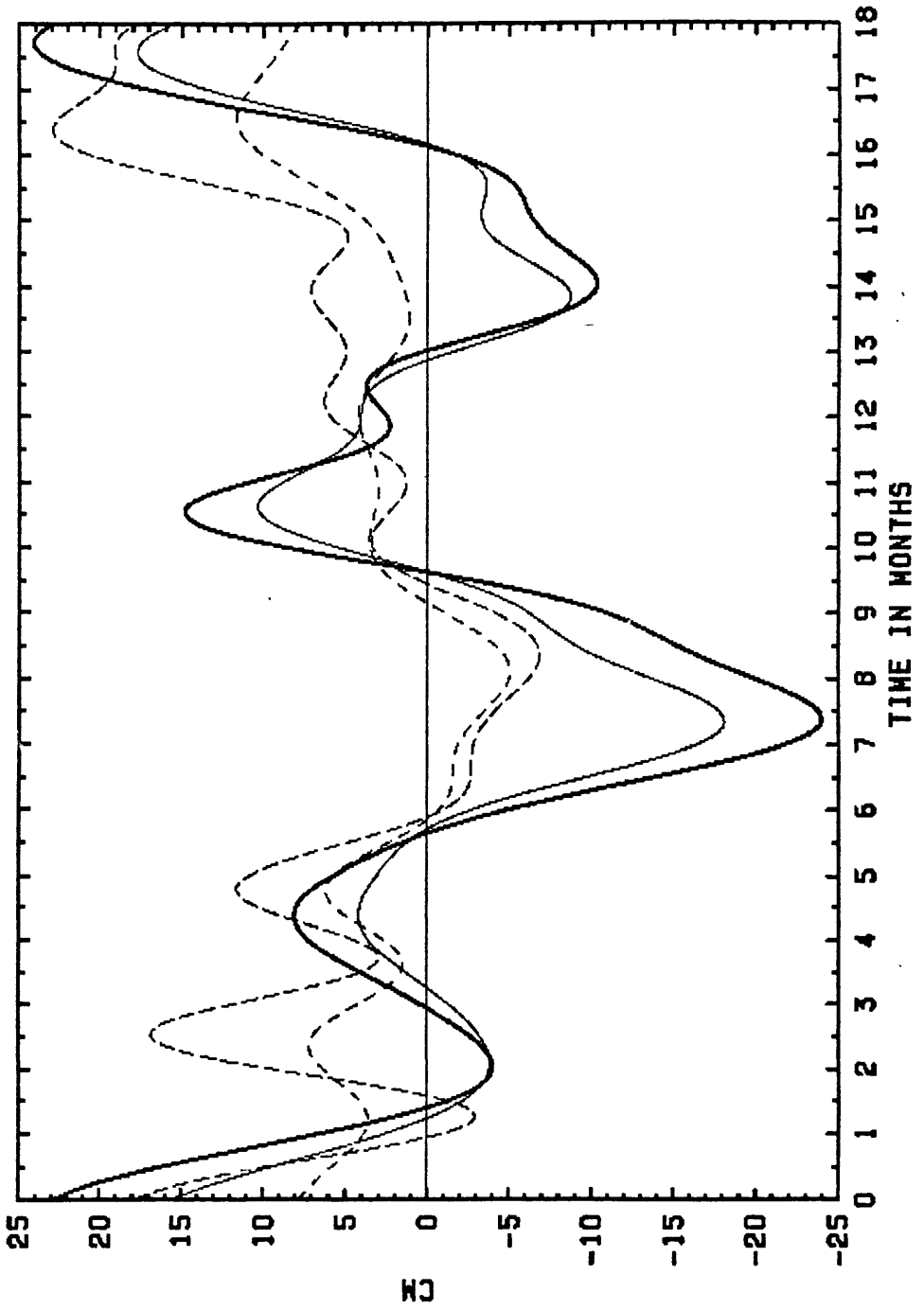

FIGURE 5.4Q

Jarvis (5S,161W)
Sea Surface Error

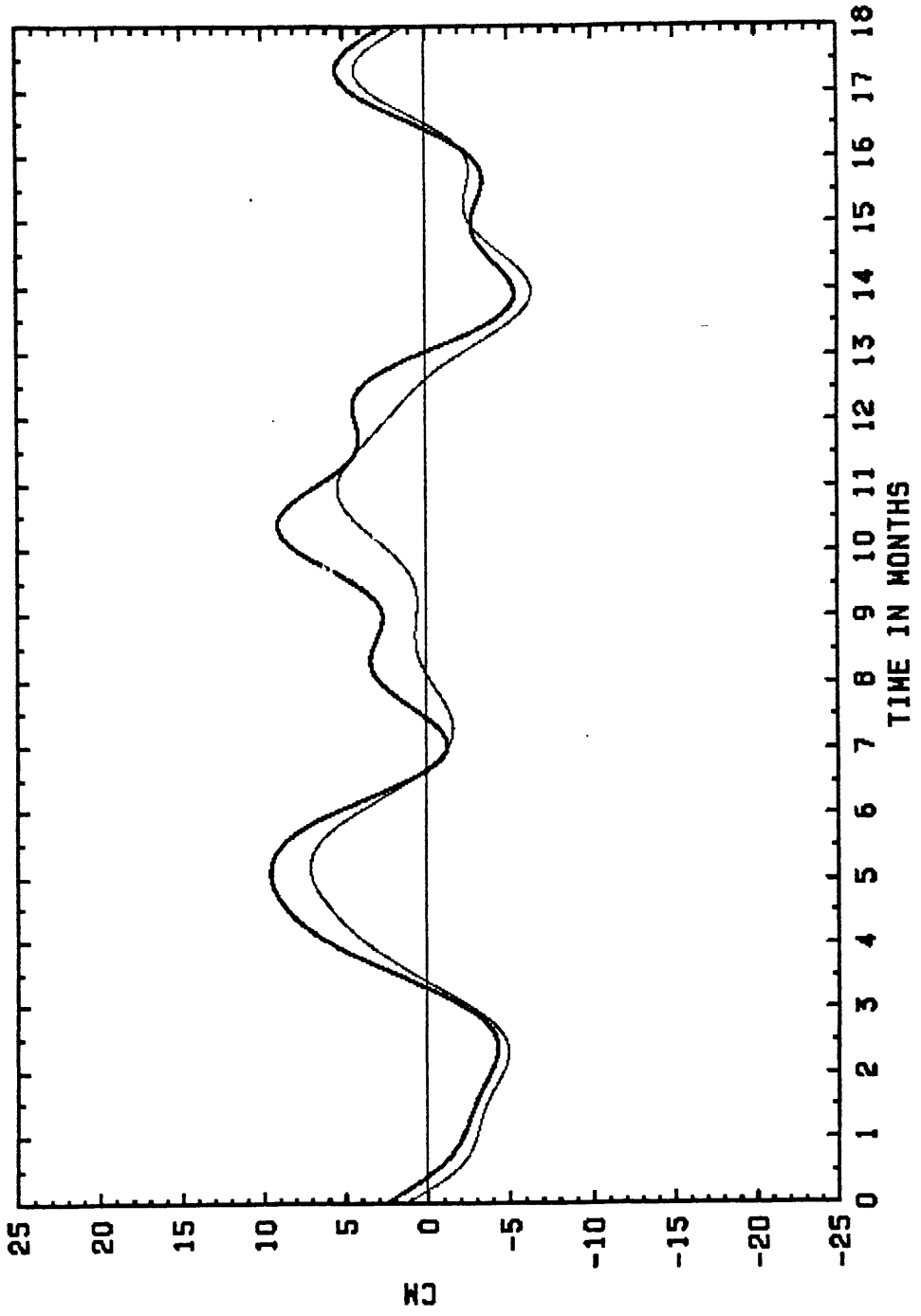

FIGURE 5.41

Canton (3S,172W)
Sea Surface Error

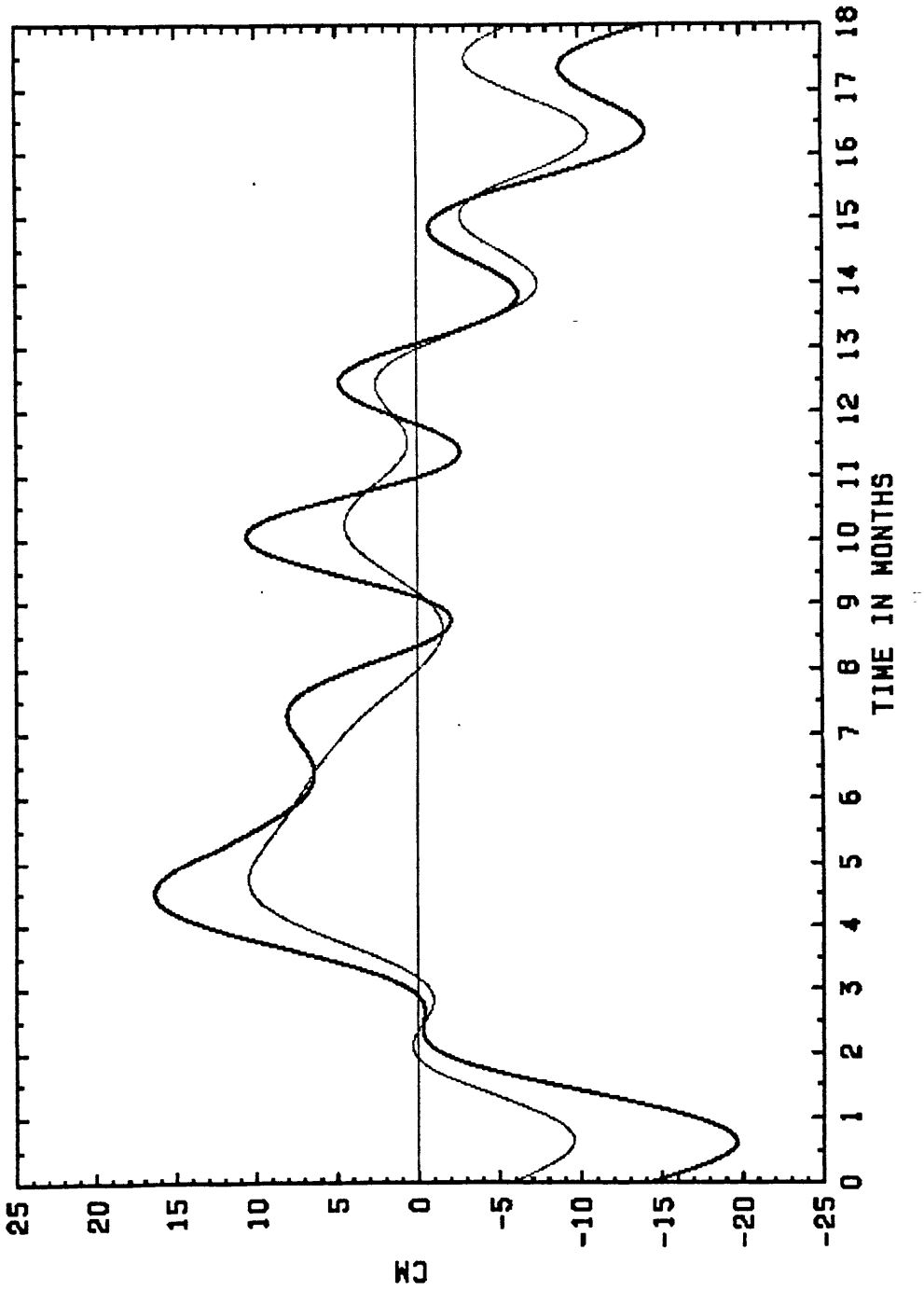

FIGURE 5.42

Kwajalien (8.5N,168E)
Sea Surface Error

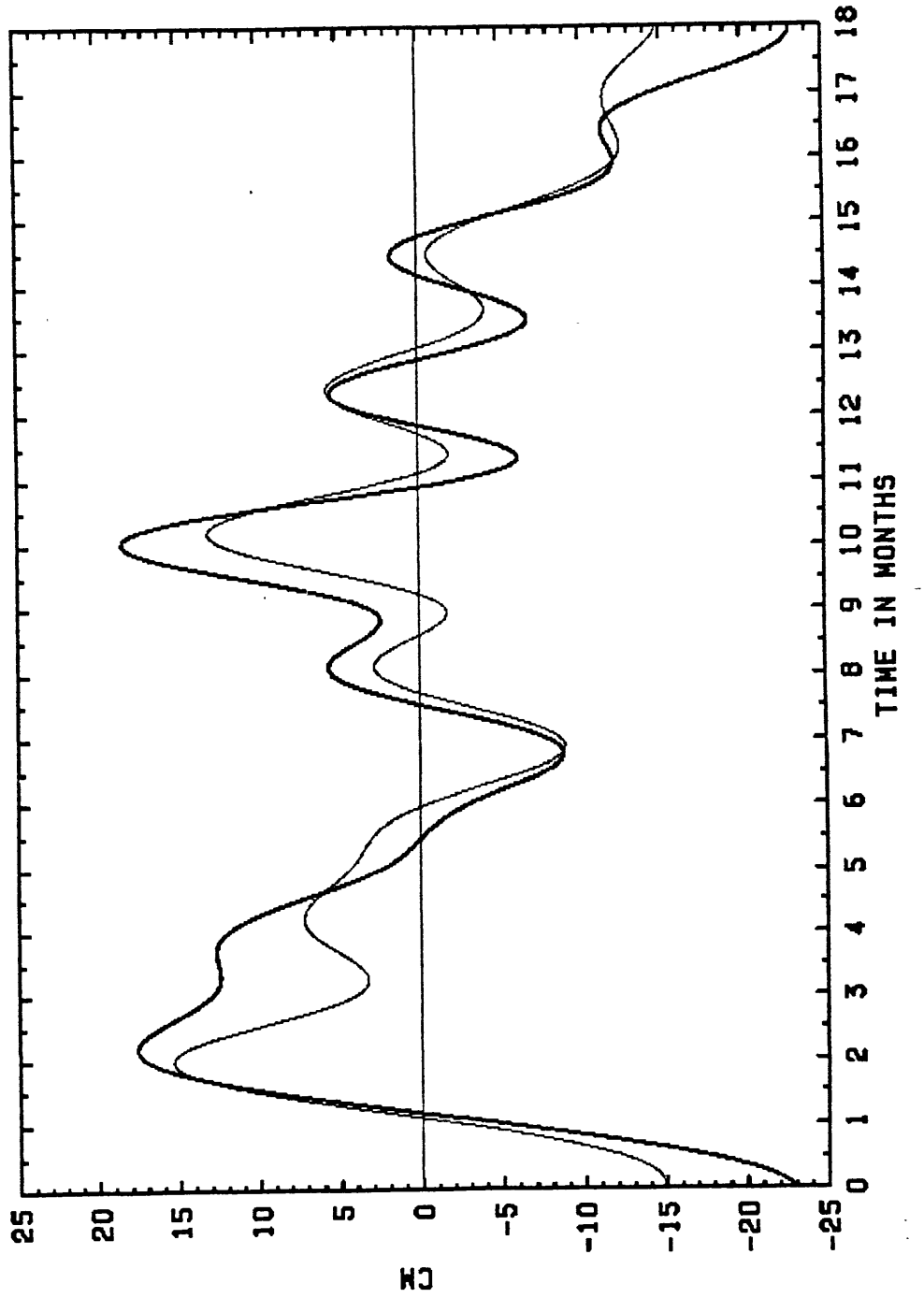

FIGURE 5.43

Nauru (1S,167E)
Sea Surface Error

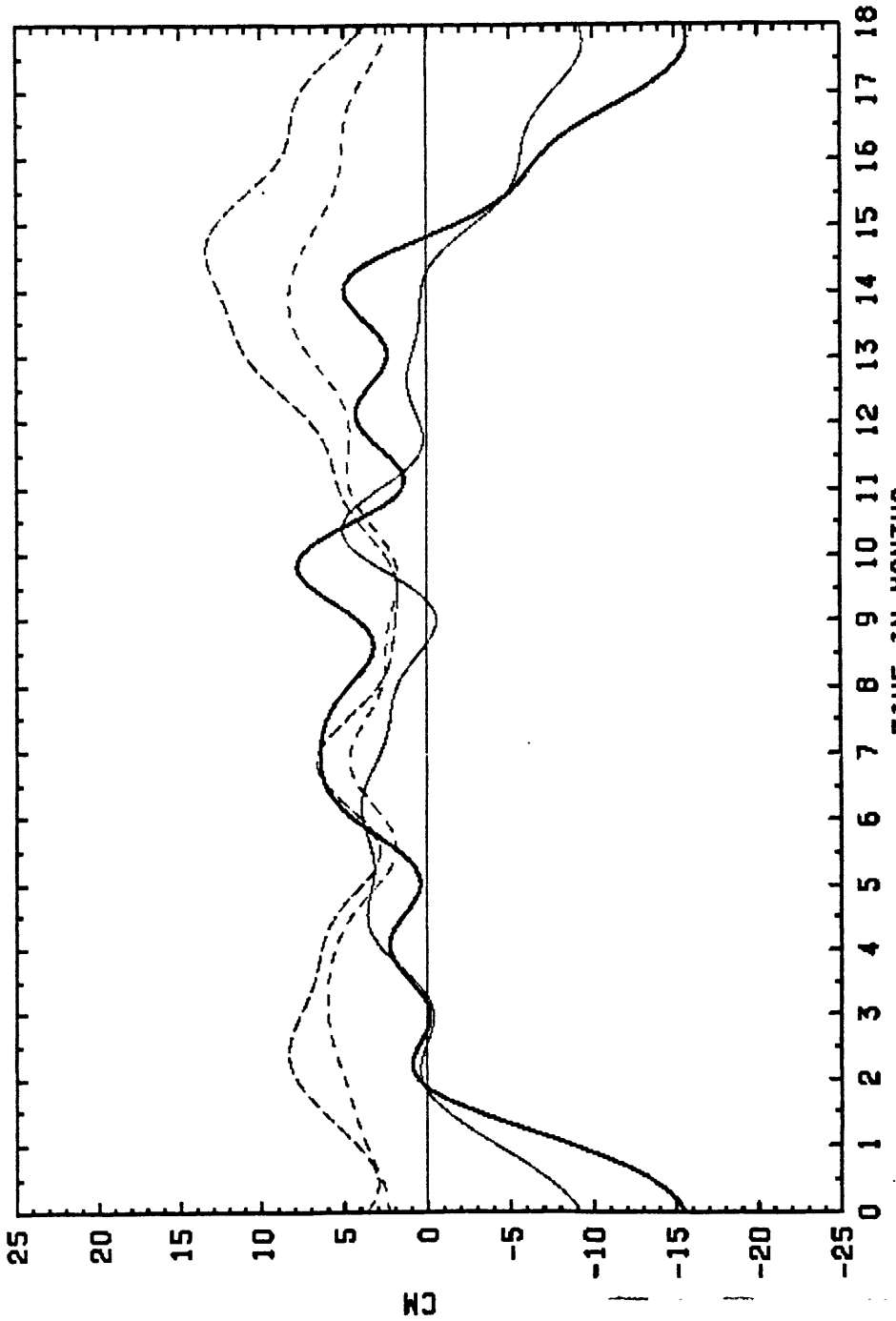

FIGURE 5.44

Truk (7N,151E)
Sea Surface Error

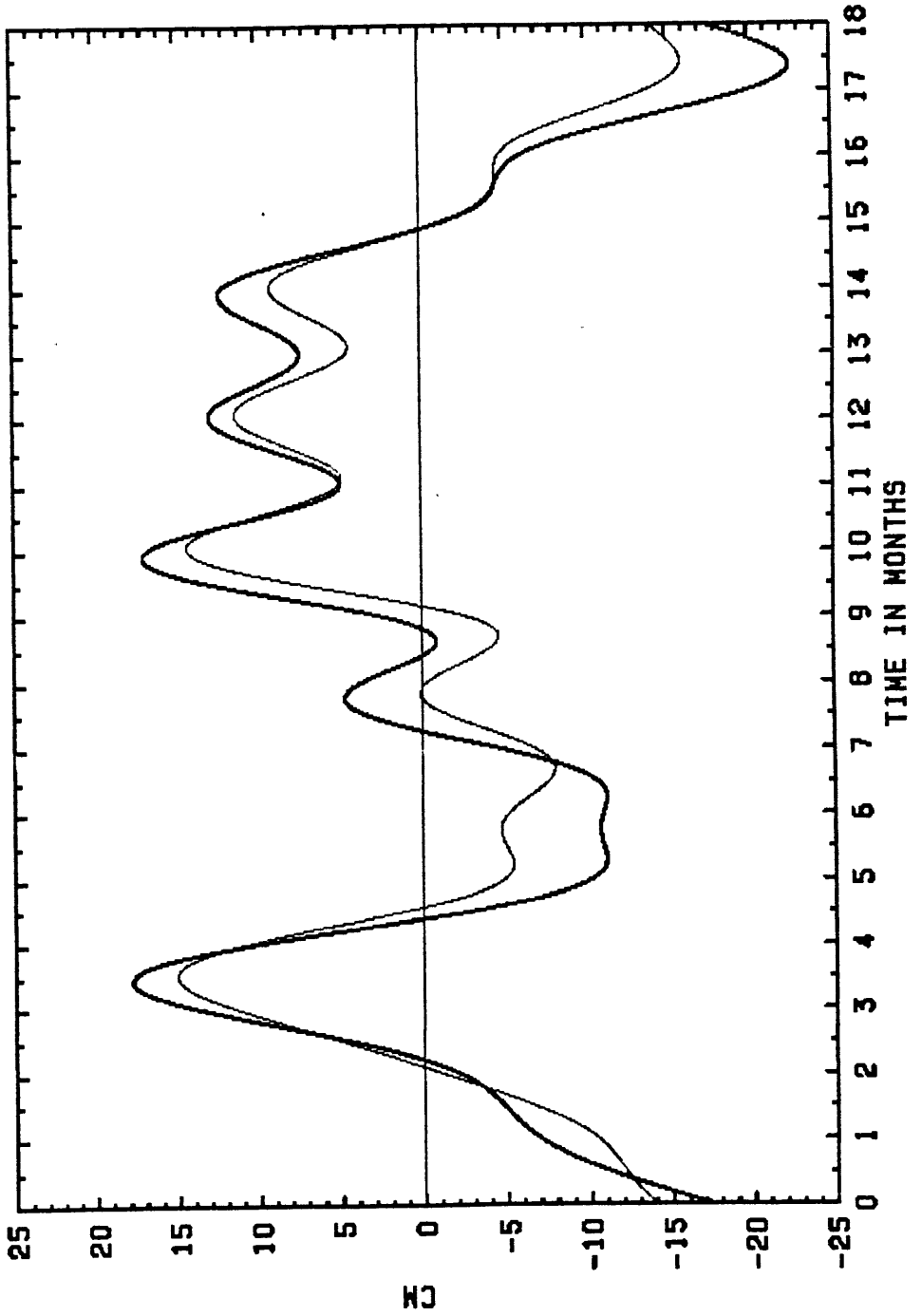

FIGURE 5.45

Rabaul (4S,152E)
Sea Surface Error

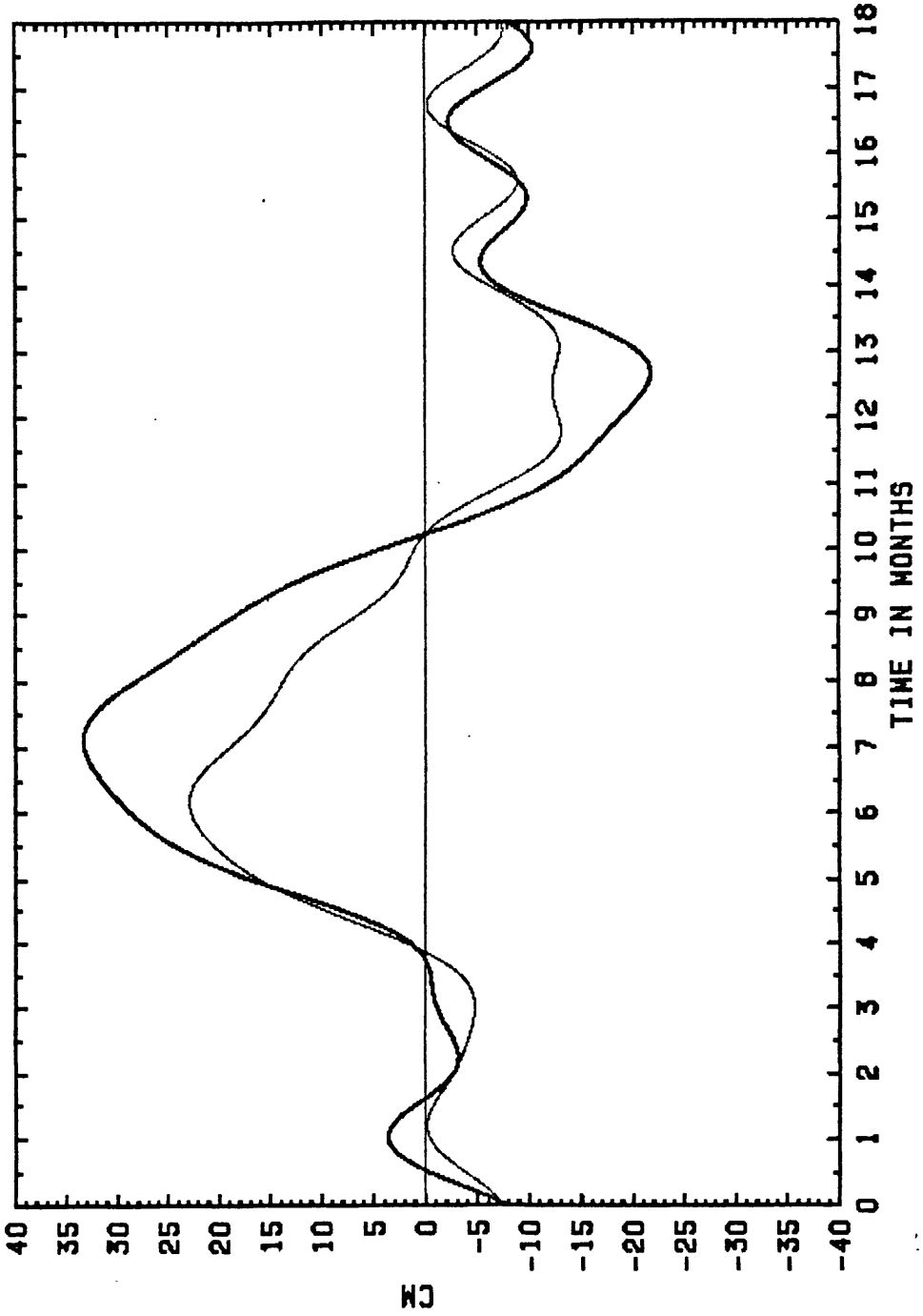

FIGURE 5.46

Malakal (7N,134E)
Sea Surface Error

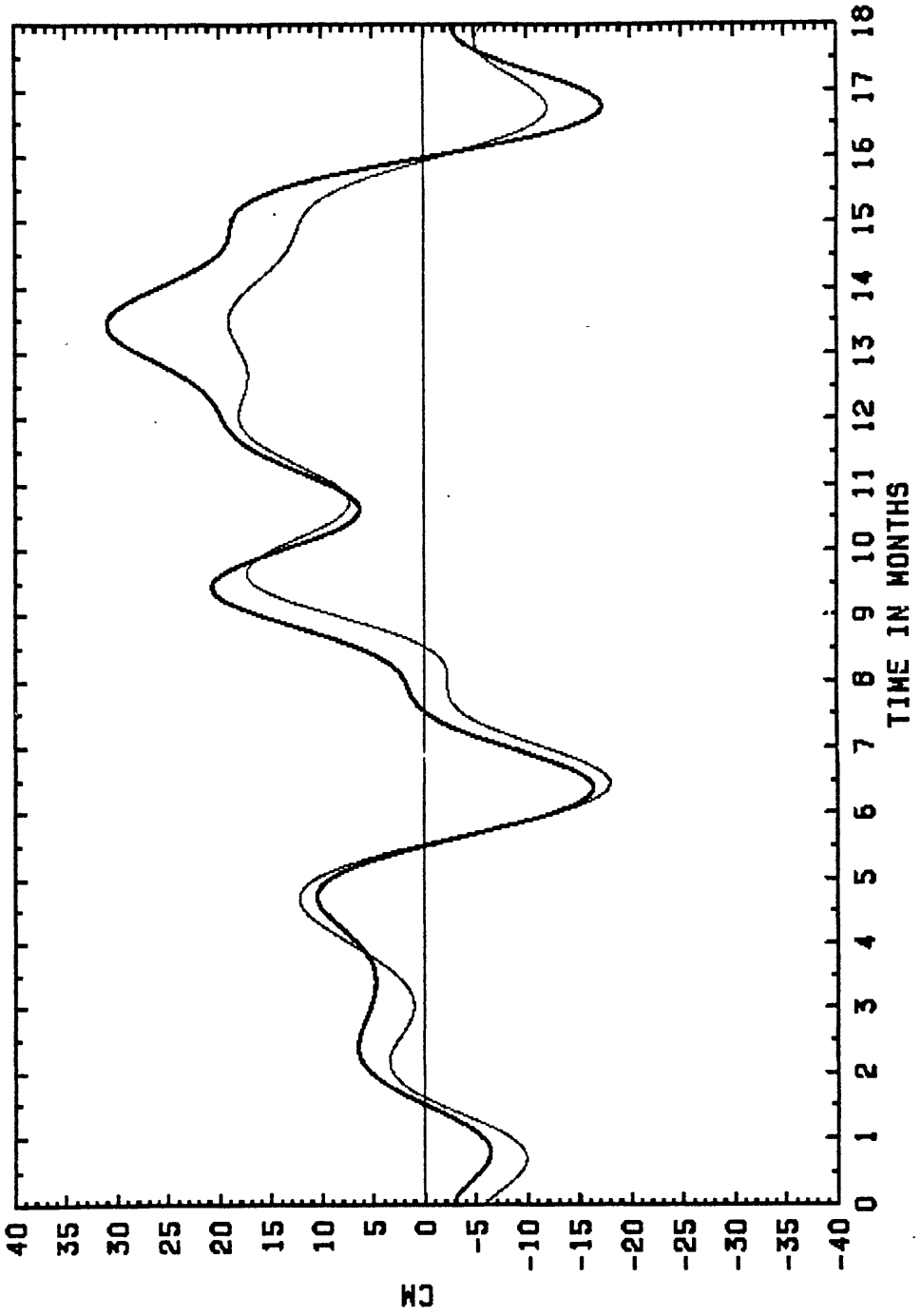

FIGURE 6.1

Indian Observation Stations

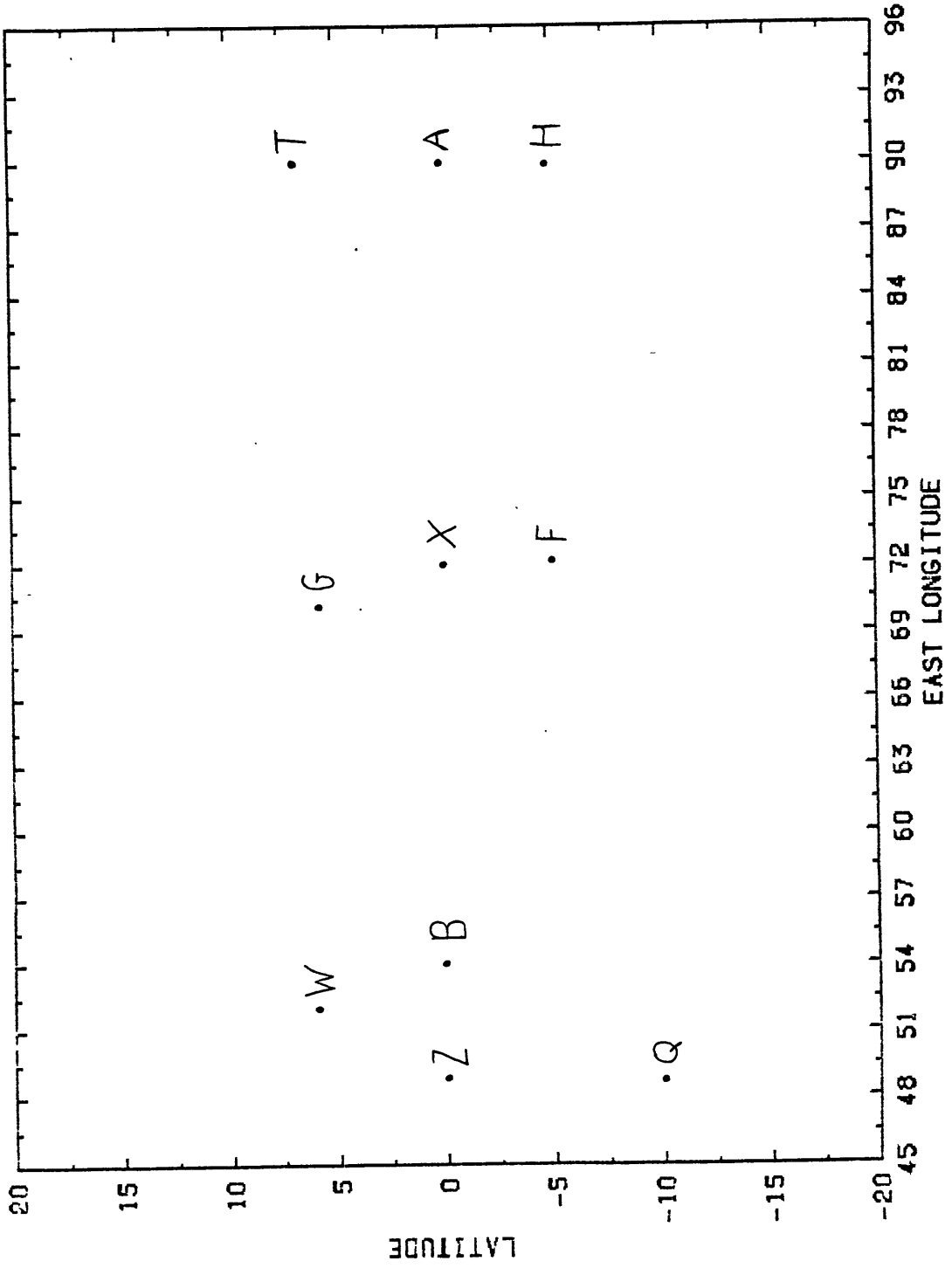

FIGURE 6.2

EMC Zonal Stress (dynes)
December 1978

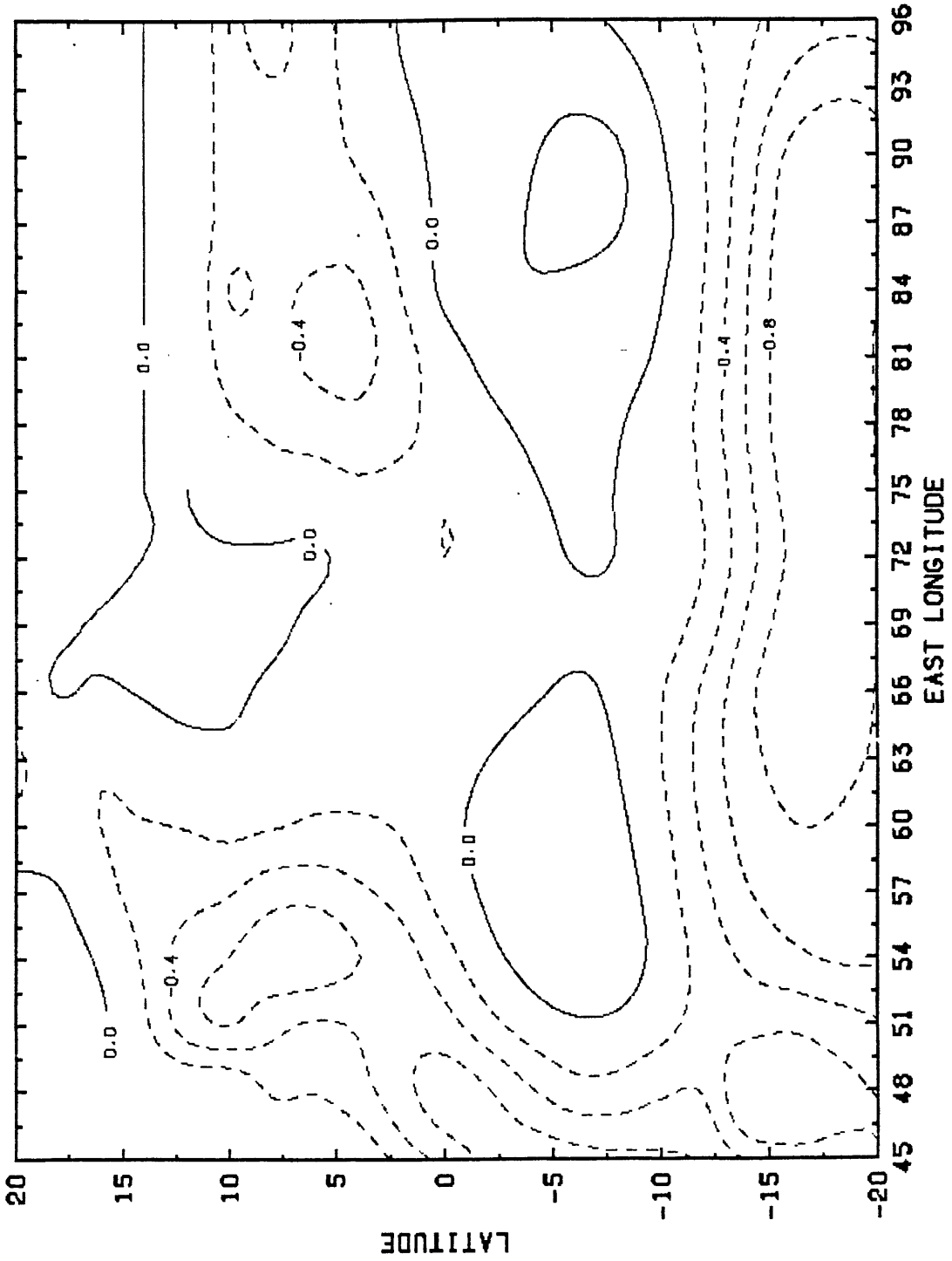

FIGURE 6.3

EMC Zonal Stress (dynes)
January 1979

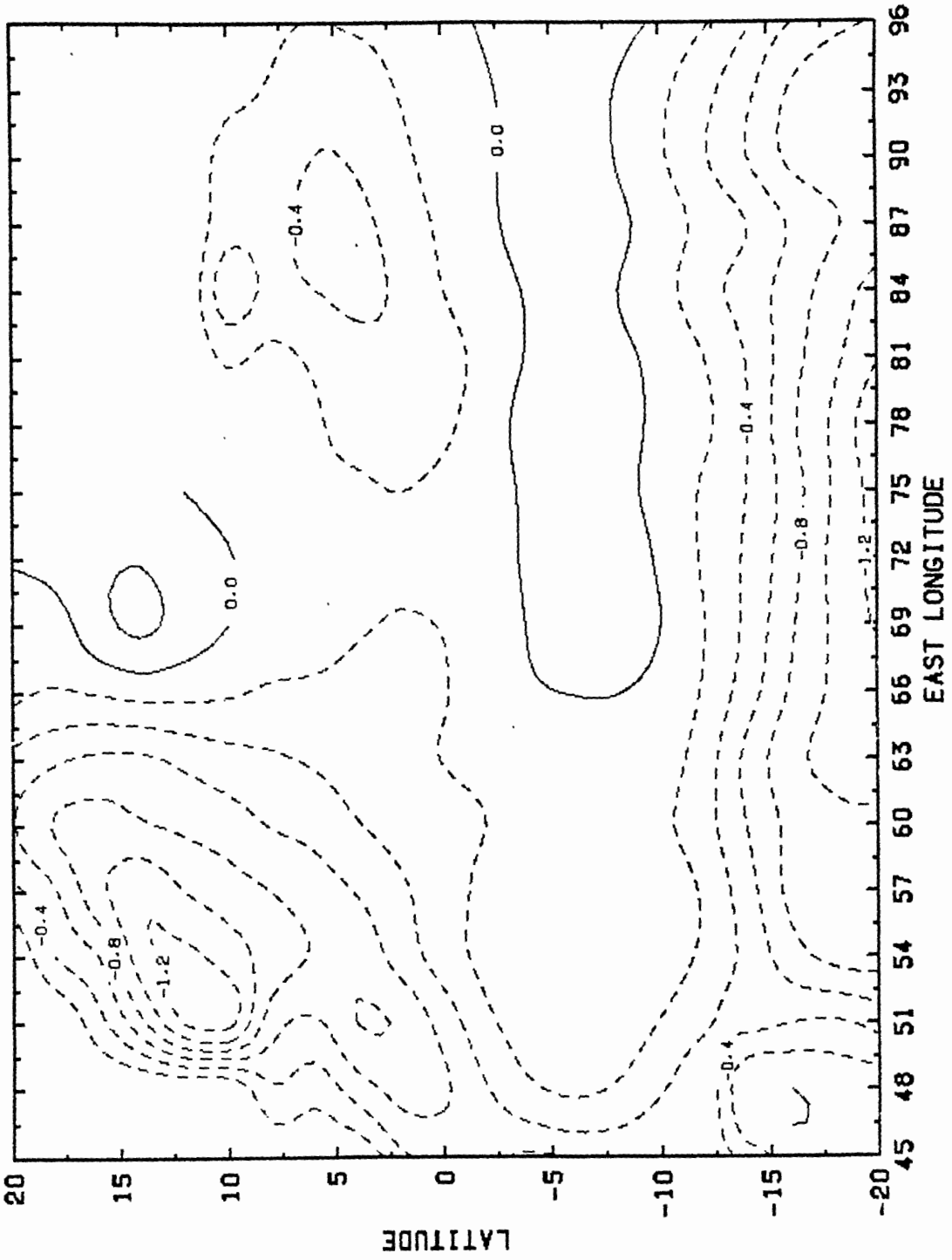

FIGURE 6.4

EMC Zonal Stress (dynes)
February 1979

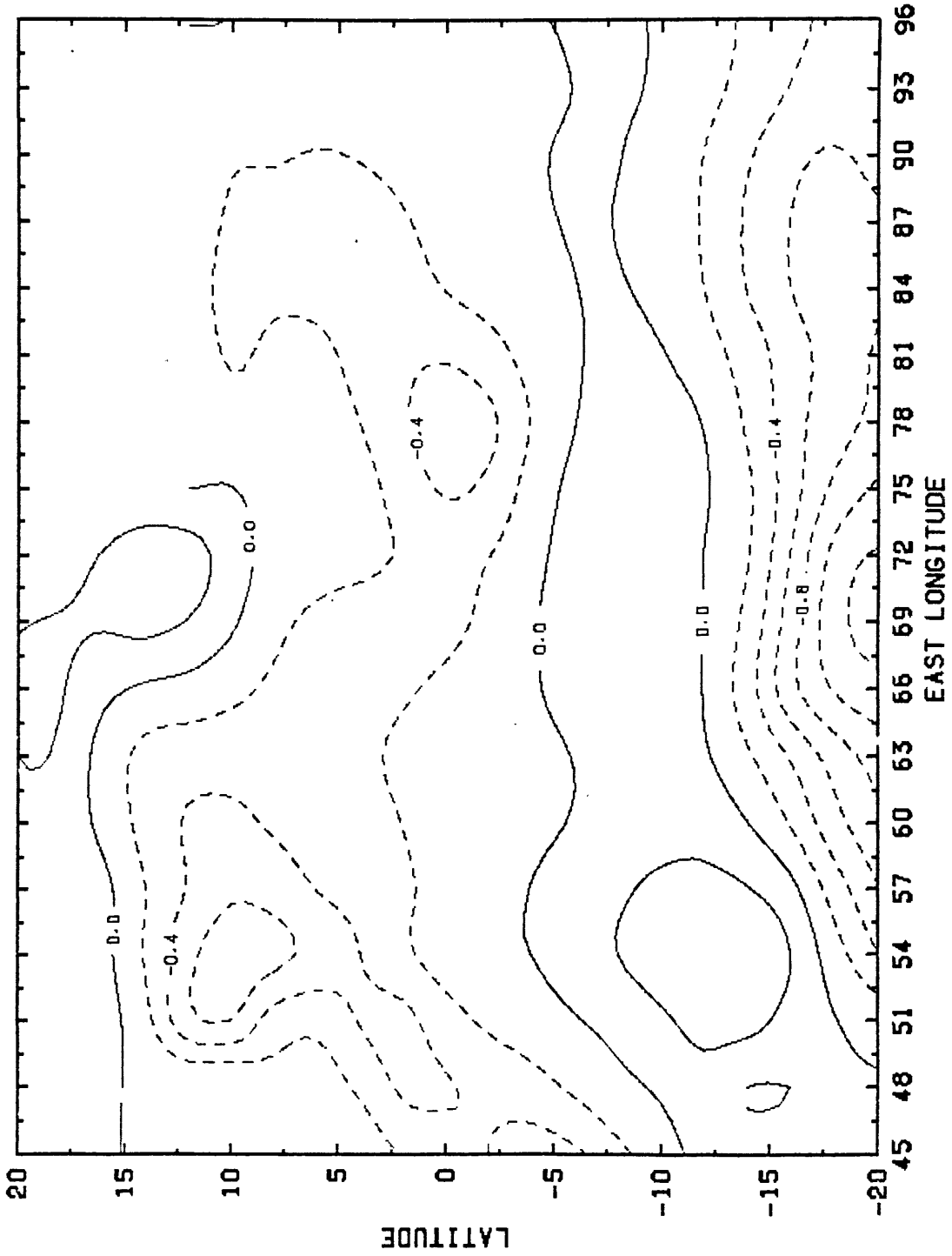

FIGURE 6.5

EMC Zonal Stress (dynes)
March 1979

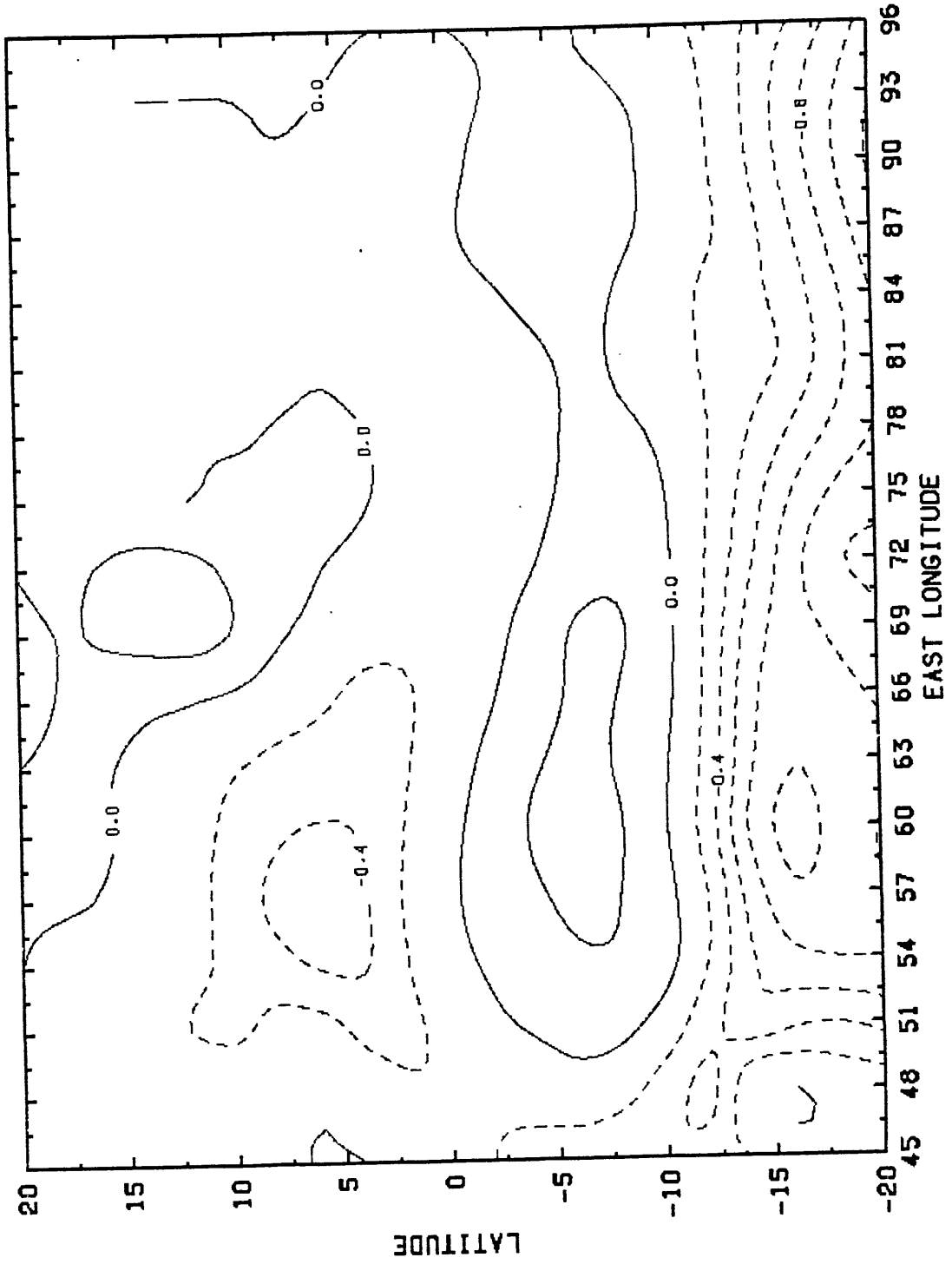

FIGURE 6.6

EMC Zonal Stress (dynes)
April 1979

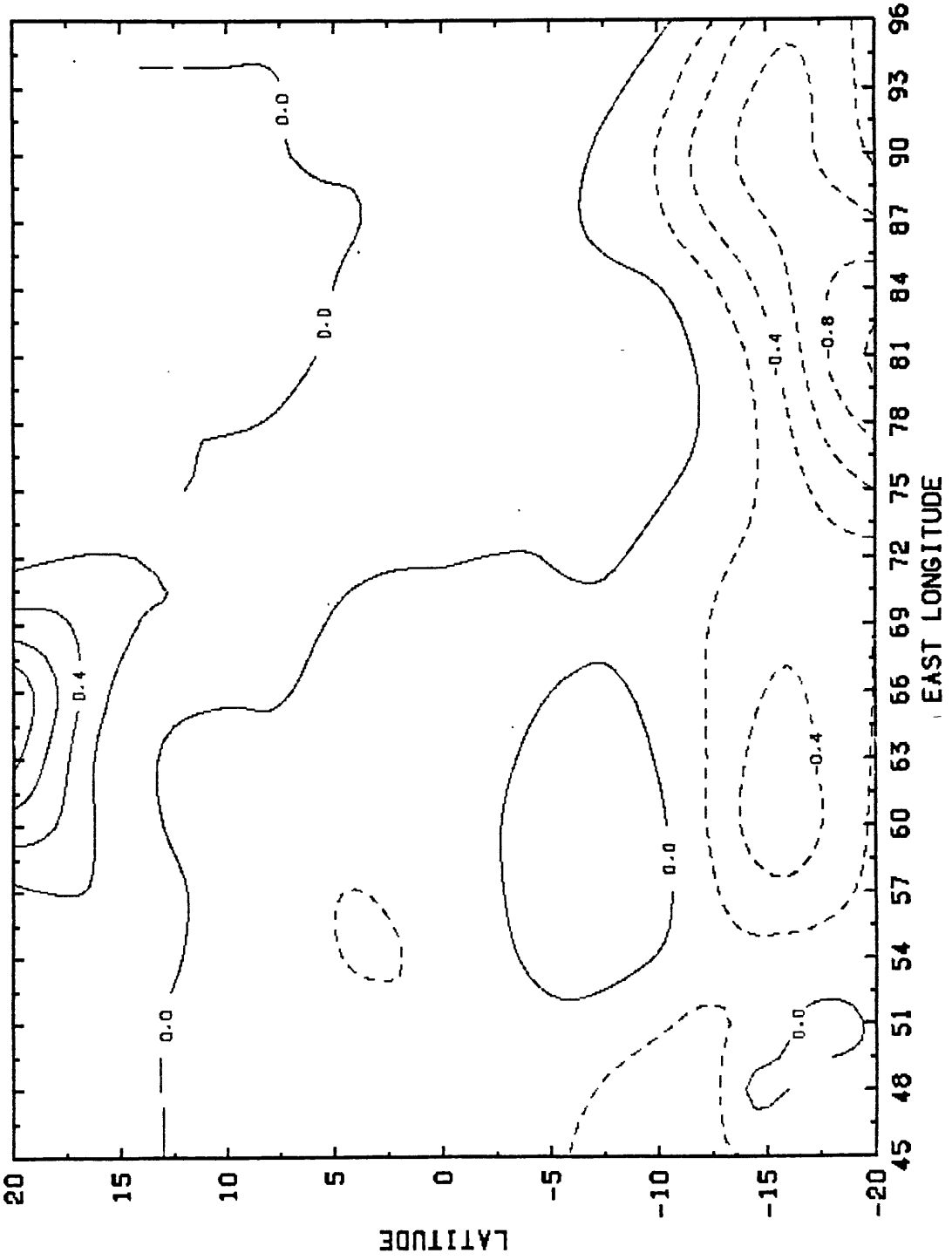

FIGURE 6.7

EMC Zonal Stress (dynes)
May 1979

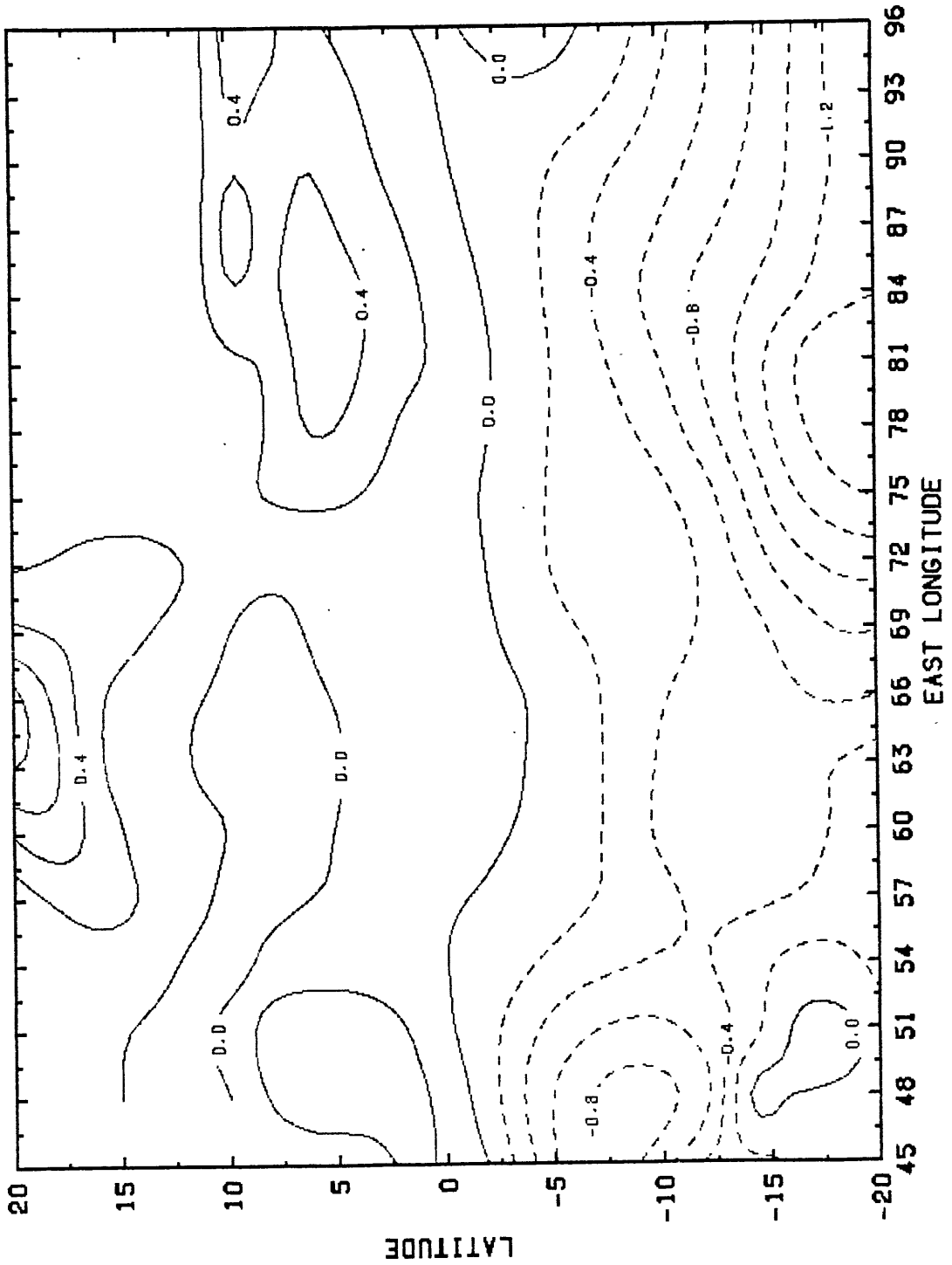

FIGURE 6.8

EMC Zonal Stress(dynes)
June 1979

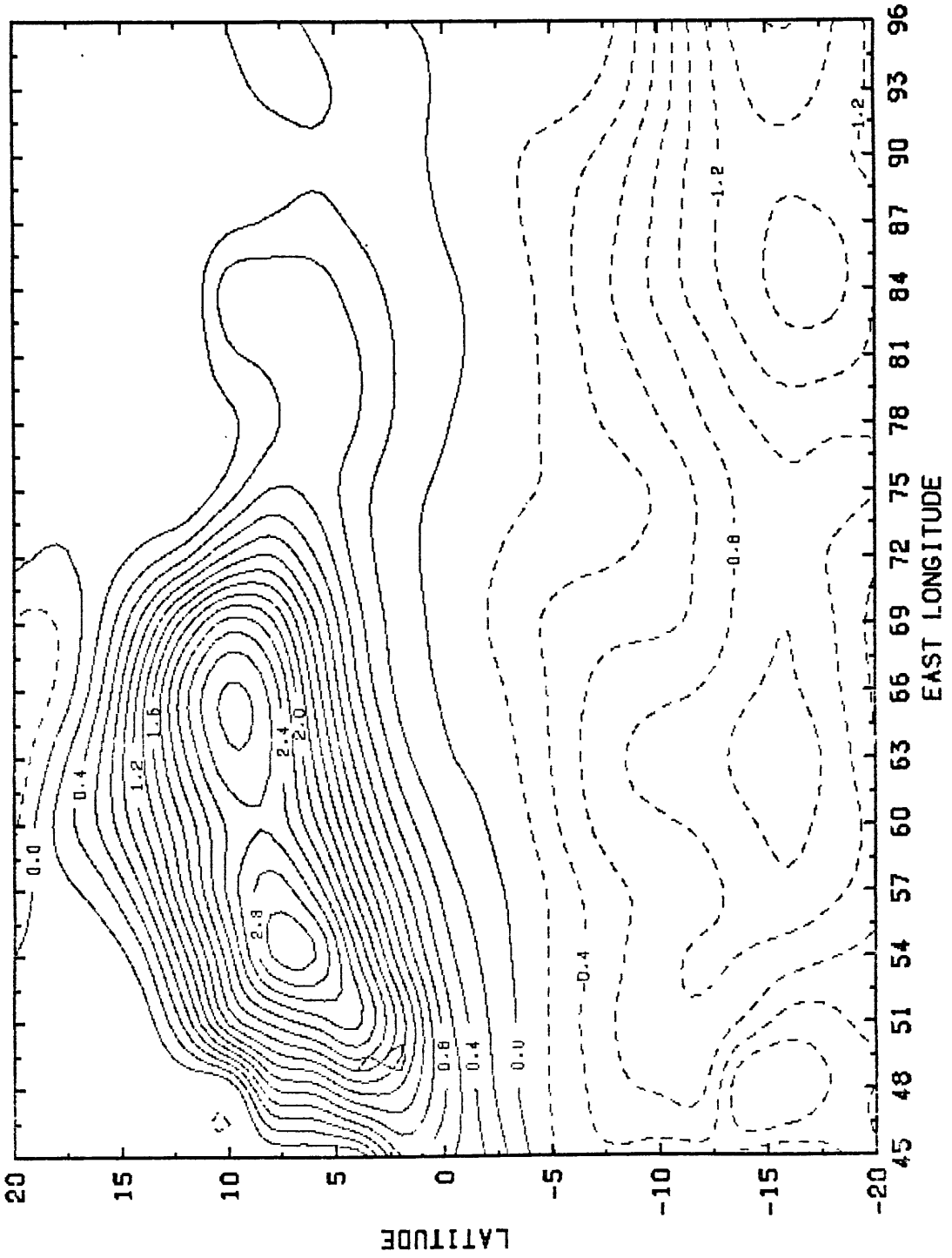

FIGURE 6.9

EMC Zonal Stress (dynes)
July 1979

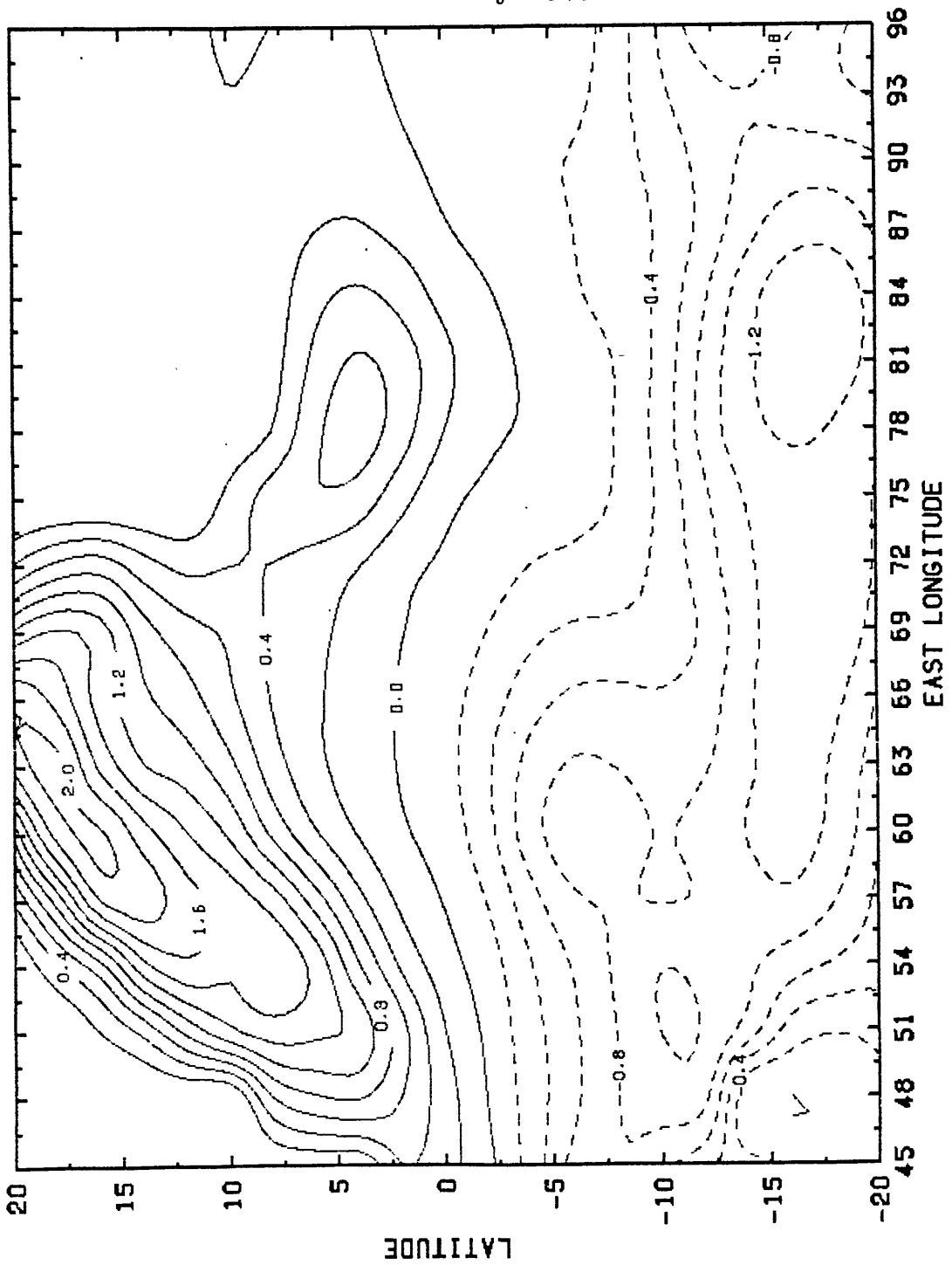

FIGURE 6.10

EMC Zonal Stress (dynes)
August 1979

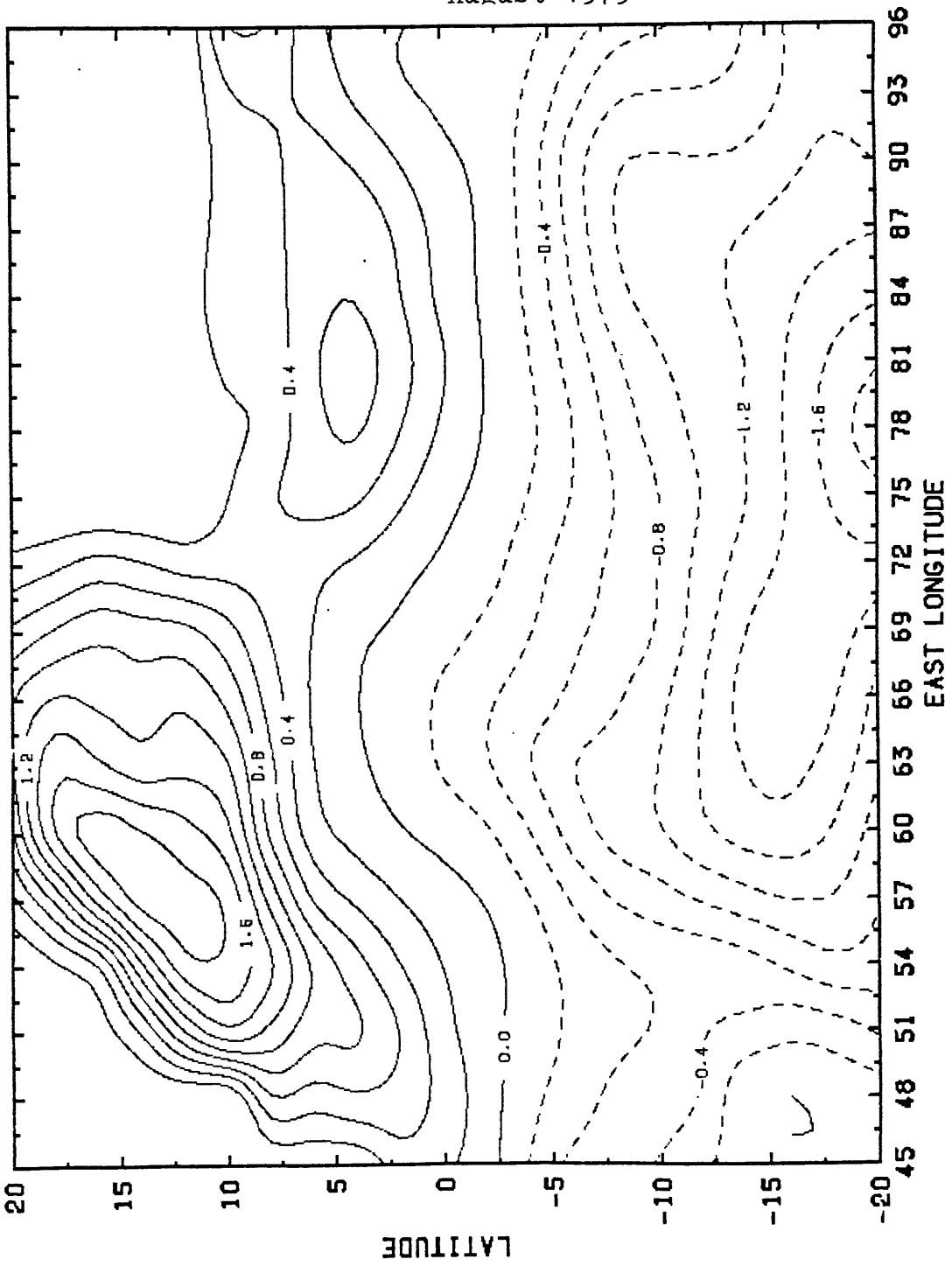

FIGURE 6.11

EMC Zonal Stress (dynes)
September 1979

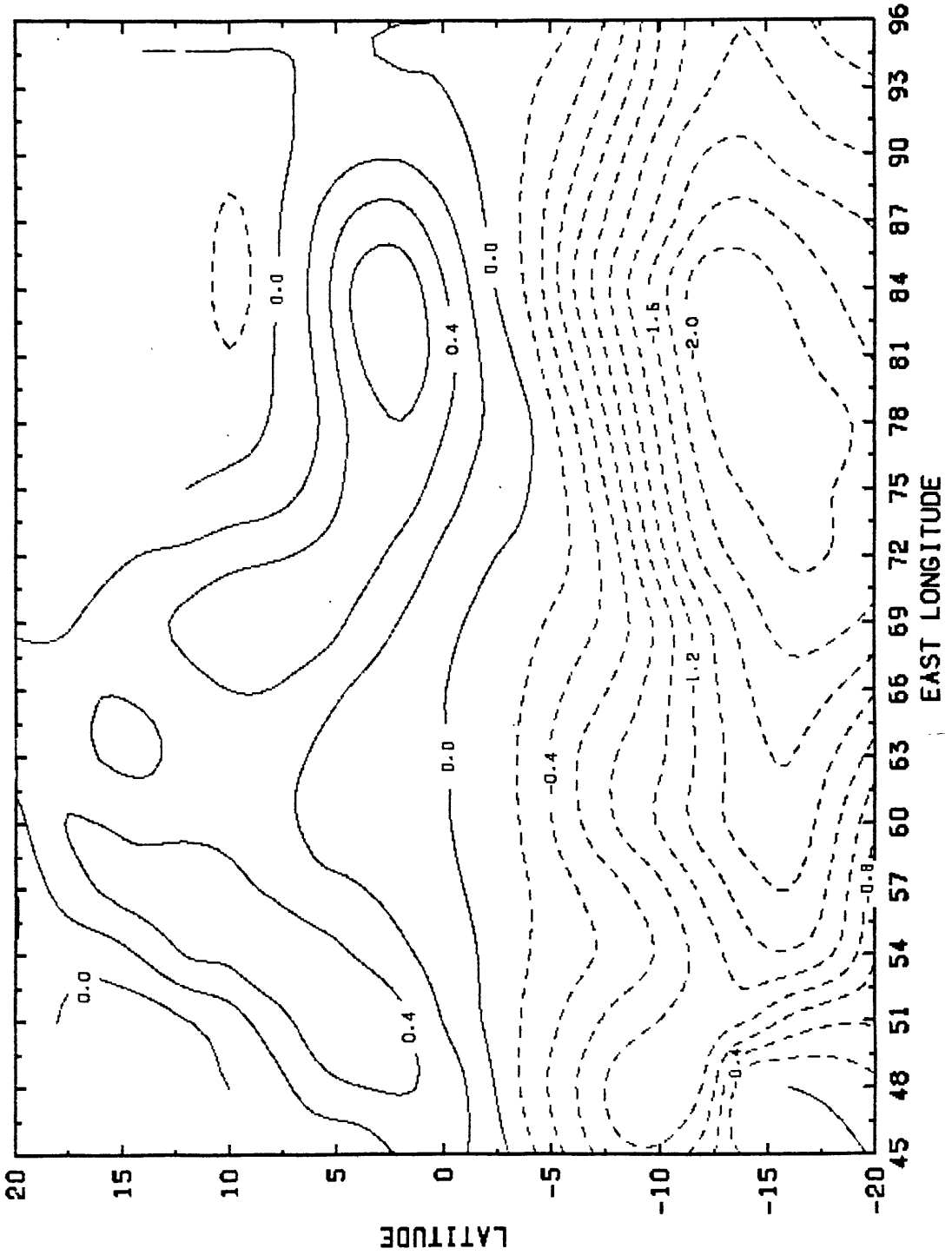

FIGURE 6.12

EMC Zonal Stress (dynes)
October 1979

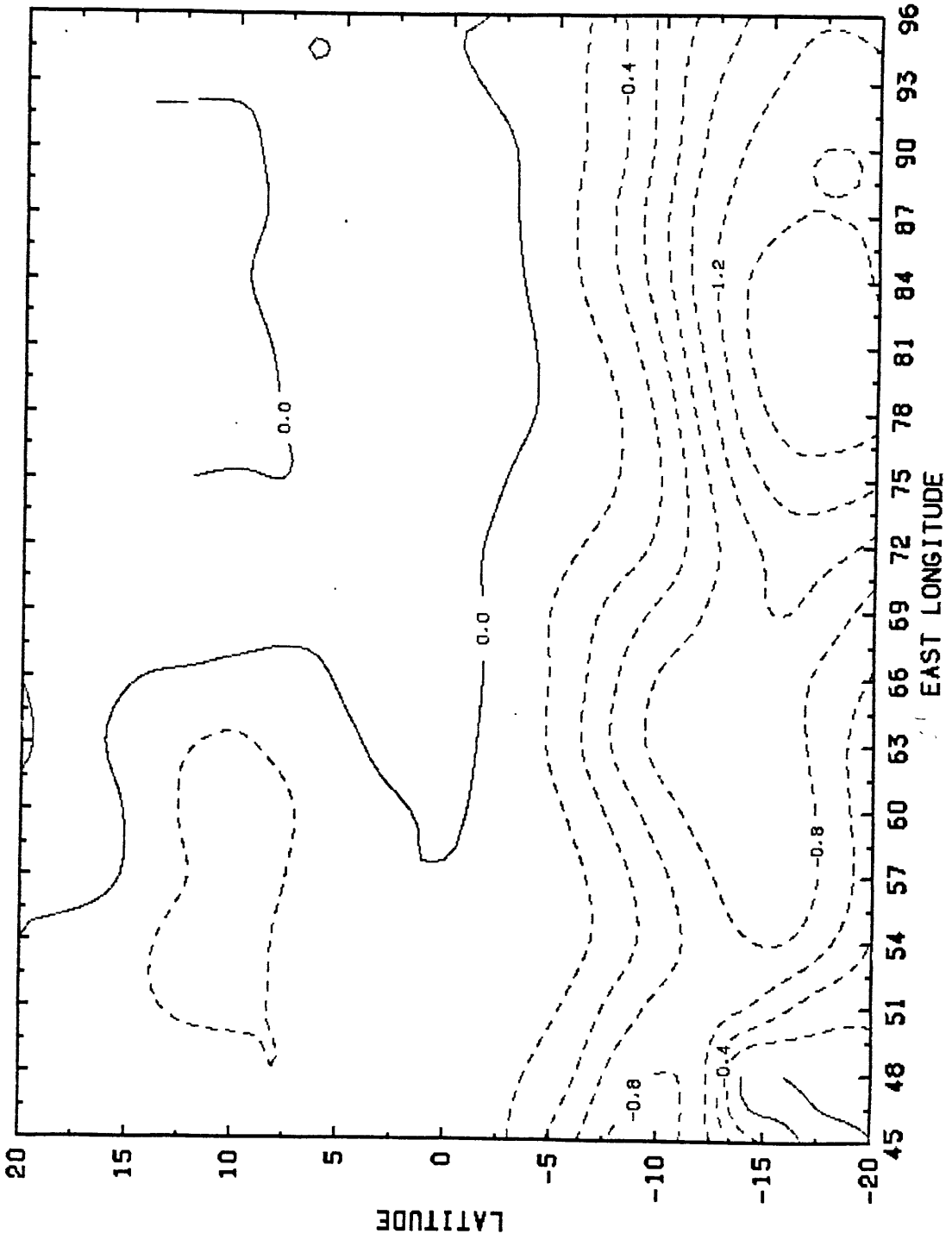

FIGURE 6.13

EMC Zonal Stress (dynes)
November 1979

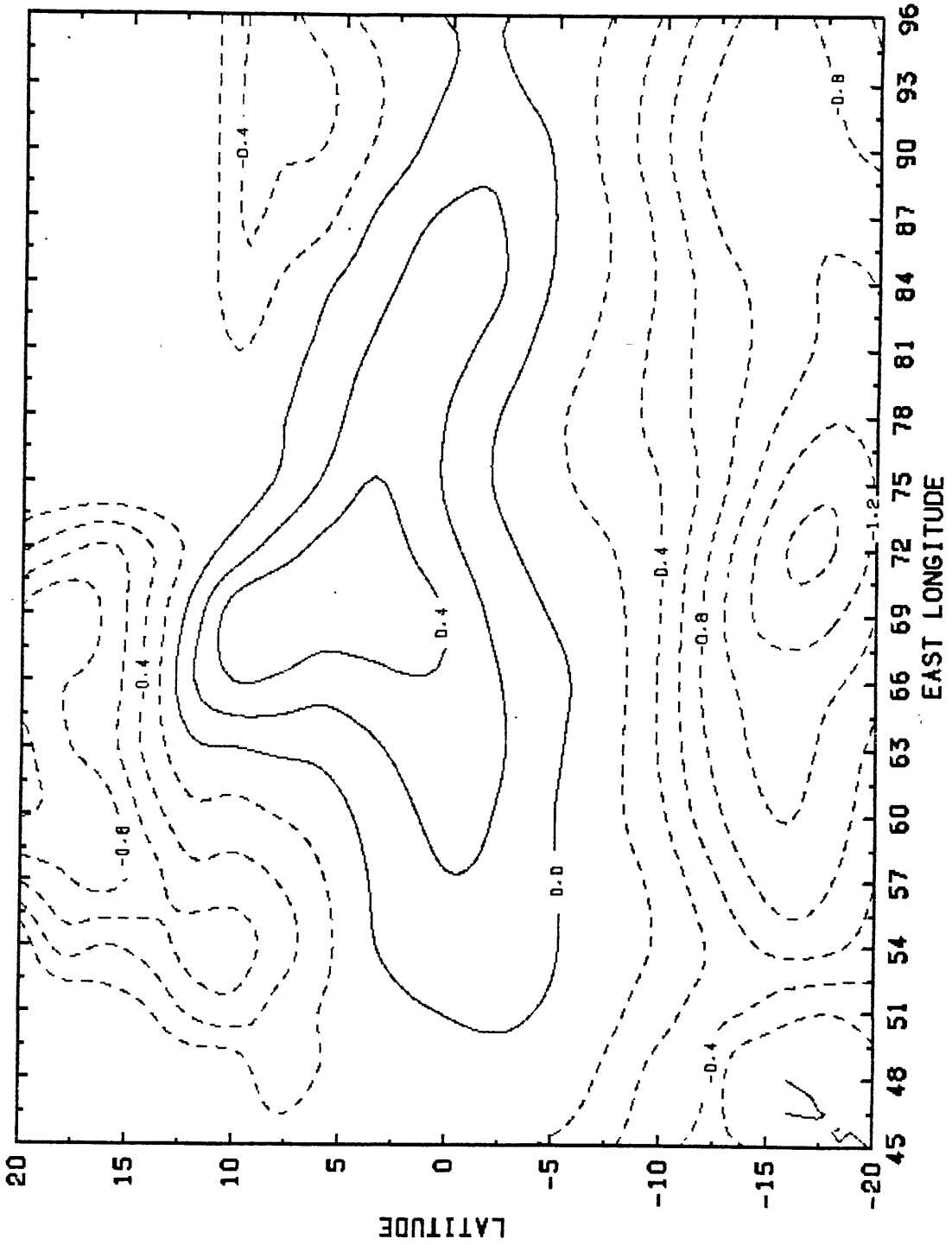

FIGURE 6.14

Stress Error Transform
Forcing Period = DC

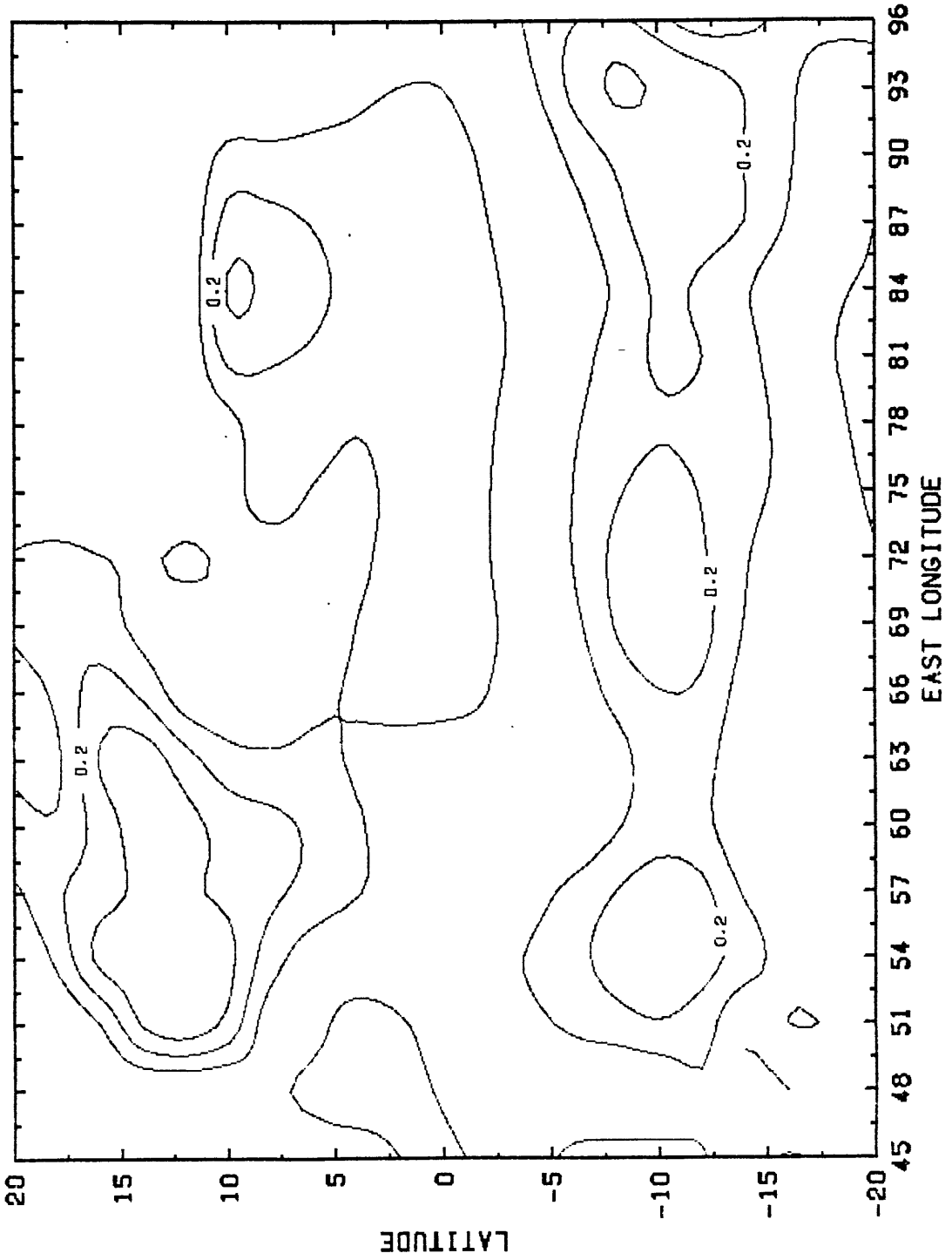

FIGURE 6.15

Stress Error Transform
Forcing Period = 12 Months

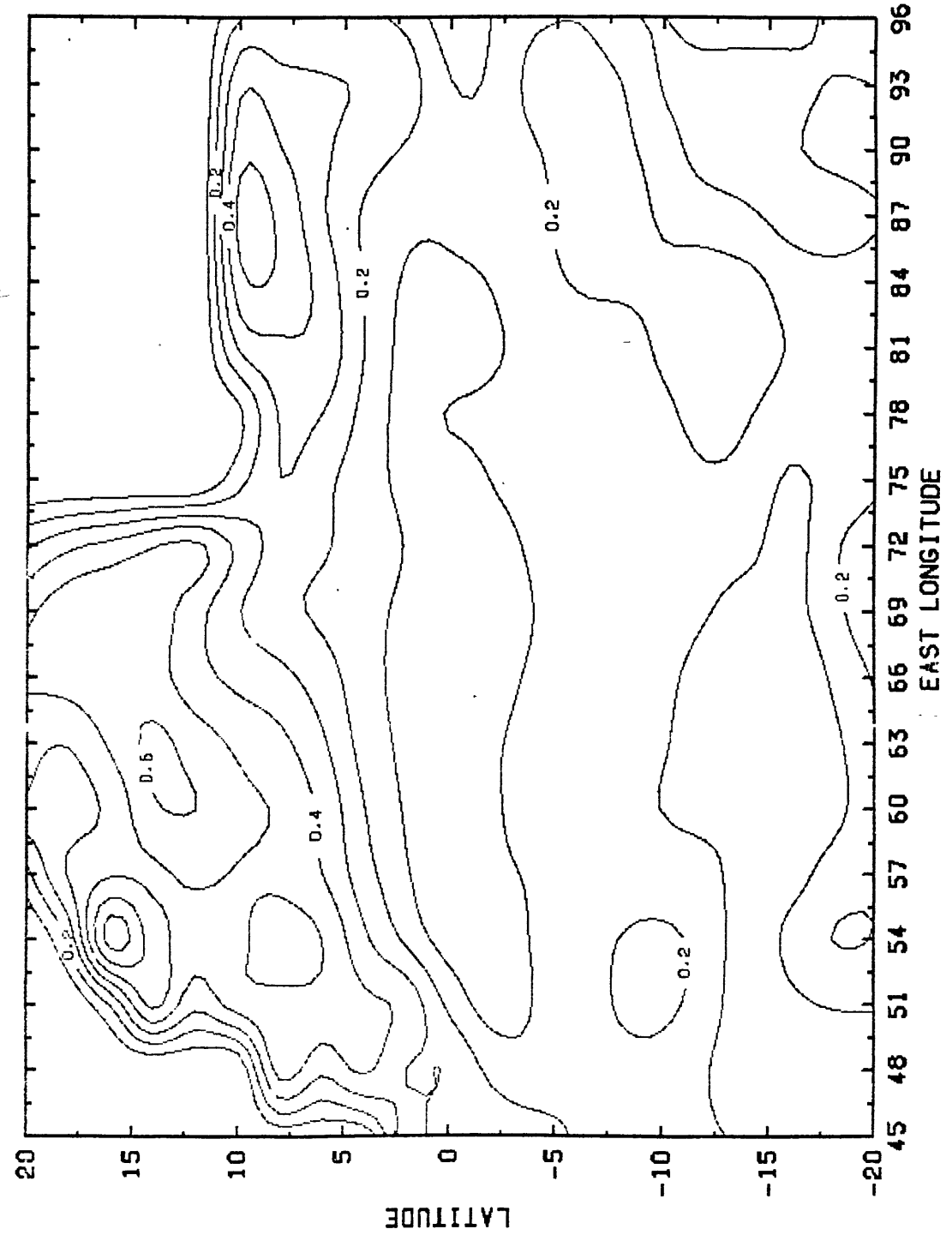

FIGURE 6.16

Stress Error Transform
Forcing Period = 6 Months

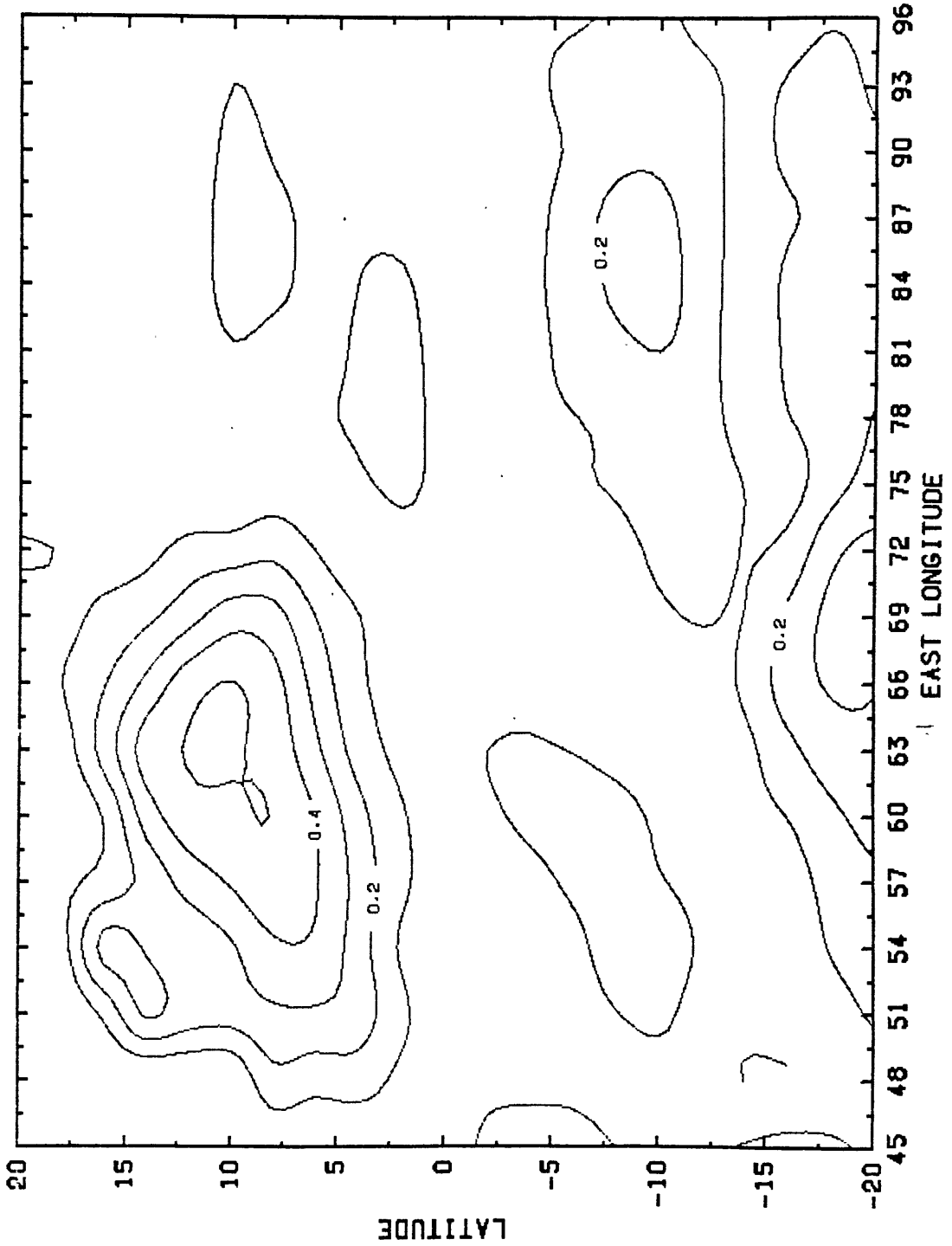

FIGURE 6.17

Stress Error Transform
Forcing Period = 2 Months

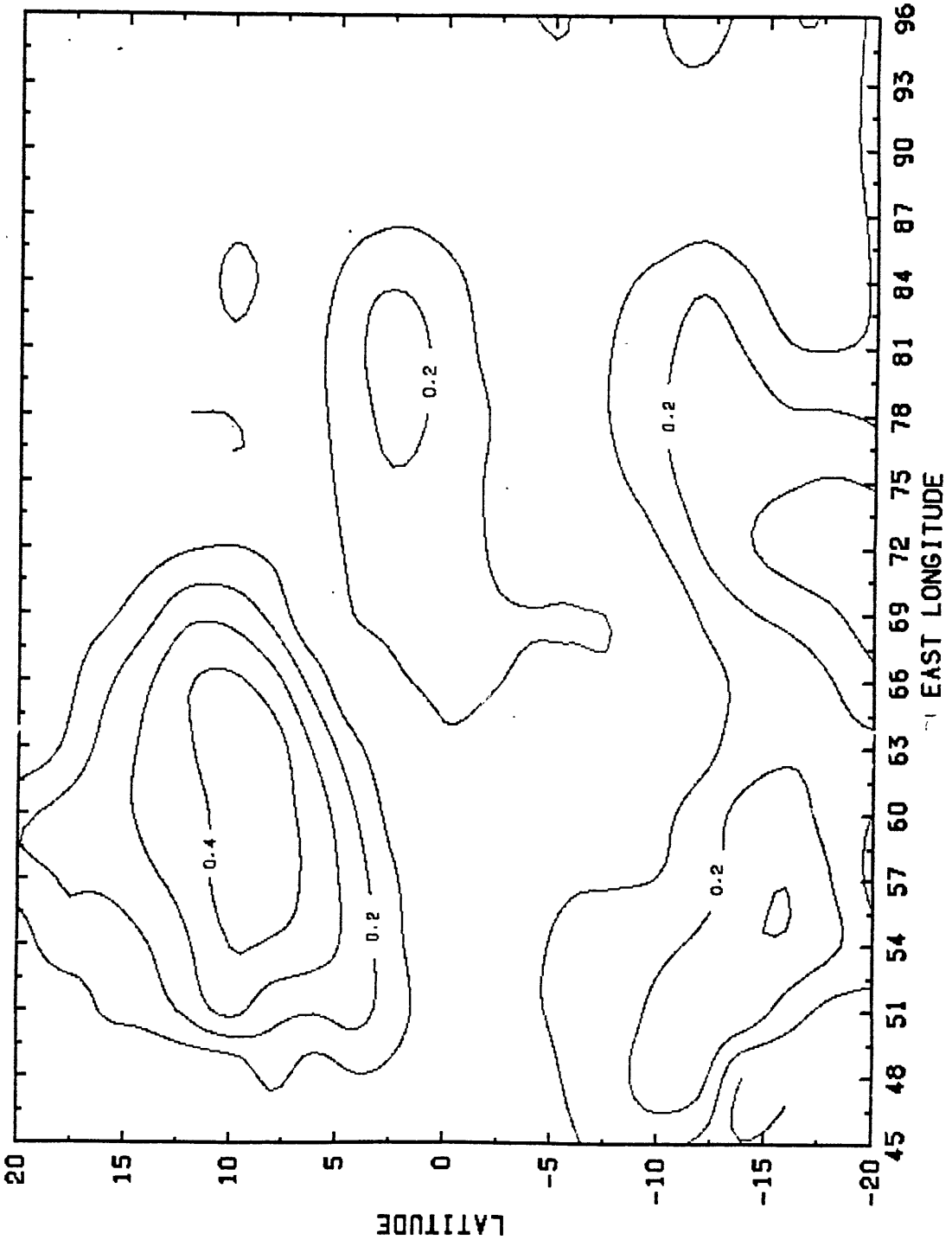

FIGURE 6.18

Station A (0,91E) Response Function
Forcing Period = DC

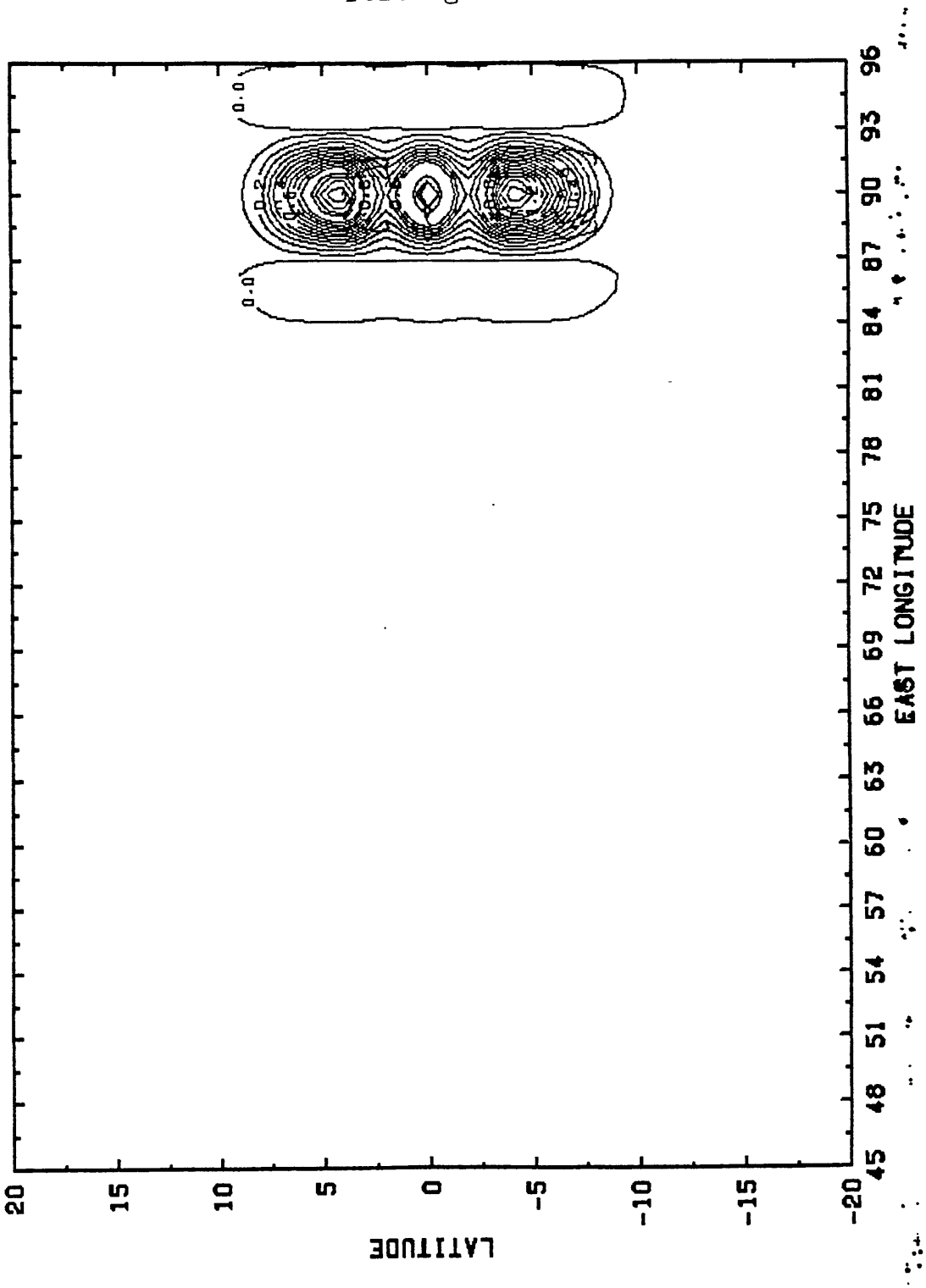

FIGURE 6.19

Station A (0,91E) Response Function
Forcing Period = 12 Months

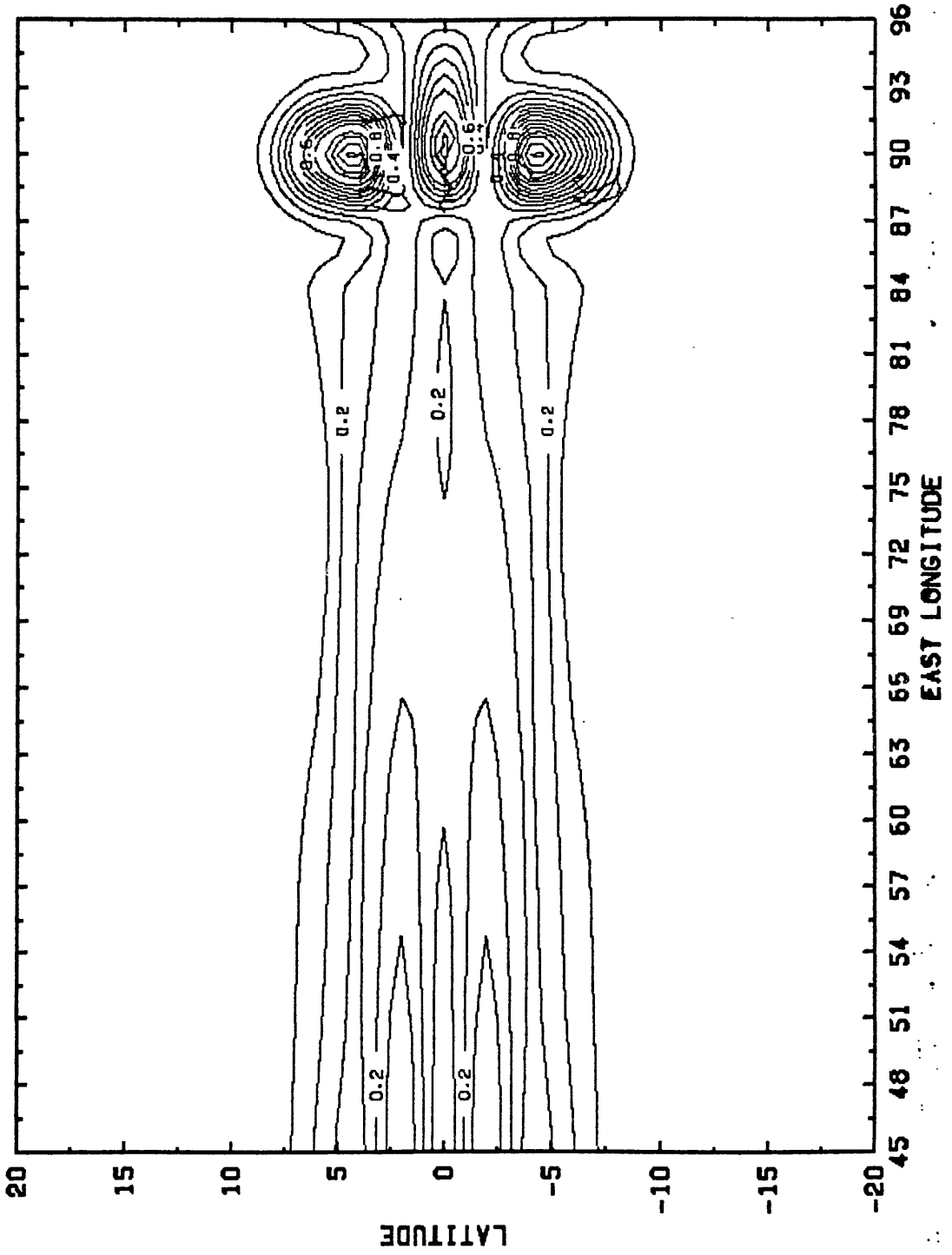

FIGURE 6.20

Station A (0,91E) Response Function
Forcing Period = 6 Months

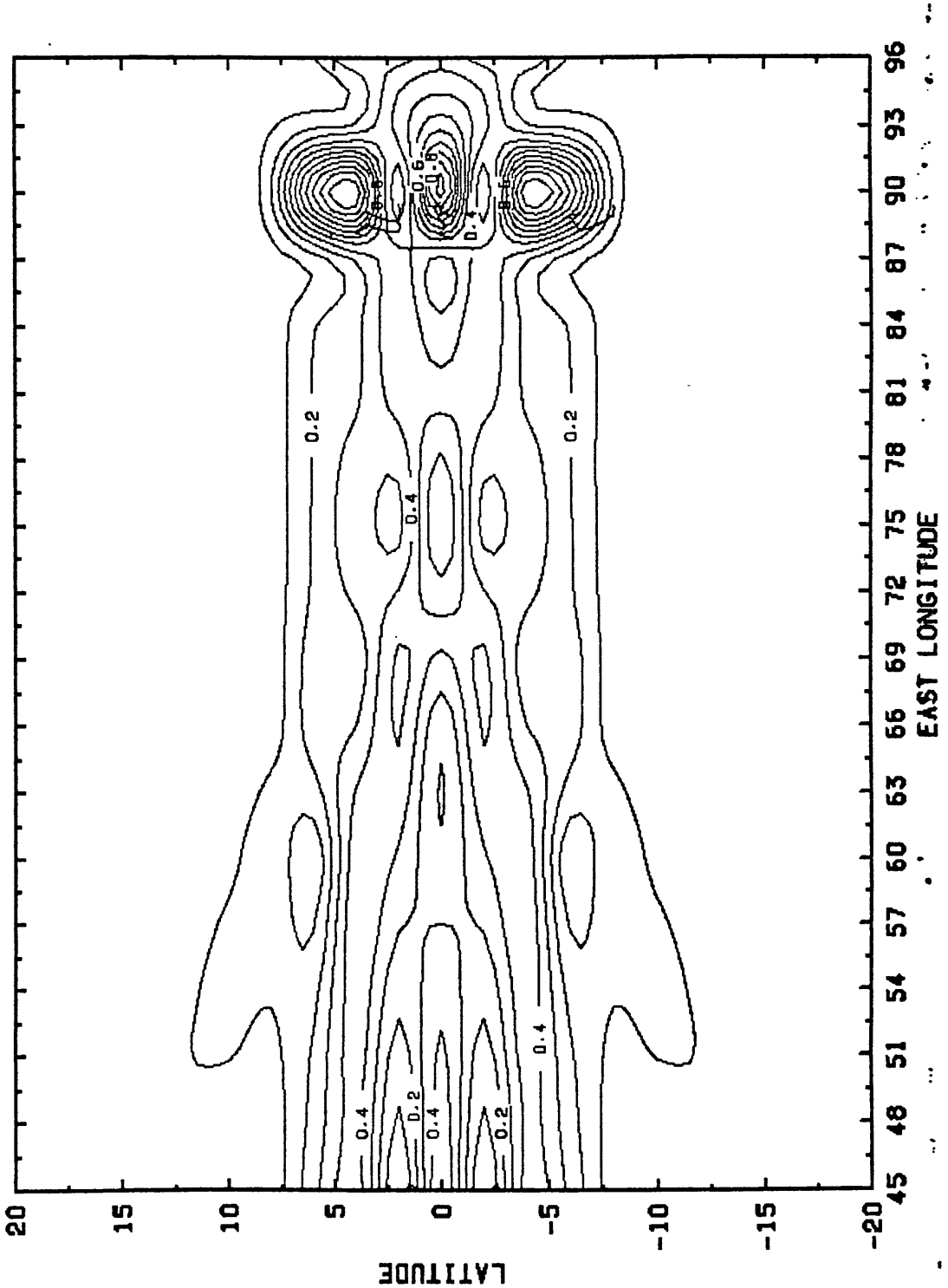

FIGURE 6.21

Station A (0,91E) Response Function
Forcing Period = 2 Months

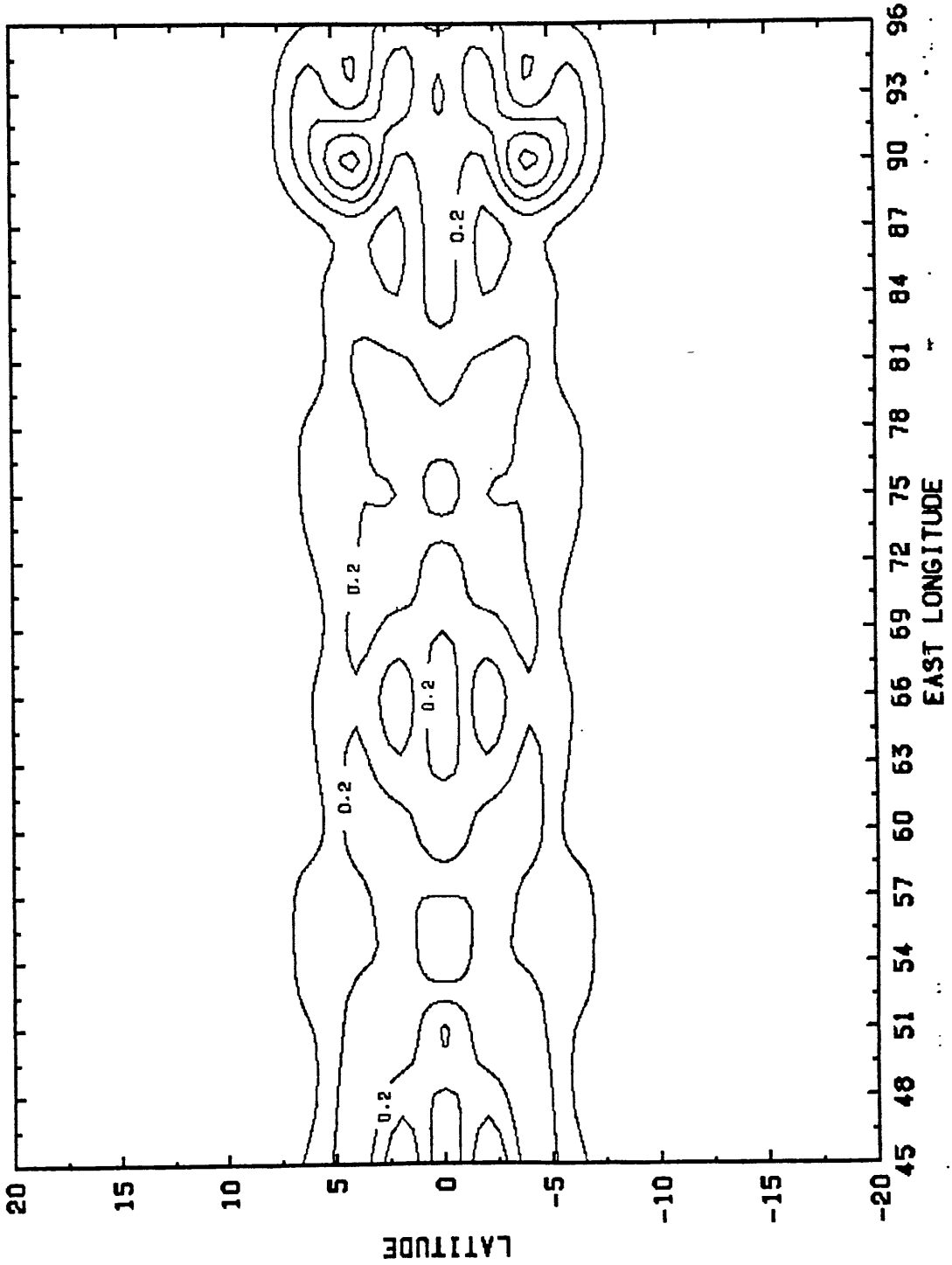

FIGURE 6.22

Station H (5S,91E) Response Function
Forcing Period = 4 Months

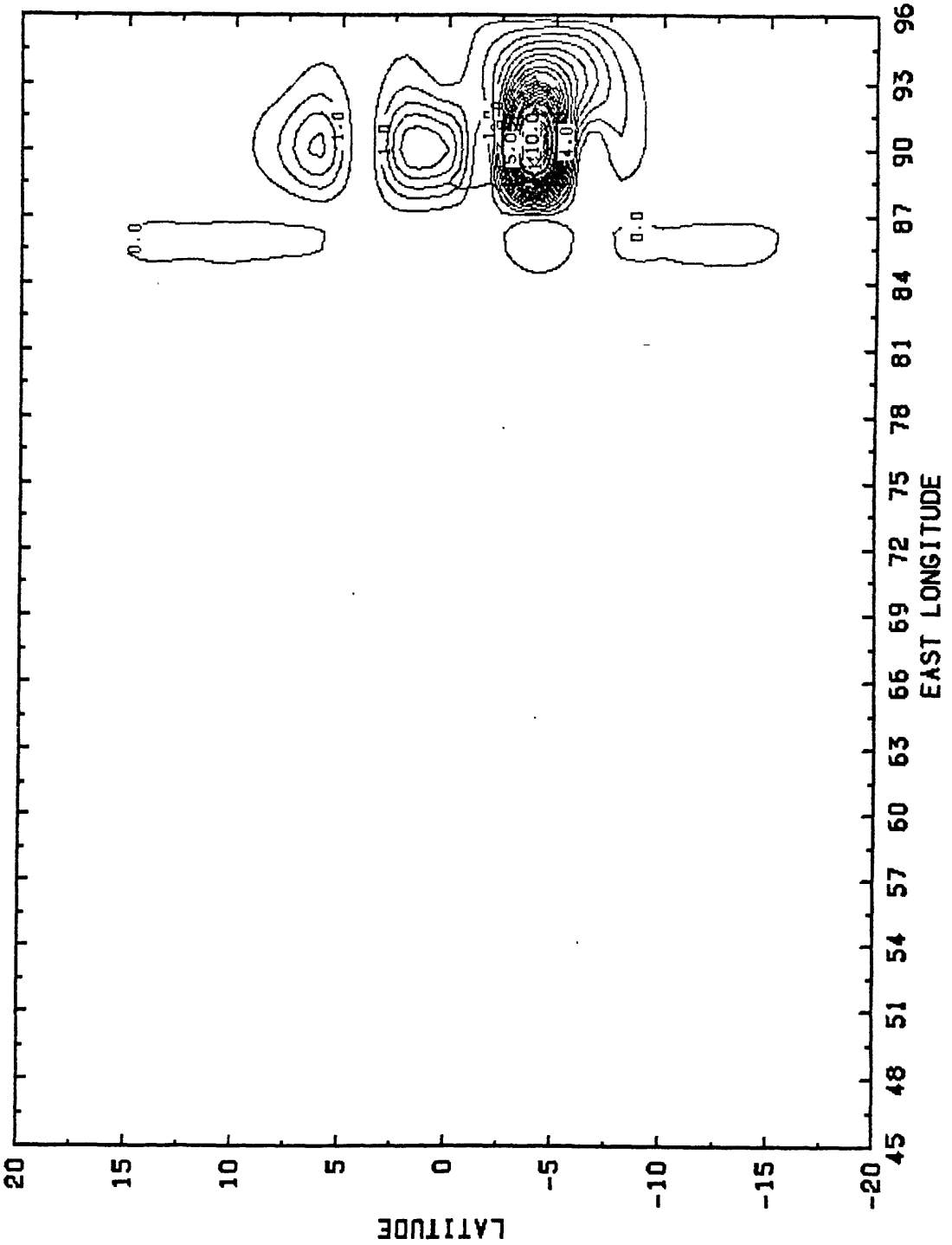

FIGURE 6.23

Station X (0,72E) Response Function
Forcing Period = 3 Months

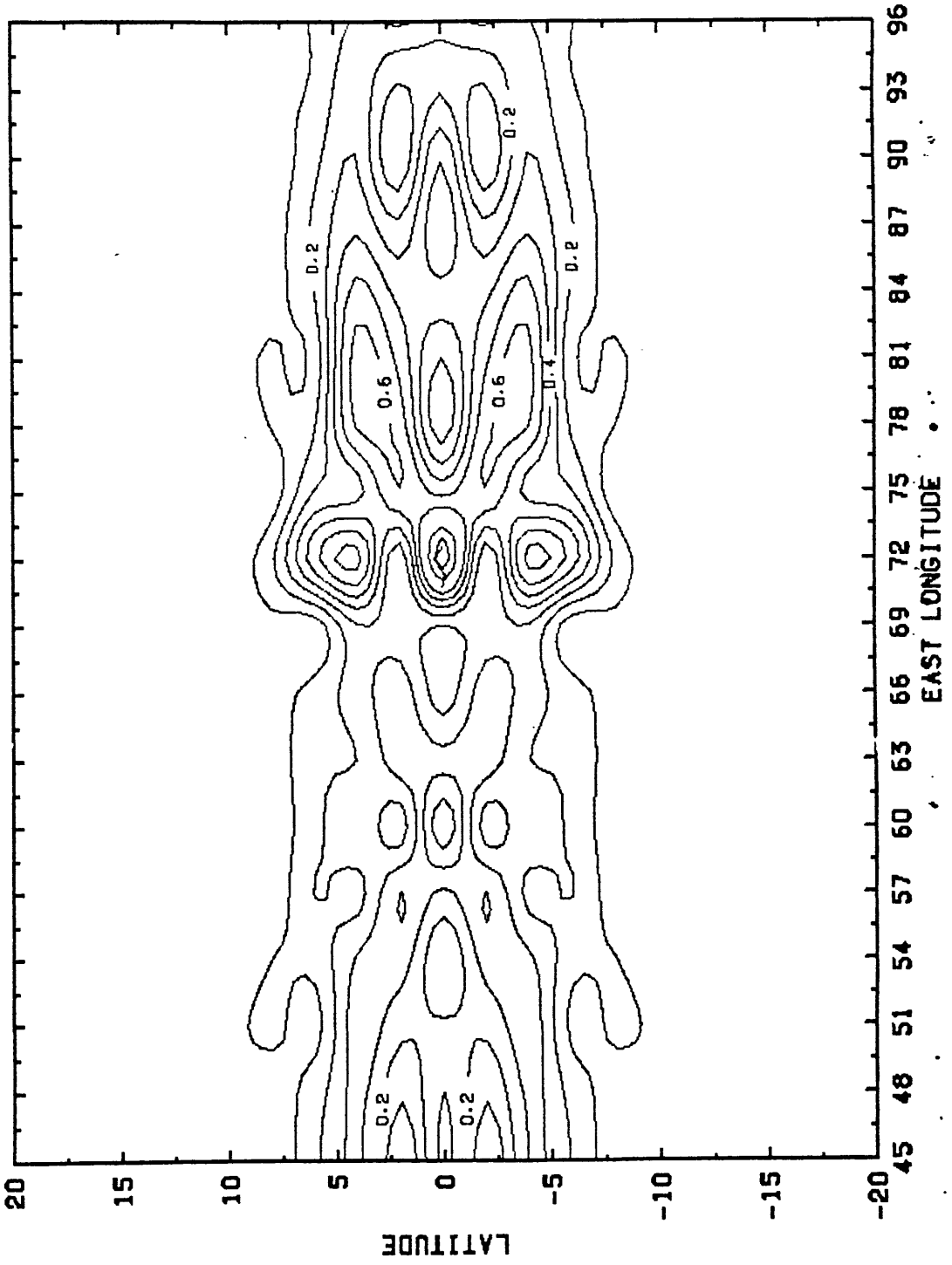

FIGURE 6.24

Station F (5S,72E) Response Function
Mode = 1 - Forcing Period = 12 Months

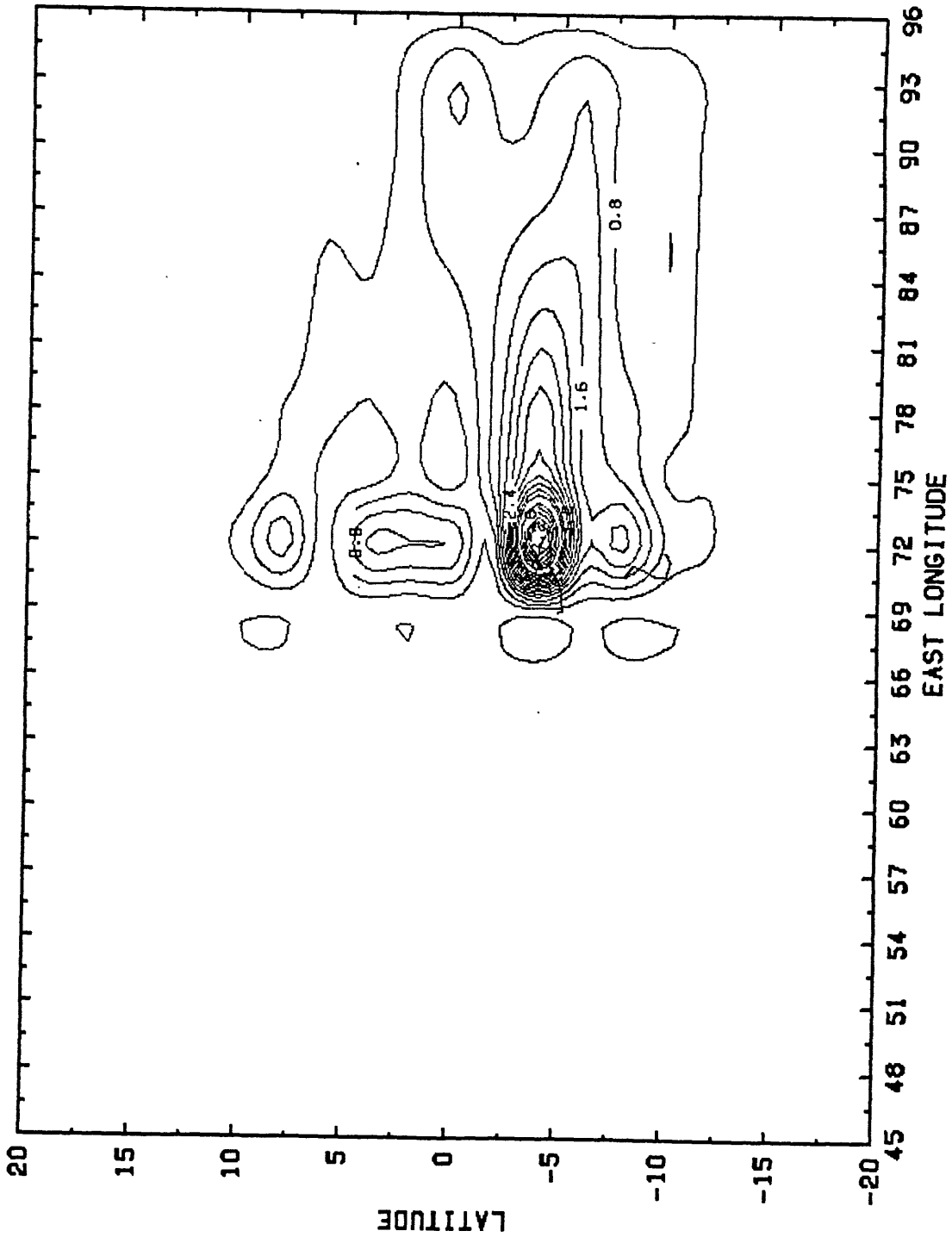

FIGURE 6.25

Station F (5S,72E) Response Function
Mode = 2 - Forcing Period = 12 Months

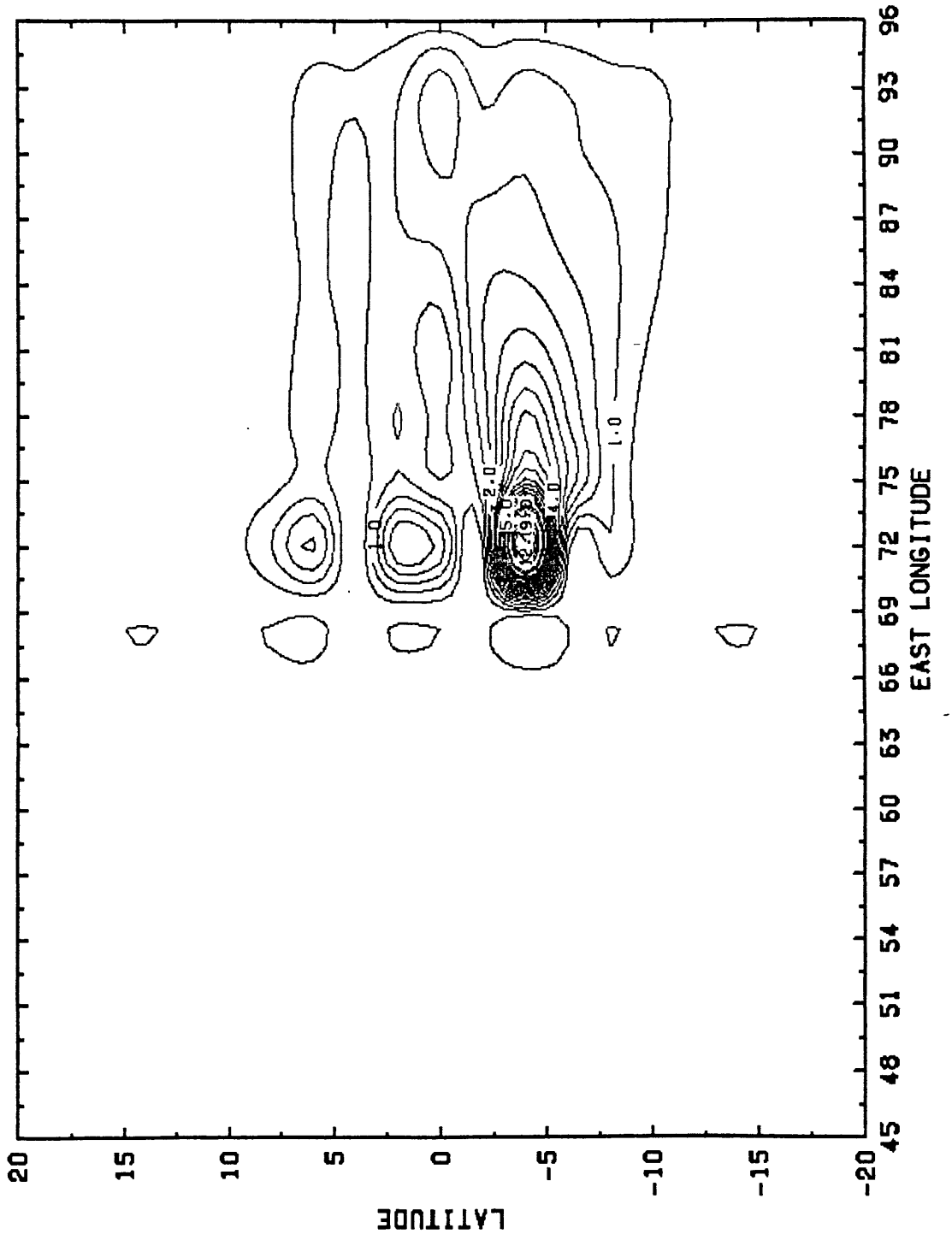

FIGURE 6.26

Station B (0,54E) Response Function
Mode = 2 - Forcing Period = 6 Months

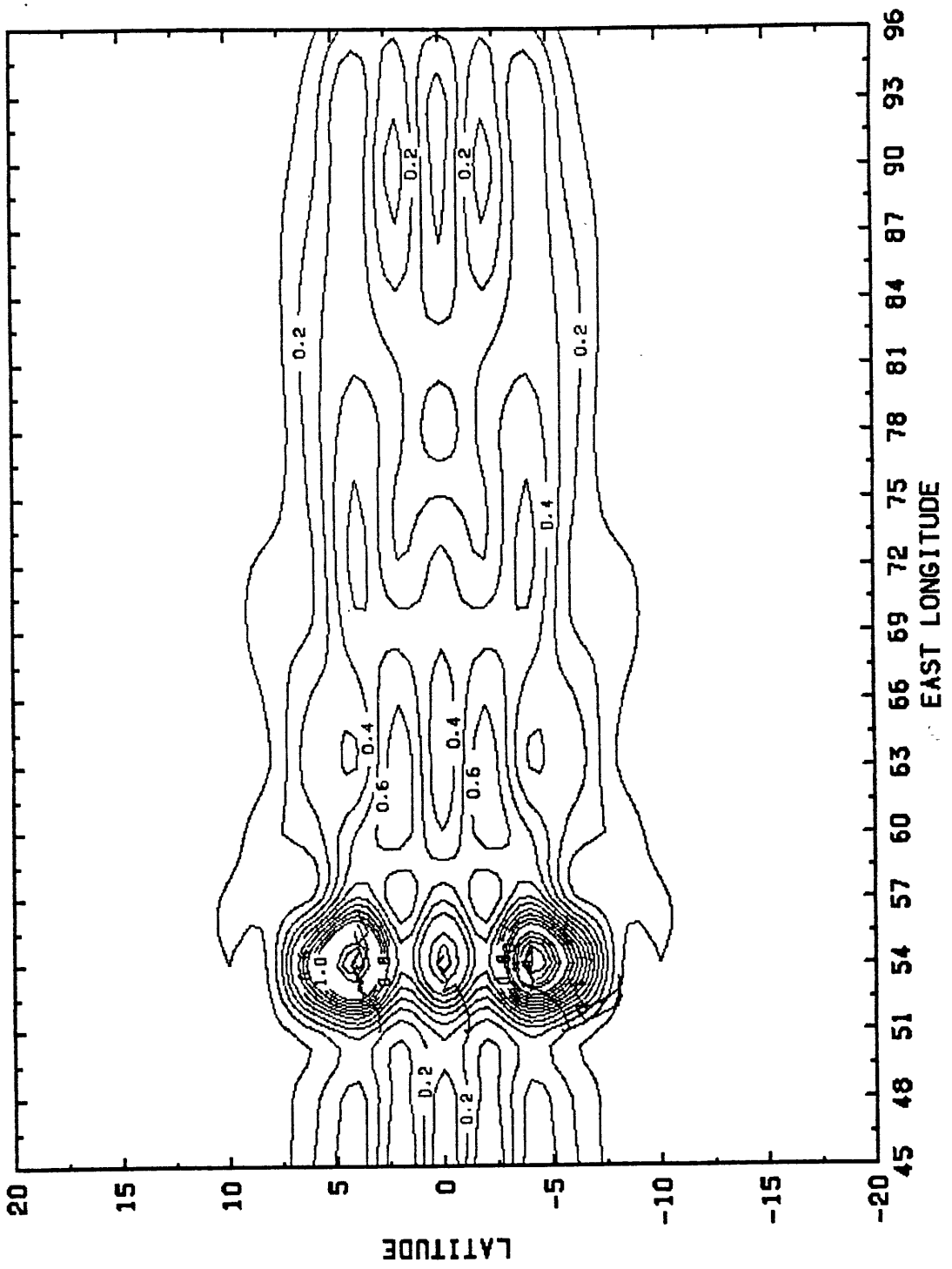

FIGURE 6.27

Station B (0,54E) Response Function
Mode = 3 - Forcing Period = 6 Months

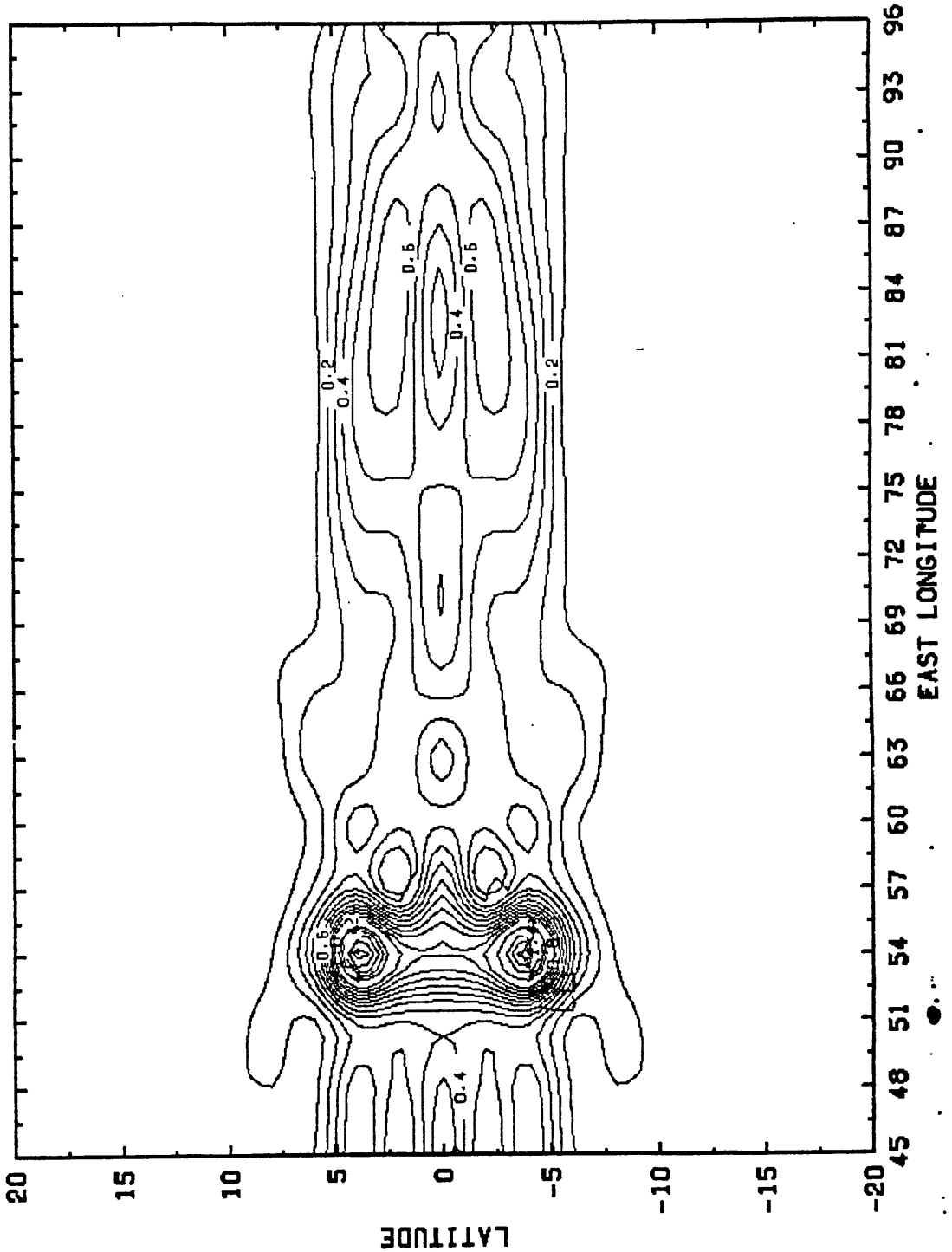

FIGURE 6.28

Station W (6N,52E) Response Function
Forcing Period = 6 Months

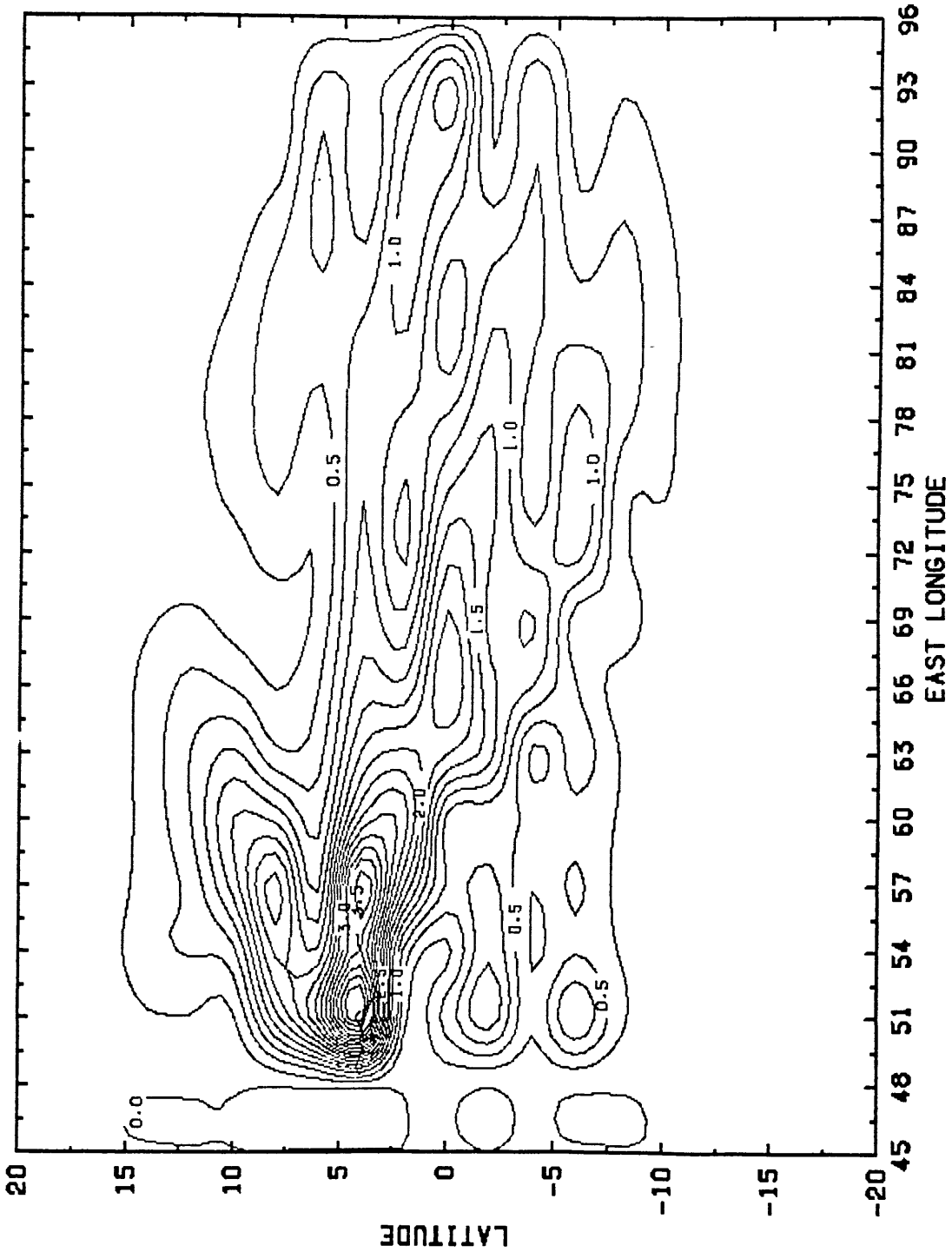

FIGURE 6.29

Station Q (10S,49E) Response Function
Forcing Period = 3 Months

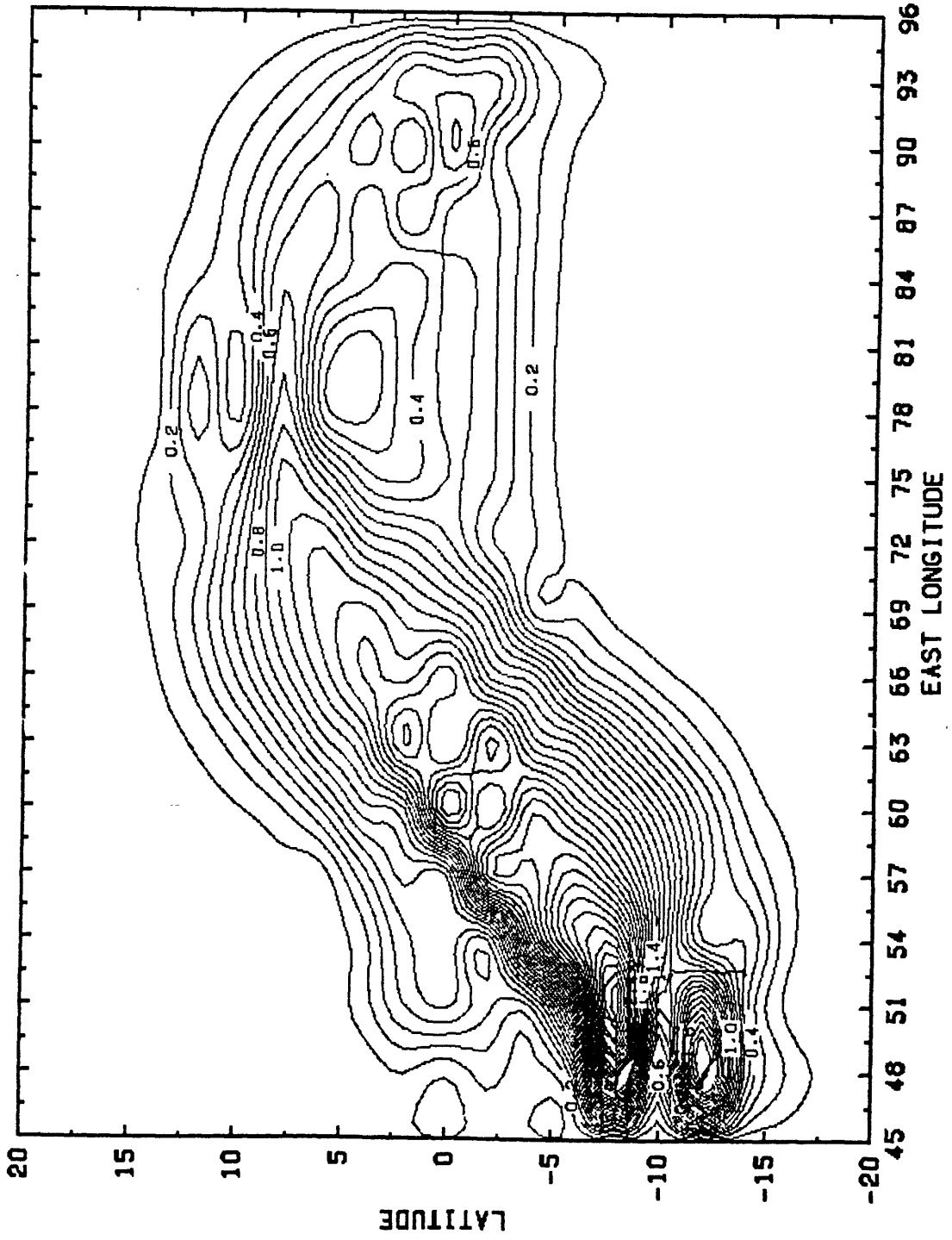

FIGURE 6.30

Station A (0,91E)
Sea Surface Error

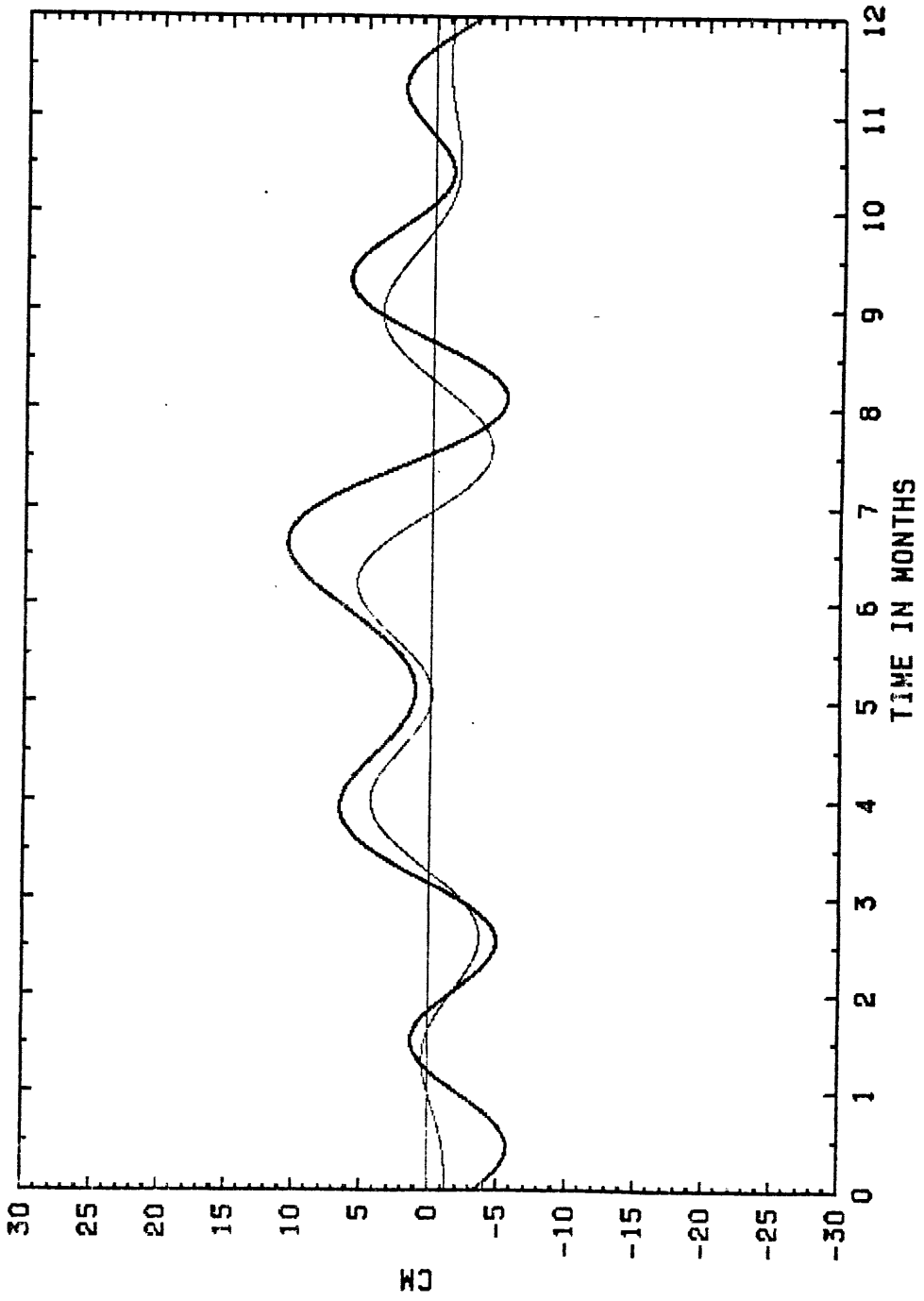

FIGURE 6.31

Station T (7N,91E)
Sea Surface Error

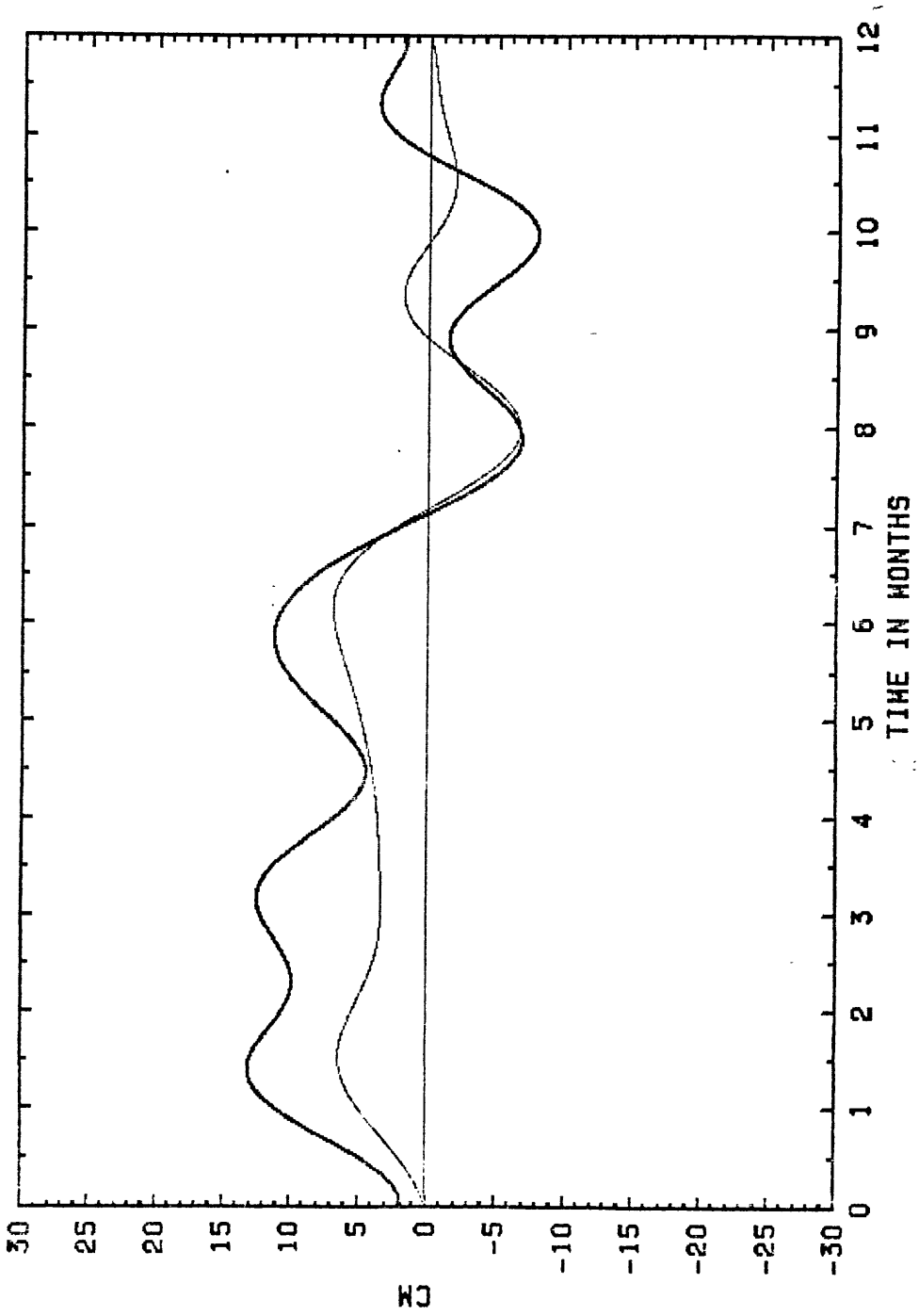

FIGURE 6.32

Station H (5S,91E)
Sea Surface Error

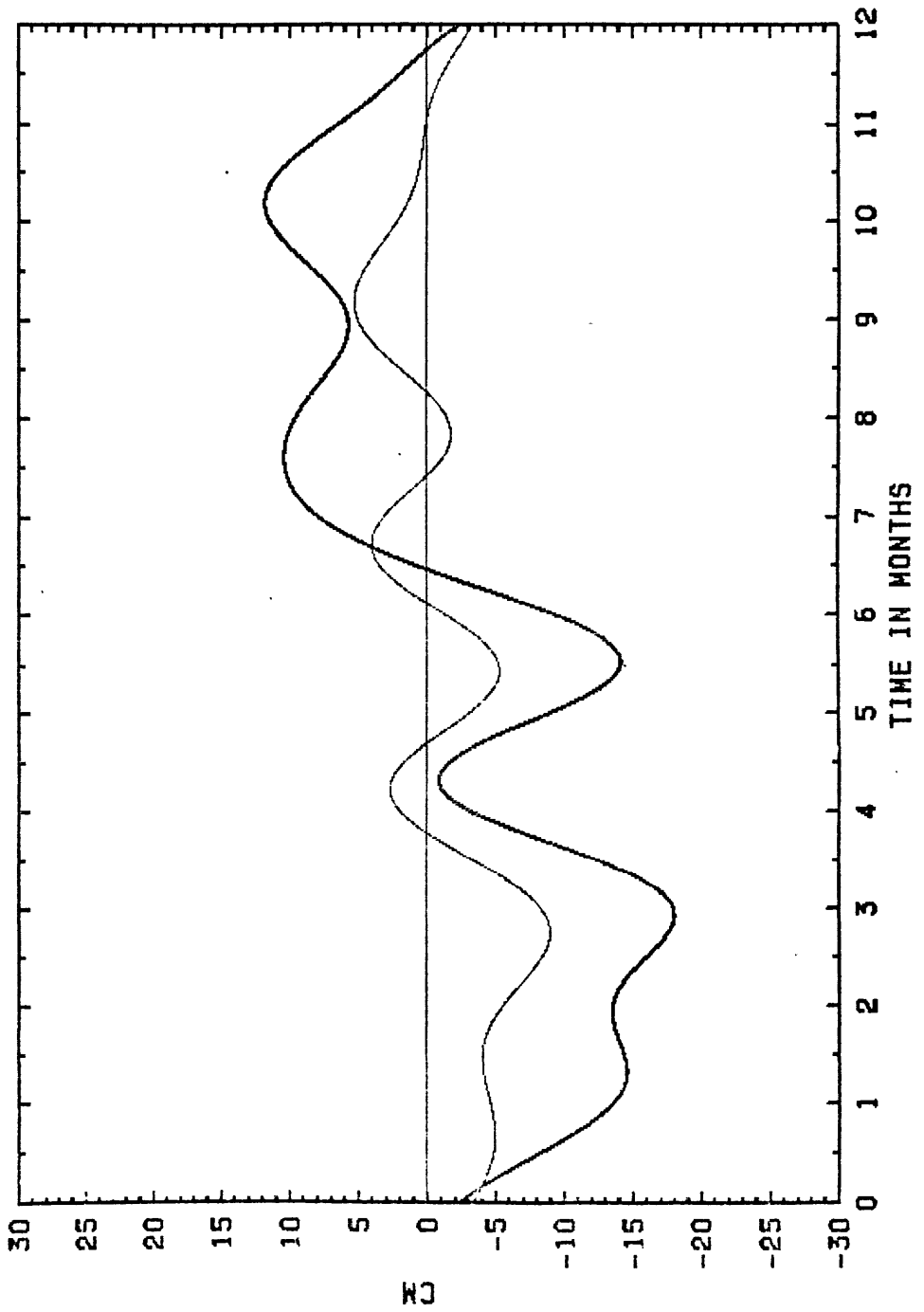

FIGURE 6.33

Station X (0,91E)
Sea Surface Error

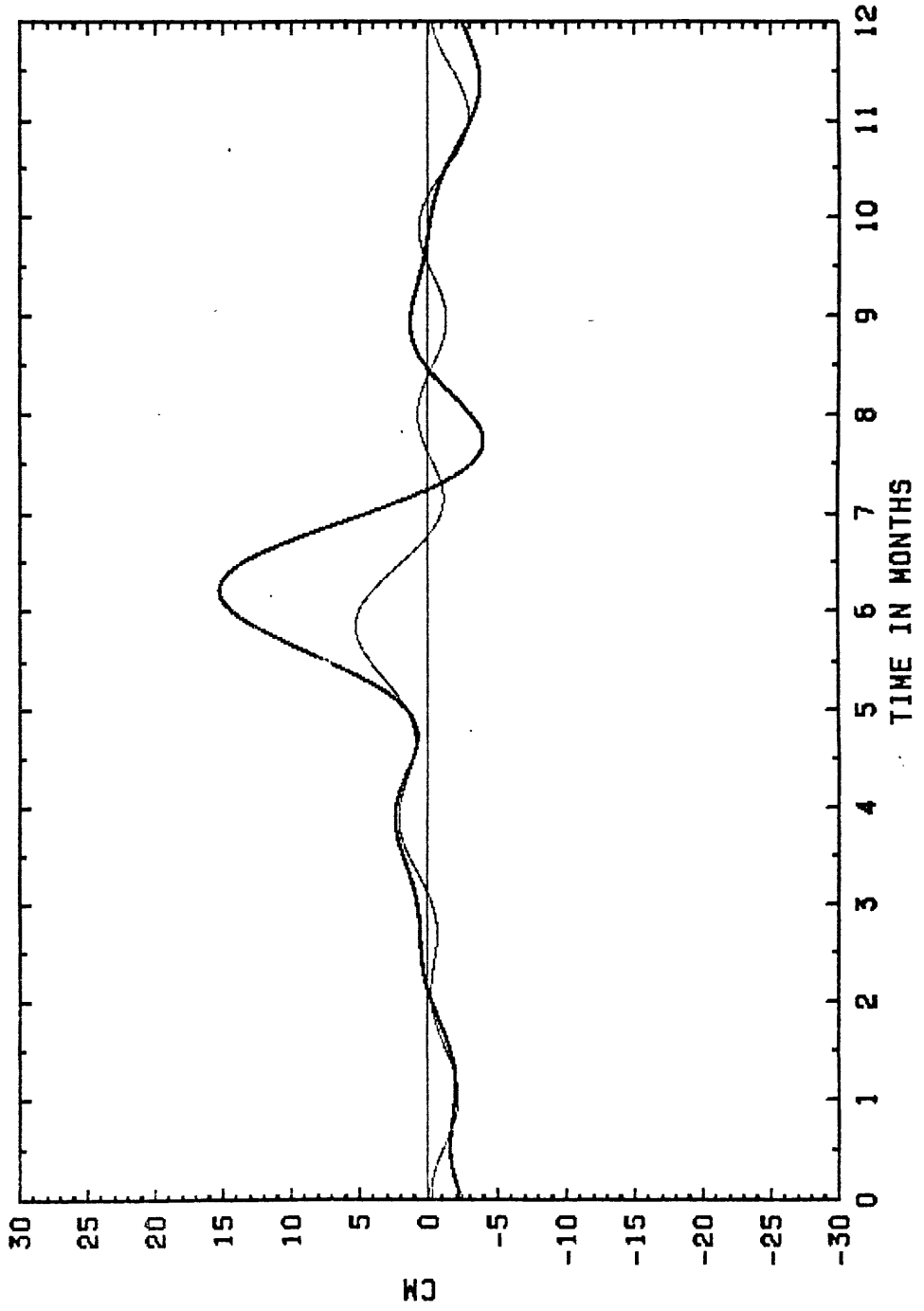

FIGURE 6.34

Station F (5S,72E)
Sea Surface Error

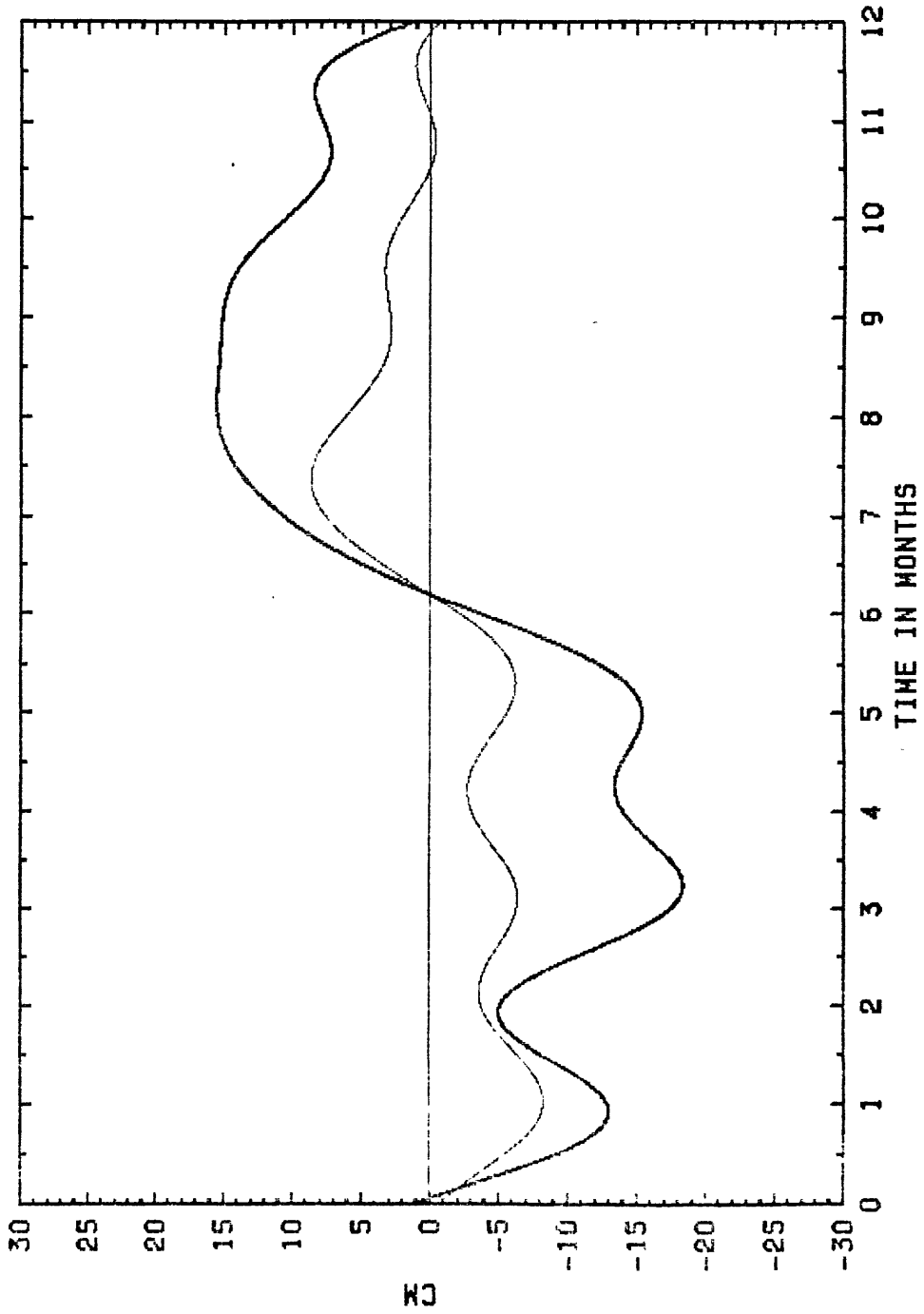

FIGURE 6.35

Station G (6N,70E)
Sea Surface Error

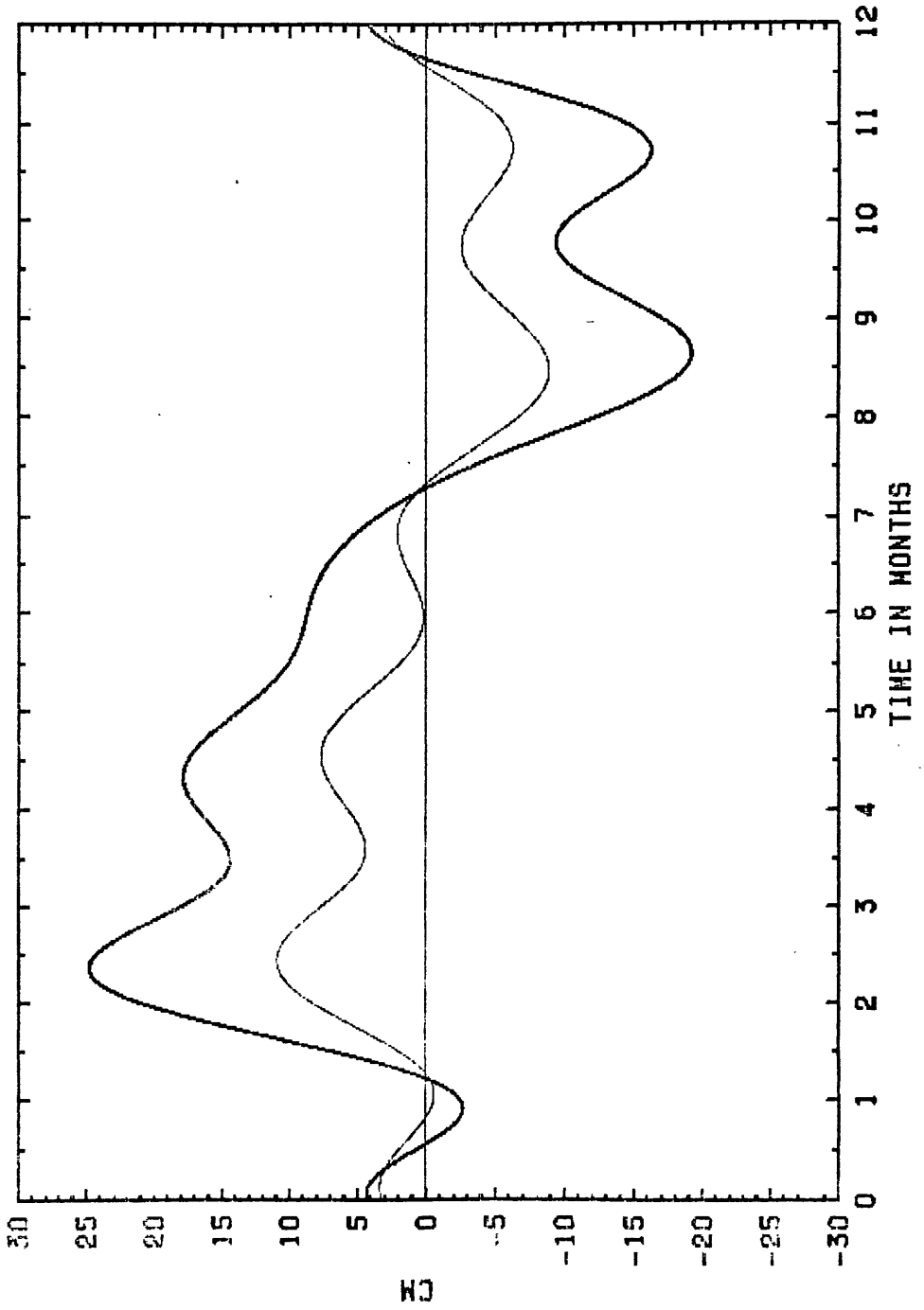

Figure 6.36

Station B (0,54E)
Sea Surface Error

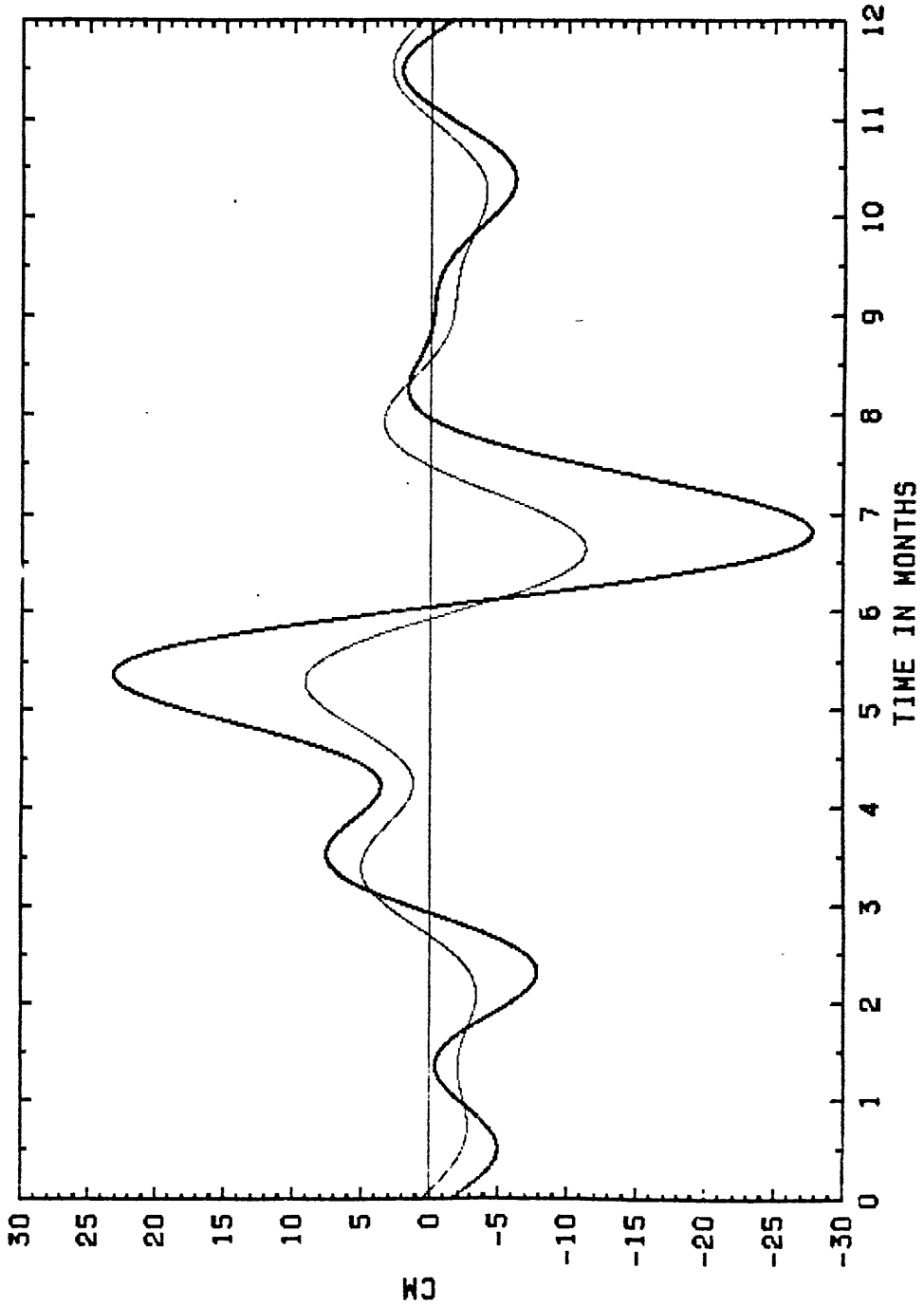

FIGURE 6.37

Station W (6N,52E)
Sea Surface Error

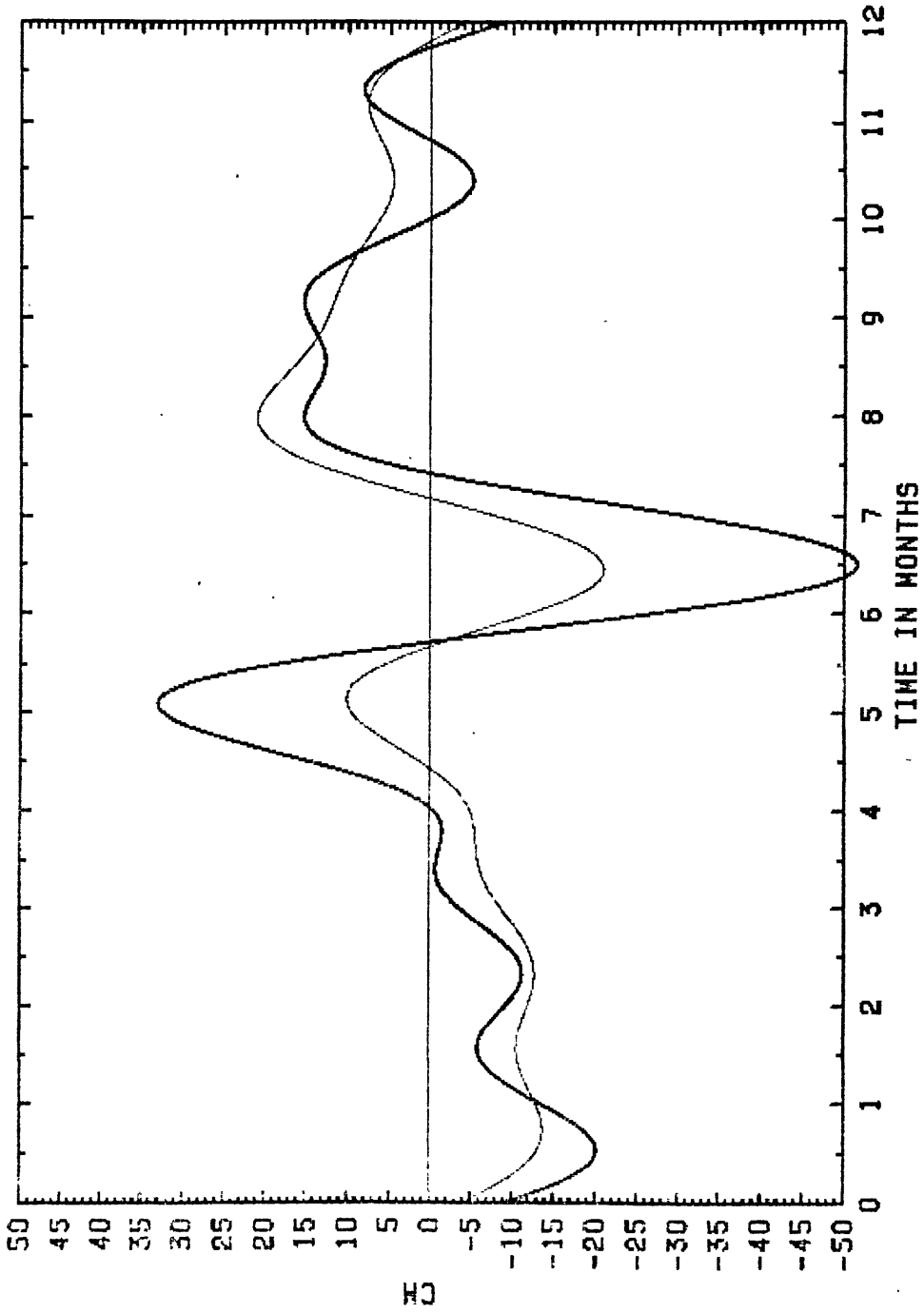

FIGURE 6.38

Station Q (10S,49E)
Sea Surface Error

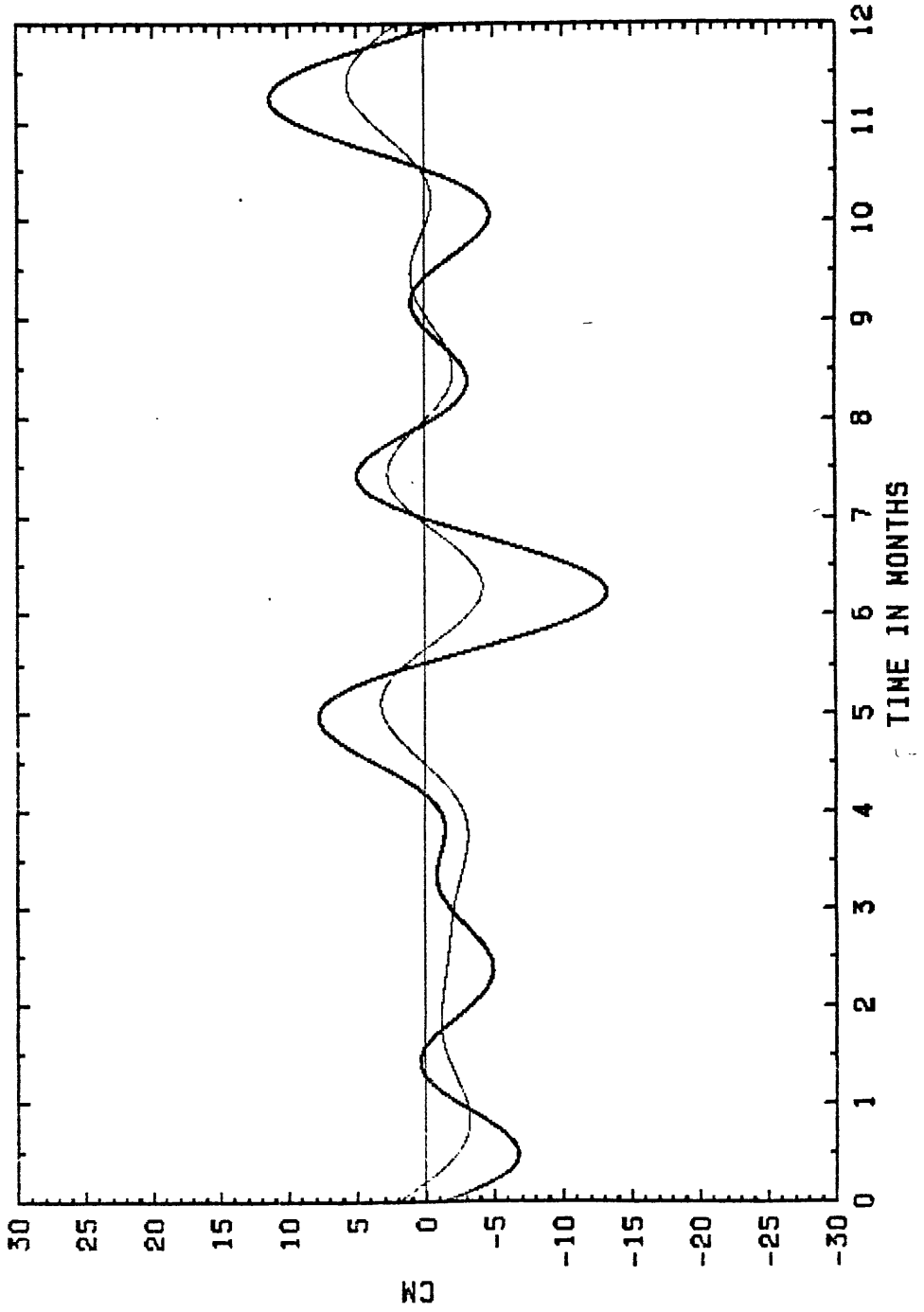

FIGURE 6.39

Station Z (0,49E)
Sea Surface Error